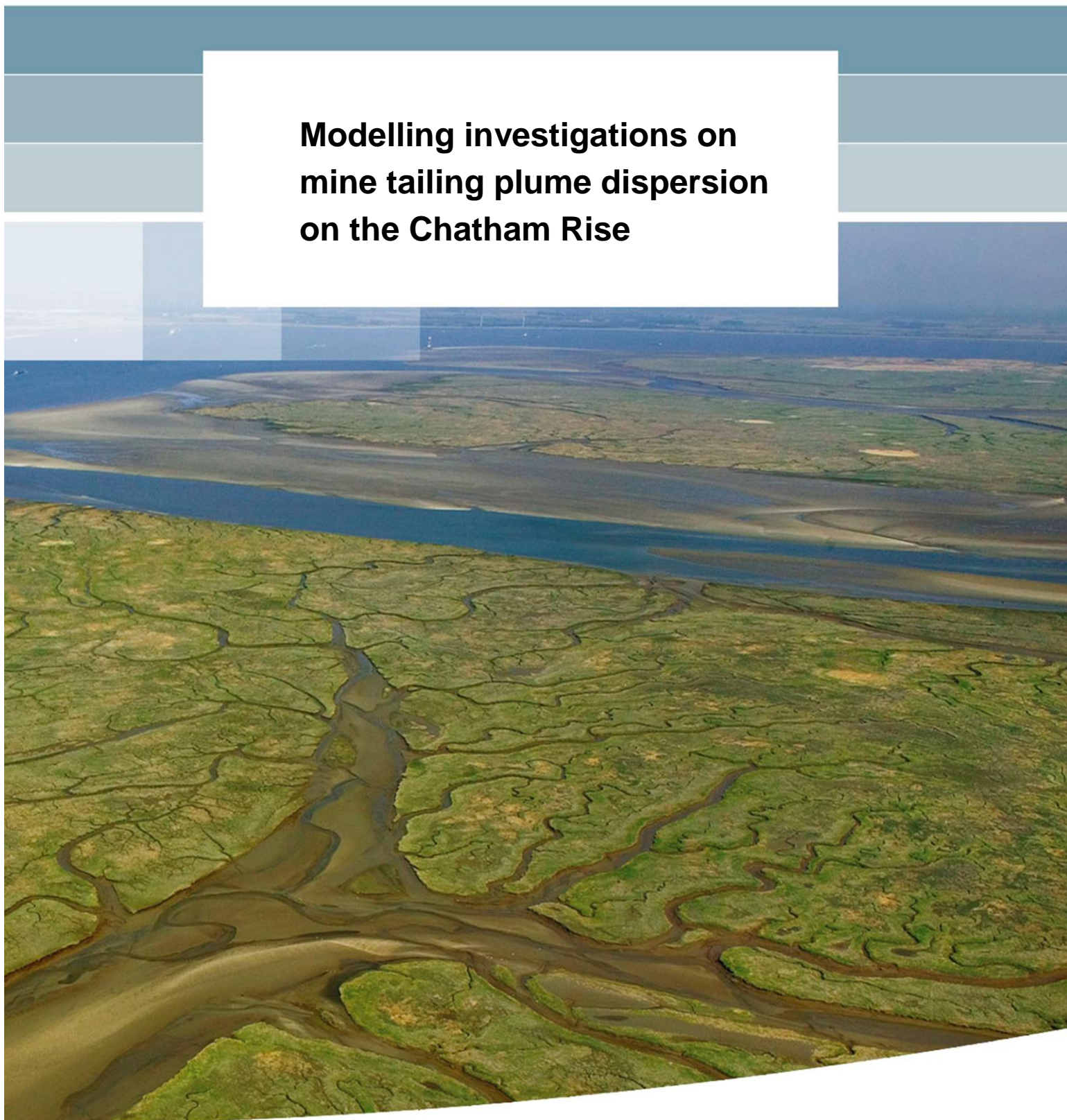


Appendix 25

Modeling investigations on mine tailing plume dispersion on the Chatham Rise (Deltares 2014b)

**Modelling investigations on
mine tailing plume dispersion
on the Chatham Rise**



Modelling investigations on mine tailing plume dispersion on the Chatham Rise

Jamie Lescinski
Claire Jeuken
Katherine Cronin
Julia Vroom
Edwin Elias

1209110-000

Title

Modelling investigations on mine tailing plume dispersion on the Chatham Rise

Client

Chatham Rock Phosphate

Project

1209110-000

Reference

1209110-000-ZKS-0007

Keywords

Deep sea mining, Modelling, Mine tailing dispersion, Chatham Rise.

Executive Summary

In the framework of the Chatham Rise Rock Phosphates (CRP) Mining Project, Boskalis and CRP asked Deltares to conduct an operations study investigating the dispersion behaviour of sediments released during the mining tailings return process (sediment resuspension during mining excavation is negligible, in comparison). The main interest is in the turbidity generated in the water column and the deposition footprint on the seabed resulting from the mining discharge. The Chatham Rise is a submarine feature that is approximately 1000 km in length, extending eastward from the South Island of New Zealand. The rise has water depths that range from roughly 80 m to 500 m, with the Chatham Islands near the eastern extent of the submarine feature. Just north and south of the Rise, water depths quickly approach 3000 m.

This study uses a dedicated modelling approach to assess the near and far-field dispersion, and sedimentation behaviour of sediments released during the mining process. The study consisted of three main phases. The far-field assessments were carried out using a Delft3D model with seasonal forcing: spring, summer and winter periods in 2011. These periods were chosen to represent periods with different hydrodynamic conditions, such that the mining disposal is occurring when the largest tidal currents are expected, resulting in conditions when the largest predicted plume advection and dispersion would occur due to tidal forcing.

The near-field mine tailing plume development was investigated using a JET3D model. The far-field study only considers the behaviour of the silt- and clay fractions. Sand is expected to settle immediately in the direct vicinity of the point of release and does not thus contribute to the dispersive plume.

The first phase (2012) was an initial mine tailing plume investigation composed of two sub-phases, Phase 1a and 1b. Phase 1a investigated the near-field plume development and far-field plume dispersion for mine tailings released at 5 m and 200 m above the seabed.

Results of the near-field plume modelling (Phase 1a) using Jet3D show that the plume, when released at 200 m above the bed, transports the sediment, including the fines, to the seabed very quickly, regardless of the individual fall velocities of the various grain sizes. Flow velocity and sediment concentration of the near-field mine tailing plume quickly decrease as a function of distance from the release point. Only coarse particles will settle faster than the plume (sand and gravel) and only a minor fraction of the plume will be entrained in the water before it has reached the seabed (stripping). However, the effect of stripping is neglected. It is predicted the plume will result in a suspension layer near the bed after the plume contacts the bottom. In this suspension layer, the fine silt fractions will settle over wider areas. However, the very fine colloidal or clay fractions (finer than 2 µm) are not likely to settle.

Based on these results it was decided that mine tailings should be disposed of near or at the seabed to minimize plume dispersion effects. Therefore the subsequent initial investigations of Phase 1b, as well as the optimized investigations of Phase 2, considered mine tailing release at the seabed and 10 m above the seabed. Additionally, an initial comparison of simulated and measured far-field flow velocities was made using moored RDI ADCP current data. Finally, model sensitivities for key physical factors were tested.

Results of far field modelling (Phase 1b) show that during periods of active mining high sediment concentrations occur along the mining track. Most of these sediments (both the clay and silt) directly deposit along the track line (as can be observed from the sedimentation footprints). A minor part is picked up by the flow and transported throughout the model domain, with maximum dispersion occurring near the end of mining. During the 5-day break in mining, the plume silt and

Title

Modelling investigations on mine tailing plume dispersion on the Chatham Rise

Client

Chatham Rock Phosphate

Project

1209110-000

Reference

1209110-000-ZKS-0007

clay concentrations in the entire model domain drop below 0.1 mg/l and 1 mg/l respectively. In addition:

- Plume dispersion tends to occur in a predominantly northern to north-western direction.
- Plume spreading is largest in the Summer scenario.
- The finer clay fraction is subject to a larger dispersion than the silt fraction.
- Suspended sediment concentrations rapidly decrease with increasing height off the seabed.

The second phase (2013) used an optimized Local Delft3D Model co-located to the location where monitoring instruments were installed. The grain size distribution of the mine tailings was further adjusted. With this new Local Model the single-cycle mining operations were re-run with, for most simulations, the mine tailings material returned directly to the seabed. Multiple mining cycles were simulated with material discharged at the seabed and approximately 10 m above the bed, including resuspension from the seabed of the fine sediments originating from the mine tailings.

The objective of this phase was to determine if the predicted sedimentation patterns by the single-cycle scenario are cumulative for multiple cycles. Additionally, the multiple cycles' investigation also provides an increased understanding in the role of the natural variability on the mine tailings fate and transport. A last objective of this second phase was to provide advice on the likelihood of the incident events having an impact above and beyond the normal mining operations.

Results of the far field modelling (Phase 2) show that during active mine tailings disposal, high sediment concentrations occur along the mining track. Most of these sediments (both the clay and silt) directly deposit along the track line (as can be observed from the sedimentation footprints). Plume dispersion patterns for silt in spring and winter look similar and display dispersion in a north-western direction. In the Summer scenario the silt plume dispersion is somewhat larger. Maps of clay dispersion reveal considerable intra-seasonal variation in plume spreading that is similar to the predicted seasonal variation. Temporal and also spatial variation in plume dispersion is not surprising given the complex hydrodynamics on the Chatham rise. The multiple cycle simulations further revealed that near-bed suspended clay fraction can remain locally in suspension between mining cycles and results in a temporal build-up of concentration in the model domain. Besides the intra-seasonal variations in plume dispersion, this building-up behaviour will also affect the cumulative sedimentation footprint.

The maximum sedimentation height (excluding sand) when disposing 10 m above the bed is less than 2.5 cm, as compared to the predicted maximum local peaks reaching above 15 cm when disposing at the seabed. The sedimentation patterns when disposing 10 m above the bed are also more diffuse closer to the mining area as compared to when discharging on the seabed.

The third phase (2014) consists of an in-depth analysis and comparison of modelled and measured tidal and non-tidal flows using the results of the Oceanographic study (Deltares, 2014a). The velocity profiles measured by an ADCP and the near bed velocities measured by an Aquadopp are used in the comparison. In the mining area both tidal and non-tidal flows are important for plume advection and dispersion. Tides together with internal tides are potentially important for resuspension of sediments because of the bed shear stresses they exert. Residual currents are important for the advection of suspended sediments and the eventual location of sedimentation. The main aspects of the model performance that will influence the transport and dispersion of the sediment plume are:

- Current velocities are at times overestimated in the lower half of the water column.
- Though Delft3D is capable of modelling internal tides internal tides are not resolved in the model because of the tidal boundary conditions being uniform over depth (in the Regional model).

Title

Modelling investigations on mine tailing plume dispersion on the Chatham Rise

Client

Chatham Rock Phosphate

Project

1209110-000

Reference

1209110-000-ZKS-0007

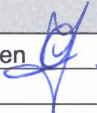
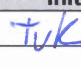
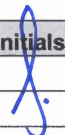
- Residual flows, though small, are overestimated by the model. However, the time averaged residual direction in the lower water column is simulated correctly, though north north-west instead of north-west.
- There are large gradients of water properties across the rise, associated with the subtropical convergence. A large temperature front across the rise, as present in HYCOM (global ocean model used to force Delft3D), is captured in the model but temperature and salinity observations are needed to investigate the strength and motion of this front across the rise and its effect on current velocities.
- The tidal signal and tidal ellipses are well reproduced by the model so these diurnal and semi-diurnal speeds and directions which influence the sediment plume on varying time-scales are correctly represented.

Both horizontal and vertical dispersion in combination with settling velocity determine the time scale over which sediment from an injected plume (re-) deposits. Dispersion is dependent on the degree of stratification therefore dispersion of the sediment plume in horizontal direction will be greater during periods of stronger stratification (but smaller in vertical direction). In periods where the profiles over depth are more uniform, for both model and measurement, the degree of horizontal dispersion simulated by the model will be closer to that in reality. This occurs in less-stratified periods.

READERS GUIDE: At the end of each chapter a blue text box provides a summary of the main outcomes of that chapter.

References

1209110-000-ZKS-0007.

Version	Date	Author	Initials	Review	Initials	Approval	Initials
1.0	Mar 2014	C. Jeuken		T. van Kessel		F. Hoozemans	

State

final

Contents

1 Introduction	1
1.1 Project Background	1
1.2 Study Location	2
1.3 Study approach and history	2
2 Model Setup	1
2.1 General	1
2.2 Regional Delft3D Model	2
2.3 Local Delft3D Models	3
2.4 Seabed sediment grain size	8
2.5 Schematisation of the mining process in the models	10
2.5.1 Proposed mining	10
2.5.2 Schematization of the mining cycle(s)	12
2.5.3 Schematization of mining tracks	12
2.5.4 Schematization of the mine tailing discharge input in Delft3D	14
2.5.5 Summary of settings used in the simulation of a single mining cycle	16
2.6 Modelling Assumptions	17
2.7 Model Simulation Overview	18
3 Model Simulations - Initial Investigation (Phase 1a and Phase 1b)	21
3.1 <i>Near field</i> plume development	21
3.1.1 Disposal at 200 m above the seabed	21
3.1.2 Disposal at and near the seabed – deposition of the sand fraction.	27
3.2 Far-field Model performance – initial assessment	28
3.2.1 Information sources	28
3.2.2 Performance	31
3.2.3 Sensitivity Tests of the Regional Model	36
3.3 <i>Far-field</i> mine tailing dispersion for 3 seasonal scenarios	38
3.3.1 Suspended sediments	38
3.3.2 Sedimentation	45
4 Model Simulations – Optimized Investigation - Suspended Sediment (Phase 2)	49
4.1 Single Cycle Simulations – Disposal at the bed	49
4.1.1 Spring	49
4.1.2 Summer	52
4.1.3 Winter	52
4.2 Single Cycle Simulation - Disposal at 10 m above the bed	58
4.3 10-Cycle Simulations	61
4.3.1 Summer	62
4.3.2 Winter	65
4.4 Discussion	65
5 Model Simulations – Optimized Investigation – Sedimentation (Phase 2)	73
5.1 Single Cycle Simulations for a spring, summer and winter scenario	73
5.2 Single cycle simulation - disposal at 10 m above the bed	77
5.3 10-Cycle Simulations	78
5.3.1 Summer	78

5.3.2	Winter	79
5.4	Discussion	80
6	Model Verification	85
6.1	Introduction	85
6.2	Time series comparisons – Model vs. ADCP and Aquadopp	87
6.3	Tidal versus non-tidal flow	91
6.3.1	Tidal Analysis	92
6.3.2	Tidal Ellipses	99
6.3.3	Reconstructed tidal time series and residual flow	101
6.3.4	Godin filtered signal	106
6.3.5	Internal tides	111
6.4	Salinity, temperature and density	114
6.5	Implications of model verification	116
7	Incident Modelling Spill plume computation	121
7.1	Jet3D input	122
7.2	Results and discussion	123
8	Conclusions	127
9	References	131

1 Introduction

1.1 Project Background

Chatham Rise hosts economically significant amounts of rock phosphate captured in nodules present on the seabed and within the top 30-40 cm of the seabed. Rock phosphate is a primary constituent of most fertilisers used in New Zealand, most of which is currently being imported from Morocco. Extraction of the Chatham Rise rock phosphate could provide a locally produced alternative and would have a number of economic, environmental and market benefits.

The New Zealand Government awarded Chatham Rock Phosphate Ltd (CRP) the prospecting license for two 2-year terms (2010-2014, see Figure 1.1). CRP has the priority rights to either extend the prospecting permit or to apply for (a) mining license(s) after meeting all required obligations, including a detailed design study and an Environmental Impact Assessment (EIA) study. In 2011, CRP exclusively selected Boskalis to undertake the detailed design of the offshore rock phosphate nodule extraction project at Chatham Rise. Golder Associates (NZ) Limited is leading the EIA study.

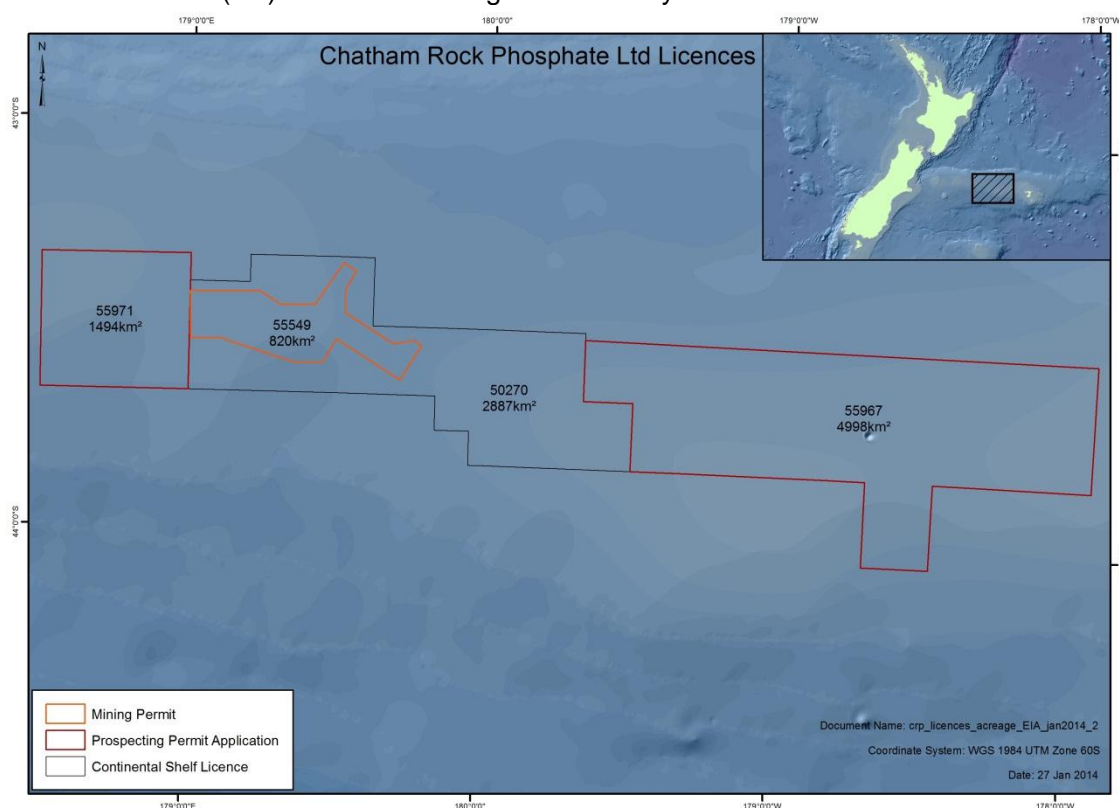


Figure 1.1 Map of CRP license area.

In the framework of the CRP Mining Project, Boskalis and CRP asked Deltares to conduct an operations study investigating the dispersion behaviour of sediments released during the mining process. The main interest is in the turbidity generated in the water column and the deposition footprint on the seabed resulting from the mining discharge.

1.2 Study Location

The study has been carried out for the first potential mining site on the Chatham Rise, located near the iX Survey mooring deployed in 2011.

The Chatham Rise is a submarine feature that is approximately 1000 km in length, extending eastward from the South Island of New Zealand (Figure 1.2). The rise has water depths that range from roughly 80 m to roughly 500 m, with the Chatham Islands near the eastern extent of the submarine feature. Just north and south of the Rise, water depths quickly approach 3000 m.

Along the top of the rise, where the mining locations sit (in roughly 400 m water depth), the flow patterns are commonly dominated by the tidal regime, cross-rise eddies and the residual flows resulting in quite complex circulation patterns. The maximum horizontal velocities are on the order of 0.5 m/s (for more details see Deltares, 2014a).

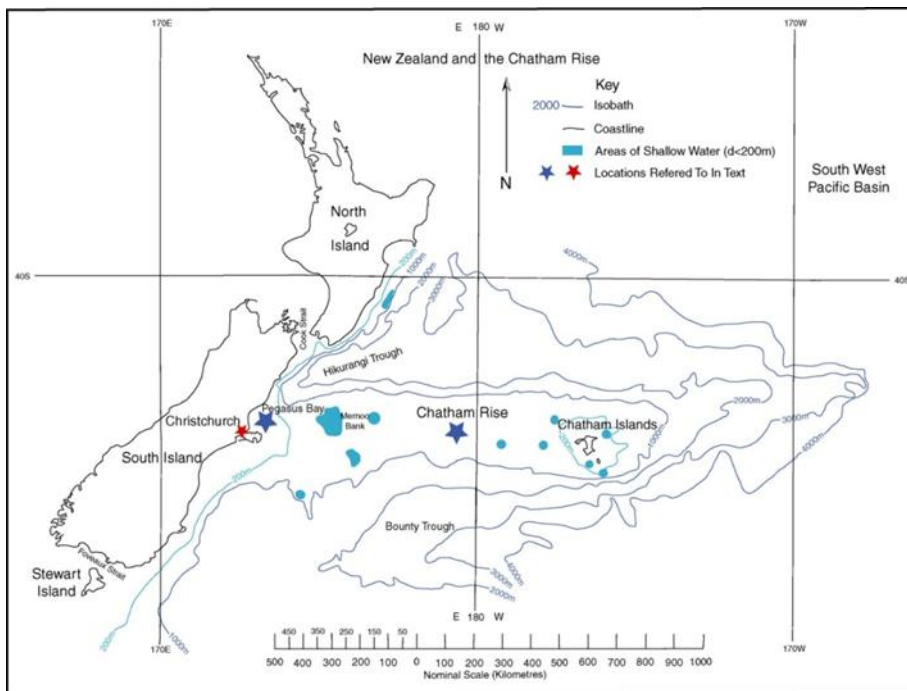


Figure 1.2 Map of New Zealand and the Chatham Rise (Wikipedia: Ngatimozart, 2010).

1.3 Study approach and history

This study uses a dedicated modelling approach to assess the far-field dispersion, and sedimentation behaviour of sediments released during the mining process (see Chapter 2 for details). The study consisted of three main phases, all of which are documented in this report:

The first phase (2012) was an initial mine tailing plume investigation composed of two sub-phases, Phases 1a and 1b (Chapters 3). Phase 1a investigated the near-field plume development and far-field plume dispersion for mine tailings release at 5 m and 200 m above the seabed. Based on these results it was decided that mine tailings should be disposed near or at the bed to minimize plume dispersion effects. Therefore the subsequent initial investigations of Phase 1b, as well as the optimized investigations of Phase 2, considered mine tailing release at the seabed and 10 m above the seabed.

During this initial investigation phase the study location, the material properties and the proposed mining design were optimized using new information and insights obtained from the survey cruises in 2011/2012 to the Chatham Rise. Additionally, an initial comparison of simulated and measured far-field flow velocities was made using moored RDI ADCP current data. Finally, model sensitivities for key physical factors were tested.

The second phase of the operations study (2013) used an optimized Local Delft3D Model. The model is referred to as optimized as it was enlarged and co-located to the iX Survey mooring location (Chapters 4 and 5). Otherwise the set up and parameter settings remain the same as previously described. The grain size distribution of the mine tailings has been further adjusted. With this new Local Model the single-cycle mining operations were re-run with, for most simulations, the mine tailings material returned directly to the seabed. Multiple mining cycles were simulated with material discharged at the seabed and approximately 10 m above the seabed, including resuspension of the fine sediments in the mine tailings. The objective of this study was to determine if the predicted sedimentation patterns by the single-cycle scenario are cumulative for multiple cycles (Chapters 4 and 5). Additionally, the multiple cycles' investigation also provides an increased understanding in the role of the natural variability on the mine tailings fate and transport. A last objective of this second phase of the mine tailing dispersion study was to provide advice on the likelihood of the incident events having an impact above and beyond the normal mining operations (Chapter 7).

During the second phase of the study two other related studies were executed in parallel: These were: an oceanographic study (Deltares, 2014a) and a resuspension study (Deltares, 2014b). The former investigated the tidal and non-tidal flow processes using the RDI ADCP data. Additionally it investigated the representativeness of the ADCP measurement period and modelling scenario's using HYCOM data. The resuspension study investigated the parameters affecting resuspension of mine tailings and the effect of mining and disposal on the local sediment characteristics.

The third phase consists of an in depth analysis and comparison of modelled and measured tidal and non-tidal flows (Chapter 6), using the results of the oceanographic study (Deltares, 2014a).

2 Model Setup

2.1 General

Numerically assessing the far-field plume dispersion and sedimentation of the mine tailings released during the mining process requires a dedicated modelling approach that accounts for:

- Large-scale oceanic flows over the Chatham Rise, including seasonal variations thereof.
- Sufficient model resolution in time and space (x,y,z,t) on top of the Rise enabling:
 - a proper simulation of the far-field sediment mine tailing plume dispersion and;
 - a proper schematisation of the mining track and cycle and;
 - associated mine tailings release characteristics.
- An appropriate characterization and schematisation of the mine tailings (i.e. grain size distribution and sediment characteristics).
- An appropriate schematisation of the mine tailings disposal during the mining process.

To achieve these requirements, Delft3D simulations were set-up using a Regional model (section 2.2) and higher resolution Local Models (section 2.3). The Regional Model, including the large-scale oceanic flow effects and seasonal variations, provides boundary conditions for the (nested) Local Models. The latter were set-up to model the far-field plume dispersion and the mining process using schematized characteristics of the seabed sediments obtained during the 2012 survey cruises (section 2.4). The schematization and simulation of the mining track and cycle (section 2.5) was done using the Local Delft3D Models and Jet3D. Jet3D computes the near-field plume and was used to provide input to the Local Delft3D model in the case when sediment was released at 200 m above the seabed.

The coordinates of the Delft3D models are with respect to UTM zone 60S. The model bathymetries were derived from the new multi-beam data obtained within the marine mining license areas and older single beam data, both provided by Boskalis, and the GEBCO 08 data, in order of importance. Section 2.6 summarizes the assumptions made and used in the modelling undertaken in this study. Finally section 2.7 provides an overview of executed simulations during all three phases of the study

Delft3D has been used to model complex hydrodynamics environments worldwide for many different applications in stratified and non-stratified conditions (Lesser *et al.*, 2004). Delft3D has been tested and validated for many of the processes relevant for plume dispersion, such as turbulent mixing, vertical shear dispersion etc. Delft3D-FLOW solves the Navier-Stokes equations for an incompressible fluid and usually the grid (horizontal and/or vertical) is too coarse and the time step too large to resolve the turbulent scales of motion. Therefore turbulence models are used (Uittenbogaard *et al.*, 1992).

Delft3D has also been used and validated in several sediment plume dispersion studies, mostly in shallower coastal waters (e.g. Cronin *et al.*, 2011; van Kessel and van Maren, 2013). In general, little is known about the performance of models to predict plume dispersion in deep water due to a lack of observations. This also applies for the Chatham Rise (NIWA, 2011). Additionally, development of new marine infrastructure projects often requires compliance monitoring, which could also provide a basis for validation of plume dispersion models.

2.2 Regional Delft3D Model

The Regional Delft3D Model was set-up to include and transfer large-scale oceanic flows into the higher resolution local models on the Chatham Rise. To achieve this, the model extends 260 km across the Chatham Rise covering the steep parts of the north and south slopes and 160 km in along-rise region (Figure 2.1).

The water depths in this model domain range from 3000 m on the north-side of the domain, to roughly 400 m along the top of the rise, and back down to 1500 m on the south-side of the domain. The Regional Delft3D Model is composed of 40 Z-layers (which are vertical layers constant in height common for ocean-scale modelling).

The marine mining license areas are roughly centred in this Regional domain.

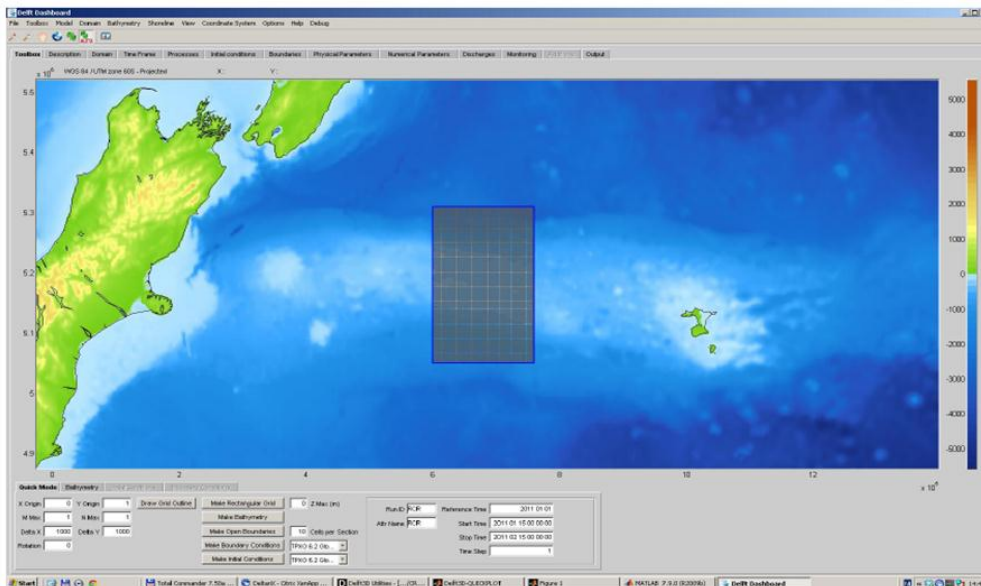


Figure 2.1 Regional Delft3D domain within Delft Dashboard.

In order to include the large-scale, oceanic circulation effects in the Regional Model, time series boundary conditions are generated using the HYCOM Global Ocean Model (HYCOM GLBa0.08, experiment 90.9 with 1/12° equatorial resolution) predictions of:

- U-velocity,
- V-velocity,
- Water level,
- Salinity, and
- Water temperature.

HYCOM (HYCOM.org) is developed by a consortium that is a multi-institutional effort sponsored by the National Ocean Partnership Program (NOPP), as part of the U. S. Global Ocean Data Assimilation Experiment (GODAE), to develop and evaluate a data-assimilative hybrid isopycnal-sigma-pressure (generalized) coordinate ocean model (called HYbrid Coordinate Ocean Model or HYCOM). HYCOM is a 3D global ocean model which is run operationally. The daily snapshots of the HYCOM output are freely available via an OpenDAP server (HYCOM Data Server).

The HYCOM model does not include tidal forcing, therefore, the Oregon State University (OSU) TOPEX/Poseidon global inverse solution TPXO ([\(TOPEX/Poseidon website\)](#)) was utilized to provide tidal forcing in addition to the HYCOM forcing. TPXO7.2 is a current version of a global model of ocean tides, which best-fits, in a least-squares sense, the Laplace Tidal Equations and along track averaged data from TOPEX/Poseidon and Jason (on TOPEX/POSEIDON tracks since 2002) obtained with OTIS. The tides are provided as complex amplitudes of earth-relative sea-surface elevation for eight primary (M2, S2, N2, K2, K1, O1, P1, Q1), two long period (Mf, Mm) and 3 non-linear (M4, MS4, MN4) harmonic constituents, on a 1440x721, 1/4 degree resolution full global grid (for versions 6 and later). The Delft3D Regional Model has a 2 km resolution and employs a 1-minute time step. Simulations run for the three phases of the study cover the entire period 15 January 2011 – 13 November 2011. Each phase of the study focussed on specific objectives and required specific simulation periods using the regional and objective-dedicated local models. For a tabular overview and explanation see section 2.7.

2.3 Local Delft3D Models

Higher resolution Local Delft3D Models were set-up to model the far-field sediment plume dispersion and sedimentation footprint.

Grid schematization for any numerical model is a trade-off between computational time and resolution of processes modelled. Grid resolution and time step should be sufficient to capture the phenomena of interest, but still allow efficient and accurate computations over the desired area. Only phenomena or features larger than (several) grid cells can be resolved by the model formulations.

Three Local Model domains were subsequently set-up and utilized in the operations study:

- Southern Local Model (Figure 2.2 and 2.4).
- Northern Local Model (Figure 2.2 and 2.5).
- Optimized Local Model which is co-located with the 2011 iX Survey ADCP mooring location (Figure 2.3 and 2.6).

Table 2.1 summarizes the main characteristics of the three models as well as some principal model settings. For comparison purposes, it summarizes the characteristics of the Regional model as well.

In contrast to the Regional Model, the vertical dimensions for the Local Models is resolved using sigma layers, vertical model layers that have a constant percentage of the water depth, i.e. the absolute height of the layers change with fluctuations in the total water depth. Sigma layers are more commonly used for coastal modelling and when modelling sediment transport, as these provide a smooth boundary near the bed. For all three local models the mining area in the model has the highest horizontal grid resolution. The grid resolution gradually coarsens towards the boundaries. This allows a large spatial domain without adding too much computational time.

Prior to the execution of Phase 1b an initial set of North and South Models was set-up and utilized in Phase 1a. These models, more widely spaced apart, were set-up for a different design of the mining operation. For a description and model results, see Appendix V2 (Section B).

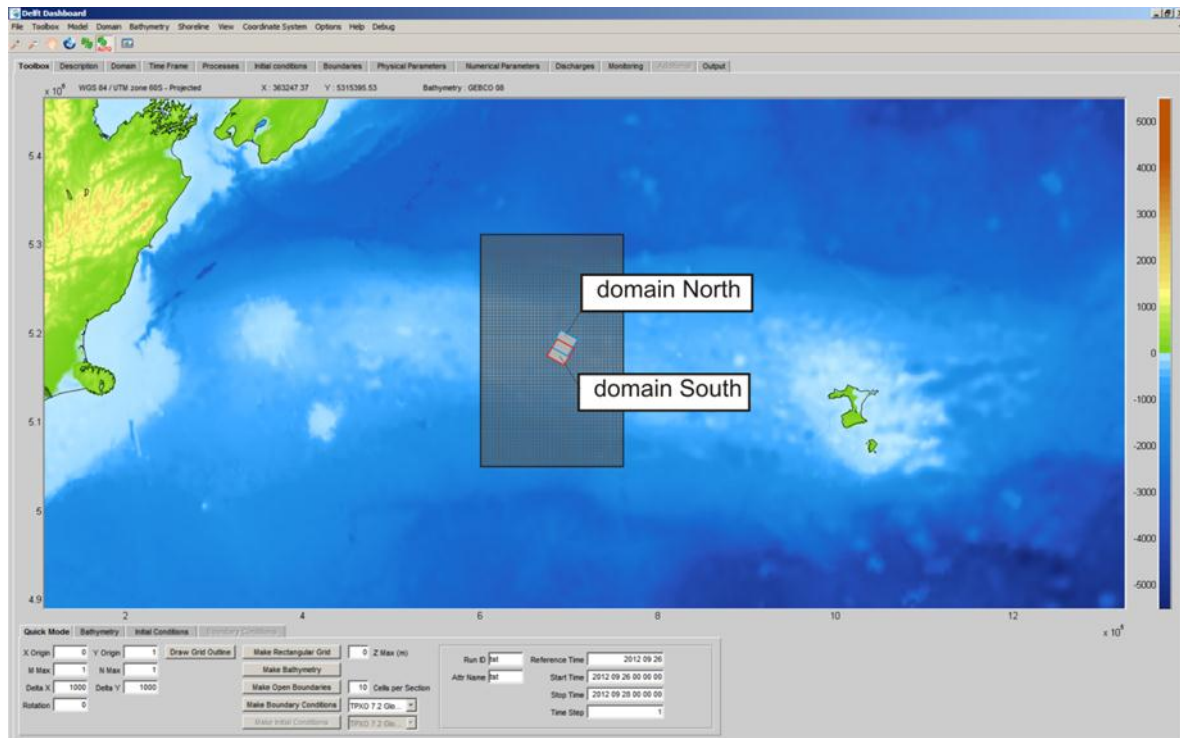


Figure 2.2 Regional Delft3D domain within Delft Dashboard with Local North and South domains (Phase 1b).

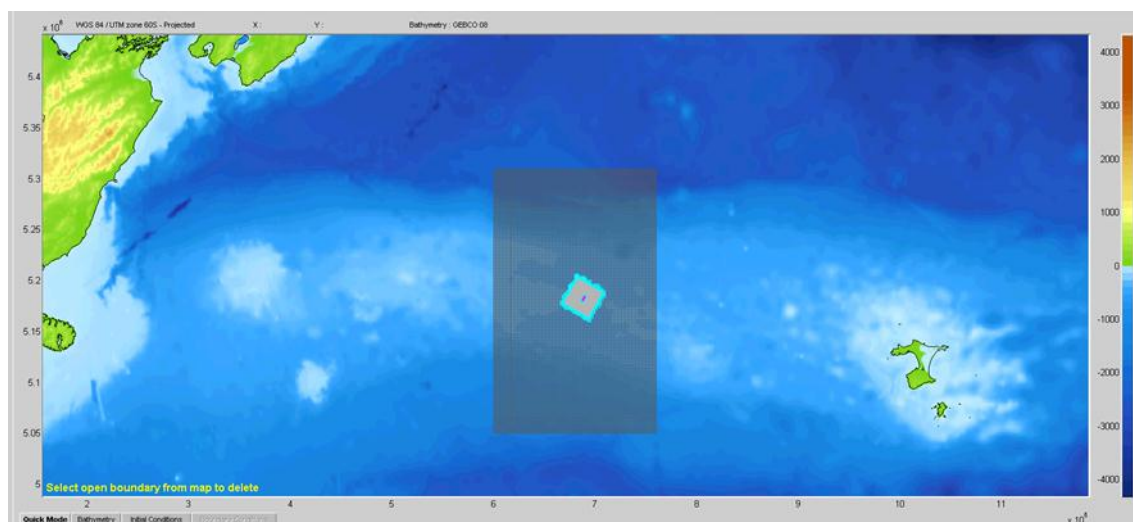


Figure 2.3 Regional Delft3D domain within Delft Dashboard with the Optimized Local domain (Phase 2). Note, the spatial extent of this model domain includes the entire area (and more) covered by the Phase 1b models and is centred on the iX mooring location.

Table 2.1 Overview of model schematization characteristics.

Characteristic	Regional Model	Northern & Southern Local Model	Optimized Local Model covering ADCP-mooring site
Water depths	400-3000 m	375-425 m	
Vertical layers	Z-layers	Sigma layers	Sigma layers
Number of vertical grid cells.	40 At boundaries of local models:	25	30
Distribution of vertical grid resolution	Layer thicknesses in m from bed to surface are: 430.35, 368.77, 316.07, 270.87, 232.17, 198.96, 170.53, 146.13, 125.25, 107.34, 92.01, 78.85, 67.58, 57.91, 49.64, 42.55, 36.45, 31.25, 26.77, 22.96, 19.68, 16.86, 14.45, 12.38, 10.61, 9.11, 7.78, 6.67, 5.74, 4.90, 4.21, 3.61, 3.10, 2.64, 2.28, 1.95, 1.65, 1.65, 1.65, 1.65. The total thickness is 3005 m and ranges from -3000 m MSL to +5 m MSL.	Logarithmic: layer thicknesses in % are: 28.189, 20.244, 14.539, 10.442, 7.5000, 5.3860, 3.8680, 2.7780, 1.9950, 1.4330, 1.0290, 0.7390, 0.5310, 0.3810, 0.2740, 0.1970, 0.1410, 0.1010, 0.0730, 0.0520, 0.0380, 0.0270, 0.0190, 0.0140, and 0.0100.	The-Layer-Thicknesses in % from surface to bed are: 0.25, 0.351, 0.492, 0.69, 0.969, 1.359, 1.907, 2.675, 3.753, 5.265, 7.387, 10.363, 14.539, 14.569, 10.337, 7.333, 5.203, 3.691, 2.619, 1.858, 1.318, 0.935, 0.663, 0.471, 0.334, 0.237, 0.168, 0.119, 0.085, 0.06 %.
Thickness of near-bed layer (m)	40-50	± 0.04	± 0.23
Spatial extent	260 x 160 km	20 x 20 km	30 x 30 km
Max. horizontal grid resolution	2000 x 2000 m	30 x 30 m	75 x 75m
Nr of grid cells (in u,v plane)	10611	30504	22059
Run time indication (days) on single node, 32-bit PC	1 day for 30 days simulation	5 days for 10 days simulations	1 day for 10 days simulations
Bed roughness	Manning, $n=0.02$	Manning, $n=0.02$	Manning, $n=0.02$
Turbulence model	k- ϵ	k- ϵ	k- ϵ
Sediment fall velocity	no sediments included	Clay: $2.7 \cdot 10^{-6}$ m/s Silt: $2.5 \cdot 10^{-4}$ m/s	Clay: $2.7 \cdot 10^{-6}$ m/s Silt: $2.5 \cdot 10^{-4}$ m/s
Shear stress for erosion $\tau_{crit,e}$	no sediments included	0.5 Pa	0.5 Pa
Erosion parameter M	no sediments included	$1 \cdot 10^{-4}$	$1 \cdot 10^{-4}$

The North Model and South Model were utilized to perform initial investigations on plume dispersion, including sensitivity testing during the first phase of the mine tailing dispersion study. The model results and initial insights in model performance and sensitivities (Chapter 3) were used to optimize the grid schematization and resolution of the model during the 2nd phase of the operations study, besides co-locating the model with the iX Survey mooring. The results of phase 1 indicated that the model domain needed to be increased (1.5 times) to ensure that the fine suspended sediment concentrations above 5 mg/l remain within the model domain for the single mining cycles. Additionally, the horizontal grid resolution of the Optimized Local Model is coarser than that of the previous Local Delft3D Models by 2.5 times in the mine tailings disposal area. This acceptable loss in horizontal grid resolution contributes greatly to improving the computational efficiency of this physically larger Local model. Similar to the previous Local Model, the Optimized Local Model grid resolution smoothly coarsens towards the boundaries, increasing to approximately 300 m. Again, this allows a large spatial domain without adding too much computational time. In general, the grid adaptations of the Optimized Local Model resulted in:

- A 30 x 30 km domain which for the single-cycle seasonal runs suspended sediment concentrations above 5 mg/l remain within the model boundaries
- A Local domain with the mine tailings discharge tracks co-located with the 2011 iX Survey mooring location and the proposed initial mining region
- Maximum vertical resolution at the bed of 23 cm.
- Maximum horizontal resolution of 75 m x 75 m at the mine tailings discharge location, which still sufficiently resolves the bed features in the discharge region
- Increased vertical resolution in the upper part of the water column compared to the Northern and Southern Local Models.
- Increased computational efficiency by at least four-fold compared to the Northern and Southern Local Models.

These grid adaptations resulted in a more flexible Local Delft3D Model better apt for future applications.

Model bathymetries for the three Local Models are composed from the old single beam data and new multi-beam data (first priority data) within the marine mining license areas, both provided by Boskalis. Areas not covered by these data (far field corners) were filled in using GEBCO 08 data. All transitions between data sources were smoothed to optimally fit the surrounding data points.

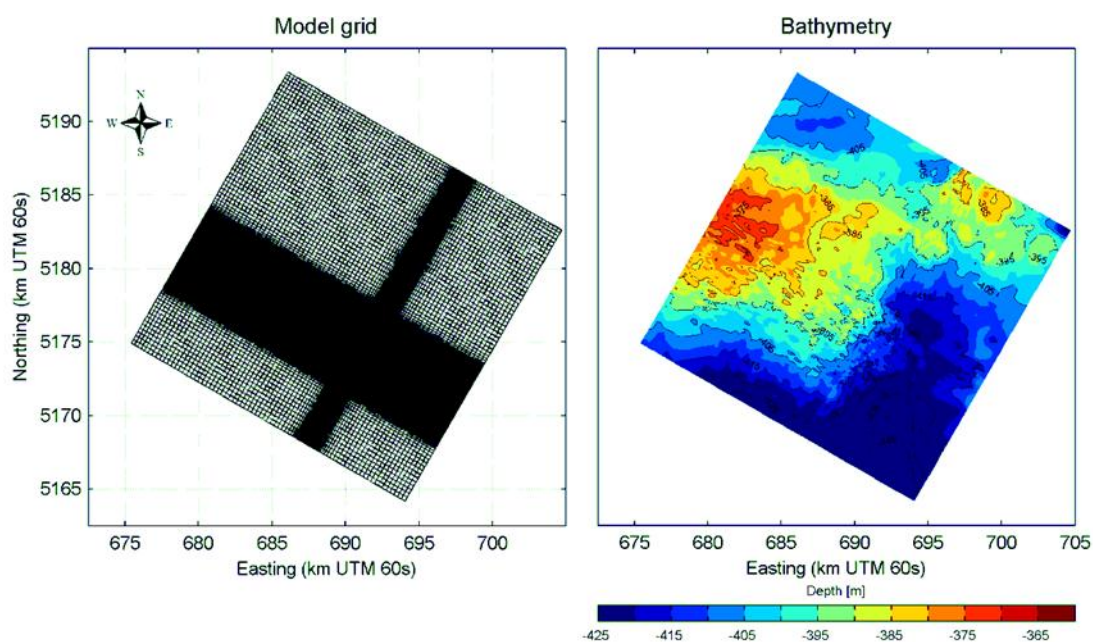


Figure 2.4 Model grid and schematization for the Local Delft3D southern domain.

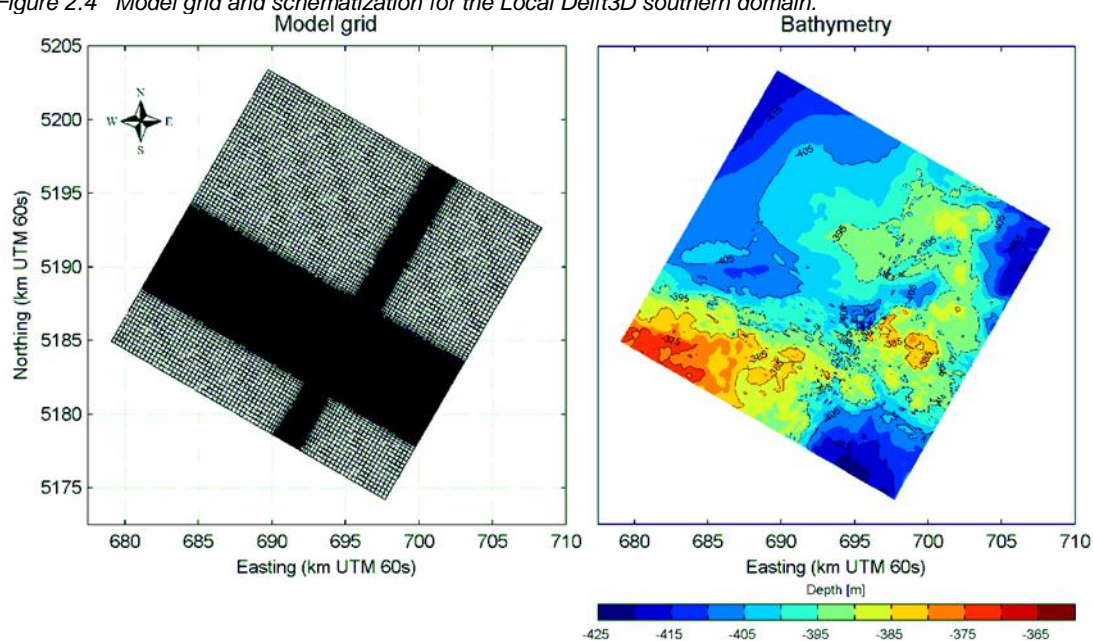


Figure 2.5 Model grid and bathymetry for the Local Delft3D northern domain.

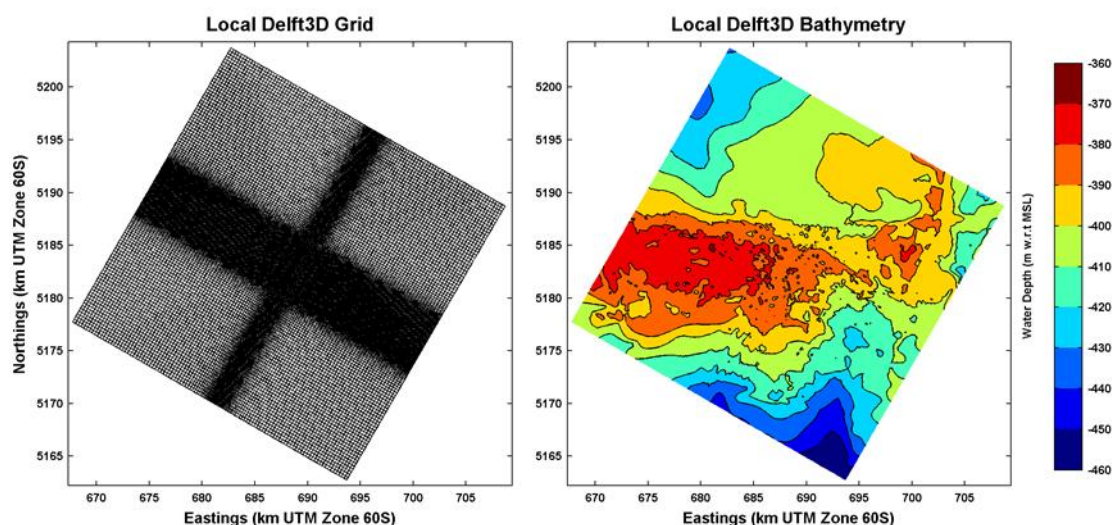


Figure 2.6 Model grid and bathymetry for the Optimized Local Delft3D domain (please note the different colour bar compared to Figure 2.4 and Figure 2.5).

2.4 Seabed sediment grain size

The grain size distribution of the seabed sediments is based on analyses of bed samples obtained during the 2012 investigation cruises. Over the course of the different phases, the grab and core samples have been analysed to further improve the sediment characteristics understanding, thus the grain size distribution has also been updated between the various modelling phases. Phase 1 of the study investigated two different grains size settings (Table 2.2, Figure 2.7 and Figure 2.8), with differences in the percentage of fines (largest in Phase 1b). The Phase 2 study uses a higher percentage of silt compared to clay; however, the sand fraction assumed to deposit instantly remains roughly the same as in Phase 1b.

Table 2.2 Comparison of grain size distribution settings used during the different phases of the operations study.

Characterization of grain sizes	Phase 1 - a	Phase 1 - b	Phase 2
% between 100 μm and 1000 μm	55	43	46
% between 60 μm and 100 μm	10	14	10
% between 20 μm and 60 μm	12	13	20
% between 4 μm and 20 μm	8	12	16
% smaller than 4 μm	15	18	8
Specific gravity (ton/m ³)	2.70	2.70	2.70

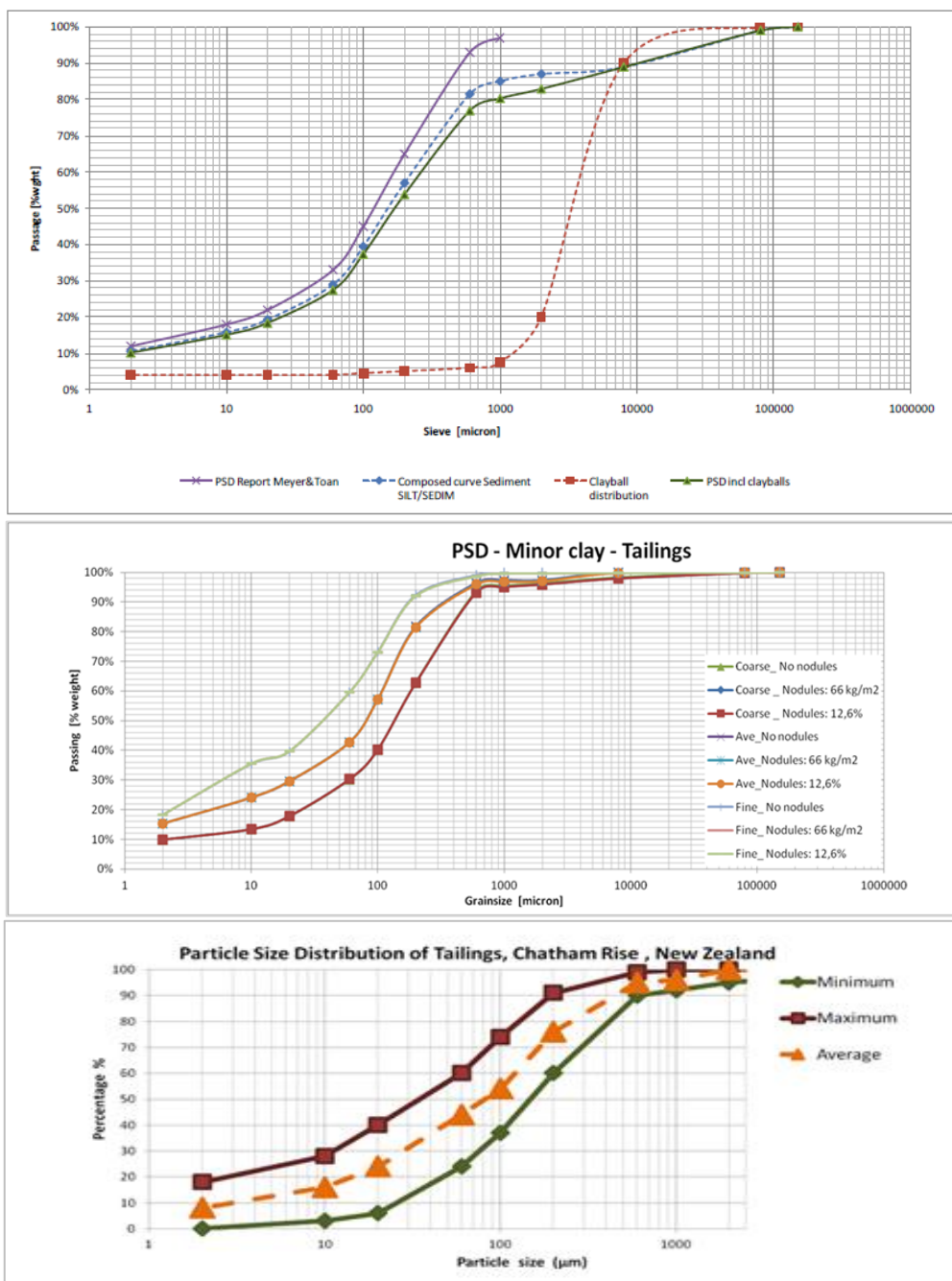


Figure 2.7 Grain size distribution (as provided by Boskalis) for Phase 1a (top), Phase 1b (middle) and Phase 2 (bottom). For Phase 1a, Purple curve utilized as assumed grain distribution in study area. Orange (middle) curves utilized as assumed grain distribution in study area (Phases 1b and 2, see Table 2.2).

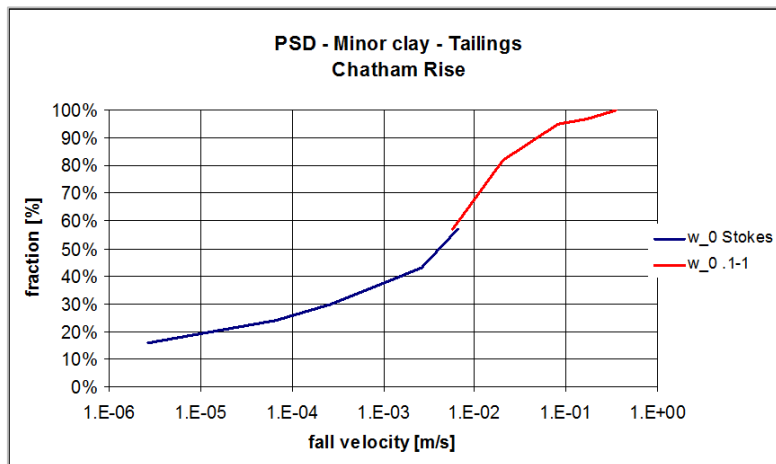


Figure 2.8 Computed fall velocity distribution (bottom) based on particle size distribution (blue = Stoke's Law for fines, red = intermediate expression for sand > 0.1 mm).

Herein, clay is defined as the fraction below <4 μm , silt <63 μm and sand > 63 μm . The very fine sediments (clays < 2 μm) will probably have a larger fall velocity in reality due to flocculation. However, the effect of flocculation is not modelled in the current study because not enough information is available on the sediment properties to accurately represent this complex process. Flocculation and aggregation depend on the concentration of fines, residence time, hydrodynamic conditions and mineralogical composition. In addition, sand is assumed to deposit immediately and so is not modelled.

Instead, a sensitivity analysis has been made to investigate the effect of fall velocity of the fines on plume dispersion (Appendix V2-B). The Stoke's fall velocity of 2 μm particles (0.0027 mm/s) is taken as an absolute lower limit for the clay fraction, but also simulations with about a 10- and 100-fold increased fall velocity (0.025 and 0.25 mm/s) were made (see Appendix V2-B). Typical values for observed particle fall velocities in oceans are in the range of 0.1 mm/s or above.

2.5 Schematisation of the mining process in the models

2.5.1 Proposed mining

Figure 2.9 schematically visualizes the mining track, including the central strip where no mining will occur. The central part, referred as the residual strip, is an area where no mining is planned to leave the seabed relatively undisturbed.

The mining tracks are 5 km long with an assumed orientation of 30 – 210 degrees. Each subsequent track ring is spaced 5 m out from the previous track. In total, 24 rounds are made per mining cycle and the tracks are sailed with a vessel speed in the order of 0.75 m/s. Each track line, therefore, takes 1.85 hours. In total, each mining run consists of 24 rounds amounting to a total mining time of approximately 102 hours (see Table 2.3). Between each mining cycle, there is a waiting period of at least 5 days when no mining takes place.

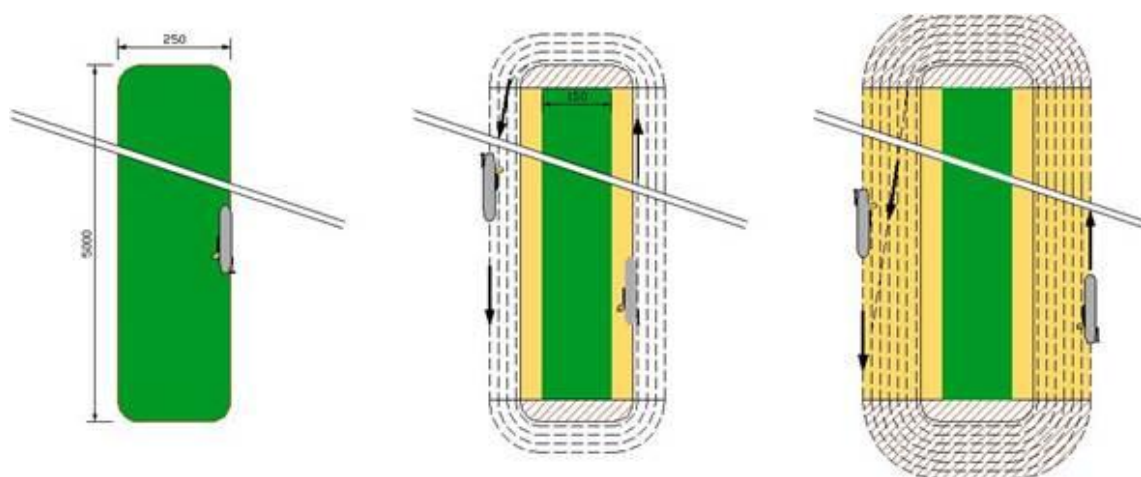


Figure 2.9 Dredge track as provided by Boskalis .The green areas have not been mined and the yellow areas have been mined

Different production characteristics were investigated in the phases of the operation study (see Table 2.3). Table 2.3 summarizes the principal model settings in simulating a mining cycle.

Table 2.3 Production characteristics used in the various phases of the study.

	Phase 1a	Phase 1b and 2
Mixture outflow (m ³ /s)	2.48 (0.44 m ³ /s solids and 2.04 m ³ /s water)	2.15 (0.31 m ³ /s solids and 1.84 m ³ /s water)
Mixture density (kg/m ³)	1325	1265
Sediment release rate (kg/s)	1195	827
Release height (m above bed)	200 m, 5 m	0 m i.e. at the bed and 10 m above the bed
Release velocity (m/s)	1.0 ±0.25	0.75 (equal to sailing speed)
No production time between tracks (hours)	0	0.28
Progressive outward shift of tracks after each round (in m).	3-5	3-5

Simulation of this mining cycle in the Local Delft3D Model(s) requires schematization of the following aspects:

- 1 The mining cycle
- 2 The mining tracks
- 3 Sediment release associated with mine tailing disposal

The paragraphs below explain these aspects of implementation in the model in more detail.

2.5.2 Schematization of the mining cycle(s)

A *single* mining cycle is simulated as a roughly 10-day period, including:

- A two-day spin-up period; (the model spin-up is typically completed in less than one day)
- A mining and disposal period
- A break between before a subsequent mining and disposal cycle begins, while the vessel transits to shore to offload and return to the mine site.

Different durations for disposal time and after-disposal for a single mining cycle were assessed in Phase 1b and Phase 2 (Table 2.4)

Table 2.4 Schematization of a single mining cycle, applied in this study.

Aspect	Phase 1 a	Phase 1(b) using North, South Local Models	Phase 2 using optimized co-located model
<i>Schematization of mining cycle</i>			
Spin-up (days)	2	2	2
Disposal time (hours)	72	70	102
Break after dredge disposal (days)	5	5	4.75

2.5.3 Schematization of mining tracks

Single cycles

Figure 2.10 illustrates the Delft3D interpretation of the proposed mining (Figure 2.9). The mining track and outflow are schematized by a series of disposal points and a time-series of outflow rates that mimics the above described characteristics. To account for the 30° orientation, the standard north-south model grid was rotated in the direction of the mining track. The 5 m jumps between following lines cannot be represented with the resolution of the Local Models (30 m and 75 m). Therefore the 5 m jumps between following track lines results in an approximately 120 m-wide mining track for one cycle consisting of e.g. 24 rounds (phase 2 cycle settings, Table 2.3). For simplification purposes, the sediment is disposed along only two track lines to represent the SW-NE-oriented disposal lengths. These two track lengths are located roughly 250 m apart, thus three grid cells apart. Each of the 24 rounds are run over these two track lengths resulting in a total disposal of approximately 1.2 million m³ of fine sediment into the Local Model domain (over a period of 102 hours) per single-cycle simulation.

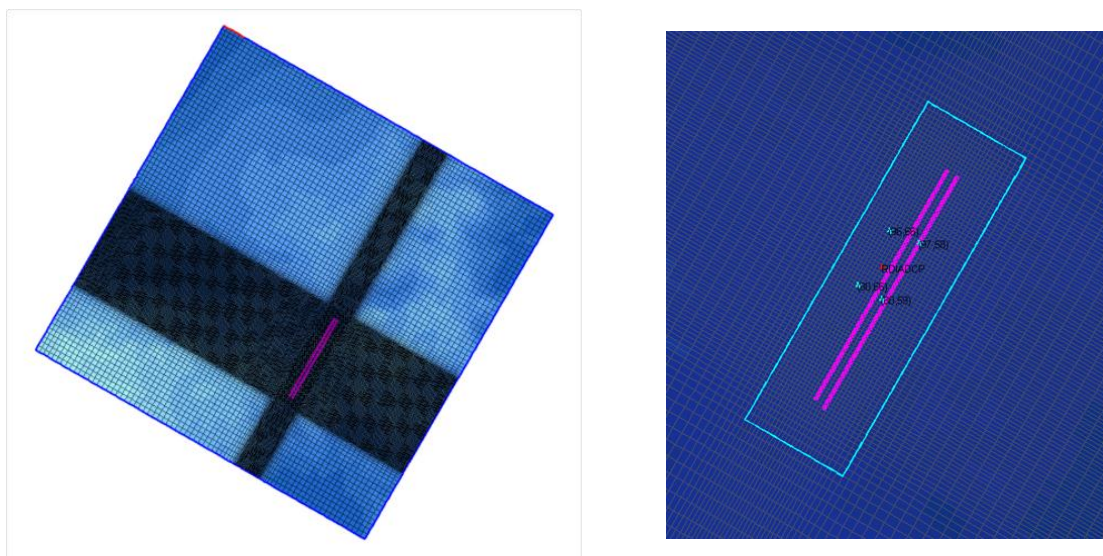


Figure 2.10 Implemented of track tracks in the model schematizations (cf. Figure 2.9).

Multiple cycles

For the multiple cycle simulation, the track lines are progressively moved apart by two grid cells (one grid cell outwardly for each track line) per mining cycle to represent the increasing distance between tracks over time. The time to transition between tracks of 0.28 hours is maintained with this increasing distance between tracks, thus the overall discharge time and model scenario period remain the same.

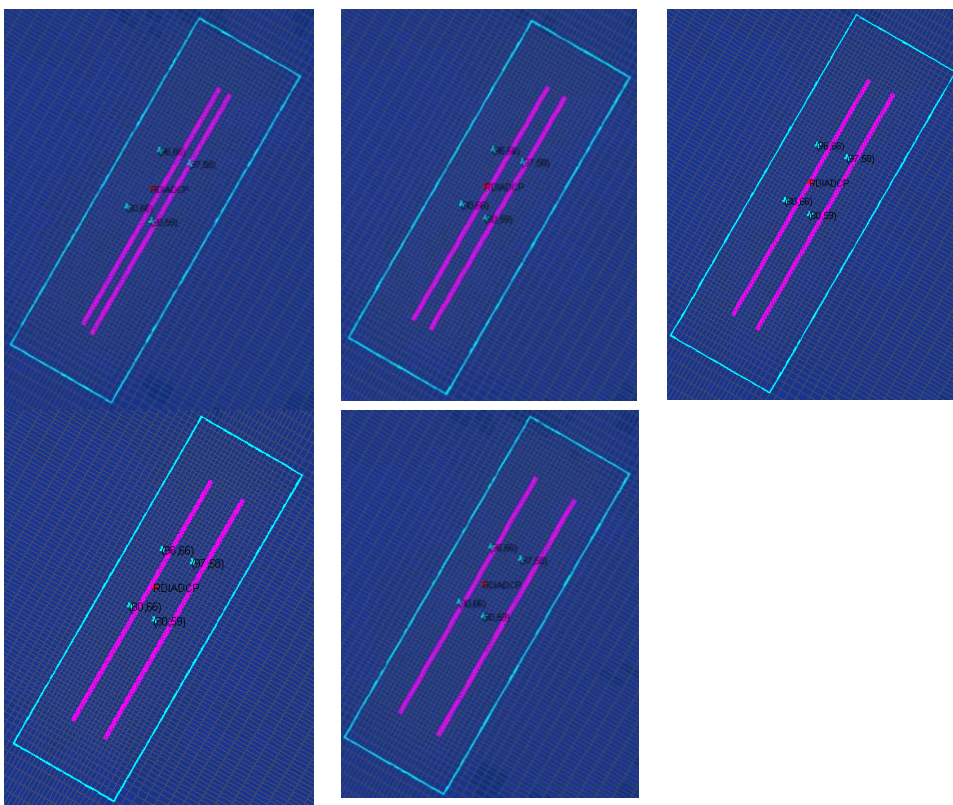


Figure 2.11 Example for implementing multiple cycles, (see Chapter 4 and 5 for results). Mining tracks for Cycle 1 (upper left), Cycle 2 (upper middle), Cycle 3 (upper right), Cycle 4 (lower left), and Cycle 5 (lower middle).

2.5.4 Schematization of the mine tailing discharge input in Delft3D

The mine tailing release is included in the model by translating the mine tailing discharge information into a discharge file suitable as input for the Local Delft3D Models.

The files were divided according to the possible depths at which mine tailings would be discharged (see also Table 2.5):

- Sediment disposal at mid-water column (approximately 200 m above the sea bed);
- Sediment disposal near the seabed
- Sediment disposal at the seabed.

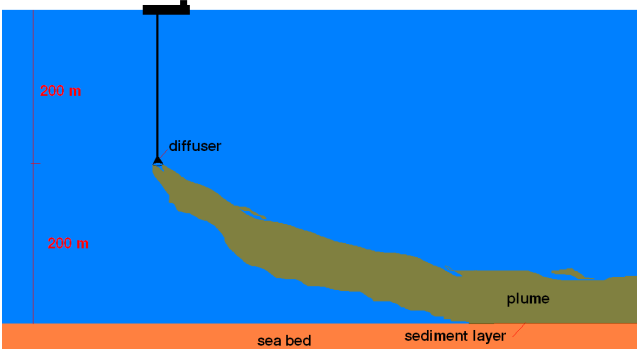
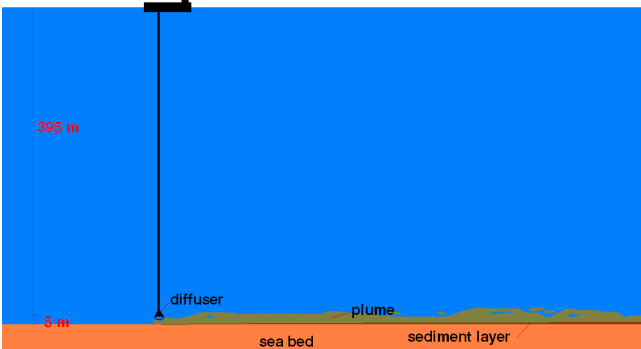
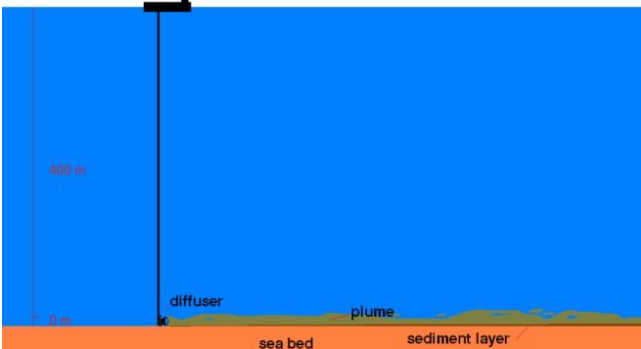
In the first phases (phase 1a and 1b) several discharge options were considered. Mine tailings release was made at three heights above the bed: mid-water column (approximately 200 m above the seabed), at 5m above the bed, and lastly at 10 m above the seabed. The calculations with sediment release at mid-water depth were made using Jet3D and Delft3D. Based on these tests, suitable settings were chosen to provide input for the Delft3D Model at the end of the near-field simulation (see section 4.1, for more information). During the remaining phases of the study only sediment release near (10 m) or at the seabed was considered.

During the testing of the different scenarios using the near-field model Jet3D, it was determined that utilizing the end of the near-field plume dispersal predictions, can be applied successfully at a larger water depth (e.g. mid-water column) where there is enough distance between the discharge depth and the seabed enabling the plume to become fully developed. However, when releasing the mine tailings close to the seabed this is not possible since a fully developed sediment plume, as computed with Jet3D, will not establish due to depth limitations. Close to the bed, sediment leaves the outfall pipe as undiluted slurry, in a free-fall, and hits the bed without any significant change. As the still undiluted slurry hits the seabed, it spreads out (under supercritical flow condition) and forms a highly concentrated sediment suspension layer on the bed (Table 2.4, middle panel)

Delft3D run with hydrostatic assumptions, as is employed in this study, is not fit for computing momentum-driven flows due to discharges; therefore, it is not apt for modelling the suspended sediment concentrations in the region of momentum-driven flow (at the discharge location). However, Delft3D is well-suited for modelling the suspended sediment concentrations and sedimentation in the far-field, thus outside of the momentum driven flow region. In Delft3D, it is most important to ensure the sediment mass flux discharged into the model domain is correct, while trying to represent the suspended sediment concentrations near the discharge location as well as possible in balance with achieving a reasonable computational efficiency. In order to resolve the sediment discharge into the model accurately a small vertical grid size for the bottom bins, such as 23 cm and 32 cm, was applied.

Thus, in this study, the mine tailings are discharged into the model through one vertical grid cell, and whereas the discharge concentration at the discharge location is not representative as the discharge is diluted within the model grid cell, the actual amount of discharge being released is conserved. From an operational point the discharge is spatially varying but temporarily constant as much as possible (assuming constant ship speed and production rate). This is an acceptable approach when investigating the large-scale spreading and sedimentation footprint of the mine tailings. It is important to note that the sediment concentrations in the near-field (within the momentum-driven flow) region as predicted by Delft3D should not be taken into consideration, i.e. the first few hundred metres from the discharge location

Table 2.4 Models and methods of computing the sediment discharge.

Location of Sediment discharge	Model Implementation:
<p><u>Mid-depth disposal (Phase 1)</u></p> 	<p>Jet3D is used to compute the sediment plume;</p> <p>Schematized Jet3D results are used as boundary conditions for Delft3D. Delft3D computes the far field effects.</p>
<p><u>5m above the bed disposal (Phase1):</u></p> 	<p>Jet3D does not compute a fully-developed sediment plume due to the close distance to the bed.</p> <p>The sediment mixture leaves the pipe as a slightly diluted plume and falls to the seabed, creating a suspended sediment layer on the bed. The sediment concentration of the diluted plume needs to be estimated and incorporated into the Delft3D Model. Delft3D cannot compute this process.</p> <p>Delft3D can be used to compute far field effects once an estimate of the diluted plume is made.</p>
<p><u>On bed disposal (Phase 2)</u></p> 	<p>Sediments are deposited directly on the bed as undiluted slurry. No plume of sand material develops (in combination with diffuser and sailing method). Delft3D can compute this process, but needs a fine grid schematization to get reasonable assumptions for the inflow sediment concentration.</p>

2.5.5 Summary of settings used in the simulation of a single mining cycle

Table 2.5 Schematisation and simulation of a single mining cycle.

Aspect	Phase 1(b) using North, South Local Models	Phase 2 using the optimized co-located model
<i>Schematization of mining cycle</i>		
Spin-up (days)	2	2
Disposal time (hours)	70	102
Break after dredge disposal (days)	5	4.75
Conditions	during spring summer and winter 2011	
<i>Production characteristics</i>		
Mixture outflow (m ³ /s)	2.15 (0.31 m ³ /s solids and 1.84 m ³ /s water)	2.15 (0.31 m ³ /s solids and 1.84 m ³ /s water)
Mixture density (kg/m ³)	1265	1265
Sediment release rate (kg/s)	827	827
Release velocity (m/s)	0.75 (equalling sailing speed)	0.75 (equalling sailing speed)
Release height (m above bed)	0 m i.e. at the seabed	0 m and also 10 m (for 10-cycle simulations)
<i>Schematization of mining tracks</i>		
Location of mining tracks centre.	Location south: X= 43 33.5200 Y= 179 22.0100 (Boskalis reference: Box 3, BOS 18) Location North: X= 43 28.0500 Y= 179 24.5000 (Boskalis reference: Box 7, BOS 24)	iX Survey location: X = 688825m, Y = 5182856m. with respect to UTM Zone 60s
24 track, 5 m displaced	2 tracks	2 tracks for single cycle, 10 tracks and 20 tracks for 10 cycles
Model time step (minutes), to ensure accuracy of the flow and sediment solver.	0.125	0.5
<i>Schematization of sediment release</i>		
Height of sediment release	<ul style="list-style-type: none"> Mid-water (using Jet3D) near-bed (5 m and 10 m above bed) At bed 	<ul style="list-style-type: none"> At bed 10 m above bed
Boundary condition mid-water sediment release	Mass flux (mass conserving)	Not applicable
Boundary condition near and at bed	Mass flux (mass conserving) in one vertical grid cell along mining track	Mass flux (mass conserving) in one vertical grid cell along mining track

2.6 Modelling Assumptions

Given the available information on sediment characteristics (which were partly investigated in Deltares 2014b), the following conservative assumptions were applied in this study which were partly investigated in Deltares, (2014b):

- 1 No flocculation effects are included, resulting in a lower settling velocity for clay particles (a sensitivity analysis was performed to assess the effect of using a fall velocity (w_s) equal to 0.0027, 0.025 versus 0.25 mm/s) which indicated the predictions were not sensitive to such a range in fall velocities (Appendix V2-B4);
- 2 No burial of fine sediments or armouring by coarser sediments when plume settles on the bed;
- 3 Full segregation of sand and fine sediments (silts and clay fractions);
- 4 Sand fraction immediately settles upon disposal, hence no sand fraction is modelled

Additionally, a few non-conservative assumptions were made in the Delft3D modelling:

- No resuspension or movement of the sand fraction due to bed shear stresses is taken into account. This assumption is supported by the Resuspension Study (Deltares 2014b); In addition, the turbidity approximated by the ADCP and the OBS (Optical BackScatter) sensors reveal that background concentrations are low (Deltares, 2014b) and no clear relation was found with residual flow patterns or tidal resuspension,
- No background organic material is considered in the model. In reality organic material will settle to form a layer of very easily erodible material on the sediment surface and can contribute to any increase in turbidity as the seabed is disturbed.
- A very high critical shear stress for sedimentation is applied in the model in order to ensure that any sediment that does settle can enter the bed. Therefore sedimentation is only determined by the currents and settling velocity.
- Lastly, an average silt settling velocity is utilized in this study, whereas, in reality, the silt settling velocity could be one order of magnitude larger or smaller depending upon the actual grain size, and somewhat on the flocculation properties, of the silt at the mining location. In this study, a silt settling velocity of 0.25 mm/s is used. Sensitivity tests were performed on this parameter and are reported in Appendix V2-B4

Default settings for the other parameters important in sediment transport, such as the critical shear stress for erosion (0.5 Pa) and the erosion parameter ($1 \times 10^{-4} \text{ kg/m}^2/\text{s}$) were utilized in the model set-up. Calculations on a range of previous in situ bed samples showed the critical shear stress for erosion of these in situ sediments to be between 1 and 2 Pa (Deltares, 2014b). The critical erosion threshold for erosion of the mine tailings (after settling) was estimated to be lower ($\sim 0.4 \text{ Pa}$), as a result of the fact that the mixture is less dense. Therefore the modelled critical shear stress for erosion value is very close to the critical shear stress for erosion estimated for the mine tailings as calculated by the resuspension study. Whether any resuspension of the settled sediments from the plume occurs in the model depends on the modelled bed shear stresses. In reality little resuspension of natural bed material occurs. Only very fine material or loose organic material (e.g. detritus) on the surface of the seabed is available for resuspension (Deltares, 2014b).

However, it should be noted that erosion of sediments follows a probabilistic erosion curve as the shear stresses vary both in time and in space due to turbulent forces and changes in bed roughness (van Prooijen and Winterwerp, 2010). Due to turbulent fluctuations around the mean bed shear stress, and the natural variations in critical bed shear stress, erosion may occur even when the bed shear stress is less than the critical bed shear stress for erosion.

2.7 Model Simulation Overview

Table 2.6 provides an overview of applied simulation periods and conditions used in the models as well as a summary (Table 2.7) of all types of simulations carried during the various phases of the study, including reference to the sections in this report where the results are reported upon.

Table 2.6 Simulation periods applied in the Regional and Local Models

Regional			
	Start time	Stop time	Description
Summer	15-01-2011	25-04-2011	(a) Nest simulation Summer local, single cycle. (b) Nest simulation Summer local, multiple cycles.
Spring	01-09-2011	01-10-2011	(a) Nest simulation Spring local, single cycle.
Winter	01-07-2011	01-10-2011	(a) Nest simulation Winter local, single cycle. (b) Nest simulation Winter local, multiple cycles.
Summer – multiple (10) cycles	15-01-11	25-04-11	
Winter – multiple (10) cycles	01-07-11	01-10-11	
Model validation	21-05-11	13-11-11	
Local			
Summer–single cycle	01-02-2011	10-02-2011	
Spring – single cycle	20-09-2011	30-09-2011	Not available for Phase 1b
Winter – single cycle	10-07-2011	20-07-2011	
Summer – multiple (10) cycles	01-02-2001	23-04-2011	Phase 2 Model
Winter – multiple (10) cycles	10-07-2001	30-09-2011	Phase 2 Model
Model validation	21-05-11	13-11-11	Phase 2 Model

The far-field assessment was carried out using Delft3D under seasonal forcing: spring, summer and winter periods in 2011 (see Table 2.6) These periods were chosen such that a variation of hydrodynamic conditions would be represented and that the mining disposal occurs when the largest tidal currents are expected, resulting in conditions when the largest predicted plume suspension and dispersion would occur due to tidal forcing. It should be noted that the simulated periods for the Regional Model are longer than for the Local Model to allow for adequate model spin-up time prior to the Local modelling period.

It was found in the Oceanographic Study (Deltares, 2014a), based on an analysis of HYCOM that with respect to the three seasonal modelling periods, the summer, winter and spring period seem reasonably representative with respect to the near-bed currents. Additionally, the flows of the chosen 2011 period were strongly directed towards the northwest, where as historically there is a more limited excursion and somewhat southerly directed.

It is important to note that the Summer and Spring modelling periods were found to be representative because their flow patterns fall within the historical HYCOM variability (Deltares, 2014a); however, because the environment is highly variable, the various seasonal months in different years can produce different sedimentation and plume dispersion patterns.

Therefore, the multi-cycle simulations, specifically simulations that are real-time and cover longer time periods, are quite important because they capture the range of likely plume dispersion patterns within this highly three dimensional hydrodynamic region.

It is also important to note that longer time period simulations were run covering the period 15 January to 16 March, 15 January to 23 April and 1 July to 30 September to provide boundary conditions to the Local Delft3D Model for the multiple cycle investigations (Chapters 4 and 5).

Table 2.7 Summary of investigations performed during this study

Aspect	Phase 1a	Phase 1b	Phase 2
Local Models (see Table 2.6)	<ul style="list-style-type: none"> North 1 South 1 	<ul style="list-style-type: none"> North 2 South 2 	Optimized model
Reasons for changing the local model set-up	n.a.	New design of mining cycle: <ul style="list-style-type: none"> Orientation of tracks Release height → at bed and not above the bed → higher near-bed resolution needed. 	<ul style="list-style-type: none"> Co-locate with RDI location to enable hydrodynamic validation (Ch.6, 3rd Phase) Optimize grid resolution in vertical and horizontal domain to enable larger domain (to keep 5mg/l SSC within the domain) and multiple cycles in a computational efficient manner.
Investigation objectives and (location in this report)	<i>Near-Field plume:</i> <ul style="list-style-type: none"> (§ 3.1.1, 3.1.2): 2 base scenarios with release heights at 200m and 5 m above bed, including sensitivity of 200 m case for: <ul style="list-style-type: none"> Ambient water density (1) Ambient flow (2x) Outflow/release rate <i>Far-field sensitivity:</i> <ul style="list-style-type: none"> Geographical location during summer (near Northern flank and southern flank). Appendix V2-B Fall velocity of clays (2x), Appendix V2-B 	<i>Near-Field</i> <ul style="list-style-type: none"> Release at bed (§3.1.3) 2 complementary release scenarios: 1) at 10 m and 200 m, 2) Other release characteristics at 200m. (Appendix V2-A) <i>Far-field (§3.2 and 3.3)</i> <ul style="list-style-type: none"> Effect of release at bed on far field (§ 3.2) Different mining duration and sediment characteristics set 2 (less sand, more fines) Initial comparison model RDI-observations (100 km spaced apart). (§ 3.2) Sensitivity testing for wind, roughness and viscosity (§ 3.2.3) 	<i>Far-field effects of</i> <ul style="list-style-type: none"> Different sediment characteristics, set 3 (less sand clay and more silt than in set 1) Repeat 1 cycle simulation with new model and settings (§4.1, and 5.1) Discharge release at 10 m above the bed (§4.2 and 5.2) 10-cycle simulation, using both SSC and available mass at the bed at the end of each cycle to start a new cycle (§4.3 and 4.3). Disposal at the bed and 10 m above the bed. Incident modelling (Ch.7)
Number mining cycles	1	1	1 and 10
Simulation conditions For definition of periods see Table 2.4	Winter, Spring and Summer scenario	Winter, Spring and Summer scenario	<ul style="list-style-type: none"> Single cycle: winter, spring and summer. Single cycle release height - summer 10 cycles in summer and winter

Model set up in brief

Numerically assessing the far-field plume dispersion and sedimentation of the mine tailings released during the mining process requires a dedicated modelling approach. To achieve these requirements, Delft3D simulations were set-up using a Regional Model and higher resolution Local Models. The Regional Model extends 260 km across the Chatham Rise covering the steep parts of the North and South slopes and 160 km in along-Rise region. The marine mining license areas are roughly centred in this Regional domain. Boundary conditions were derived from the global ocean model HYCOM and TOPEX/Poseidon global inverse solution TPXO.

The Regional Model provides boundary conditions for the (nested) Local Models. The Local Models were set-up to model the far-field plume dispersion and the mining process using schematized characteristics of the seabed sediments obtained during the 2012 survey cruises.

Three Local Models were used. A northern and southern domain was used initially, with which a series of sensitivity tests were performed. Finally a larger domain was centred over the iX survey mooring location, which provided validation data for the model. The mining area in the model has the highest horizontal grid resolution. The model bathymetries were derived from the new multi-beam data obtained within the marine mining license areas and older single beam data, both provided by Boskalis, and the GEBCO 08 data.

The schematization and simulation of the mining track and cycle and sediment release associated with the mine tailing disposal was done using the Local Delft3D Models and Jet3D. Jet3D computes the near-field plume and was used to provide input to the local Delft3D Model in the case when sediment was released at 200 m above the seabed. Simulations were performed and analysed for different seasons to capture varying hydrodynamics and for different release heights of the mine tailing disposal above the bed.

3 Model Simulations - Initial Investigation (Phase 1a and Phase 1b)

3.1 Near field plume development

As part of *phase 1a*, the near-field mine tailing plume development was investigated using Jet3D for the two base discharge scenarios, as defined by Boskalis. Based on calculations made using Jet3D suitable settings were chosen to provide input for the Delft3D model. Additionally, a variety of sensitivity test cases investigated the effects of density, as well as current direction and magnitude. This section presents the results of this Phase 1a near-field investigation.

The following outflow parameter definitions, and set-up for two base discharge scenarios:

- Outflow parameters
 - Sediment flow : 0.75 m³/s or 1200 kg dry solids/s (dry density 1.6 ton/m³)
 - Concentration of outflow 1.325 ton/m³ (seawater 1.025 ton/m³)
 - Mixture outflow: 2.48 m³/s (0.44 m³/s dry solids and 2.04 m³/s water)
 - The total sediment release rate is 1195 kg/s
 - For sediment characteristics see Table 2.2
- Discharge Scenario 1:
 - Release height is 395 m below sea level = 5 m above sea bed
 - Diffuser with radial horizontal outflow, reducing outflow velocity to below 0.5 m/s (e.g. diameter 6 m, gap height 0.25 m)
 - Duration 72 hours, followed by at least 120 hours of no release
 - Linear speed of 1 m/s, up and down over stretch of 4 km
- Discharge Scenario 2:
 - Release height at 200 m below sea level = 200 m above seabed
 - Another type of diffuser was proposed with outflow velocity at least below 2 m/s, however no diffuser was used in the study because the effects of a diffuser would be negligible at this height above the seabed.
 - Duration 72 hours, followed by at least 120 hours of no release
 - Linear speed of 1 m/s, up and down over stretch of 4 km

The following sections present the results of the near-field study.

3.1.1 Disposal at 200 m above the seabed

The Jet3D simulations for scenario 2, with an outflow half-way the water column (200 m) (see Figure 3.1), used the following input:

- 1 *Ambient density* is assumed constant over depth. Sensitivity scenarios are performed looking into the variation of the ambient seawater density between 1025 – 1027 kg/m³ due to temperature effects (as observed in summer period).
- 2 *Ambient velocity* is set equal to the trailing velocity since the plume is computed relative to the vessel. Sensitivity scenarios are performed looking into the variation of the ambient currents +/- 0.25 m/s at 200 m above the seabed (representing currents in trailing direction, values as observed).
- 3 *Jet orientation* was initially set horizontally (0° is in direction of ambient velocity) and then vertically (-90° is vertically downward direction). The jet orientation and initial release velocity were found to be of minor importance. This can be explained since

gravity effects dominate the initial momentum effects at a distance greater than approximately 50 m. The plume flow is driven mainly by gravity and not by initial velocity and momentum. A “virtual” input jet diameter of 2.5 m is chosen to satisfy sediment mass flow rate with initial velocity at diffuser as given by Boskalis (0.5 m/s).

- 4 Initial jet density of 1325 kg/m^3 was used.

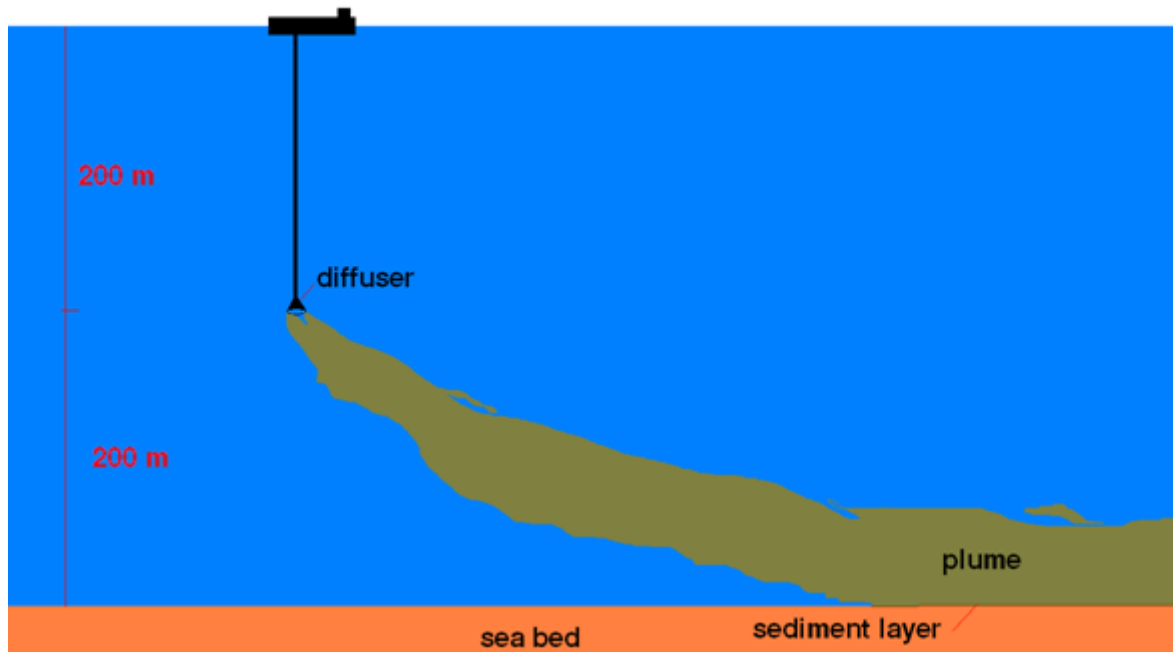


Figure 3.1 Discharge Scenario 2 Discharge schematic with diffuser approximately 200 m above the seabed.

The Jet3D figures for this scenario (see Figure 3.2 to Figure 3.5) show the plume from three different directions, side view, profile view and plan view. Note the interaction with the bed is not computed by Jet3D (Top view shows the plume as if it continues). When at the bed, the flow width is approximately 200 m. When evenly spread over a width of 200 m, the sediment release results in a sediment layer thickness of 3 – 4 mm. The plume height is about 50 m above the bed. Flow velocity and density in the plume are decreased strongly due to entrainment (dilution).

The plume transports the sediment, including the fines, to the seabed very quickly, regardless of the individual fall velocities of the various grain sizes (including clay particles). Actually, the fall velocity is to be super-positioned on top of the plume subsidence velocity. Only coarse particles will settle faster than the plume (sand and gravel). Additionally, only a minor fraction of the plume, at its surface, will be suspended in the water before it has reached the seabed (stripping). However, this effect was neglected.

As a note, to control the outflow velocity and pressure in the 200 m vertical pipe line, the excess density has to be compensated with additional friction elements.

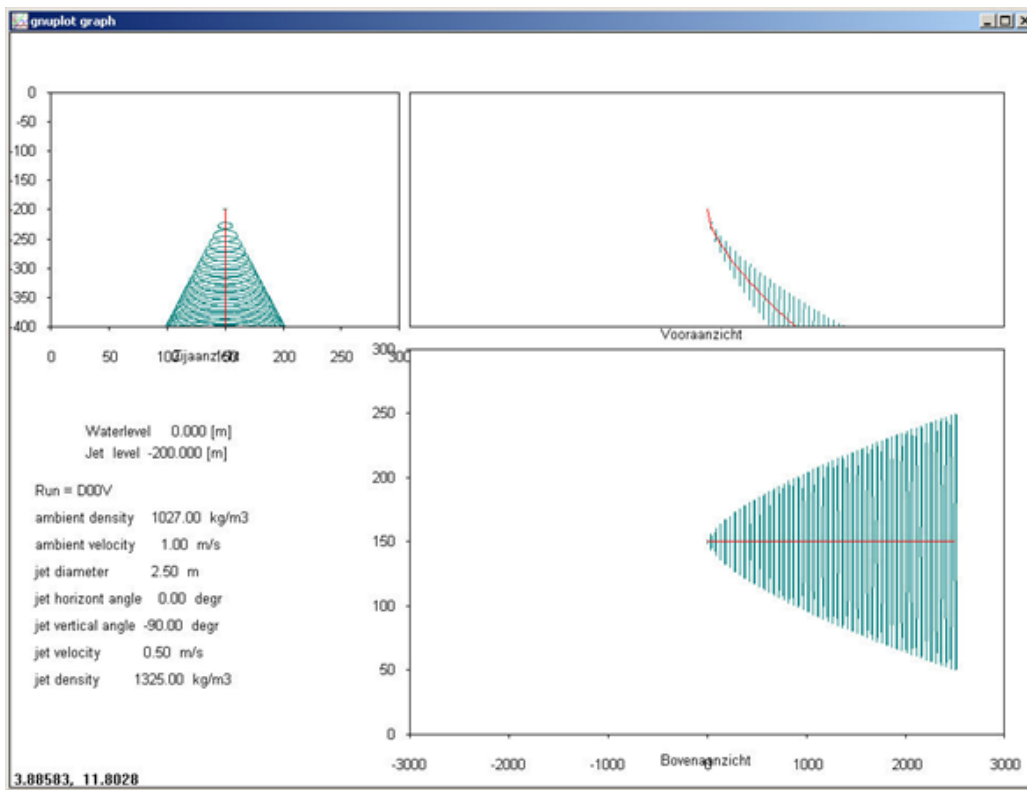


Figure 3.2 Sediment plume development JET3D for a vessel speed 1m/s, no currents, and density ambient seawater 1027 kg/m³.

In the base case of discharge scenario 2, where the vessel speed is 1 m/s, there are no ambient currents and the density of the ambient seawater is 1027 kg/m³, the plume contacts the seabed 900 m from the discharge location (Figure 3.2).

For the simulation with a vessel speed of 1 m/s, no ambient currents and an ambient seawater density of 1025 kg/m³, there is no significant difference between this result and the previous results (by comparing Figure 3.2 and Figure 3.3).

For the simulation with a vessel speed of 1 m/s, an ambient current of 0.25 m/s heading along the Rise and against the vessel, with an ambient seawater density of 1027 kg/m³, the plume contacts the seabed 550 m from the discharge point (Figure 3.4).

Finally, for the simulation with a vessel speed of 1 m/s, an ambient current of 0.25 m/s heading along the Rise and in the same direction as the vessel, with an ambient seawater density of 1027 kg/m³, the plume contacts the seabed 1300 m from the discharge point (Figure 3.5).

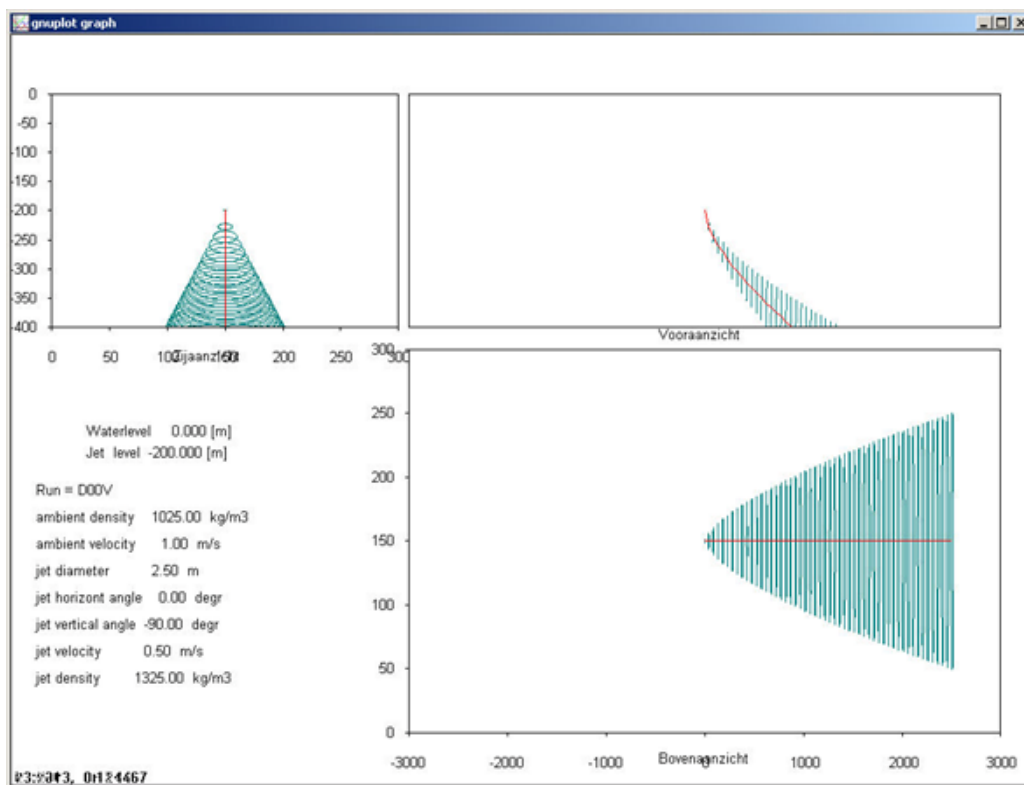


Figure 3.3 Sediment plume development JET3D for a vessel speed of 1 m/s, no currents, and an ambient seawater density of 1025 kg/m³.

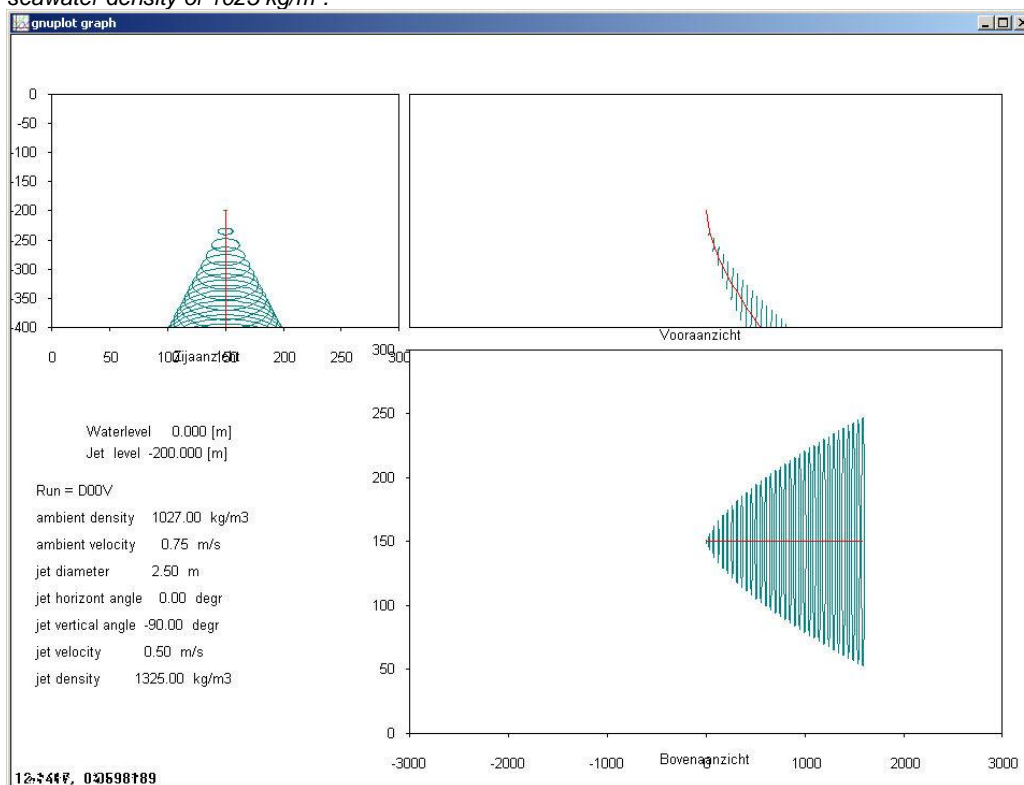


Figure 3.4 Sediment plume development JET3D for a vessel speed of 1 m/s, ambient current 0.25 m/s along the Rise heading against the vessel, and an ambient seawater density of 1027 kg/m³.

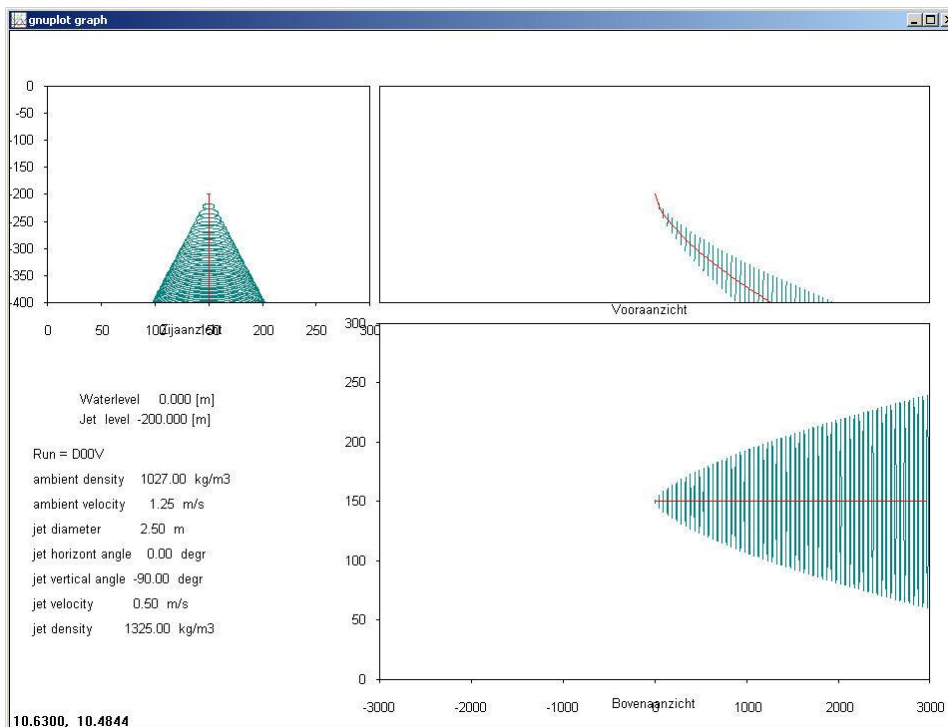


Figure 3.5 Sediment plume development JET3D for a vessel speed of 1 m/s, and ambient current of 0.25 m/s along the Rise heading in the same direction as the vessel, and an ambient seawater density of 1027 kg/m³.

Flow velocity and sediment concentration of the near-field mine tailing plume quickly decrease as a function of distance from the release point (Figure 3.6). All sediment particles travel to the bed in the plume with a velocity that is much larger than the individual fall velocity of the fines. The coarser particles will likely segregate.

The fall velocity of particles with grain sizes above 400 μm (16% by weight) is larger than the final plume velocity near the bed (about 0.05 m/s). Therefore these particles will probably segregate from the plume. In contrast, the finer particles will remain suspended above the seabed.

Jet3D predicts the plume will result in a suspension layer with a height of about 50 m (refer to the profile panels in Figure 4.2 through Figure 4.5) and a speed of 0.05 m/s at the bed after the plume contacts the bed. In this suspension layer, the fine silt fractions (finer than 63 μm) could settle within 1 km. However, the very fine colloidal or clay fractions (finer than 2 μm), according to the PSD still 10% by weight, will likely stay in suspension and may be transported outside the model domain.

The far-field modelling, by Delft3D, will show that the fine silt fractions will only partially settle within a 10 km distance from the Delft3D discharge locations due to the large-scale and local currents.

Appendix V2-A provides a complementary scenario for discharging at 200 m above the bed, using different grain size characteristics of the mine tailings.

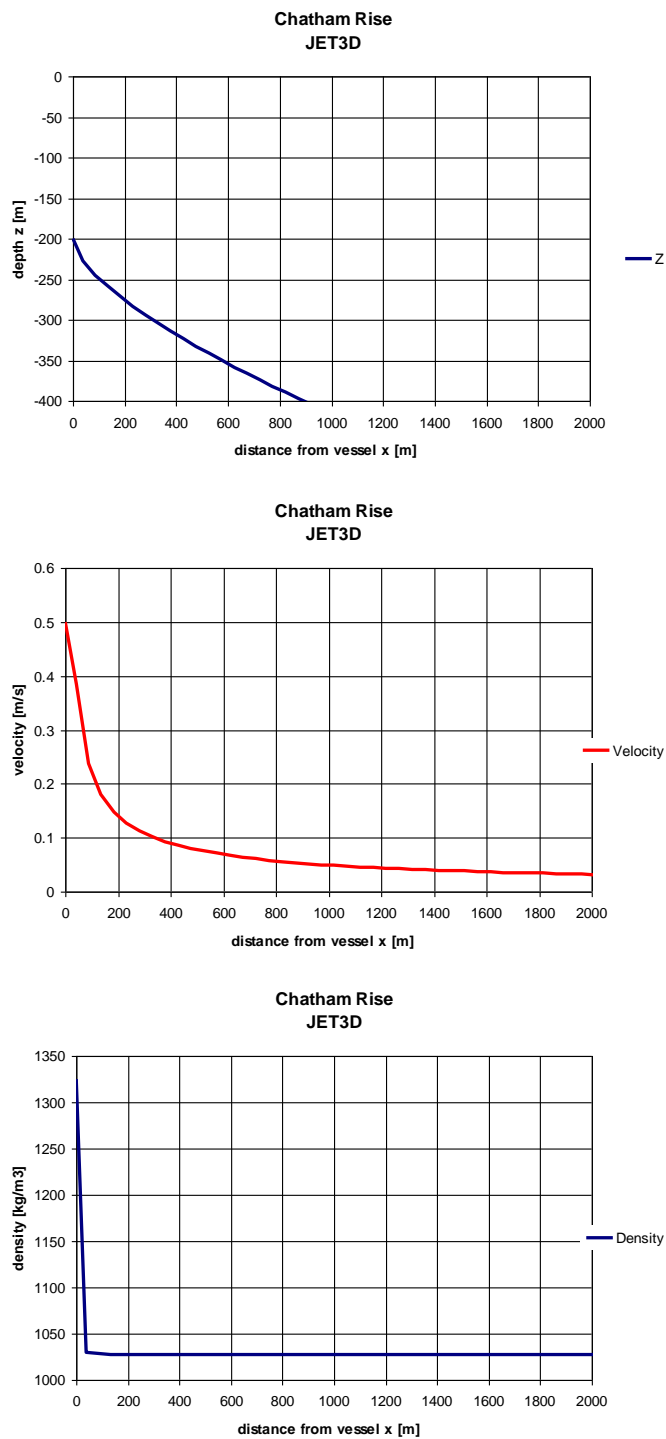


Figure 3.6 Trajectory (top), flow velocity (middle) and density (bottom) of the sediment plume.

3.1.2 Disposal at and near the seabed – deposition of the sand fraction.

This section provides estimates of the deposition of the sand fraction along a single mining track for discharging at and near the bed, i.e. cases where the plume flow cannot fully develop and therefore cannot be computed with JET3D. General production characteristics and assumptions for these estimates are:

- sailing speed is 0.75 m/s
- flow spreading 1:7 from 6 m diameter diffuser
- segregation of sand and fines

Phase 1A-disposal at 5m above the bed

The total flow rate is $2.48 \text{ m}^3/\text{s}$, with an initial density of 1325 kg/m^3 . The total sediment release rate is 1200 kg/s . It is assumed that the fines (with grain size $d < 63 \mu\text{m}$) will segregate completely and remain suspended and can be considered as input to Delft3D, while the sand (with grain size $d > 63 \mu\text{m}$), in this case 55% of the total sediment load (Table 2.2), will be deposited directly after passage of the diffuser. When released at a height of 5 m above the bed and evenly spread, the width of the deposited sand layer will be about 7.5 m and the layer thickness 0.07 m per single track with a layer bulk density of 1600 kg/m^3 (as given by Boskalis, see table 2.3).

Phase 1b and Phase 2-disposal at the bed and 10 m above the bed

For the conditions assumed for phase 1b the total sediment load is 825 kg/s . Released at a height of 10 m above the bed the spreading width will be about 9 m. The sand fraction is now 43% and the layer thickness 0.03 m per single track. At this height still no plume development will have taken place.

When released at the bed the spreading width will be about 6 m and with a sand fraction of 46% the sand layer thickness will be 0.05 m per single track.

In reality, part of the material will be suspended in the plume as schematically shown in Figure 3.7. The fate and transport of this suspended plume is modelled using the far-field model, Delft3D (see section 4.2 and Chapters 5 and 6).



Figure 3.7 Discharge Scenario 1- Discharge schematic with diffuser approximately 5 m above the seabed.

3.2 Far-field Model performance – initial assessment

3.2.1 Information sources

As part of phase 1b an initial assessment of the far-field (Delft3D) hydrodynamics was carried out using field observations (Table 3.1). The validation material received contained the following data:

- CTD Profile
- A temperature profile
- Near bed velocities measured by a Aquadopp instrument
- Current measurements over the vertical measured by an RDI ADCP and
- Turbidity measurement measured by an Aquatec instrument

A summary of the velocity and turbidity data from the moorings is presented by Bowen (2012) and Deltares (2014a).

Velocities through the water column were obtained by an RDI ADCP moored at a depth of 362.74 m at location 43°29.003' S - 179°20.099' E. The centre of the first depth bin was located at 30.5 m above the bottom. An Aquadopp attached to the same frame measured velocities closer to the bed (at 8 m above the bed). The ADCP and Aquadopp were mounted on a frame about 10 m above the seabed. All data are transformed to UTC date and time, and current directions were corrected for local magnetic declination.

Table 3.1 Overview available field data.

Instrument	Location	Depth	Time Frame Start-end (UTC)	Parameter
RDI ADCP	43°29.003' S - 179°20.099'	362.74	21/05/2011 19:00 - 13/11/2011 0:00	Current profile
RDI Aquadopp	43°29.003' S - 179°20.099'	372.28	21/05/2011 19:00 – 11/12/2011 0:00	Bottom Current
Aquatec Aqualogger Top	43°29.003' S - 179°20.099'	359	18/07/2011 10/12/2011	Temperature / turbidity
Aquatec Aqualogger Bottom	43°29.003' S - 179°20.099'	372	18/07/2011 10/12/2011	Temperature / turbidity

Figure 3.8 illustrates the measured speed and direction derived from the ADCP. Speeds generally ranged between 0 and 50 cm/s. Maximum values recorded between 55 and 75 cm/s. A distinct tidal signal is visible in both the speed and direction signals. Figure 3.9 illustrates this by plotting time series for the top, middle and bottom bin. The pressure, a proxy for water level, shows the tidal elevation changes. Tidal ranges are at their maximum during spring tides, with maximum tidal elevation values of 0.75 m above the mean water level, and are at their minimum during the neaps.

The near-bed speeds measured with the RDI Aquadopp (Figure 3.10) show a maximum of 45 cm/s, but are generally between 10 and 40 cm/s. These magnitudes are comparable to the lowest ADCP bin. Tidal component analysis using the T-tide toolbox (Pawlowicz *et al.*, 2002) reveals the dominance of the M2 tidal component. The strongest flows measured are associated with the tides. Tides account for 70% of the total variance.

The Aquatec Aqualogger timeseries of temperature (not shown) reveal a near 2-degree temperature variation over the measurement timeframe. The top and bottom instruments show similar temperature variations. In general, bottom values are 0.02 degrees warmer than

the top values, which might indicate a small offset in the instruments. The limited differences between top and bottom layer velocities indicate that (local) temperature driven flows are not important.

Turbidity sensors recorded measurements over a five-month timeframe. The Turbidity time series in general show sustained background values around 2 FTU (Formazin Turbidity Unit) (Figure 3.11). The increasing turbidity, and maintained high values above 4 FTU since October, is questionable. An increasing trend in turbidity over time, without a known disturbance, is commonly linked to biofouling of the sensors. Several short-term events with significantly higher values (> 10 FTU) were recorded during the deployment.

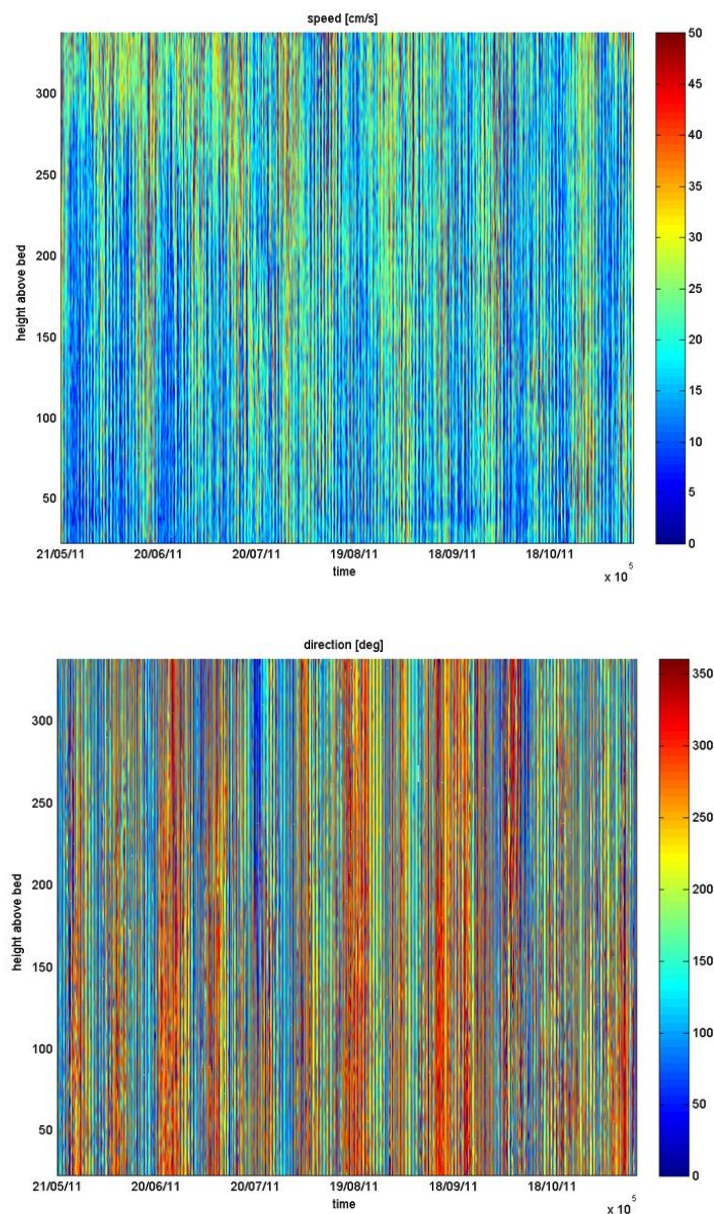


Figure 3.8 RDI ADCP measurements for speed (top) and direction (bottom).

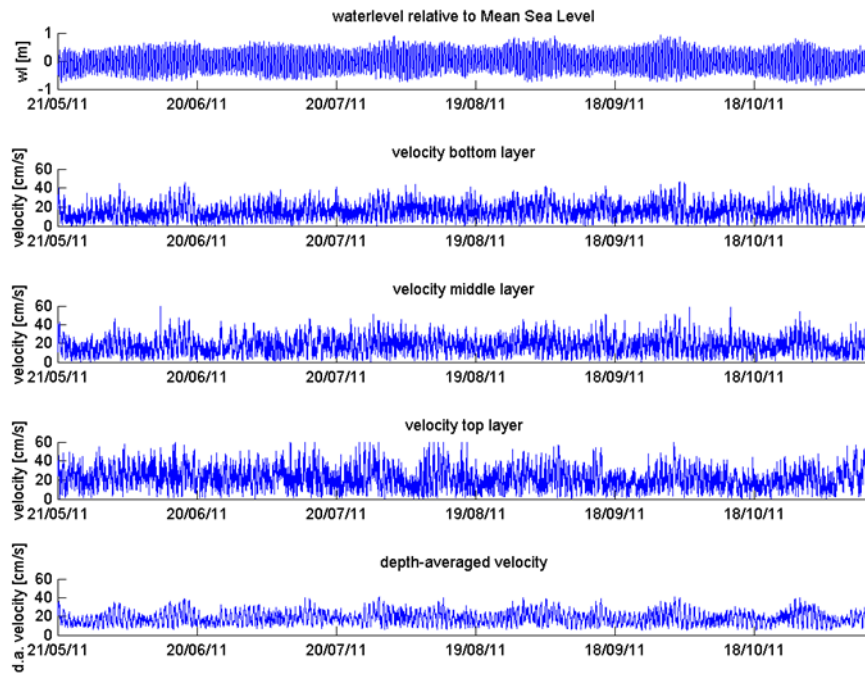


Figure 3.9 Timeseries derived from the RDI ADCP measurements (from top to bottom): pressure (m) and velocities for the bottom and top layers, and depth averaged-velocities (cm/s).

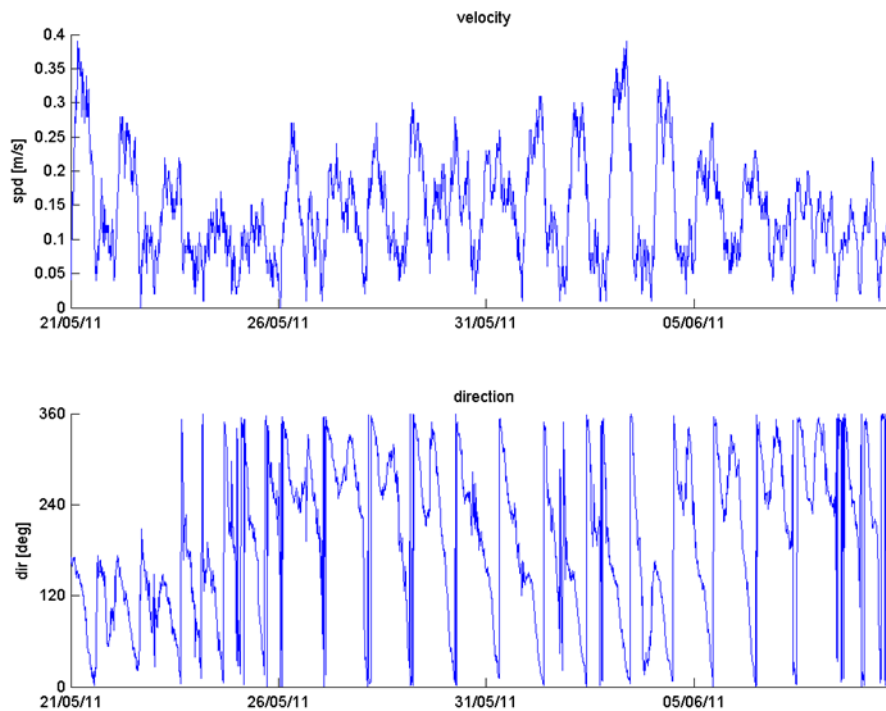


Figure 3.10 Flow speed and direction from RDI Aquadopp.

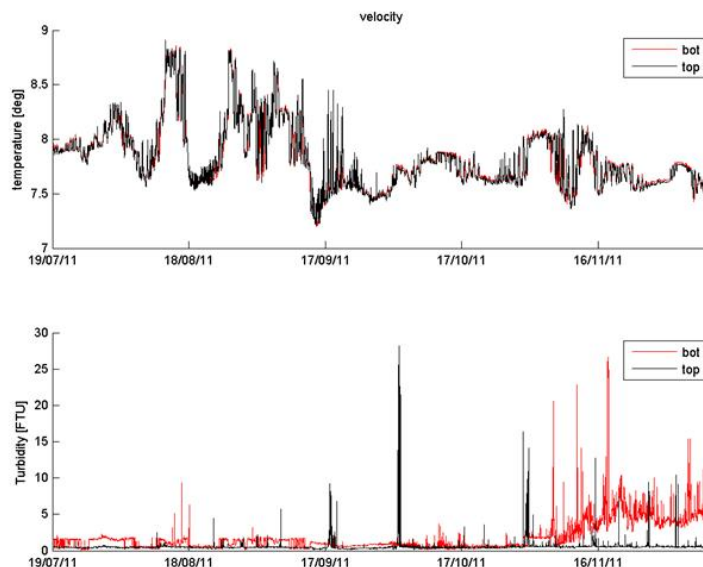


Figure 3.11 Timeseries of bottom and surface of Turbidity (bottom) and temperature (top) measured with the Aquatec Aqualoggers.

3.2.2 Performance

As a first step, the measured and modelled time-series of water levels and depth-averaged flow velocities were harmonically analysed separately over the three modelling periods (spring, summer, winter). Herein a correction for an observed phase difference, of about two hours, between model and data was applied to the modelled data. During the execution of Phase 3 it became clear that the processed ADCP data contained a timing error of 2 hours related to day light saving time.

The major tidal constituent is the M2 tide. This constituent is resolved accurately by the model, with a mean error below 10% for both water level and velocity (Table 3.2). For the following comparisons, please note that the location of the observations and the location of the utilized model results is not exactly the same. In the original simulation, no observation point existed at this location and the nearest available station had to be used. The velocity magnitudes are less sensitive compared to direction. Figure 3.12 summarizes the observation-model comparison by plotting velocity relative to range. Detailed comparisons of velocity time series are presented in Figure 3.13 to Figure 3.19 for the regional and local models. All time-series show a similar picture of accurately resolved water levels. Velocity magnitudes are reproduced fairly well. There is a directional-offset between the observed versus modelled velocities resulting in a deviation between the observed and modelled depth-averaged x-component and y-component signals (for example, in the bottom two panels of Figure 3.13 and Figure 3.14, and also can be seen in Figure 3.16). Such directional differences can arise as the model contains a fairly coarse grid schematisation and is forced by its boundaries only. Local effects of bathymetry generation of flow due to phenomena within the domain are not covered.

Overall, the initial model-to-data comparisons indicate the models are performing well at reproducing depth averaged flow, and thus provide confidence in the hydrodynamic modelling performed thus far. A more in depth-analysis is required to assess the performance for near-bed plume dispersion, considering near-bed tidal and residual flows. This analysis is provided in Chapter 6

Table 3.2 Comparison of observed and modelled tidal constituents for water levels (top) and velocities (bottom).

Water level		Amplitudes [m]						
Const	Freq.	Measured	Model			Model		
		[m]	Winter [m]	Summer [m]	Spring [m]	Mean error [m]	Mean Error [%]	Relative mean error [%]
K1	0.042	0.0232	0.0361	0.0363	0.0280	0.010	44	2
*M2	0.081	0.5353	0.5356	0.4544	0.5007	-0.038	-7	-7
M3	0.121	0.0054	0.0024	0.0043	0.0036	-0.002	-36	0
M4	0.161	0.0018	0.0022	0.0030	0.0033	0.001	57	0
2MK5	0.203	0.0024	0.0014	0.0009	0.0009	-0.001	-56	0
M6	0.242	0.0030	0.0016	0.0014	0.0019	-0.001	-46	0
*3MK7	0.283	0.0028	0.0013	0.0014	0.0014	-0.001	-51	0
*M8	0.322	0.0022	0.0013	0.0002	0.0015	-0.001	-55	0
Velocities								
[m/s]								
K1	0.042	0.019	0.116	0.075	0.06030	0.038	92	3
*M2	0.081	0.187	0.175	0.167	0.11603	0.008	9	1
M3	0.121	0.014	0.004	0.006	0.00571	-0.042	-35	-3
M4	0.161	0.004	0.004	0.005	0.03252	-0.043	-27	-3
2MK5	0.203	0.006	0.003	0.004	0.00406	-0.067	-33	-5
M6	0.242	0.003	0.001	0.002	0.01082	-0.078	-32	-5
*3MK7	0.283	0.002	0.002	0.002	0.00409	-0.093	-33	-6
*M8	0.322	0.001	0.001	0.002	0.00292	-0.106	-33	-7

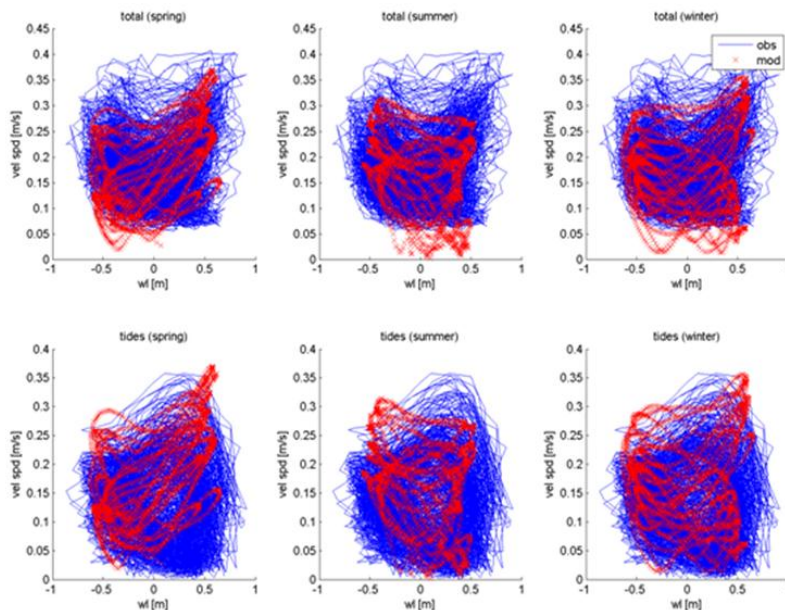


Figure 3.12 Modelled (red) and observed (blue) tidal range (x-axis) versus velocity (y-axis) for spring, summer and winter conditions (left to right). Top plots illustrate the total velocity signal; bottom plots show tide-only. Predicted flow variability falls within the observed range of variations

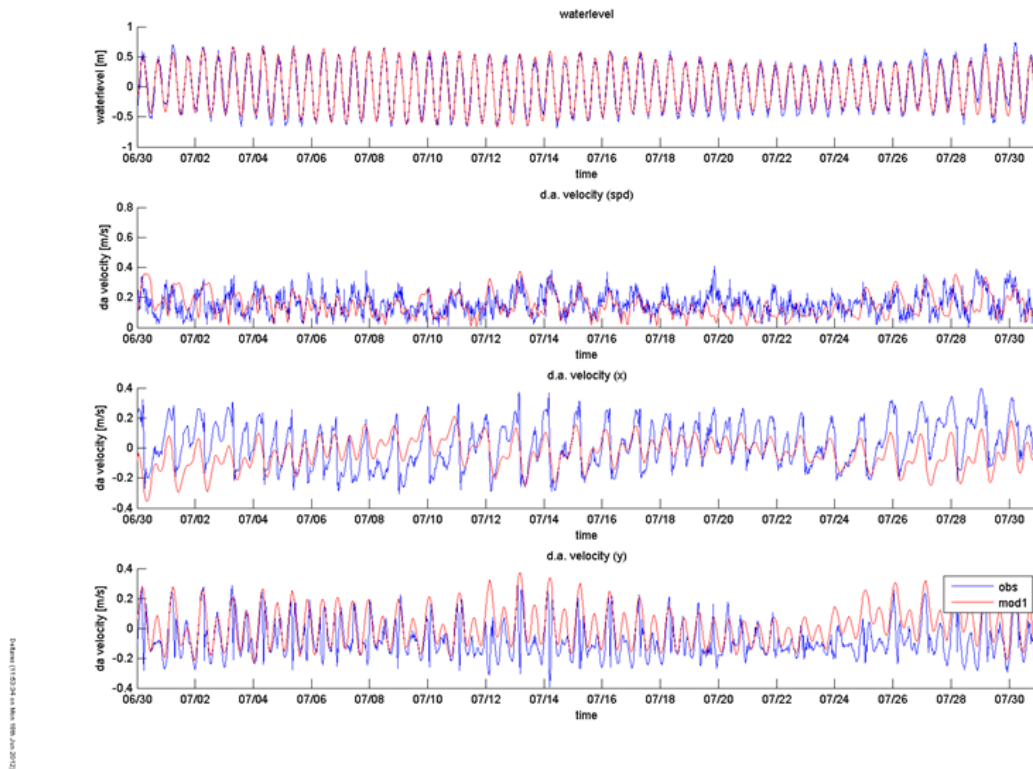


Figure 3.13 Comparison of observations (blue lines) and regional model results (red lines) for water levels, depth-averaged velocity magnitude, depth-averaged velocity x and y components (from top to bottom).

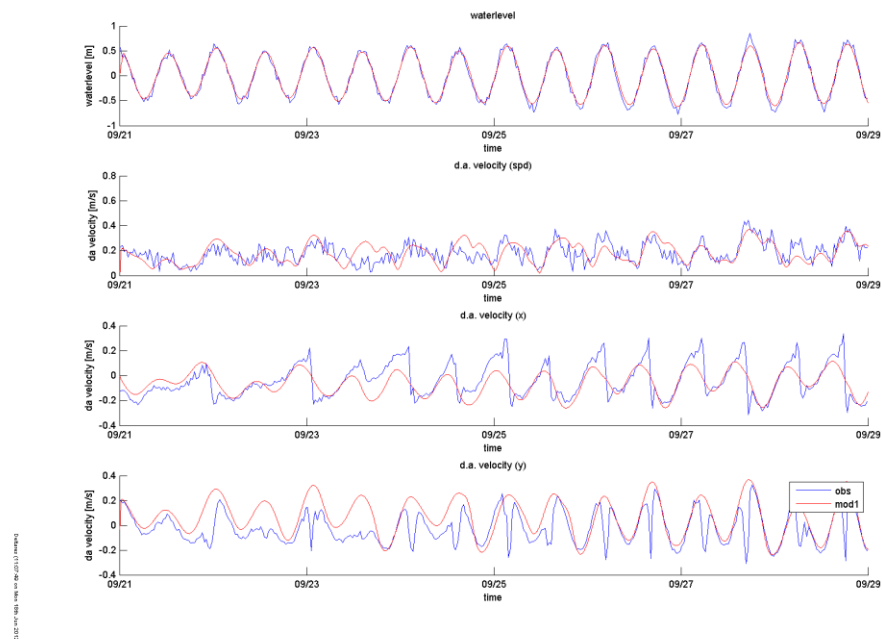


Figure 3.14 (from left to right): Modelled (local model) and observed water levels (from pressure), depth averaged velocity magnitude and depth averaged velocity in x and y component for spring simulation.

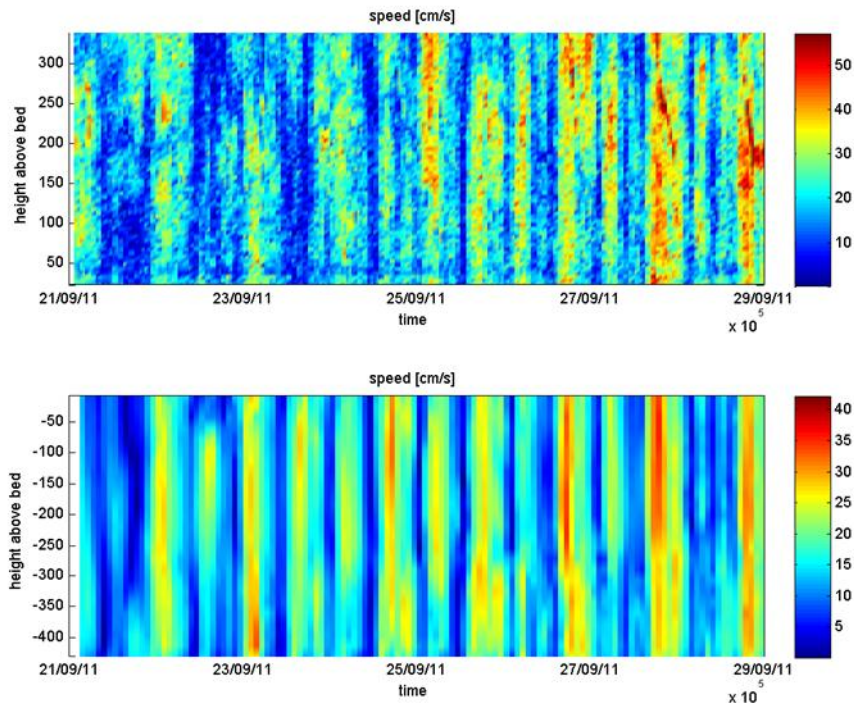


Figure 3.15 Observed (top) and modelled (bottom) velocity magnitude (cm/s) for spring simulation.

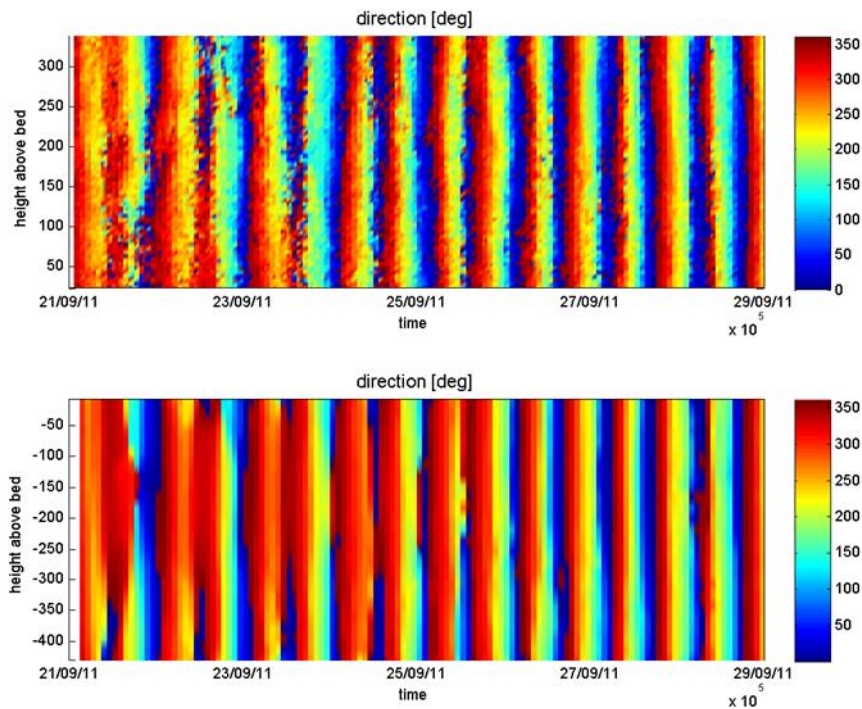


Figure 3.16 Observed (top) and modelled (bottom) velocity directions (°) for spring simulation.



Figure 3.17 Modelled (Local Model) and observed water levels (from pressure measurement), depth-averaged velocity magnitude and depth-averaged velocity in x and y component for winter simulation.

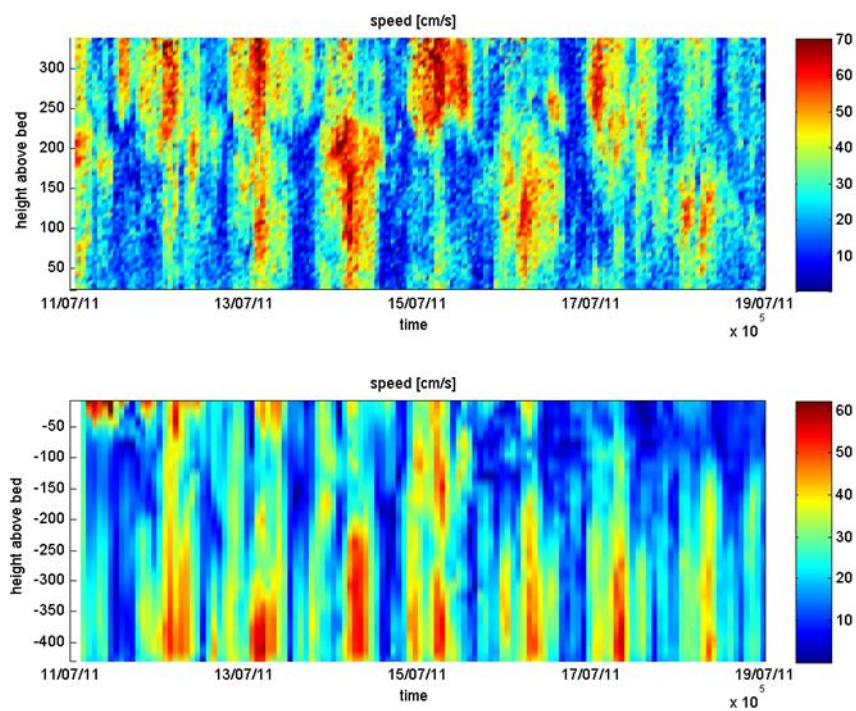


Figure 3.18 Observed (top) and modelled (bottom) current magnitude (cm/s) for winter simulation.

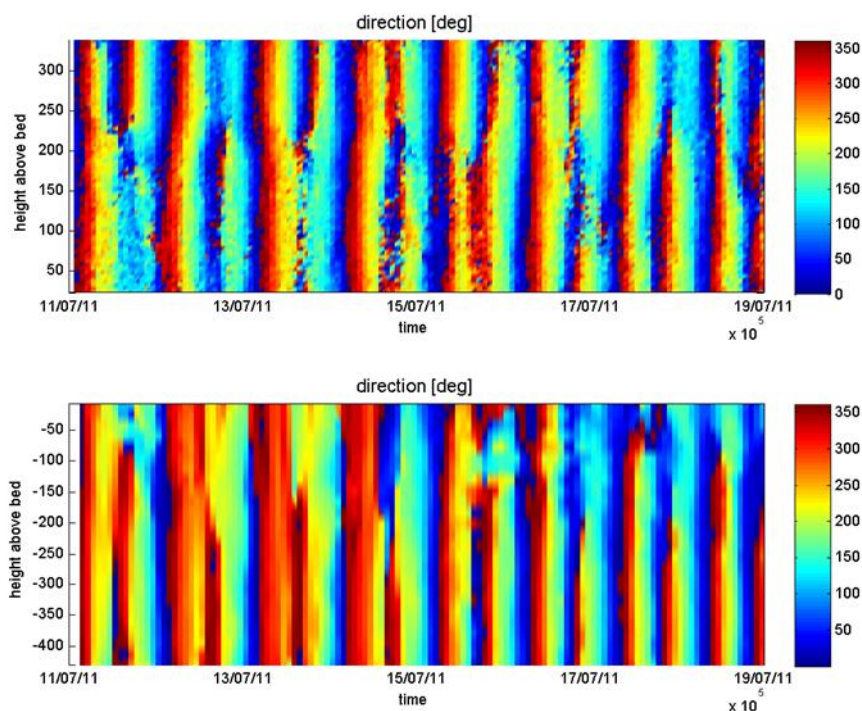


Figure 3.19 Observed (top) and modelled (bottom) current directions (°) for winter simulation.

3.2.3 Sensitivity Tests of the Regional Model

A number of tests were performed to investigate the response to various processes (Figure 3.20) and parameter settings of the Regional Model (Table 3.3). All simulations are based on the winter period. The results of the model simulations are comparable to the results discussed in the previous section (differences below 10%) and are subsequently not repeated here. These comparable results indicate that:

- The model is robust. A robust model provides confidence in the model results as these prove to be relative insensitive to (small) changes or fine-tuning. It is unlikely that large variations in the flow arise when adjustments to the model are made within realistic ranges. Hydrodynamic results will be comparable to those presented in this memo.
- The flows are driven by non-local processes. Changing the processes within the model domain (for example, the wind forcing) does not improve or change the results significantly. The larger scale ocean forcing is dominant.

Table 3.3 Overview of sensitivity simulations regional model.

runid	Description
R0	Default simulation
R1	No wind simulation
R2	Space-varying wind fields
R3	Space varying wind + Manning bed roughness 0.02
R4	No wind + manning bed roughness 0.02
R5	Chezy bed roughness of 75 (+ wind)
R6	Viscosity of 0.1 (+ space varying wind)

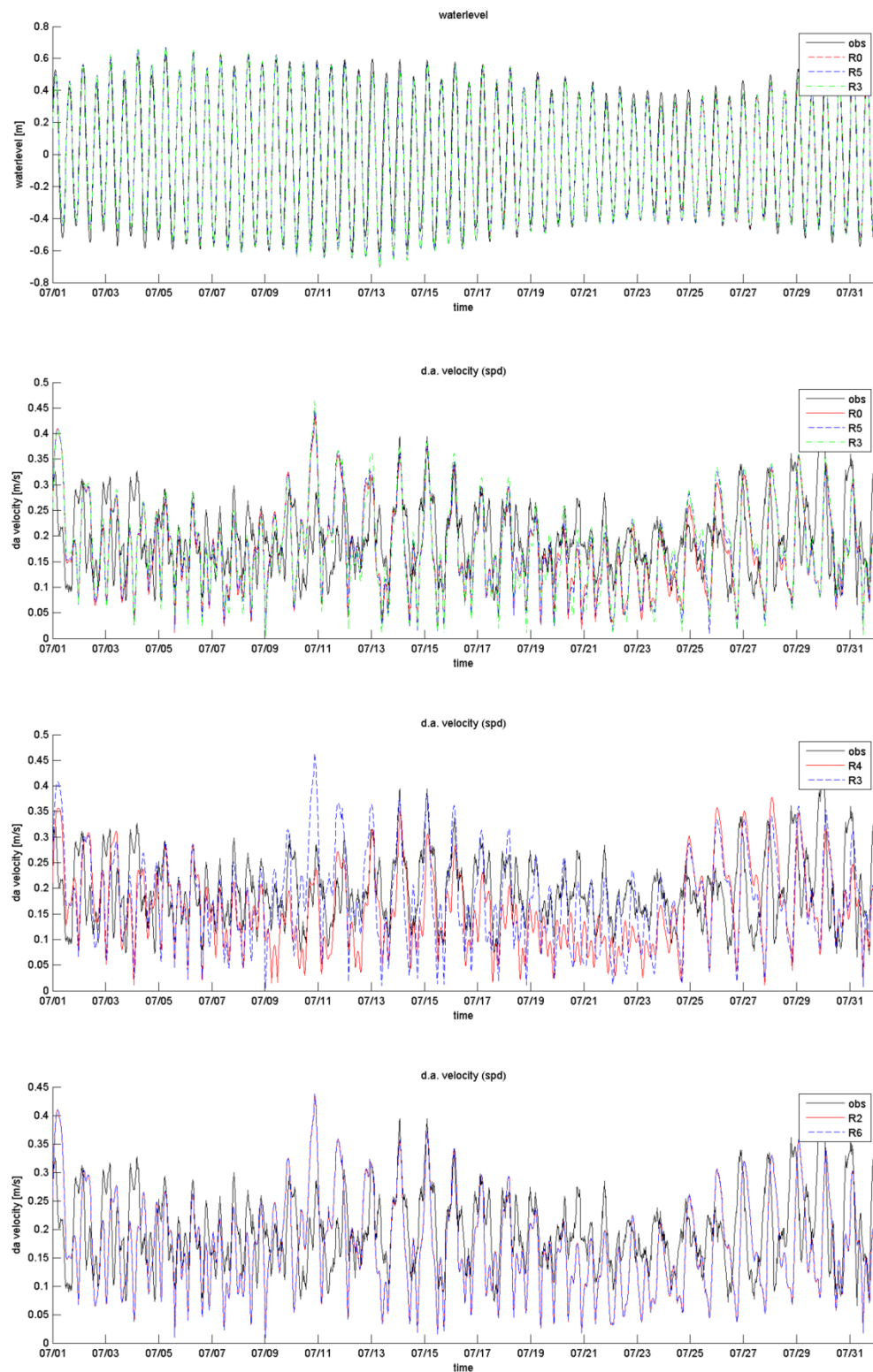


Figure 3.20 Overview results for sensitivity testing. From top to bottom: Effects of bottom roughness value and formulation on water level (panel 1) and depth-averaged velocity (panel 2). Effect of including wind on depth-averaged velocity (panel 3). Effect of viscosity on the depth-averaged velocity (panel 4). For legend description, see Table 3.3

3.3 Far-field mine tailing dispersion for 3 seasonal scenarios

3.3.1 Suspended sediments

Based on the results of the first initial investigations (phase 1a) it was decided to only consider mine tailing discharged at the bed and at 10 m above the bed. This section presents the results of the initial investigations on far-field mine tailing plume dispersion of Phase 1b with the following characteristics:

- Mine tailings are discharged at the bed
- Three seasonal scenarios are considered, viz. a Spring, Summer and Winter scenario
- Using the two overlapping North and South models domains (Figure 2.2).

Thereby, these investigations address both temporal and spatial variations in predicted mine tailing dispersion. For summarized details on set-up of the simulations see Chapter 2, Table 2.5 and Table 2.7 in particular.

Different types of plots are used to visualize the far-field dispersion of the mine tailings for a single mining cycle:

- Suspended Sediment Concentrations (SSC) maps: maps of the near-bed (bottom grid cell) suspended silt and clay concentrations (in g/l) during a mining cycle (Figure 3.21 and Figure 3.22). In these plots the transition from light blue to light brown is at 1 mg/l (0.001 g/l). Threshold exceedence maps, capturing the percentage of time that the maximum suspended silt and clay concentrations at any height in the water column exceed a certain threshold. Four thresholds were considered: i.e. 1 mg/l (far left sample in Figure 3.21), 10 mg/l (second from left sample in Figure 3.21), 30 mg/l and 50 mg/l. Herein total time refers to the period of disposal and transit period, roughly 8 days in total. In these plots a light blue colour represents 20% of the time that the concentration is exceeded, yellow represents 30% of the time the concentration is exceeded and red represents 40% of the time when the concentration is exceeded.

SSC-maps

Figure 3.21 shows, as an example, snapshots of the near-bed suspended concentrations of the silt and clay fraction over the course of a mining cycle in the Southern domain. Appendices V2-C shows similar maps for the other seasonal scenarios for the Northern and Southern Model domain. This figure shows high sediment concentrations occurring along the mining track during periods of active mining. Most of these sediments, the silts in particular, directly deposit along the track line (as can be observed from the sedimentation footprints, see section 3.3.2 and Appendix V2-C). A minor part is transported throughout the model domain, with maximum dispersion occurring near the end of mining, i.e. after track 24 (=3 days). During the five day break in mining, while the vessel transits to shore to offload and return to the mine site, the plume silt and clay concentrations in the entire model domain drop below 0.1 mg/l and 1 mg/l respectively.

The plots below show the maximum plume dispersion at the end of mining, track 24. To grasp both the seasonal and spatial variation in one comprehensive overview, Figure 3.22 shows the near-bed (bottom grid cell) suspended silt and clay concentrations (in g/l) at the end of mining (track 24) in each seasonal scenario, for both the North model and the South model. It reveals the following observations:

- In the Spring (for South domain only) and Winter scenario plume dispersion tends to occur in a predominantly northern to north-western direction.
- In the Summer scenario dispersions towards the southwest can be observed.
- The plume spreading is largest in the Summer scenario
- These seasonal variations in dispersion direction can be observed in both the North and the South domain.

- The finer clay fraction is subject to a larger dispersion than the silt fraction. This difference is most obvious in the concentration class 0.1-5 mg/l.
- Besides these general tendencies, the details of the plume dispersion in the North and South domain point at considerable small-scale spatial variations.

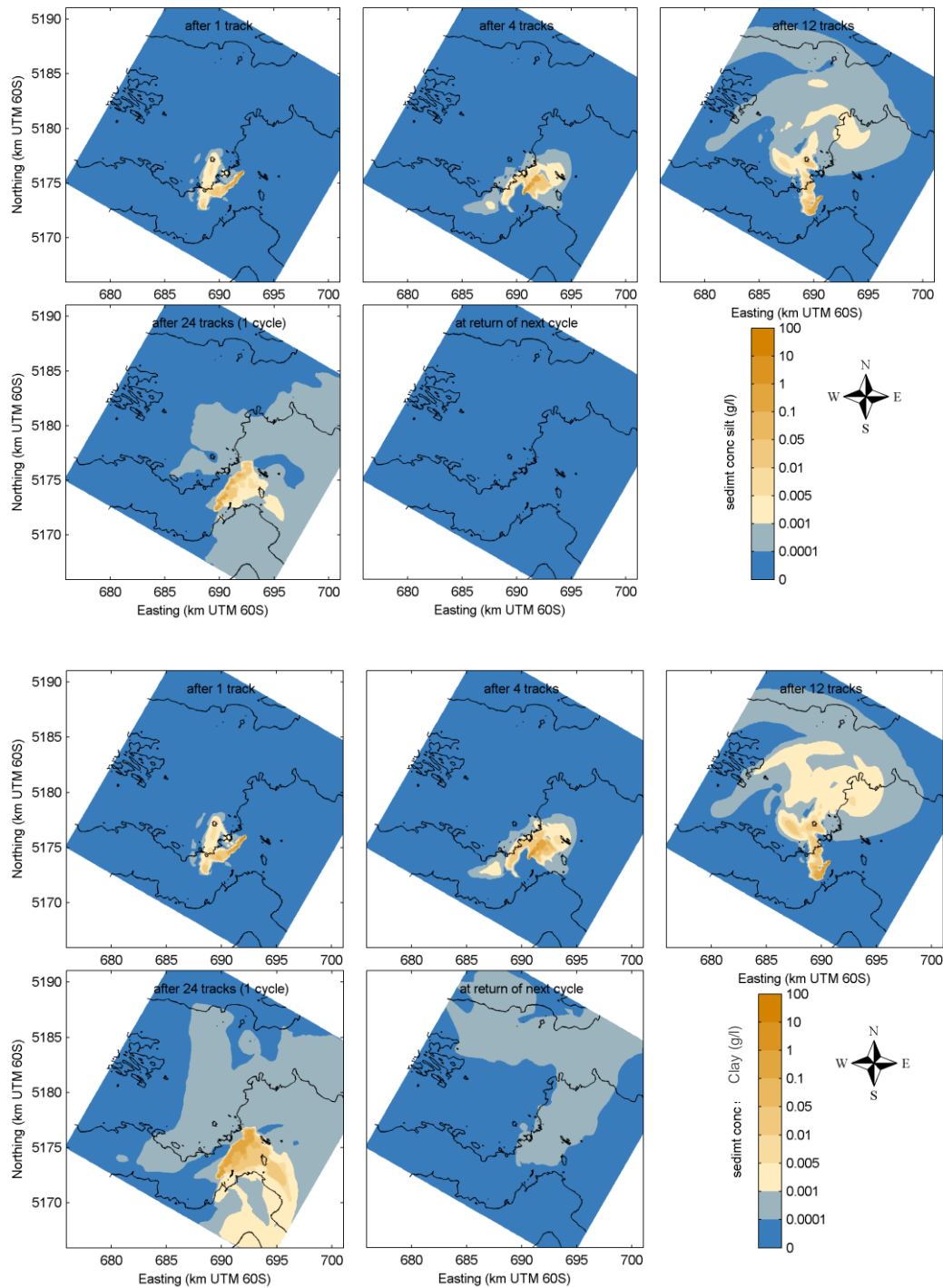


Figure 3.21: **SSC-maps – snapshots** Overview of the **near-bed** (bottom grid cell) suspended sediment concentration (g/l) of the **silt (top)** and **clay (bottom)** in **South domain – summer for discharge at the bed**. Snapshot times: over 1 completed track line, 4 track lines, 12 track lines, a complete cycle, and at the start of a new cycle (=5 days after mining stopped).

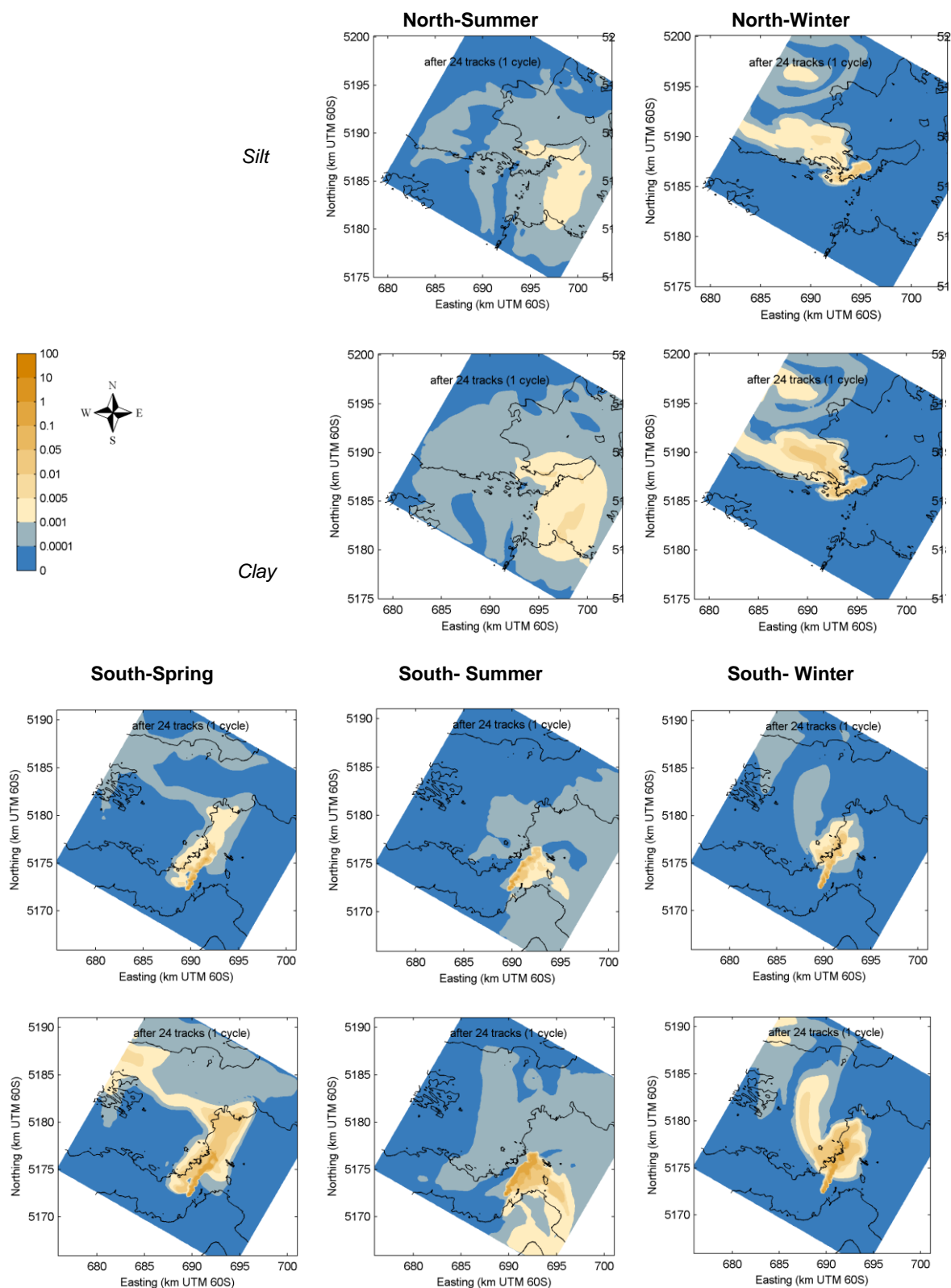


Figure 3.22 Seasonal variation in near-bed suspended silt (upper) and clay (lower) concentrations (g/l) at the end of a single mining cycle in the Northern and Southern model domain for discharge at the bed. Spring, Summer and Winter scenario. Northern domain Note that for this model domain the Spring scenario is not available

Threshold exceedence maps

Figure 3.23 illustrates for the Northern domain-Summer scenario, the percentage of time that the maximum concentration of the silt and clay concentration over the height over the water depth exceed 1 mg/l, 10 mg/l, 30 mg/l and 50 mg/l. It reveals the following representative characteristics:

- Outside the approximately 2 km-wide mining areas, the concentrations do not exceed 50 mg/l.
- Sediment concentrations higher than 10 mg/l are only observed in the direct vicinity of the track line up to 20 % of the time in a confined area. The area where 10 mg/l is exceeded roughly equals the 1-5 mm sedimentation contour (Figure 3.27, section 3.3.2) and is limited to the area directly adjacent to the track line (with a slight northwest bias for the spring and winter simulations, and more equally northwest-southeast for the summer simulations).
- Low concentrations of fine suspended sediment, 1-10 mg/l, appear to remain for a relatively long time in the model domain (50% of the time during the simulation period).

The plots for the threshold level of 1 mg/l most obviously reveal the pattern of plume dispersion, both for clay and for silt. Therefore the next figures focus on this threshold level.

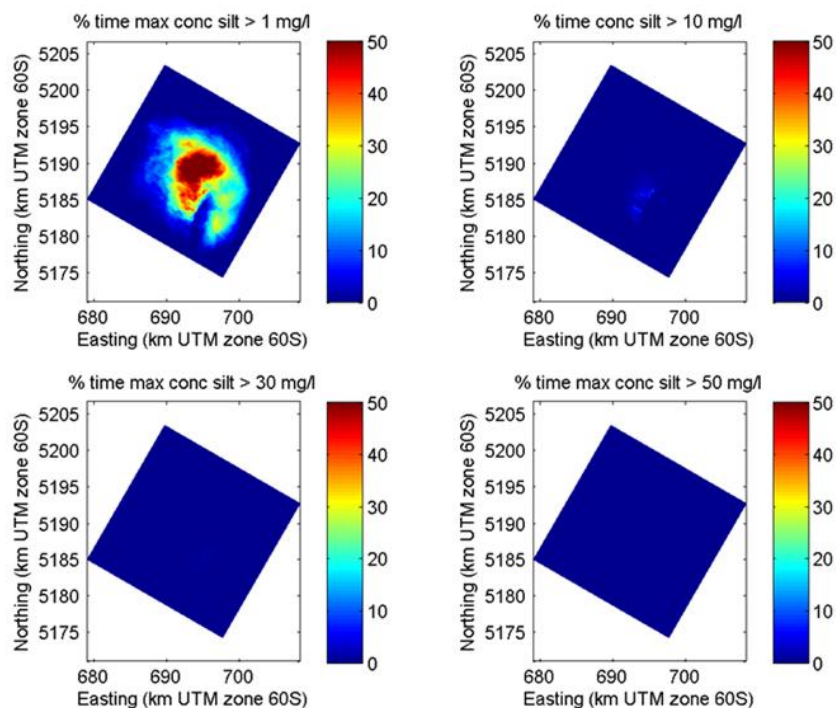
To further illustrate the extent of vertical dispersion in the water column, Figure 3.24 shows exceedence plots for silt and clay concentrations larger than 1 mg/l at 10 m and 50 m above the bed, together with the concentrations over all affected layers from the previous Figure 3.23. It can be seen that: 1) concentrations rapidly decrease with increasing height off the seabed and 2) the 'maximum concentration over the water depth' refer to concentrations in the lowest 10 m of the water column.

Therefore, Figure 3.25 summarizes the percentage of time that the maximum suspended silt and clay concentrations over the height of the water column exceed 1 mg/l, for all three seasonal scenarios in the South model and the North model. This Figure reveals the following phenomena:

- Concentrations of 1 mg/l are exceeded throughout much of the mining cycle.
- For the silt fraction, this area (exceeding 1 mg/l) mostly remains within the Local model domain.
- For the clay fraction, especially in the Summer scenario, this area extends beyond the model boundaries. It is important to note therefore, that these boundaries only allow outflow, therefore once the sediment leaves the model domain it can no longer return to the model domain, which results in a slight underestimation of total concentration at the end of the mining cycle.
- Differences in plume dispersion are most apparent in the North domain, with relatively strong dispersion in the Summer scenario. In the Southern domain these seasonal differences are much less pronounced, pointing at spatial variations in addition to temporal variations.

Appendix V2-C gives graphs as in Figure 3.21 and Figure 3.23 for both the North and the South domain and the three considered seasonal scenarios and reveals similar observations.

Silt



Clay

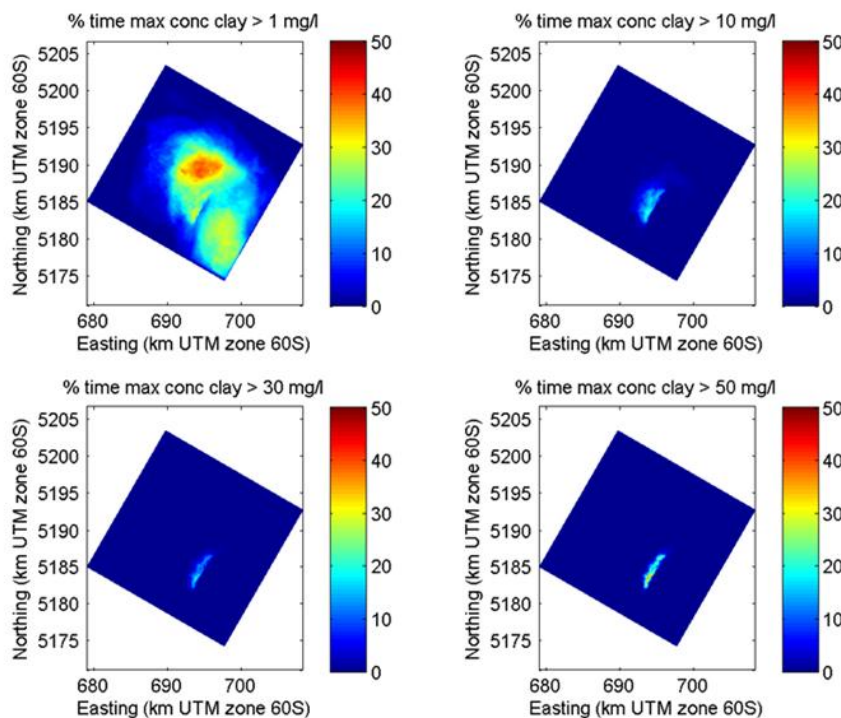


Figure 3.23 **Threshold maps SSC.** Overview of the % time (of the mining cycle) that the observed **maximum SSC** suspended **silt** and **clay** concentration **looking up into the water column** exceeds 1 mg/l, 10 mg/l, 30 mg/l and 50 mg/l for discharge at the bed - **Summer North domain**

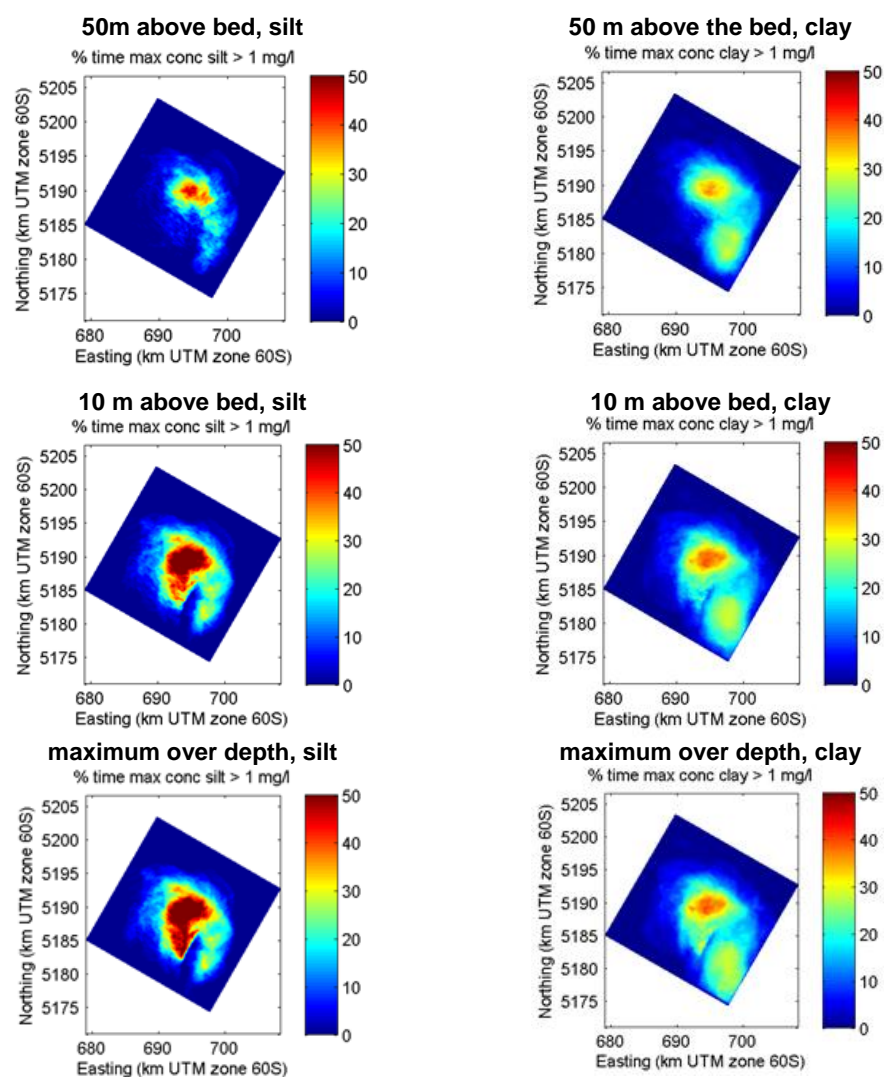


Figure 3.24 Overview of the % time (of the mining cycle) that the observed **SSC** suspended **silt** (left) and **clay** (right) concentrations at **50m** (top), **10 m** (middle) above the bed and looking up into the water column (bottom), exceed 1 mg/l for discharge at the bed. **Summer North domain**

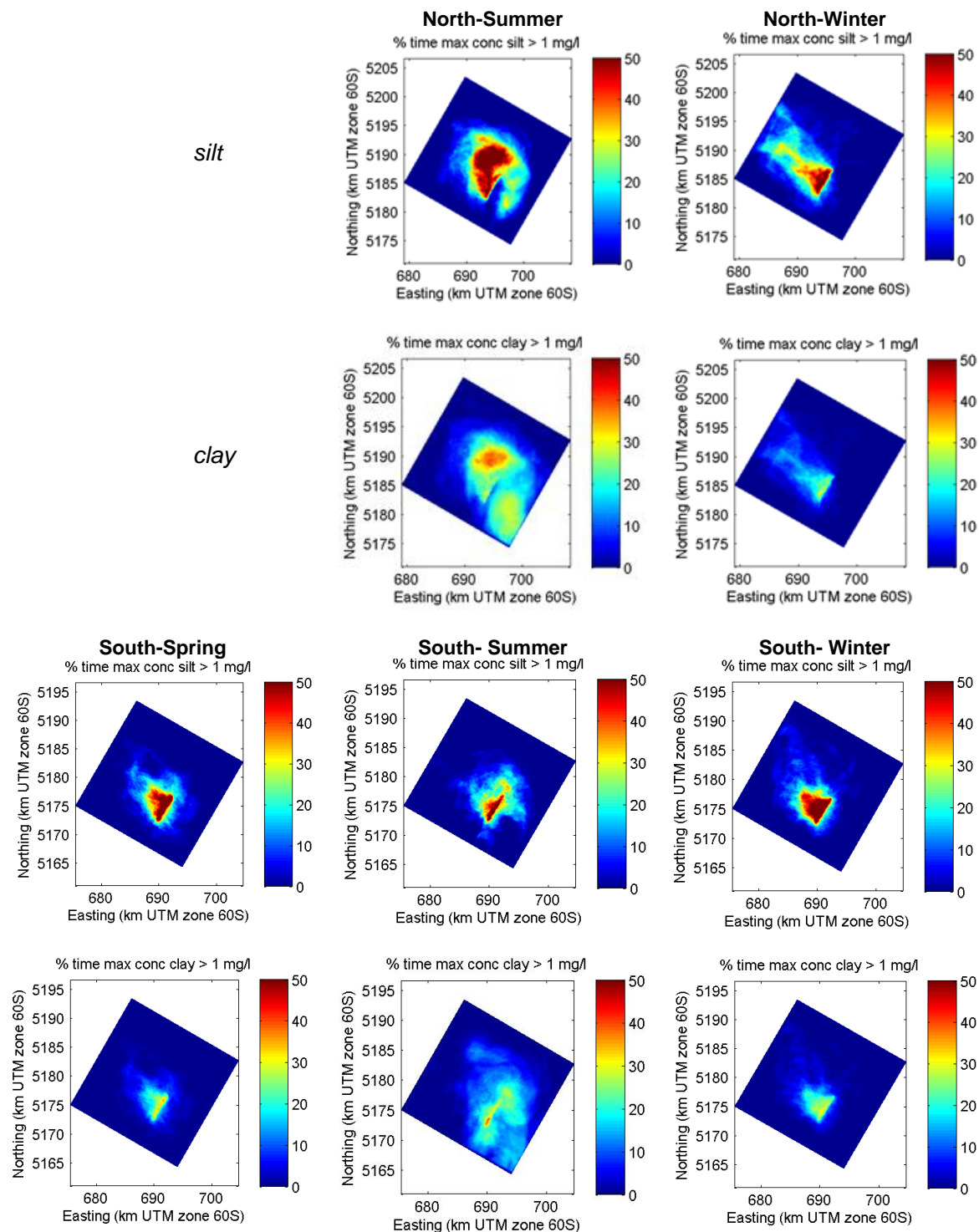


Figure 3.25 Overview of the % time (of the mining cycle) that the observed **maximum SSC** suspended **silt** and **clay** concentration exceeds 1 mg/l **looking up into the water column** for 3 seasonal scenarios in the northern and southern Local Model domains for discharge at the bed. Note: for the northern domain no spring simulation results are available.

3.3.2 Sedimentation

Figure 3.26 illustrates the development of the fine sediment (silt and clay) deposition over the course of one mining cycle for the South domain in summer (Appendix V2-C contains snapshots for other seasons and both model domains). Figure 3.27 summarizes the results using the total sedimentation of the silt and clay fractions at completion of the mining cycle (including return time) in all seasonal scenarios and for both the North and South domain.

All simulations show comparable results in terms of total sedimentation magnitude. The sedimentation is expressed in [m] deposited sediment layer thickness or height. The darkest colour represents 0.1 m of sedimentation, brighter red 0.01 m and the predominately yellow colour 0.001 m (less than 1 mm) of sedimentation. The sedimentation mainly occurs along the mining track. The mean depositional height varies between 0.10 and 0.15 m, with small local peaks up to 0.20 m. Note that this sedimentation comes on top of the sand deposition, which is concentrated in an approximately 10-15 m wide path, directly behind the diffuser: thickness of this deposit is in the order of 0.1 to 0.2 m.

In comparison to the large deposition within the mining discharge area, outside this area deposition values are small (note the non-linear scaling in the colour schemes). The sedimentation profile shown in Figure 3.28 clearly illustrates the peak in deposition along the track lines, and rapid decay on both sides. For the North domain winter simulation, sedimentation reduces to below 0.01 m within the first kilometre of the track line. Similar conclusions can be drawn from the analysis of the other scenarios; the 0.01 m sedimentation contour extends on average 1 km to the northwest and 500 m to the southeast. In general, the sedimentation pattern shows a northwest bias during winter and spring. The summer simulation shows more sedimentation to the south-southeast of the mining area.

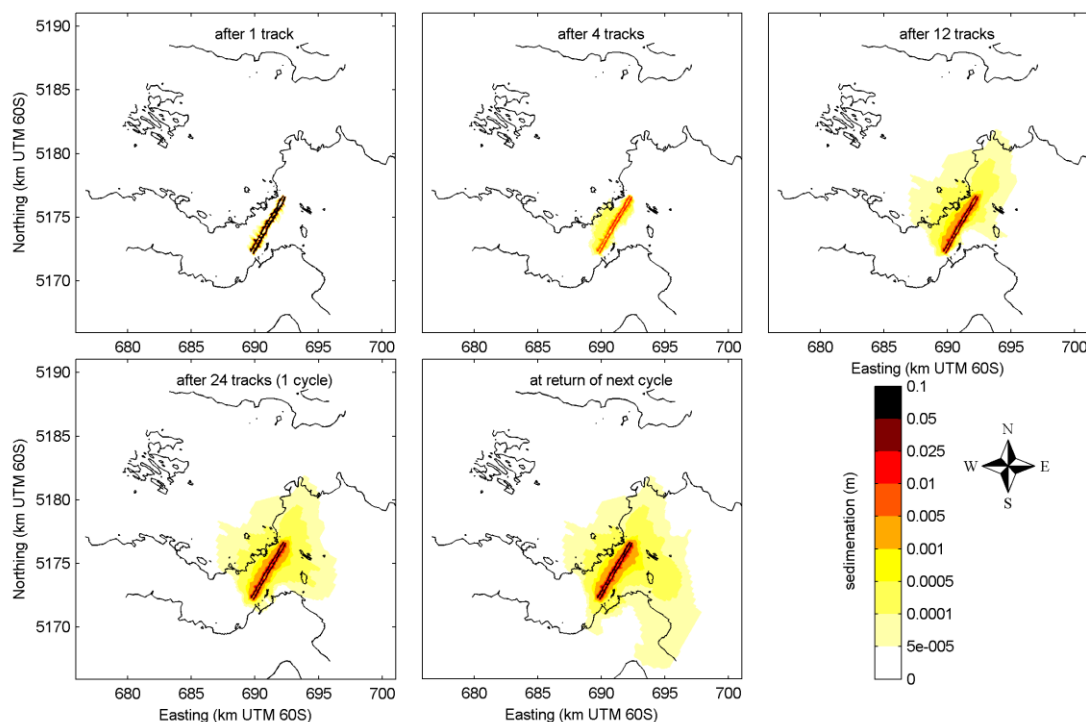


Figure 3.26 Snapshots of sedimentation over a mining cycle for discharge at the bed. **South domain – summer**

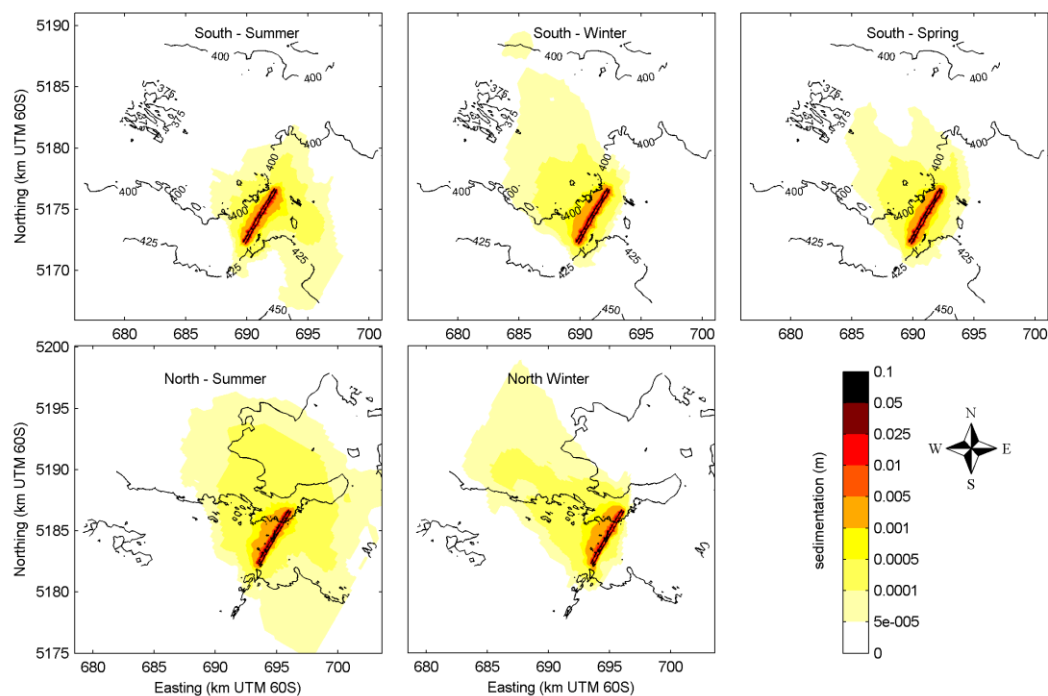


Figure 3.27 Total sedimentation of silt and clay after one mining cycle showing both spatial and seasonal variations for discharge at the bed.

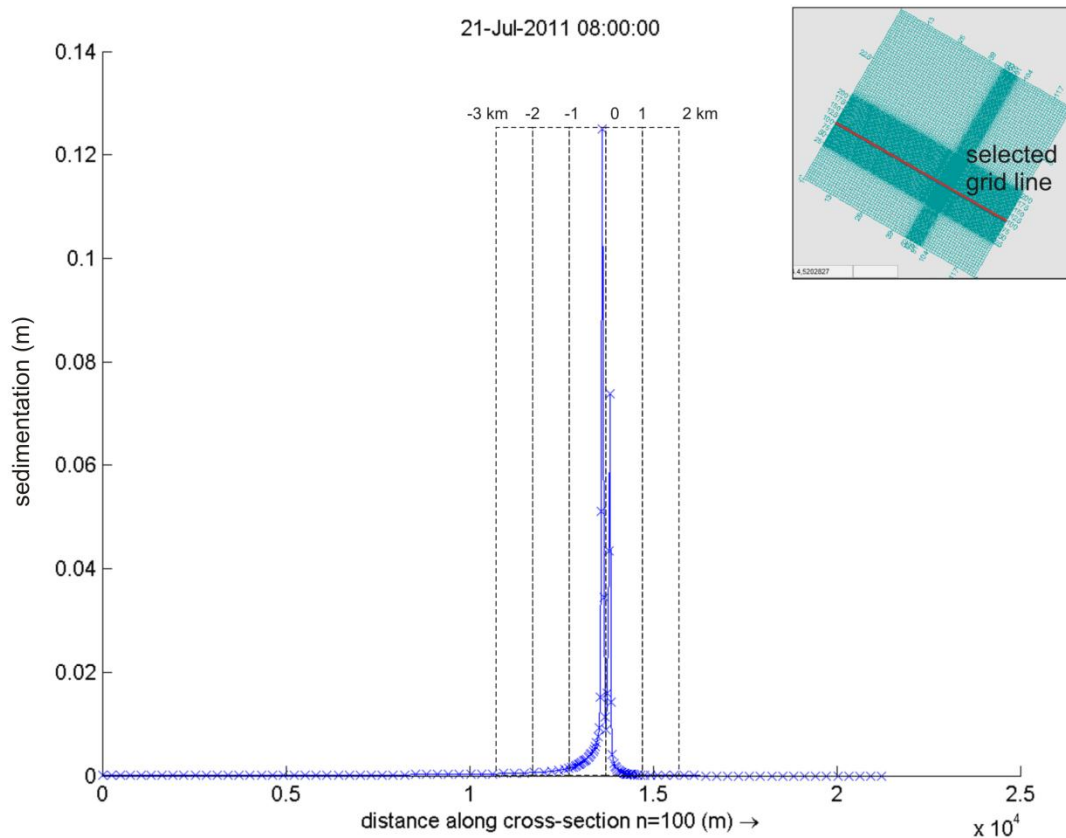


Figure 3.28 Profile (25 km) of total sediment (silt+clay) accumulation (m) over 1 completed cycle (insert shows location of grid line) for discharge at the bed. North domain – Winter.

Model simulations – Initial Investigation - main outcomes

As part of phase 1a, the near-field mine tailing plume development was investigated using Jet3D for the two base discharge scenarios, as defined by Boskalis. Based on calculations of the plume made using Jet3D suitable settings were chosen to provide input for the Delft3D model – phase 1b.

Results of the near-field plume modelling (Phase 1a) using Jet3D show that the plume, when released at 200 m above the bed, transports the sediment, including the fines, to the seabed very quickly, regardless of the individual fall velocities of the various grain sizes. Flow velocity and sediment concentration of the near-field mine tailing plume quickly decrease as a function of distance from the release point. Only coarse particles will settle faster than the plume (sand and gravel) and only a minor fraction of the plume will be entrained in the water before it has reached the seabed (stripping). However, the effect of stripping is neglected. It is predicted the plume will result in a suspension layer near the bed after the plume contacts the bottom. In this suspension layer, the fine silt fractions will settle over wider areas however, the very fine colloidal or clay fractions (finer than 2 μm), are not likely to settle.

Based on these results it was decided that mine tailings should be disposed of near or at the bed to minimize plume dispersion effects. Therefore the subsequent initial investigations of Phase 1b, as well as the optimized investigations of Phase 2, considered mine tailing release at the sea-bed and 10 m above the sea-bed. Additionally, an initial comparison of simulated and measured far-field flow velocities was made using moored RDI ADCP current data. Finally, model sensitivities for key physical factors were tested.

Results of far field modelling (Phase 1b) show that during periods of active mining high sediment concentrations occur along the mining track. Most of these sediments (both the clay and silt) directly deposit along the track line (as can be observed from the sedimentation footprints). A minor part is picked up by the flow and transported throughout the model domain, with maximum dispersion occurring near the end of mining. During the 5-day break in mining, the plume silt and clay concentrations in the entire model domain drop below 0.1 mg/l and 1 mg/l respectively. Sedimentation of silt and clay occurs mainly along the mining track. The mean depositional height varies between 0.10 and 0.15 m along the track, with small local peaks up to 0.20 m. Outside the mining track deposition heights are very small, less than 0.001 m. In addition:

- Plume dispersion tends to occur in a predominantly northern to north-western direction.
- Plume spreading is largest in the Summer scenario. The finer clay fraction is subject to a larger dispersion than the silt fraction.
- Suspended sediment concentrations rapidly decrease with increasing height off the seabed

4 Model Simulations – Optimized Investigation - Suspended Sediment (Phase 2)

4.1 Single Cycle Simulations – Disposal at the bed

4.1.1 Spring

The optimized single cycle simulations presented in this chapter and the next chapter (5) differ in a number of ways when compared to the simulations presented in the previous Chapter. Here an optimized model is used. This means that with respect to the previous model there are the follow differences:

- Improved grain size settings (see Table 2.2)
- A different mining cycle definition, i.e. 4 days of mining instead of 3 days (Table 2.5 and Table 2.2). The mining location is located roughly 10 km from the mining area in the South Model of Phase 1b.
- The horizontal model size has increased and the horizontal resolution decreased to 75 x 75 m around the mining area.

Hence results for the simulations presented in this section cannot be directly, i.e. in absolute terms, compared to results presented in the previous Chapter.

As before, three different types of plots are used to visualize the far-field dispersion of the mine tailing plume for a single mining cycle in spring, summer and autumn:

- Maps of the near-bed (bottom grid cell) fine suspended sediment concentration (silt and clay) (in g/l) after 1, 4, 12, 24 tracks and at the start of a new cycle (end of the transition time). The transition from light blue to light brown is at 1 mg/l (0.001 g/l). Maps illustrating the percentage of time that the maximum suspended silt and clay concentration over the height of the water column and the disposal and transit period (8 days in total) exceed a defined threshold. The four considered thresholds are: 1 mg/l, 10 mg/l, 30 mg/l and 50 mg/l. Maps for these four threshold levels are included in Appendix V3-A. These maps show that outside the mining area, suspended sediment concentrations hardly exceed 10 mg/l. Therefore the figures included in this chapter also focus on the threshold level of 1 mg/l. In these plots a light blue colour represents 20% of the time that the concentration is exceeded, yellow represents 30% of the time the concentration is exceeded and red represents 40% of the time when the concentration is exceeded.

Figure 4.1 and Figure 4.2 show these maps for the Spring scenario. They reveal the following observations:

SSC-maps

During active mine tailings disposal, highest near-bed sediment concentrations occur along the mining track during the entire mining cycle (Figure 4.1). Outside the mining area (2km-wide and 5 km long region, oriented northwest-southeast) the fine sediment concentrations decrease due to plume dispersion. During the considered spring conditions the plume disperses in a north-western direction. Silt and clay concentrations at the boundary of the Local Model domain are below 1 and 5 mg/l, respectively. These observations are largely in line with results of Phase 1b of study (South-Spring, Figure 3.21).

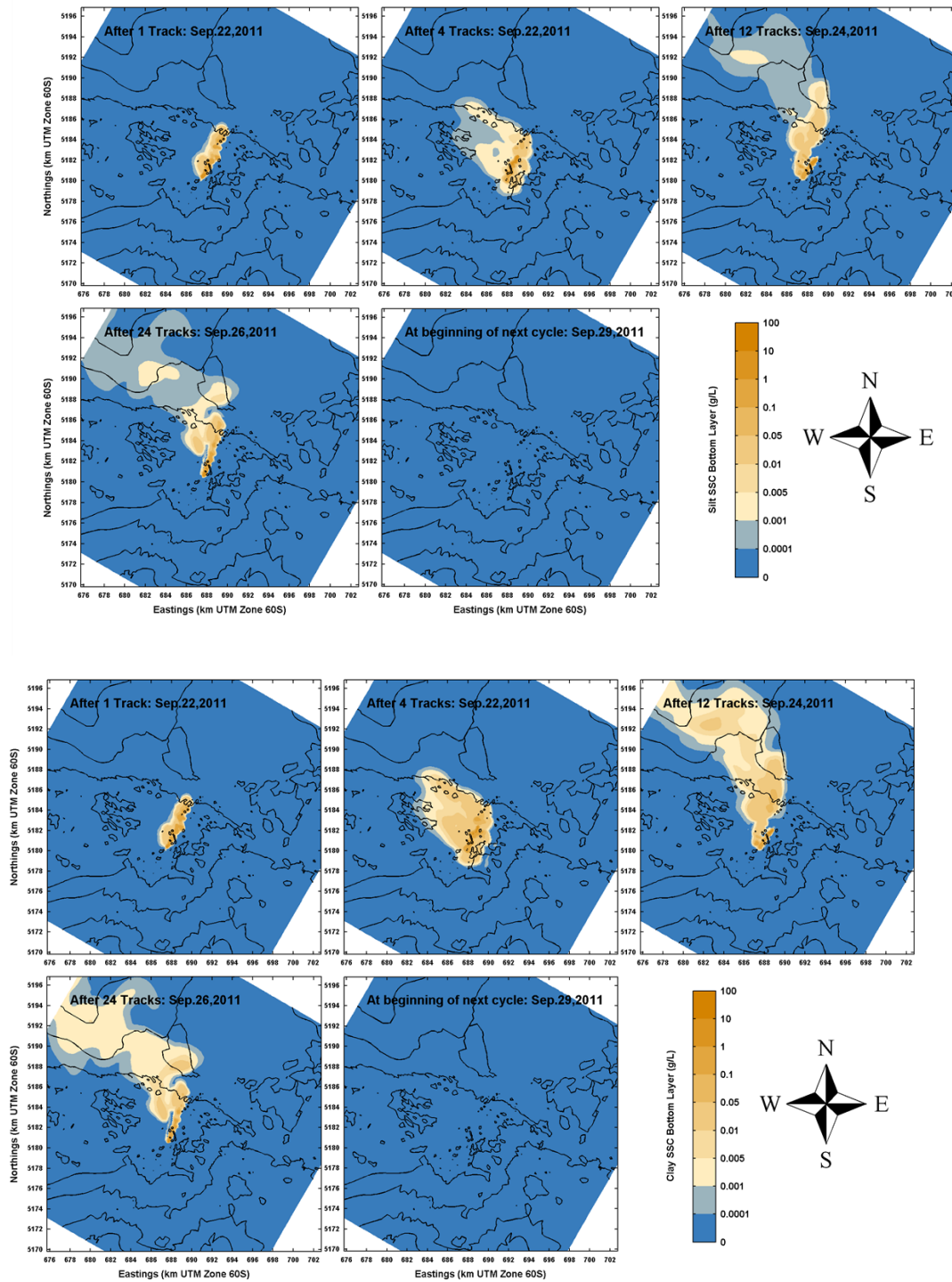


Figure 4.1: **Snapshots SSC-maps** Overview of the *near-bed* (bottom grid cell) suspended sediment concentration of the *silt* (top) and *clay* (bottom) fraction (g/l) over 1 completed track line, 4 track lines, 12 track lines, a complete cycle, and at the start of a new cycle (=5 days after mining stopped) for discharge at the bed. Local domain – **Spring**

Threshold-exceedence maps

Outside the mining area, the silt and clay concentrations are always below 50 mg/l (Figure 4.2 and Appendix V3-A). The highest values outside the mining area are along the edges of this area to the north and northwest of the mine tracks. Both inside and outside the mining area, suspended sediment concentrations decay rapidly to values below 0.1 mg/l, once mining stops limited resuspension of deposited sediment occurs over the course of one cycle. Note that resuspension depends on the model settings (specifically the critical shear stress for erosion), which are mostly supported by the findings of the Resuspension Study (Deltares 2014b). Towards the end of the simulation, or beginning of the new disposal cycle, suspended sediment concentration values have reduced to below 0.1 mg/l for silt and below 5 mg/l for clay. At 10 m above the bed, the suspended silt concentrations are always lower than 10 mg/l, whereas for the finer clay fraction this maximum concentration is 30 mg/l (Appendix V3-A).

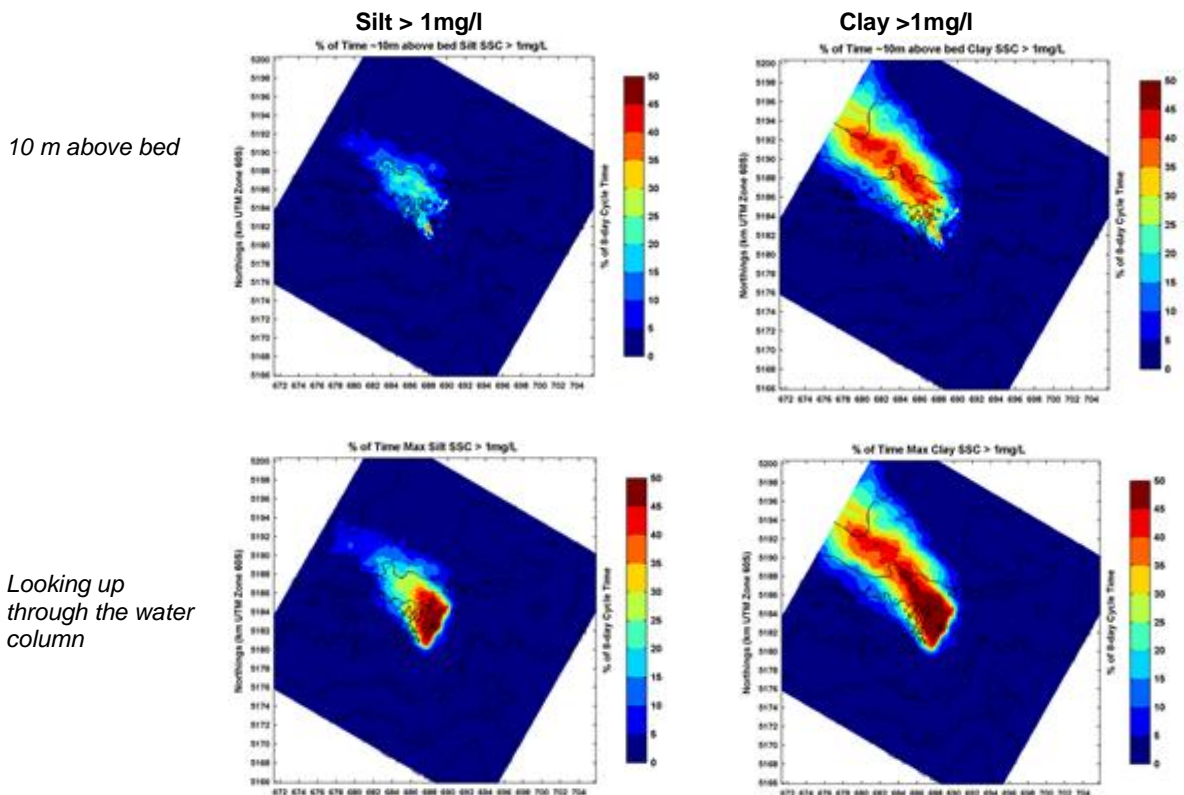


Figure 4.2 **1 mg/l - threshold maps**. Overview of the % time that the observed suspended sediment concentration of the **silt** (left) and **clay** (right) fraction exceeds 1 mg/l at 10 m above the bed (top) and for the max observed SSC looking up through the water column (bottom) for discharge at the bed. **Local Domain Spring**. Colour scale 0-50%, with 5% increment. See Appendix V3 for maps including 4 thresholds, 1, 10, 30 and 50 mg/l.

The next section present results for the Summer and Winter Scenario, focussing on how these scenarios differ from the spring scenario.

4.1.2 Summer

Figure 4.3 and Figure 4.4 show the maps characterising mine tailing plume dispersion in summer. Compared to the Spring scenario (Figure 4.1 and Figure 4.2) they reveal the following differences:

During the considered summer conditions the silt and clay plumes initially disperse to the southeast (track 4, Figure 4.3). As the mining proceeds the silt and clay plume gradually disperses in a North-western direction. Three days after the mining has concluded the silt concentrations dropped below 0.1 mg/l. The near-bed clay concentrations reach values up to 5 mg/l close to the bed, in both northwest and southeast directions.

Similar to the Spring scenario, the maximum silt and clay concentrations over the entire water column are always below 50 mg/l (Figure 4.4, Appendix V3-A). The threshold map for 1 mg/l and 10 mg/l show that clay concentrations range between 1-10 mg/l for a substantial period of time in a large area of the model domain, when compared to the silt concentrations (Figure 4.4).

Finally, Figure 4.5 shows representative time stacks of sediment concentrations over depth for two locations northwest of the disposal tracks: 1) iX Survey mooring and 2) a point southwest of the mooring location (based upon the Summer scenario). Higher sediment concentrations (greater than 25 mg/l) are only observed during the mining activities and within 10 m from the bed. Concentrations as high as 4 mg/l are predicted as high as 15 m and 25 m above the bed for the silt and clay fractions, respectively, while mining. However, during the transitional period (in between mining cycles), sediment concentrations reduce rapidly back to 0 mg/l (no background concentration in the model).

4.1.3 Winter

Figure 4.6 and Figure 4.7 show the maps characterising mine tailing plume dispersion in summer. Compared to the Spring and Summer scenario (previous two sections) they reveal the following differences:

The plume dispersion during the considered Winter scenario resembles the Spring scenario most, with a predominant plume dispersion in a north-western direction, albeit with slightly lower concentrations (cf Figure 4.6 with Figure 4.1).

The threshold plots also reflect the lower fine sediment concentrations during winter when compared to the Spring (and Summer) scenarios; outside the mining area clay and silt concentrations between 1-10 mg/l prevail considerably less long in the Winter scenario when compared to the Spring scenario (less bright colours indicating >30% of time, cf. e.g. Figure 4.7 and Figure 4.4 and Appendix V3).

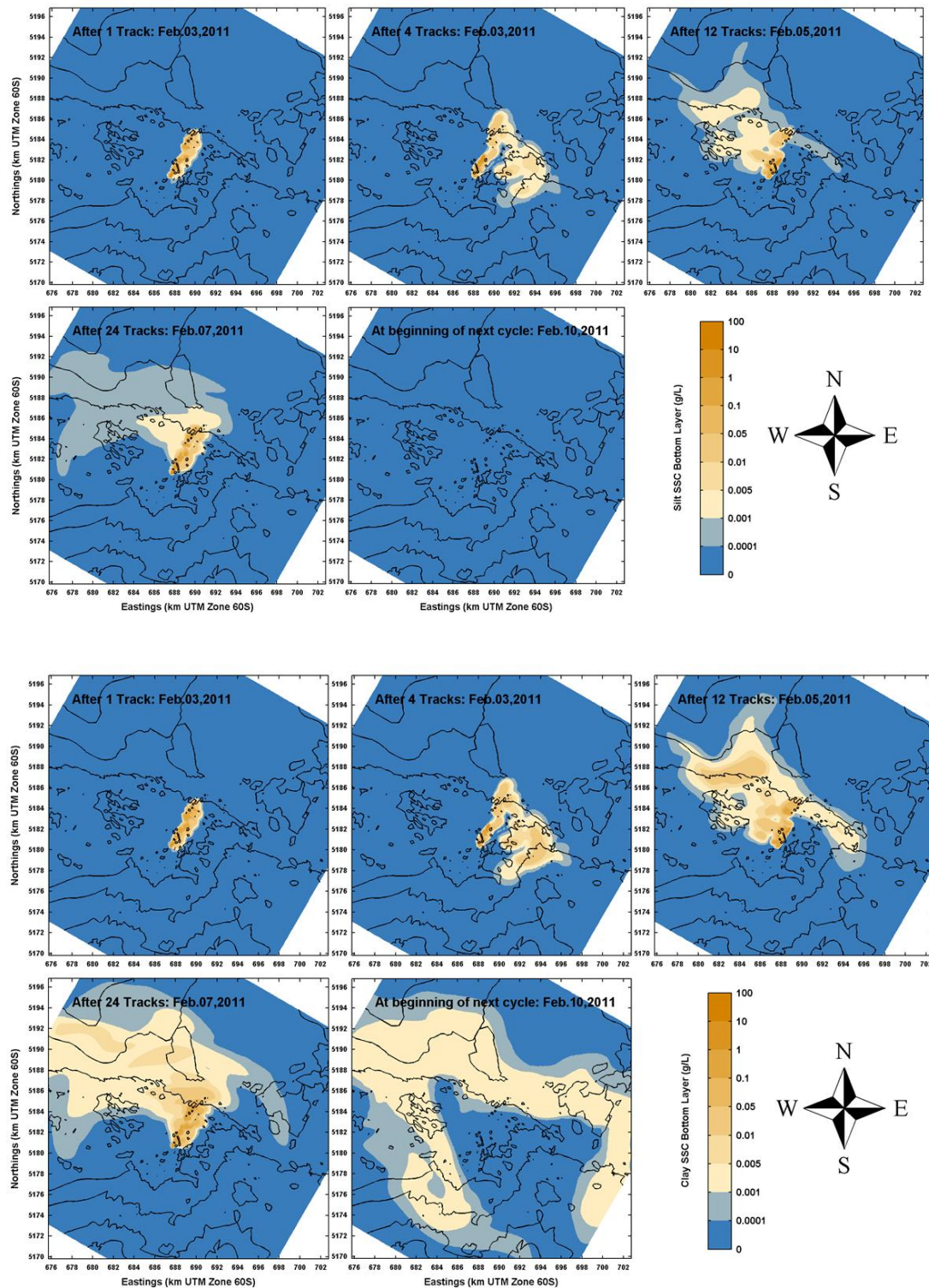


Figure 4.3 Overview of the **near-bed** (bottom grid cell) suspended sediment concentration of the **silt** (top) and **clay** (bottom) fraction (g/l) over 1 completed track line, 4 track lines, 12 track lines, a complete cycle, and at the start of a new cycle for discharge at the bed. **Summer**.

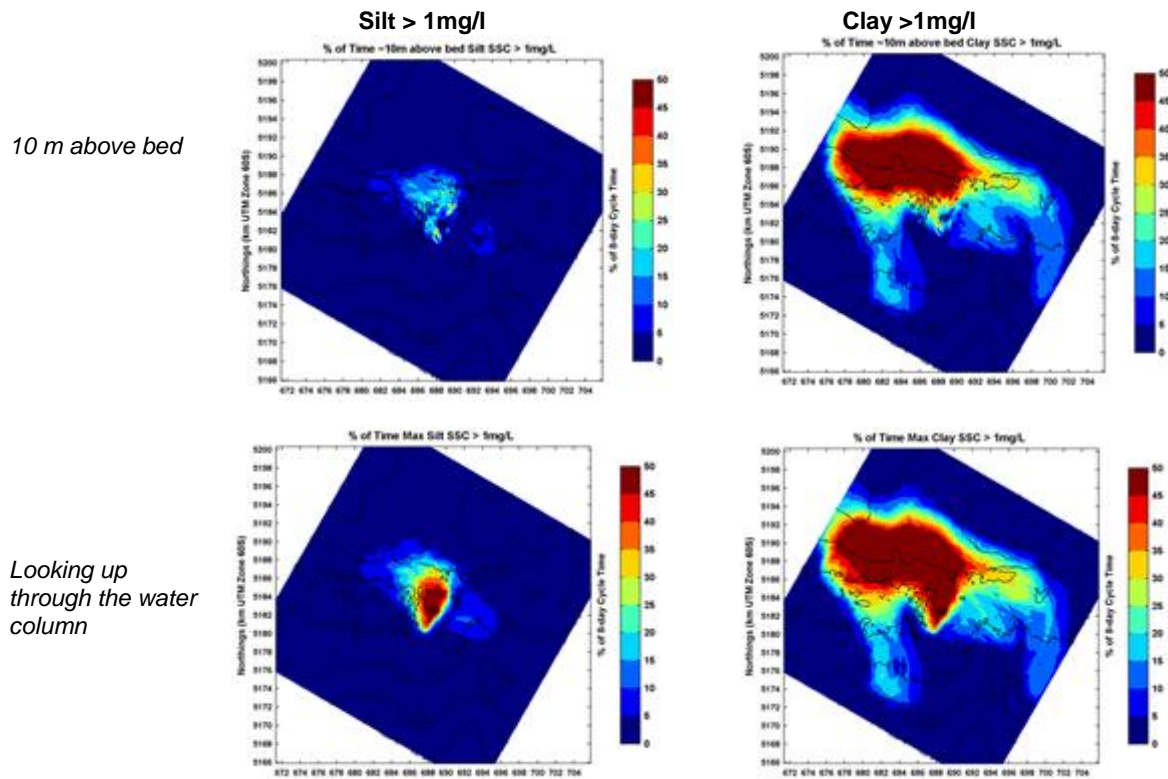


Figure 4.4 **1mg/l Threshold maps**. Overview of the % time that the observed suspended sediment concentration of the **silt** (top) and **clay** (bottom) fraction exceeds 1 mg/l (upper left), at 10 m above the bed and looking up into the water column for discharge at the bed. **Local Domain Summer**. Colour scale 0-50%, with 5% increment. See Appendix V3-A for maps including 4 thresholds, 1, 10, 30 and 50 mg/l.

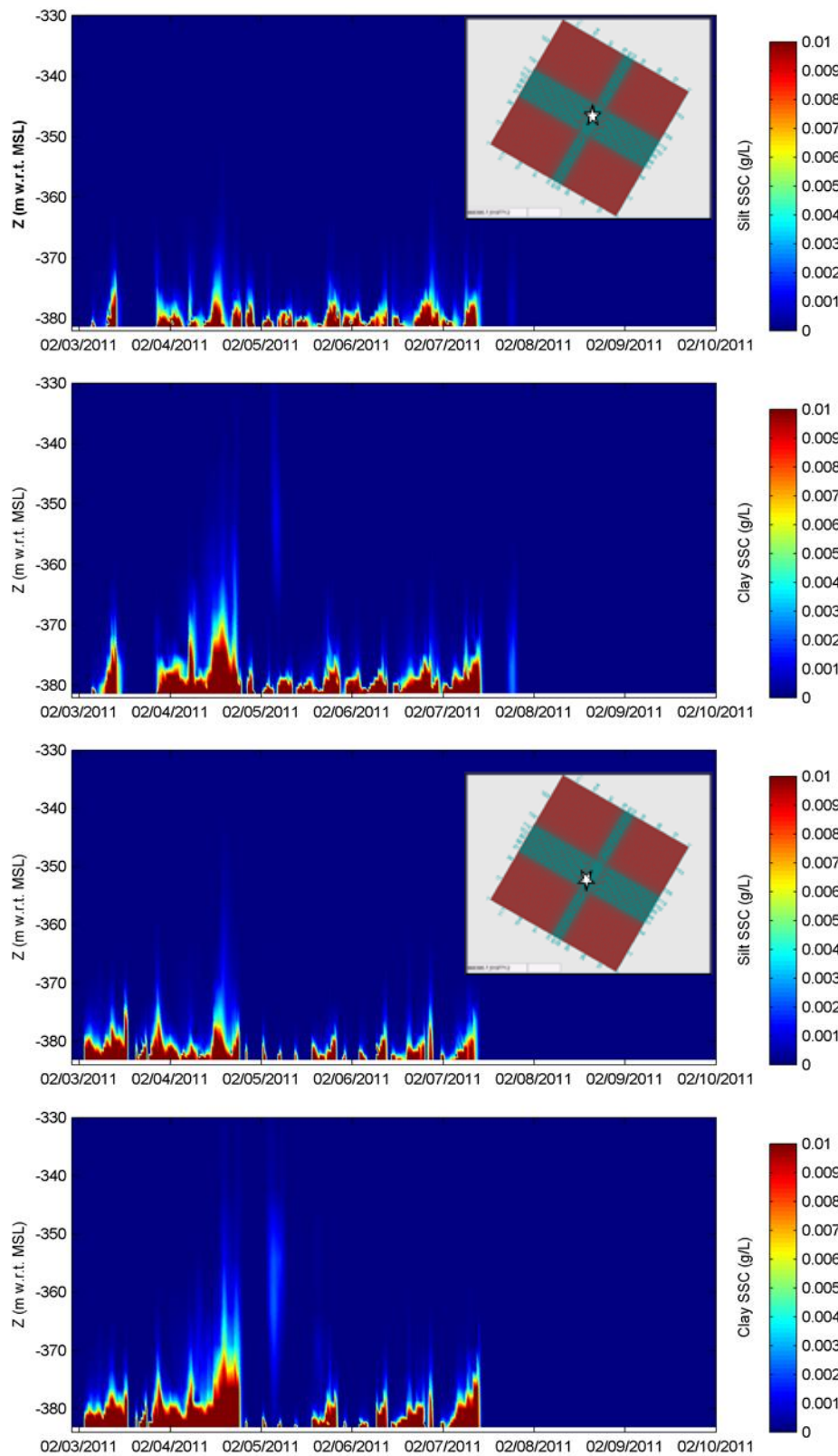


Figure 4.5: Timestack of modelled suspended sediment concentrations for the **Summer** scenario, just NW of **disposal tracks**, at the iX Survey mooring location in g/l for silt (top) and clay (top-middle) and SW of the iX survey location in g/l for silt (bottom-middle) and clay (bottom) for discharging at the bed. **Insert in top and bottom-middle panels show locations of observation points.**

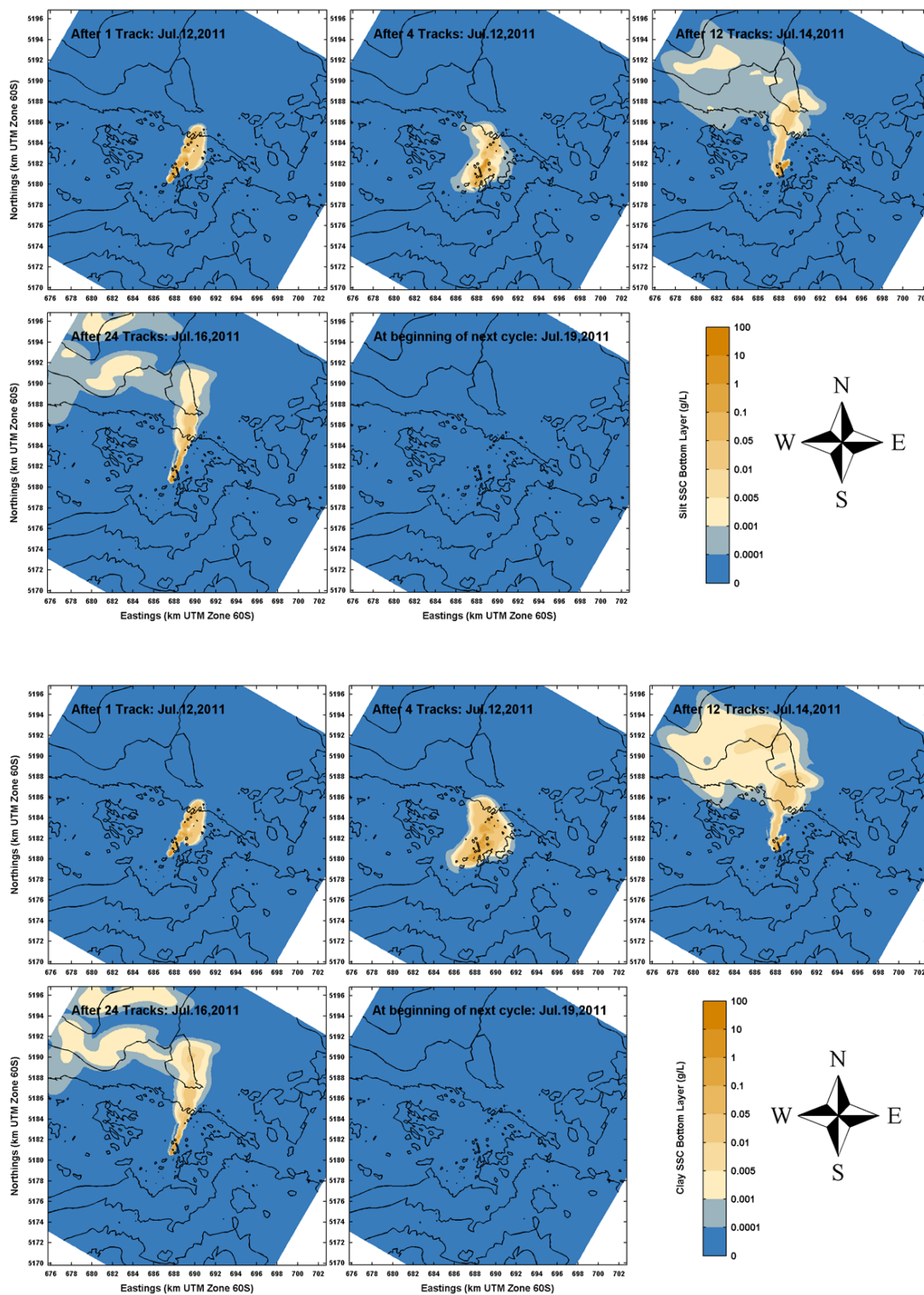


Figure 4.6: Overview of the **near-bed** (bottom grid cell) suspended sediment concentration of the **silt (top)** and **clay (bottom)** fraction (g/l) over 1 completed track line, 4 track lines, 12 track lines, a complete cycle, and at the start of a new cycle for discharging at the bed. **Winter**

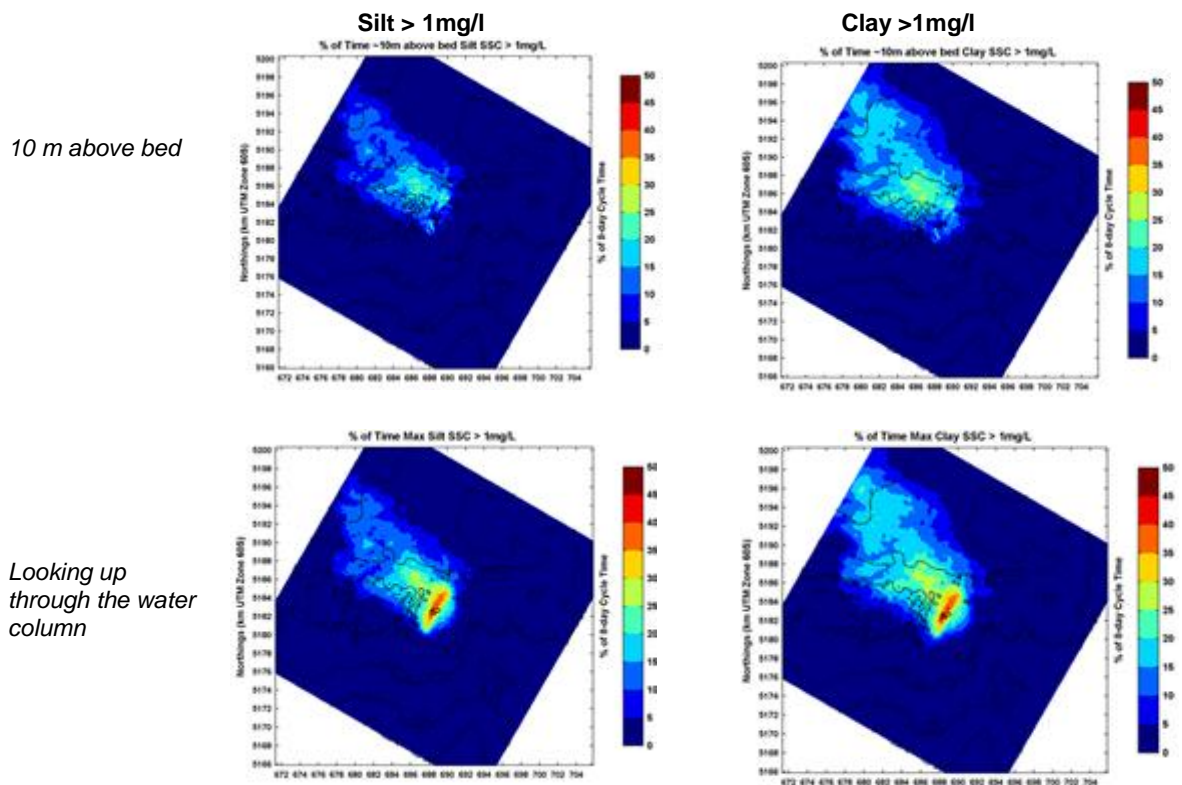


Figure 4.7 Overview of the % time that the observed suspended sediment concentration of the **silt** (left) and **clay** (right) fraction exceeds 1 mg/l, at 10 m above the bed and looking up through the water column for discharge at the bed. **Local Domain Winter**. Colour scale 0-50%, with 5% increment. See Appendix V3-A for maps including four thresholds, 1, 10, 30 and 50 mg/l.

4.2 Single Cycle Simulation - Disposal at 10 m above the bed

In the previous section of this chapter (Section 4.1), mine tailing plume dispersion has been investigated for mining operations with mine tailings discharged at the sea bed. From an operational as well as an environmental point of view it is desired to also gain a better understanding of mine tailing plume dispersion in case of discharging mine tailings at 10 m above the bed. This section therefore investigates this operational scenario for a single mine/disposal cycle using the Summer scenario. The Summer scenario was chosen for this single-cycle simulation because the largest vertical velocities are predicted during this simulation as compared to the Spring and Winter simulations, which in combination with the horizontal flows, results in the disposal plume remaining in suspension at higher concentrations for longer around the mining area.

For the scenario, with discharging at 10 m above the bed, the discharge into the model domain is through vertical layer 22. The method for prescribing the Delft3D input is similar to that at the bed scenario, for details see section 2.5.4.

Mine tailing plume dispersion for disposal at the bed and at 10 m above the bed is visualized using two compound plots (silt and clay, at bed and 10 m above bed):

- Maps of the near-bed (bottom grid cell) fine suspended sediment concentration (silt and clay) (in g/l) at the end of mining, after 24 tracks (Figure 4.8, for entire cycle snapshots of the 10 m above bed scenario, see appendix V3-B)
- Maps illustrating the percentage of time that the near-bed silt and clay concentration exceed 1 mg/l (Figure 4.9, for all 4 threshold values see Appendix V3-B).

Additionally, Figure 4.10 (section 4.2.3) shows time stacks of the concentrations at the ADCP mooring cycle for multiple cycles; the first cycle is subject of this section. These figures reveal the following phenomena:

When compared to disposing at the seabed, disposing mine tailings at 10 m above the bed results in higher but more localised suspended silt concentrations near the bed (Figure 4.8 and Figure 4.10). In contrast, the suspended clay concentrations remain slightly more elevated outside the mining area when disposing 10 m above the bed compared to when disposing at the seabed. This dispersion behaviour is in line with what can be expected.

The time exceedence patterns of the maximum silt and clay concentrations when looking up into the water column to all affected layers and at 10 m above the bed (one layer only) reveal similar general patterns, albeit with differences at a more detailed level as the sediment plume does not extend far up in the water column (Figure 4.9):

- The 10 m above bed scenario displays a larger area where 35-40% of time the near bed *silt* concentrations exceed 1 mg/l, pointing at slightly stronger plume dispersion than when discharge is at the bed. This observation is logical. A similar stronger dispersion pattern can be observed for the 15% of time area in the silt concentrations at 10 m above the bed.
- The pattern for silt varies more over the water depth than between disposal scenarios.

For the clay fraction the detailed differences are most obvious for the 15-20% time class. They however do not clearly point at a stronger dispersion or spreading of the plume. For the clay fraction the patterns varies more between the disposal scenarios than over the water depth

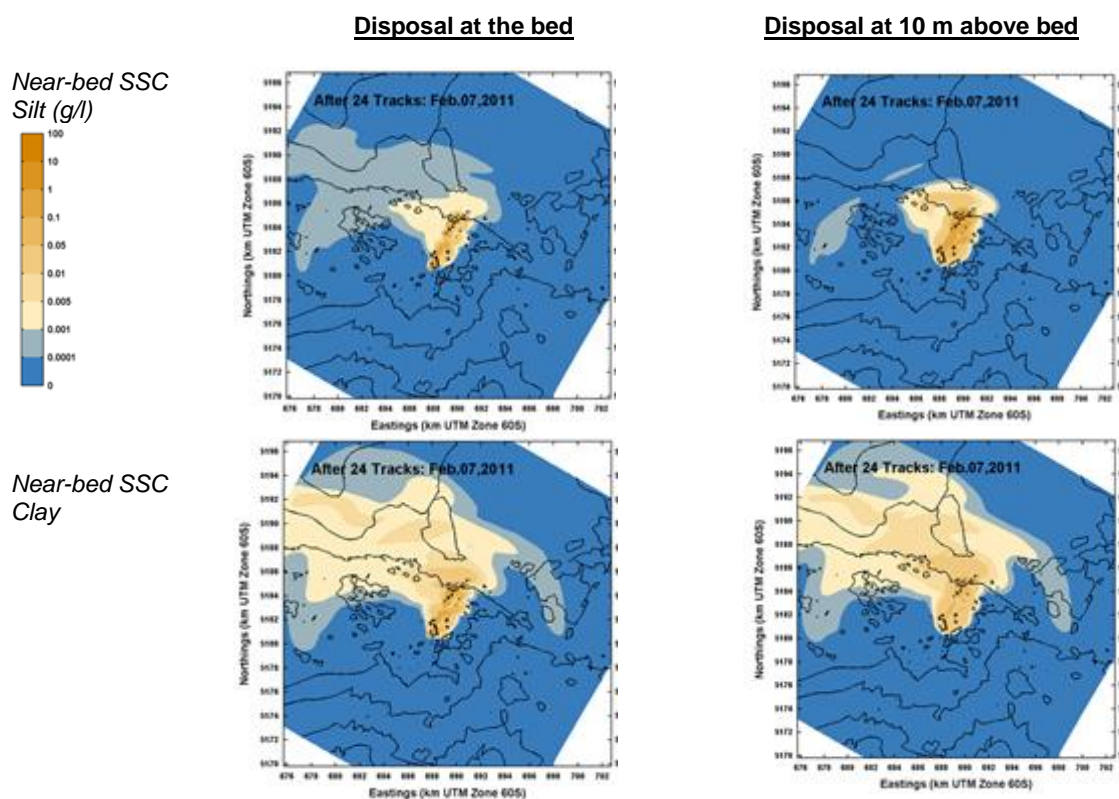


Figure 4.8 Plume dispersion showing effect of discharge release height – Near-bed (bottom grid cell) suspended sediment concentration of the **silt** (top) and **clay** (bottom) fraction at the end of mining (track 24) for disposing at the bed (left) and at 10 m above the bed (right). **Summer scenario disposal at the bed and 10 m above the bed**

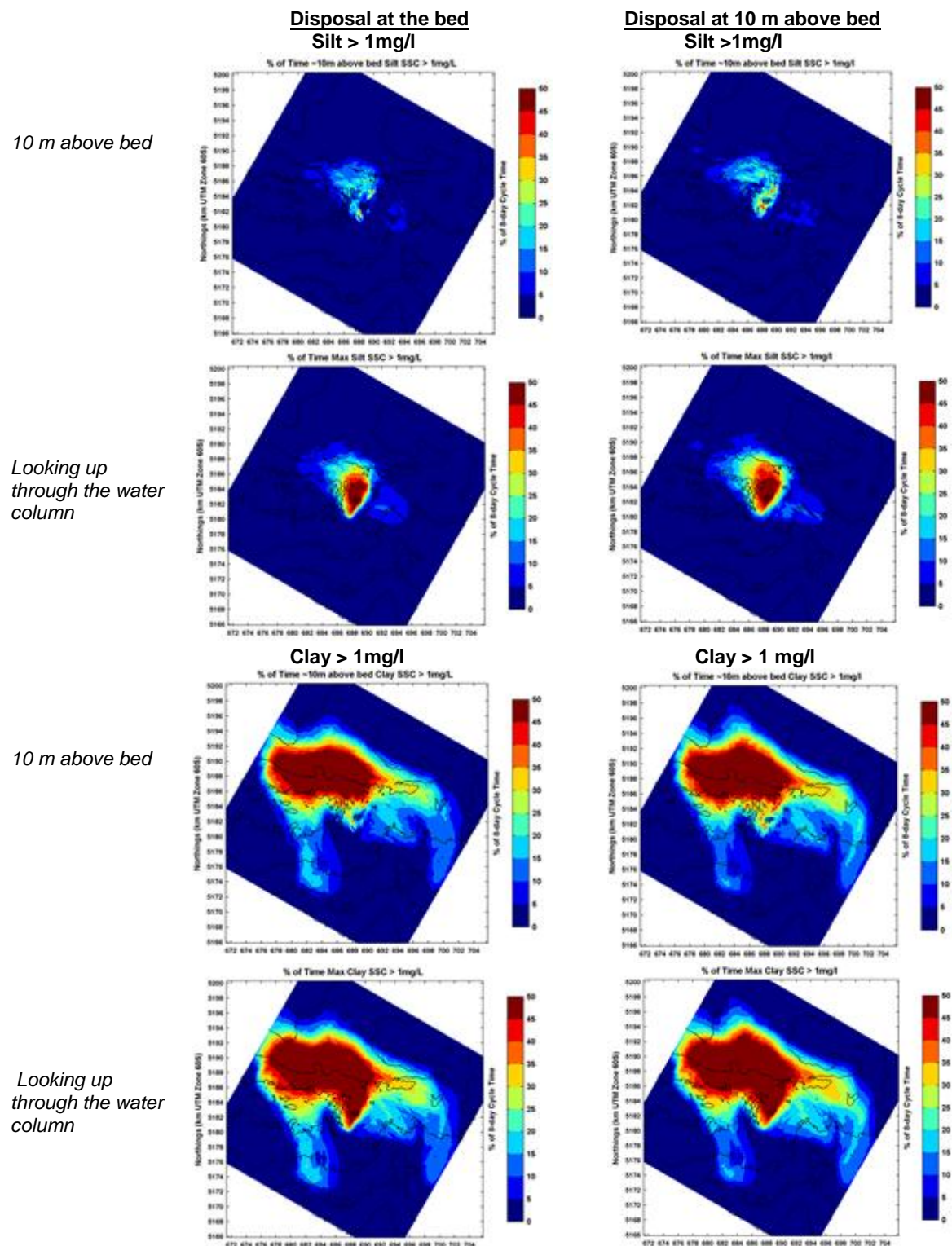


Figure 4.9 Overview of the % time that the observed (at 10 m) or maximum (over water column) suspended sediment concentration of the **silt** (top) and **clay** (bottom) fraction exceeds 1 mg/ for disposal at the bed (left) and at 10 m above the bed (right). **Summer**. Colour scale 0-50%, with 5% increment. See Appendix V3-A and V3-B for maps including 4 thresholds of 1, 10, 30 and 50 mg/l.

4.3 10-Cycle Simulations

Through the oceanographic study (Deltares, 2014a) and the seasonal scenarios (section 4.1), the variability of the hydrodynamic system in the proposed mining area has been illustrated, as well as the effect this variability has on the mine tailings plume fate and transport. Additionally, sections 4.2 (and later section 5.2) investigated the influence of the discharge release height (10 m above bed compared to at the bed), an important operational aspect, on mine tailings dispersion. In order to gain an increased understanding of how temporal hydrodynamic variability and discharge release height affect the longer-term mine tailings plume dispersion, a series of ten mining/disposal cycles were performed. More specifically, these scenarios are used to:

- 1 Assess and illustrate intra-seasonal variations in plume dispersion in the 2011 summer and 2011 winter period.
- 2 Obtain indications of cumulative effects of multiple mining cycles on plume dispersion, e.g. due to resuspension of fine sediments deposited during a previous cycle and/or settling of fine sediments in a subsequent mining cycle (i.e. uploading of suspended sediments).
- 3 Assess if and how the discharge release height influences the former two aspects.

This modelling approach is consistent with single cycle scenarios in that the Delft3D Regional Model is first run for the duration of the periods considered, i.e. July 10-September 30, 2011 for the winter period and February 1-April 23, 2011 for the summer period (Table 4.1). The Delft3D Local Model is nested within Regional Model, i.e. the Regional Model is used to generate time and space dependent boundary conditions for the Local Model.

A set of four 10-cycle simulations were investigated (Table 4.1). Two of the simulations investigated discharge at the seabed for summer and winter and approximately 10 m above the bed for summer and winter 2011. In these simulations, 82 days are modelled. This includes:

- Two days of spin-up on the first cycle, then 102.5 hours (approximately five days) disposal (i.e. mining), then 4.5 days of transit time (no disposal)
- For the second through tenth cycles, there is only the 102.5 hours of disposal followed by the three days of transit time
- First cycle begins with no available sediment within the domain (concrete bed approach) and a 0 mg/l background SSC (i.e. ambient SSC assumed 0 mg/l)
- The second through tenth cycles begin with the resulting mass of **fine** (clay and silt fractions) sediment at the bed (due to sedimentation) and SSC at the end of the previous simulation. Therefore, if resuspension does occur, not only the **fine** sediment being discharged during the current simulation can be resuspended, but also the **fine** sediment sitting on the seabed due to sedimentation in previous cycles.
- The track lines are moved outward by approximately 120 m per subsequently cycle. Therefore, the mine tailings disposal area for the 10 cycle simulations is a larger rectangular region approximately 5 km in length (parallel to the track lengths) and 2.65 km in wide (perpendicular to the track lengths).
- Like in all simulations only the fine sediment in suspension is modelled, i.e. no sand fraction included.

In addition to the figures presented in this report, plan view maps of the suspended sediment concentrations in the bottom layer (layer 30) can be found in Appendix V3-B.

Table 4.1 Four ten-cycle simulation information.

Simulation Name	Season	Time Frame (2011)	Discharge Location
Winter_DisSeabed	Winter	July 10-September 30, 2011	Seabed (Layer 30)
Winter_Dis10 m	Winter	July 10-September 30, 2011	~10 m above seabed (Layer 22)
Summer_DisSeabed	Summer	February 1-April 23, 2011	Seabed (Layer 30)
Summer_Dis10 m	Summer	February 1-April 23, 2011	~10 m above seabed (Layer 22)

4.3.1 Summer

Figure 4.10 shows the suspended silt and clay concentrations at the iX Survey mooring location up to some 50 m above the bed over the course of the ten mining cycles, including transition time. It reveals the following observations:

The differences in magnitude and vertical extent of the suspended clay and silt concentrations reflect varying hydrodynamics conditions. Suspended concentrations during the first cycle, the Summer scenario in this study, are smaller than during the other cycles. In the time stack figure this intra-seasonal variation is most obvious for the scenario with discharging at the bed. Some more detailed general information on suspended concentrations levels that can be observed in the time-stacks include:

- In case of disposal at the bed, silt and clay concentrations of 1 mg/l on average tend to occur up to about 5 m and 10 m above the bed, respectively. These concentrations are very low.
- Discharging at 10 m above the bed raises these depth levels some 5 m upward, to 10 and 15 m.
- Additionally, the number of short-lasting vertical extent peaks, with concentrations on the order of 0.1 mg/l reaching up to 50 m above the bed, occurs more frequently when disposing at 10 m above the bed. However 0.1 mg/l is so low that it will not be seen or measured in the water column.

Figure 4.10 also illustrates that the suspended silt material close to the mine tailings disposal location tends to dissipate completely in between cycles. The clay fraction also dissipates completely in between mining cycles, though there are transit periods during which concentrations remain above 0.1 mg/l off and on. However this value although numerically captured would not be visible in reality. For the considered summer period the suspended *clay* fraction is predicted to remain in concentrations, above 0.1 mg/l, at the end of the second, (sixth) and eight cycles, when the next cycles would begin. This indicates that these very low suspended clay concentrations could continue to remain locally in suspension, and thus potentially build up in concentration over time with each progressive mining cycle (sediment uploading behaviour) though concentrations will remain low. Figure 4.11 shows maps of the near-bed suspended clay concentrations in the transit time between cycles 2 and 3 and 8 and 9 for discharge at the bed. This therefore shows the suspended clay concentrations after mining in cycle 2 and cycle 8 has stopped. It indicates that cycles 3 and 9 started with locally elevated clay concentrations due to mining in the previous cycles. Similar plots for discharge at 10 m can be seen in Appendix V3-B. The fact that the clay concentrations in between subsequent cycles do not return back to 0 mg/l again, indicates that temporal uploading of the clay fraction may sometimes occur in the mining area.

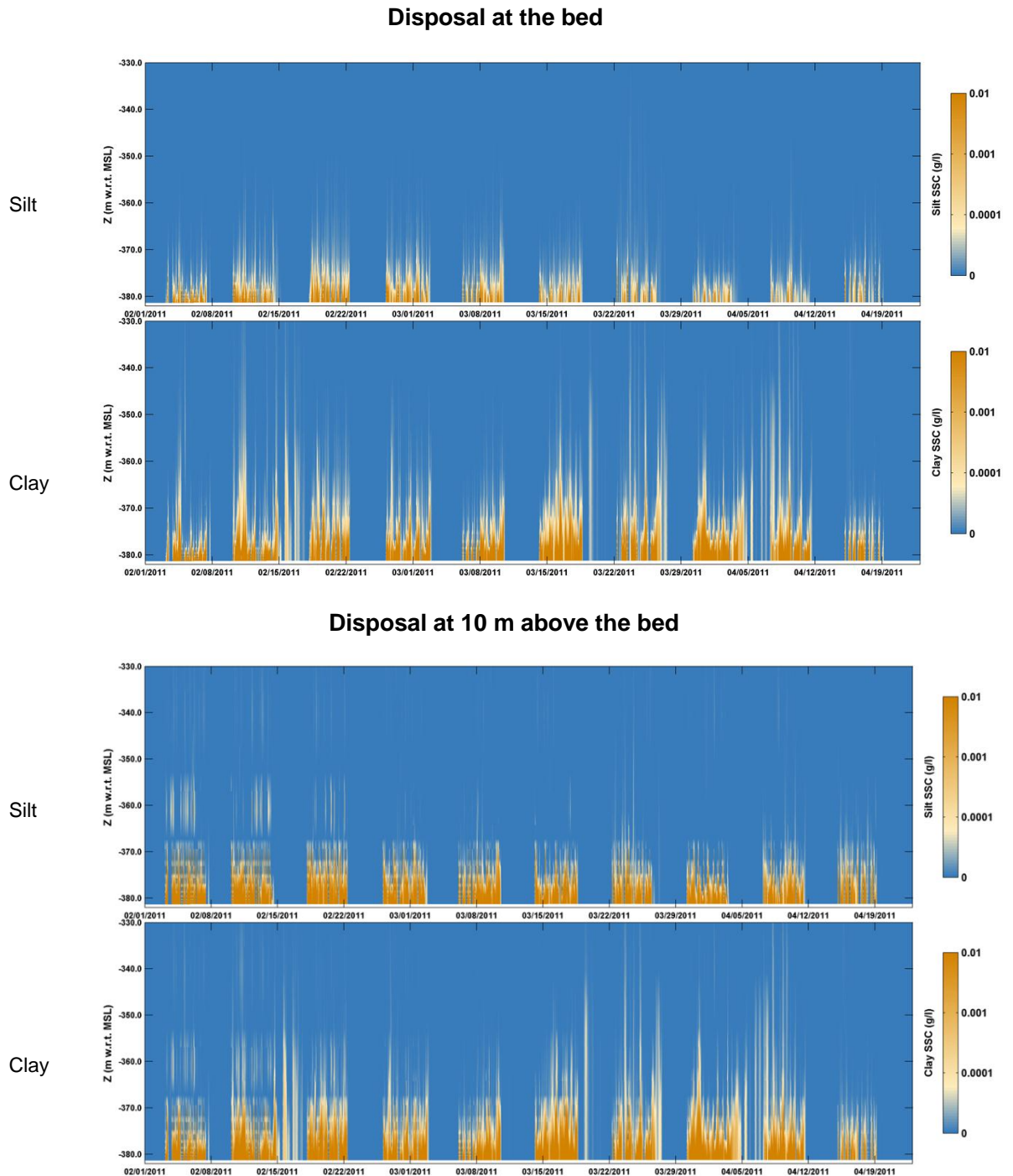


Figure 4.10 Time stacks 10-cycle simulation **Summer**. Time stack of suspended silt concentration (top panel) and suspended clay concentration (bottom panel) in the bottom 52 m of the water column at the ADCP mooring location for two operational scenarios: 1) discharging at bed (model layer 30, upper two panels) and 2) discharging at 10 m above the bed (model layer 22, lower two panels).

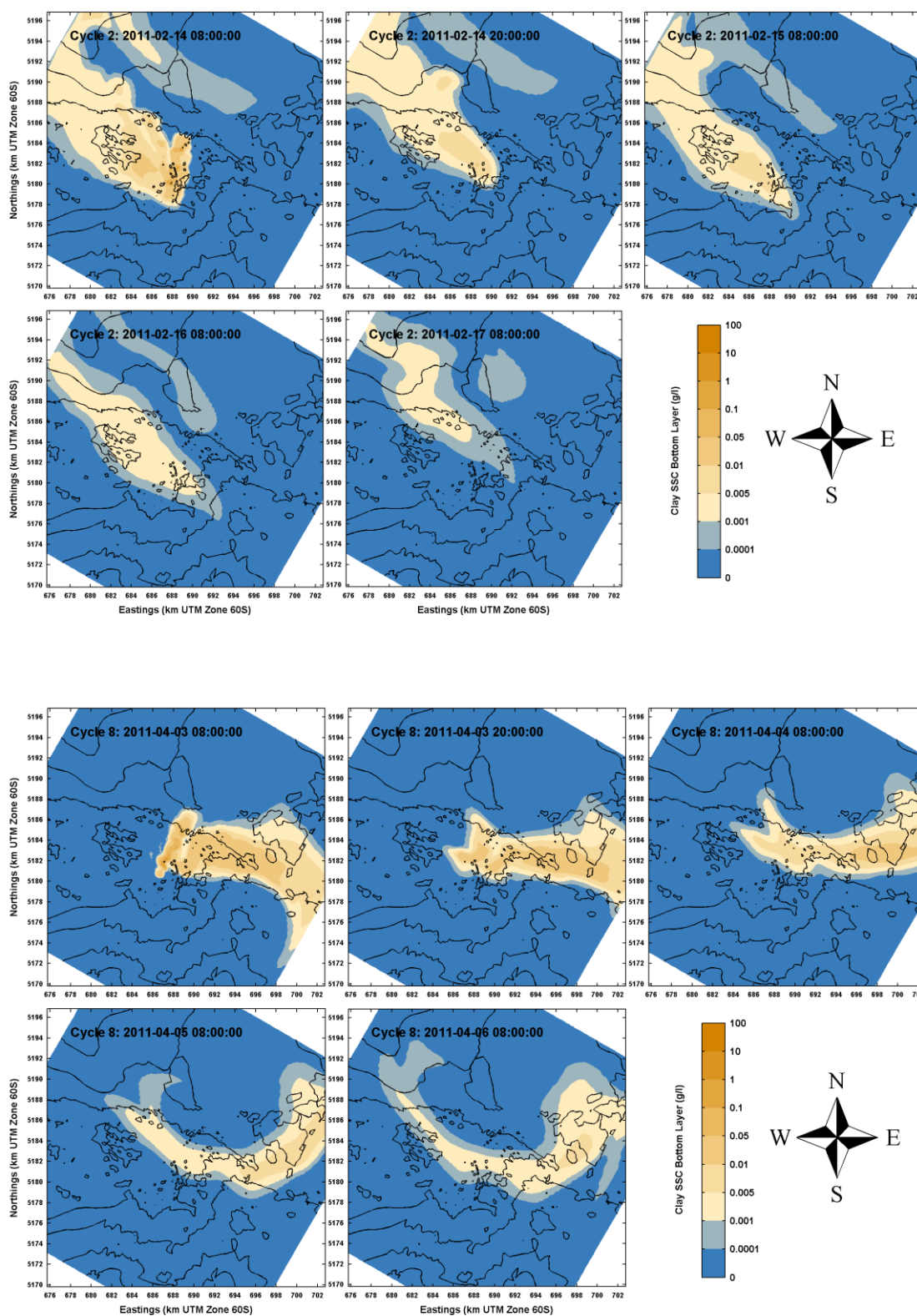


Figure 4.11 Cycle 2 (upper) and Cycle 8 (bottom) near-bed suspended clay concentrations during the 3-days break in mining, prior to commencement of a new mining cycle. **Summer, disposal at the bed.**

4.3.2 Winter

As for the summer conditions, Figure 4.12 shows the suspended silt and clay concentrations at the iX Survey mooring location for the 10-cycle simulations in winter. It reveals similar phenomena and characteristics, viz:

- Intra-seasonal variations in the suspended silt and clay concentrations;
- Compared to the Summer scenario, the suspended silt and clay concentrations due to sediment disposal are slightly higher for the Winter scenario. This is most obvious for the clay fraction, cycles 3, 5 and 8 in particular.
- Disposal at 10 m above the bed moves the average location of the 1mg/l concentration level in the water column a few metres up.
- In between mining cycles, when the vessels transit to shore and back to the mining site, suspended sediment concentrations tend to dissipate completely. However, for certain periods of time the concentration, of the clay fraction in particular, remain elevated which may result in temporal uploading behaviour of the fines in the mining area during the next cycle(s).

4.4 Discussion

Single cycles – fate and transport of mine tailings

During active mine tailings disposal, elevated sediment concentrations occur along the mining track. Most of the sediments that do settle (both the clay and silt) directly deposit along the track line (as can be observed from the sedimentation footprints in the next section, section 5.1). The sediments that settle in the domain, before a second mining cycle begins, represent only 44% of the total disposal mass, **65%** of which is fine sediments (silt and clay). The other 56% of the disposal sediment mass is sand, is assumed to settle more rapidly (within the mining region), and to be less likely to resuspend than the silt fraction.

The remaining fine sediment fraction (**35%**) that doesn't settle, which is mostly composed of the clay material, is picked up by the flow and transported throughout the model domain.

Some of this suspended fine sediment is transported outside of the Local Model domain, though in concentrations less than 5 mg/l. In the model this sediment cannot return, whereas in reality it can. This may result in enhanced temporal build-up behaviour of the clay fraction in particular but the concentrations lost are very low.

Temporal variations – seasonal and intra-seasonal variations (Figure 4.13 - Figure 4.14)

Figure 4.13 compares near-bed mine tailings dispersion at the end of a single mining cycle for three seasonal scenarios for discharge at the bed. In summary, plume dispersion patterns for Spring and Winter look similar and display dispersion in north-western direction. In the Summer scenario the plume dispersion is somewhat larger, with concentrations near the model boundary below 5 mg/l.

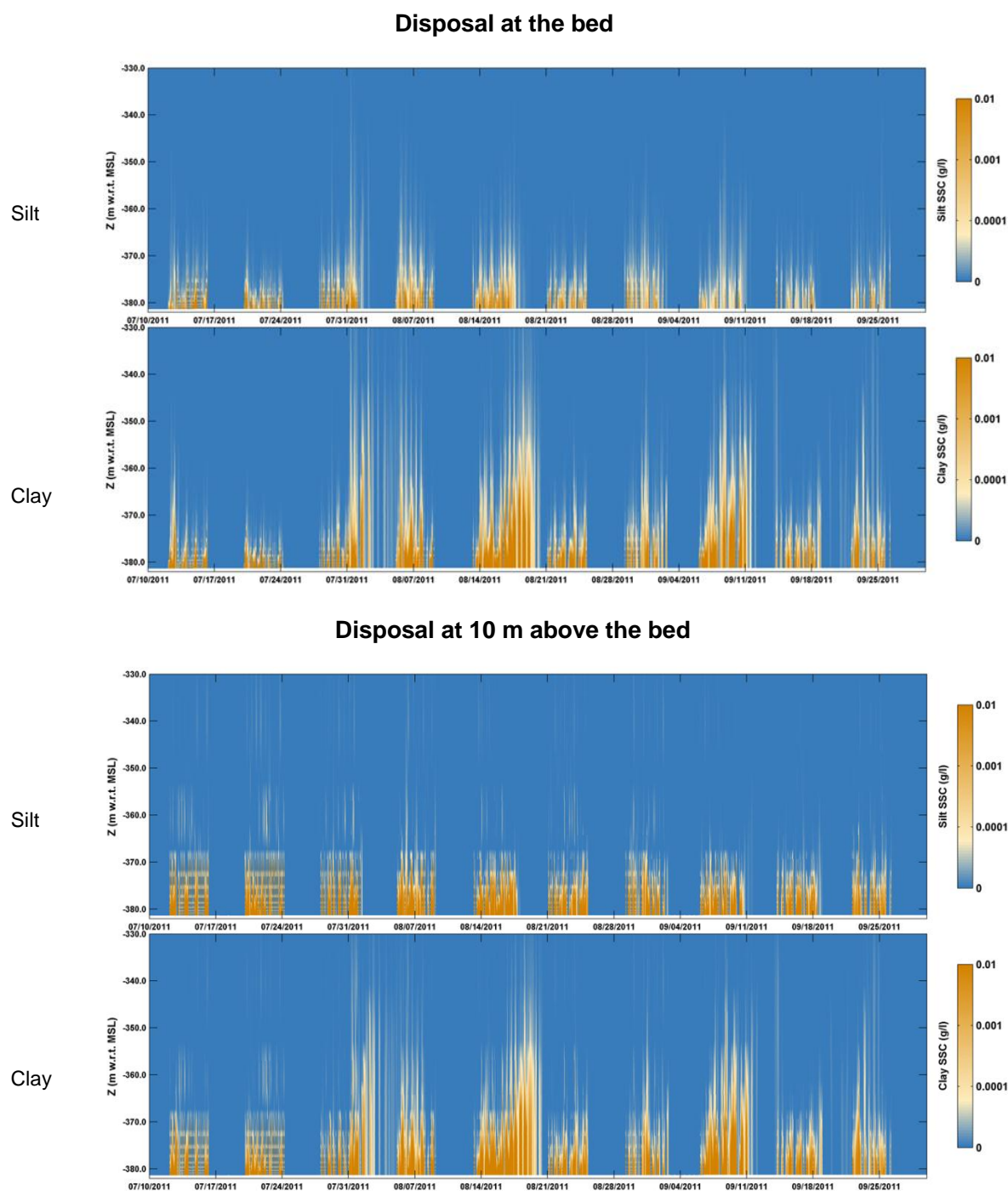


Figure 4.12 Time-stacks 10-cycle simulations **Winter**. Time stack of suspended silt concentration (top panel) and suspended clay concentration (bottom panel) in the bottom 52 m of the water column at the ADCP mooring location for two operational scenarios: 1 discharging at bed (model layer 30, upper two panels) and 2) discharging at 10 m above the bed (model layer 22, lower two panels).

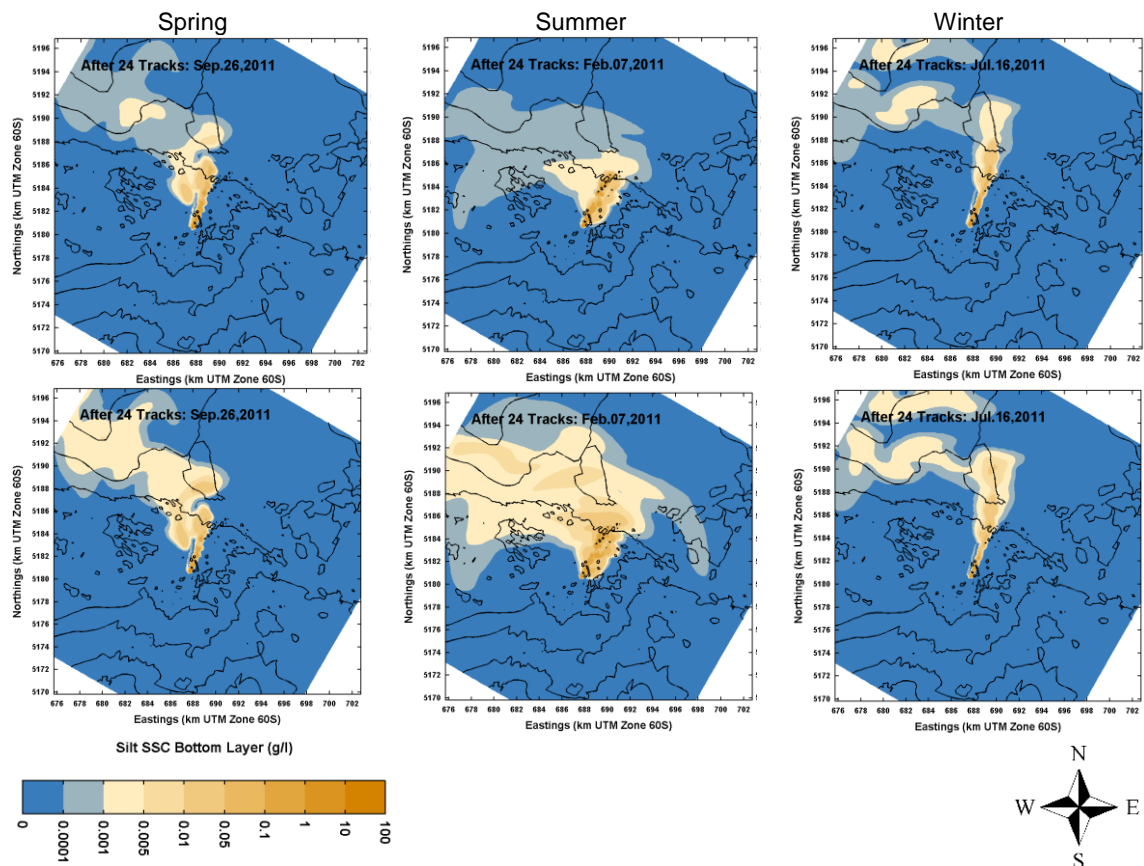


Figure 4.13 Seasonal variations in near-bed suspended silt (top) and clay (bottom) concentrations at the end of mining for discharge at the bed (i.e. after track 24).

Figure 4.14 and Figure 4.15 illustrate the intra-seasonal variation in plume dispersion using results of the 10 cycle summer simulation and the 10 cycle winter simulation for discharge at the bed. The figures show the near-bed (bottom grid cell) suspended clay concentration at the end of mining (track 24) for each mining cycle. The predominant direction of the plume transport is north-west both for the summer-cycles and the winter-cycles, albeit with small-scale variations. In the Summer scenario the plumes exhibit a somewhat larger spreading and higher concentrations when compared to the Winter scenario. This is most likely due to smaller vertical velocity gradients and hence less vertical mixing during summer, which results in a larger horizontal plume dispersion. More stratified summer conditions and therefore larger vertical density gradients may also play a role in vertical mixing and horizontal dispersion of the mine tailings plume. Finally, the maps of clay dispersion reveal considerable intra-seasonal variation in plume dispersion that is similar to the predicted seasonal variation.

Temporal and also spatial variations in plume dispersion are not surprising given the complex hydrodynamics on the Chatham rise; the Subtropical Front moving across the Rise at seasonal timescales and eastward flowing jets and meso-scale eddies along the Northern and Southern flanks of the Rise at time-scales of weeks to months (e.g. Heath, 1985, see also Deltares 2014a).

Cumulative effects

The multiple cycle simulations further revealed that near-bed suspended clay fraction can remain locally in suspension between mining cycles and result in a temporal build-up of concentration in the model domain (uploading behaviour) e.g. suspended sediments due mining cycle 2 can stay in suspension until mining cycle 4. Besides the intra-seasonal variations in plume dispersion, this building-up behaviour will also affect the cumulative sedimentation footprint. It is unlikely therefore, that sedimentation footprints of one cycle multiplied by 10 will reveal the same sedimentation footprint as a complete 10-cycle simulation under varying hydrodynamics. This will be investigated and confirmed in the next Chapter.

Operational scenarios – Disposal effects 10 m above the bed and at the bed.

Besides the operational scenario of discharging at the bed, a second scenario with near-bed sediment disposal has been investigated: Disposing mine tailings at 10 m above the bed tends to be associated with slightly more elevated fine sediment concentrations outside the mining area when compared to disposing at the bed. Figures in Appendix V3-B show the results of intra-seasonal variations near the bed for disposal at 10 m above the bed for winter and summer for both silt and clay. Implications of these operational scenarios on the sedimentation footprint will be discussed in the next section.

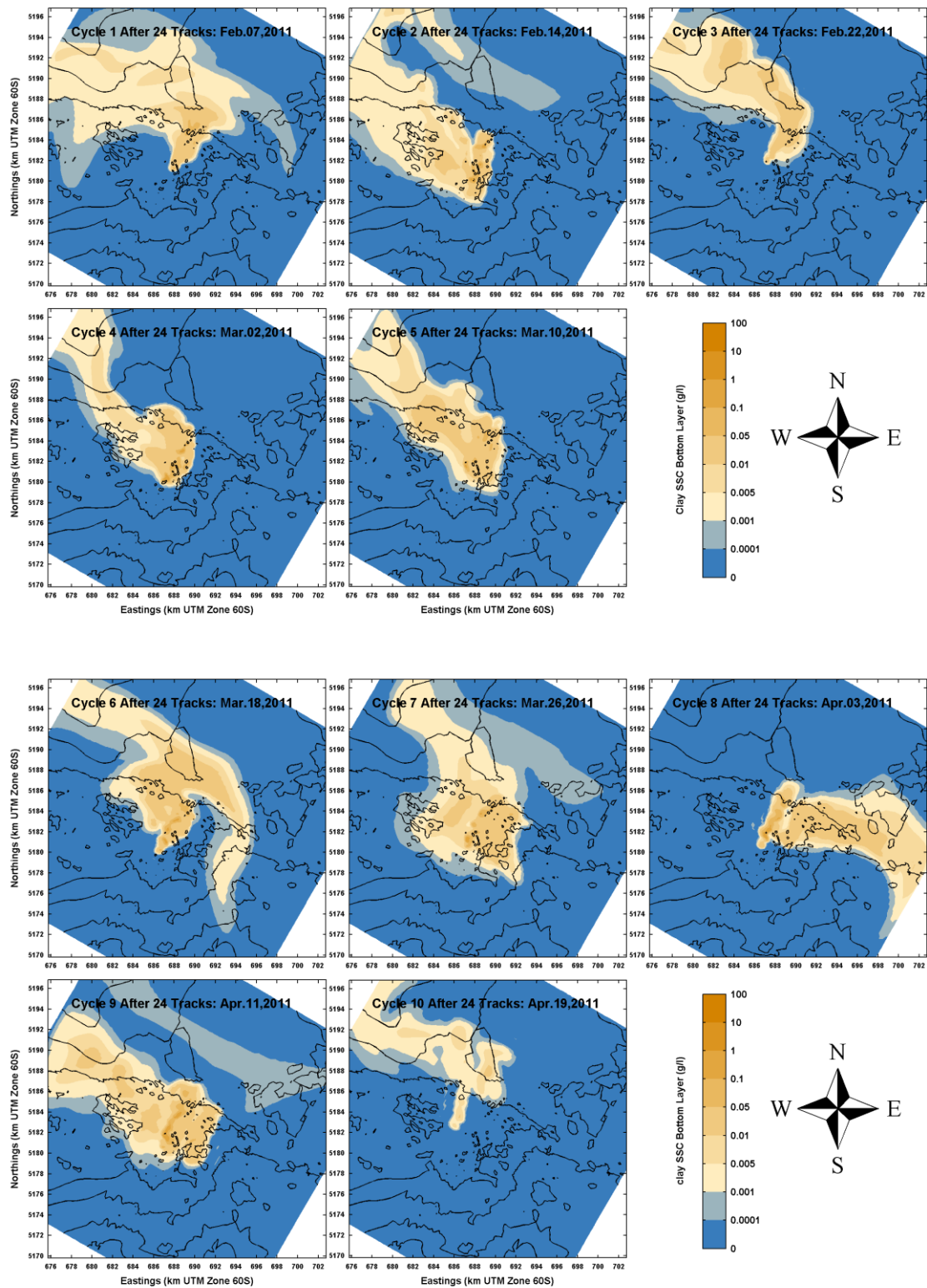


Figure 4.14 Intra-seasonal variations in near-bed suspended **clay** concentrations at the end of cycles 1-10 during the 10-cycles simulation for discharging at the bed. **Summer**. Optimized Local Model domain.

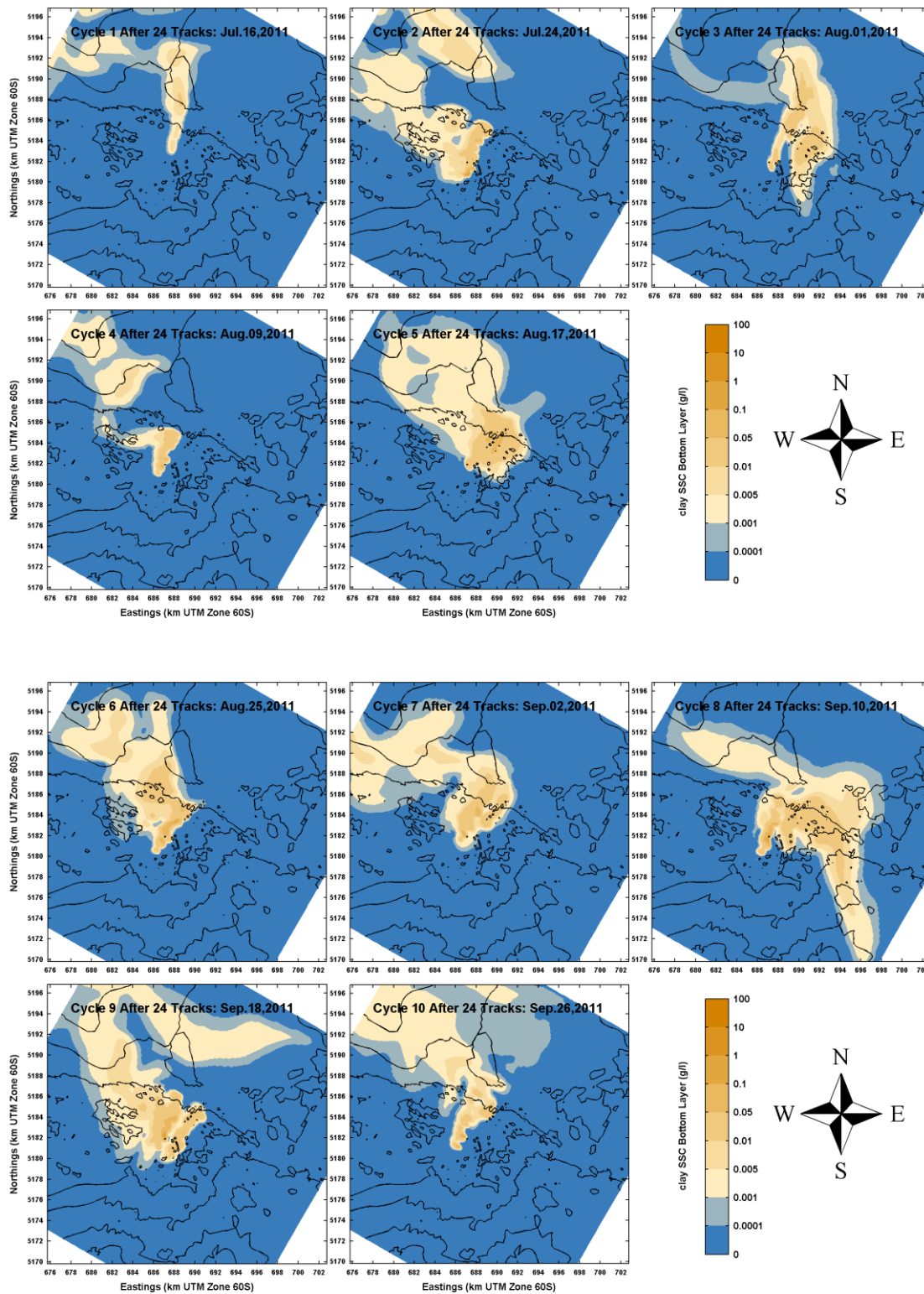


Figure 4.15 Intra-seasonal variations in near-bed suspended **clay** concentrations (g/l) at the end of cycles 1-10 during the 10-cycles simulation for discharging at the bed. **Winter**. Optimized Local Model domain.

Optimized investigation – suspended sediment - main findings

Far field modelling with the optimized model was carried out with two disposal scenarios – disposal at the bed, for spring, summer and winter (1 cycle) and disposal at 10 m above the bed for summer only (as previous results showed this was the scenario with the most plume dispersion). In order to gain an increased understanding of how temporal hydrodynamic variability and discharge release height affect the longer-term mine tailings plume dispersion, a series of ten mining/disposal cycles were also performed

Single Cycle: Disposal at the bed

Results show that during active mine tailings disposal, high sediment concentrations occur along the mining track. Plume dispersion patterns for silt in Spring and Winter look similar and display dispersion in a north-western direction. In the Summer scenario the plume dispersion is somewhat larger. Outside the mining area (2 km-wide and 5 km long region, oriented northwest-southeast) the fine sediment concentrations decrease due to plume dispersion and concentrations are always below 50 mg/l. Both inside and outside the mining area, suspended sediment concentrations decay rapidly to values below 0.1 mg/l, once mining stops; limited resuspension of deposited sediment occurs over the course of one cycle. Maps of clay dispersion reveal considerable intra-seasonal variation in plume spreading that is similar to the predicted seasonal variation. Temporal and also spatial variation in plume dispersion is not surprising given the complex hydrodynamics on the Chatham rise.

Single Cycle: Disposal at 10 m above the bed

Results of discharging 10 m above the bed show that near bed silt concentrations greater than 1 mg/l are exceeded in a larger area 35-40 % of time, pointing at slightly stronger plume dispersion. For clay the differences are less pronounced.

10 Cycle Simulation

The multiple cycle simulations further revealed that near-bed suspended clay fraction can remain locally in suspension between mining cycles and results in a temporal build-up of concentration in the model domain. Besides the intra-seasonal variations in plume dispersion, this building-up behaviour will also affect the cumulative sedimentation footprint. The suspended silt material close to the mine tailings disposal location tends to dissipate completely in between cycles

5 Model Simulations – Optimized Investigation – Sedimentation (Phase 2)

5.1 Single Cycle Simulations for a spring, summer and winter scenario

The previous chapter presented the results for the optimized investigations, focussing on the fate and transport of suspended fine sediments from the mine tailings disposal. This chapter focusses on the associated sedimentation footprints. Single cycle simulations for a spring, summer and winter period were performed using the optimized Local Model (see section 4.1 and Figure 2.3 and Table 2.2).

Figure 5.1 summarizes the results using the total sedimentation of the silt and clay fractions at completion of the mining cycle (including return time) for the three seasonal scenarios. Figure 5.2 provides, as an example, the snapshots of the development of the sedimentation footprint over a single mining cycle for the Summer scenario, (for similar graphs for winter and spring, see. Appendix V3-C. The sedimentation is expressed in [m] deposited sediment layer thickness or height. The darkest colour represents 0.1 m of sedimentation, brighter red 0.01 m and the predominately yellow colour 0.001 m (less than 1 mm) of sedimentation.

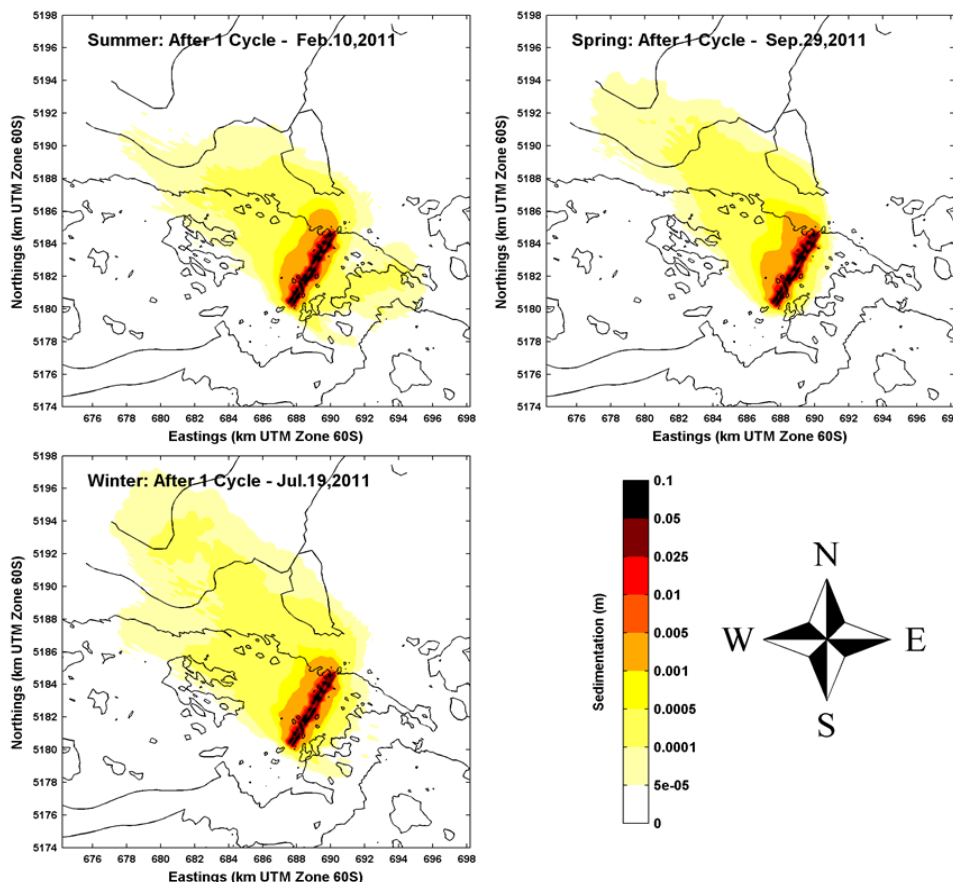


Figure 5.1 Overview of cumulative sedimentation (m) of silt and clay fractions of discharged material at the end of a completed dredge cycle for discharging at the bed (24 tracks + 114 hour return time) for the Local domain (winter, summer, spring).

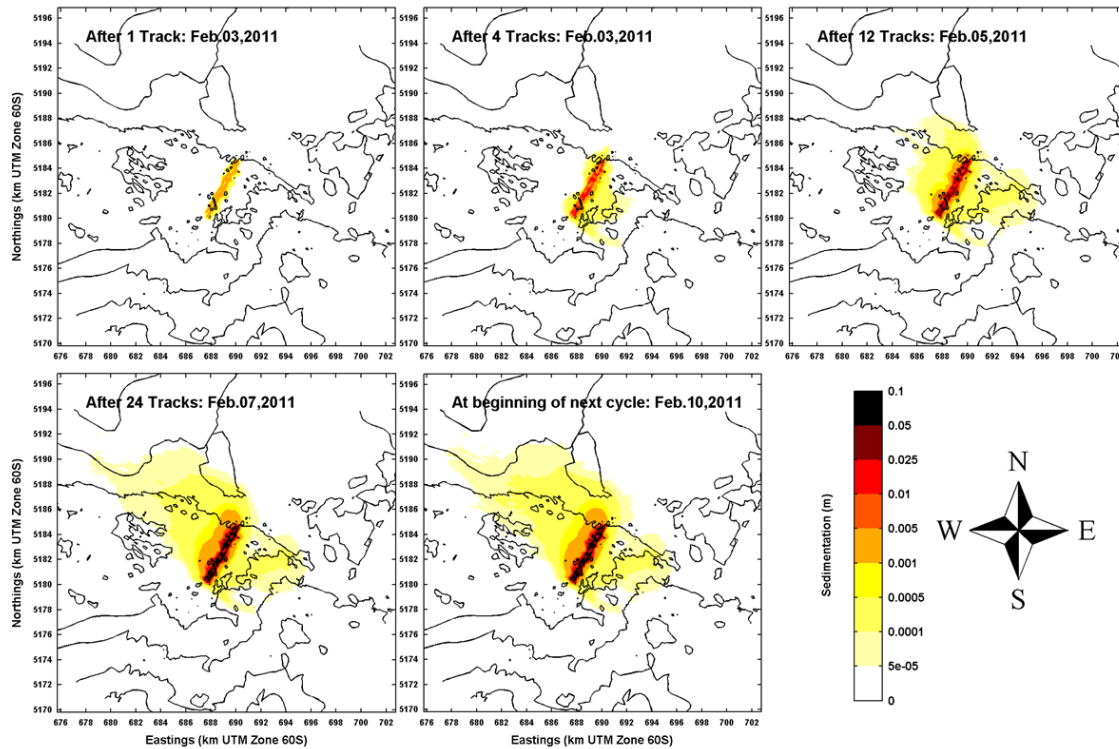


Figure 5.2 **Snapshots of single cycle footprint development in the Summer scenario.** Example overview silt and clay sedimentation (m) over 1 completed track line, 4 track lines, 12 track lines, a complete cycle, and at the start of a new cycle for discharging at the bed. For Winter and Spring, see Appendix V3-C.

The fine sediment footprints reveal the following characteristics:

- The sedimentation primarily occurs along the mine tailings disposal tracks. In the mining area the mean depositional height varies between 0.08 m and 0.10 m, with small local peaks above 0.15 m. Note that this sedimentation is assumed to occur on top of the sand deposition, which is 0.05 m per single track (section 3.1.2).
- In general, the sedimentation pattern shows a strong northwest bias during winter and spring, with the largest sedimentation footprint during the winter scenario. The summer simulation shows more sedimentation to the south-southeast of the mining area, but still with a predominant northwest bias.
- In comparison to the larger deposition within the mining discharge area, the predicted deposition outside this area is small (*Figure 5.1* note the non-linear scaling in the colour scheme).
- Approximately 2 km northwest and 1 km southeast of the disposal tracks, the predicted deposition is less than 0.001 m, respectively.

The sedimentation profile shown in Figure 5.3 clearly illustrates in more detail the peak in deposition along the track lines, and rapid decay on both sides in all three scenarios. For all three simulations, sedimentation reduces to well below 0.01 m within the first km of the track line; the 0.01 m sedimentation contour extends on average 500 m to the northwest and southeast of the two tracks lines.

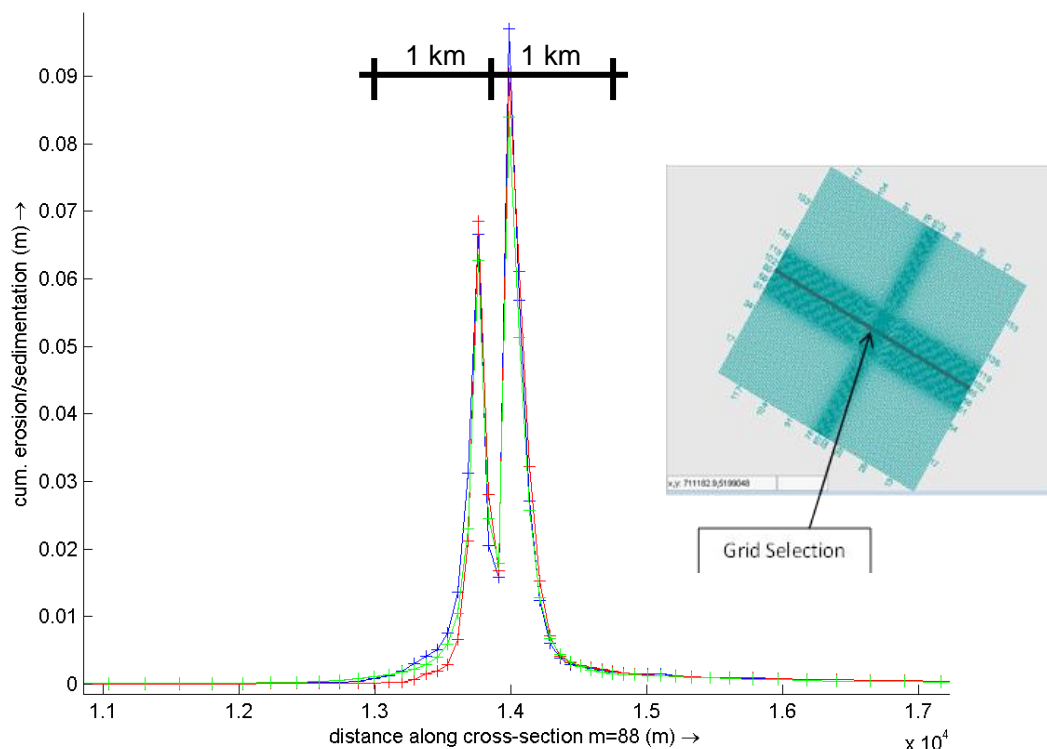


Figure 5.3 Zoomed-in profile of total fine sediment (silt + clay) accumulation (m) over 1 completed cycle for the Summer (blue), Spring (red), and Winter (green) scenarios for discharging at the bed. This is on top of the sand deposition (section 3.1.2).

Finally, Figure 5.4 shows, as an example, the daily sedimentation rates at different distances from the disposal track (see coloured dots in upper Figure 5.4) showing the following characteristics:

- In the mining area daily sedimentation rates typically amount to 0.02-0.03 m.
- At distance of 500 m from the track these rates drop to values of less than 0.01 m/day
- The sedimentation rate drops below 0.001 m/day at a distance of 3 km off the mining area.

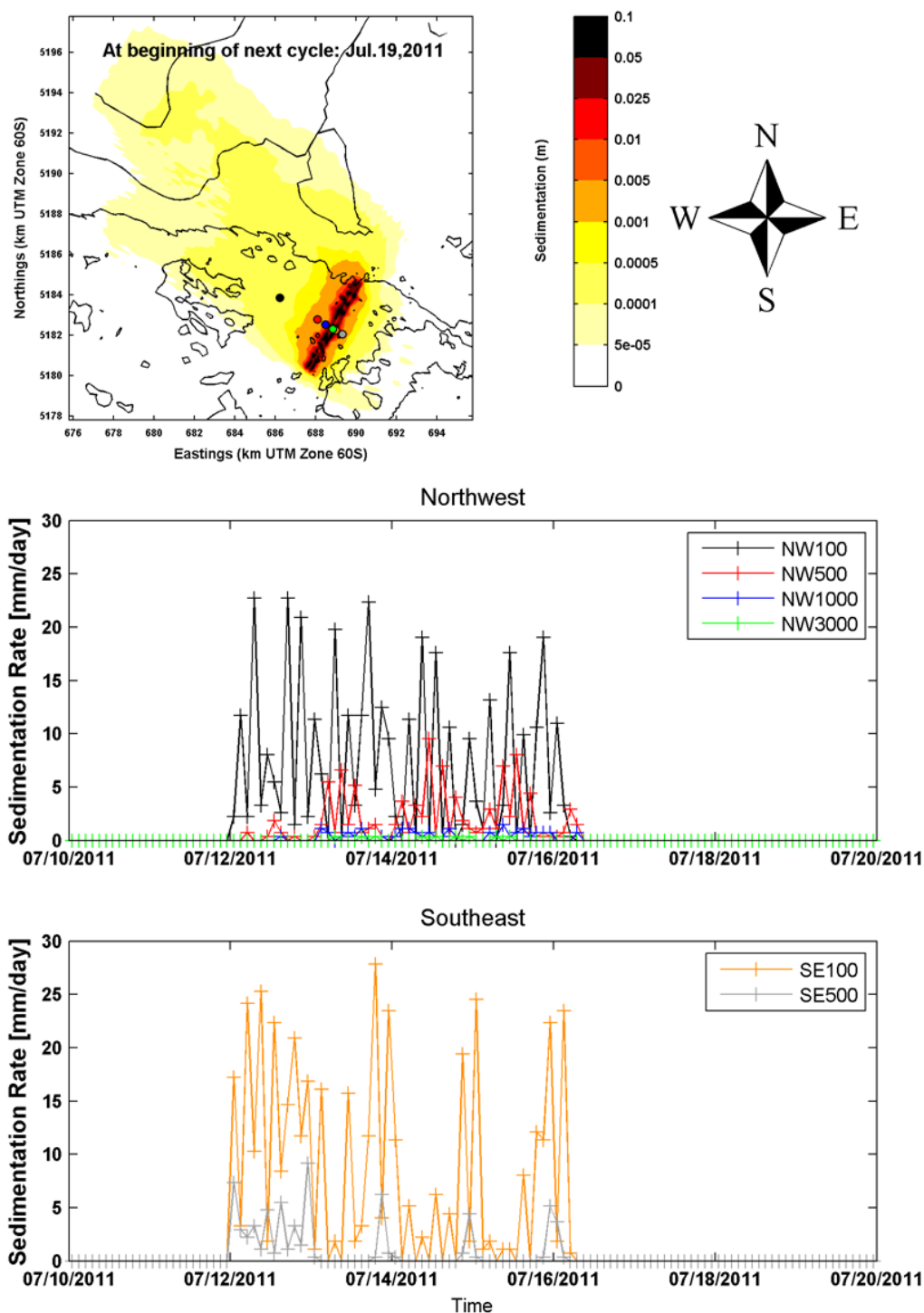


Figure 5.4 **Sedimentation footprint after one cycle (top panel) and sedimentation rates (middle and lower panel) at different distances from the disposal tracks.** Legend indicates the direction and distance in meter from the disposal track; colours correspond with dots in top panel. Results from the single cycle **winter** simulation with disposal at seabed.

5.2 Single cycle simulation - disposal at 10 m above the bed

So far, sedimentation patterns have been investigated for mining operations with mine tailings discharged at the sea bed. From an operational as well as an environmental point of view it is desired to gain a better understanding how the sedimentation footprint changes with discharging mine tailings at 10 m above the bed, as opposed to at the bed, for the Summer scenario. Section 4.2 illustrated the associated differences for the mine tailing plume dispersion.

Figure 5.7 compares results for the sedimentation footprint for the two operational scenarios, i.e. discharging at the bed and 10 m above the bed.

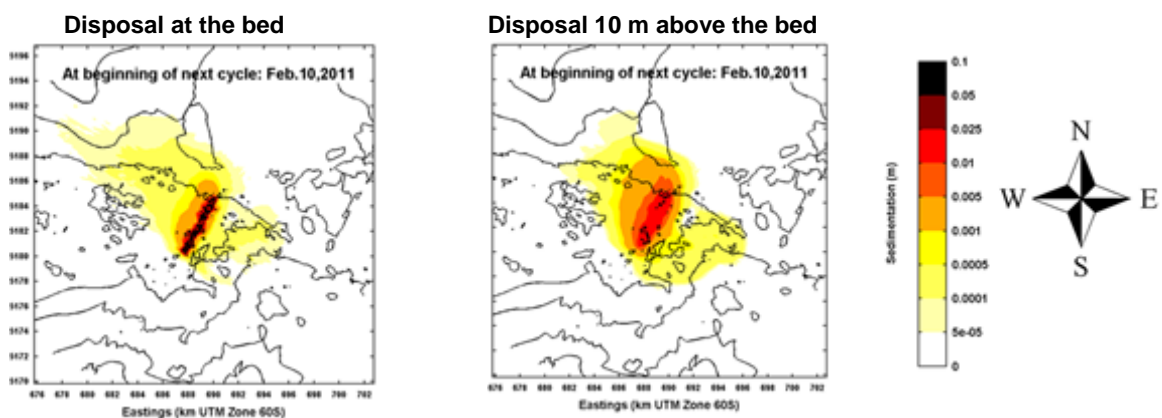


Figure 5.5: Effect of mine tailing release height on sedimentation footprint of silt and clay (m) at the end of a cycle and the start of a new cycle. **Summer**. Note that this sedimentation is assumed to occur on top of the sand deposition.

The maximum deposition height when disposing 10 m above the bed is less than 0.025 m, as compared to the predicted maximum local peaks reaching above 0.15 m when disposing at the seabed. The sedimentation patterns when disposing 10 m above the bed are also more diffuse closer to the mining area as compared to when discharging on the seabed.

For example, the width of the 0.005 m to 0.001 m depositional area is approximately 5-6 km wide when disposing 10 m above the bed, whereas it is more on the order of 3-4 km wide when disposing at the bed.

These observations are qualitatively consistent with the 1 mg/l exceedence plots discussed in section 4.2.

5.3 10-Cycle Simulations

5.3.1 Summer

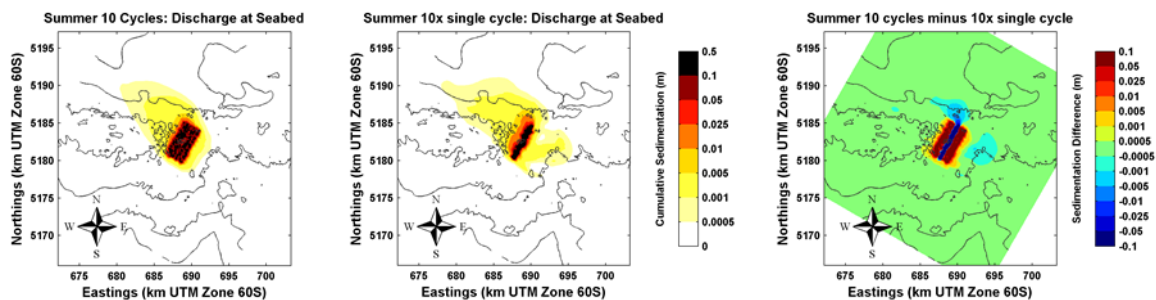
Following the discussion of the fine suspended sediment behaviour in section 4.3 and 4.4, this section considers the influence of discharge release height and cumulative effects of multiple cycles on sedimentation patterns. For this purpose the same four (two summer, two winter) 10-cycle simulations, using the suspended sediment concentrations at the end of the previous cycle to start a new cycle (see also introduction section 4.3), were analysed.

Cumulative effects and intra seasonal variation

Figure 5.6 compares the sedimentation footprint from a full 10-cycle simulation with the sedimentation footprint for the single (first cycle) simulation multiplied by 10. It gives insight into the combined (i.e. cannot be split) effect of intra seasonal hydrodynamic variations and cumulative effects of multiple cycles (due to resuspension, delayed settling). Results are given for both discharge scenarios. It reveals the following observations:

- As for the single cycle simulations, sedimentation predominantly occurs northwest of the mining area in the ten cycle simulation.
- Additionally, the central area between the two inner track lines where no mining activities are planned (see Figure 2.9), incurs less sedimentation than the rest of disposal area. Conversely, this strip is not preserved in any form when disposing ~10 m above the bed.

Discharging at the bed



Discharging at 10 m above the bed

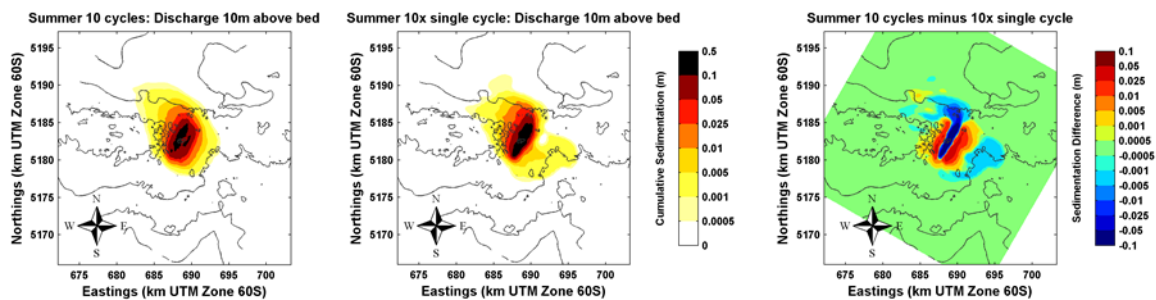


Figure 5.6 Sedimentation footprints of multiple cycles – Comparison of a full 10 cycle simulation results with single results multiplied by ten (middle).

- For discharging at the bed the difference between a full cycle and ten times a single cycle are very small outside the mining area. Inside the mining area the differences are larger, but these are due to the displacement of the mining track in the full multiple cycle situation. These small differences indicate that the effects of intra-seasonal variations on the sedimentation footprint are small. Additionally, cumulative effects caused by delayed settling and resuspension are limited.
- For the discharge scenario with mine tailing release 10 m above the bed, the difference becomes larger, reflecting additional effects of the discharge release height. These effects are outlined in the next paragraph.

Influence of disposal height

Figure 5.7 shows the sedimentation footprint after 10 mining cycles for the two disposal height scenarios. Table summarises some statistics that can be derived from these plots. In general terms disposing mine tailings at 10 m above the bed results when compared to disposal at the bed results in:

- Smaller maximum deposition heights in the mining area (half the value).
- Larger deposition (twice as large) in the first kilometre outside the mining area.
- A larger excursion of the thin edges of the footprint.

Characteristic	Disposal at the bed	Disposal at 10 m above the bed
Maximum deposition (m) in the mining area (m)	0.35	0.15
Deposition (m) at a distance 1 km NW from the mining area	0.01	0.025
Distance from the mining area where the deposition becomes less than 0.001 m	6 km in NW direction 2 km in SE direction	7 km in NW direction 4 km in SE direction

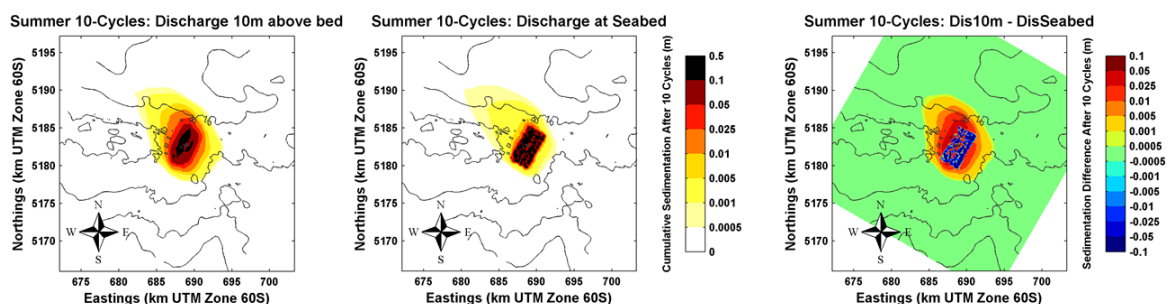


Figure 5.7 Cumulative total (fine fractions only) sedimentation at 10 cycles when discharging at the bed (middle) and ~10 m (left) above the seabed for the summer 2011 period. Right plot shows the difference plot (10 m above bed minus at bed).

5.3.2 Winter

The 10-cycle simulations for the Winter scenario reveal sedimentation footprints and characteristics that are very similar to the results described in the previous section and therefore not repeated here. Figure 5.8 shows the sedimentation footprints for discharging at 10 m above the bed and discharging at the bed, revealing the largest differences in sedimentation footprint.

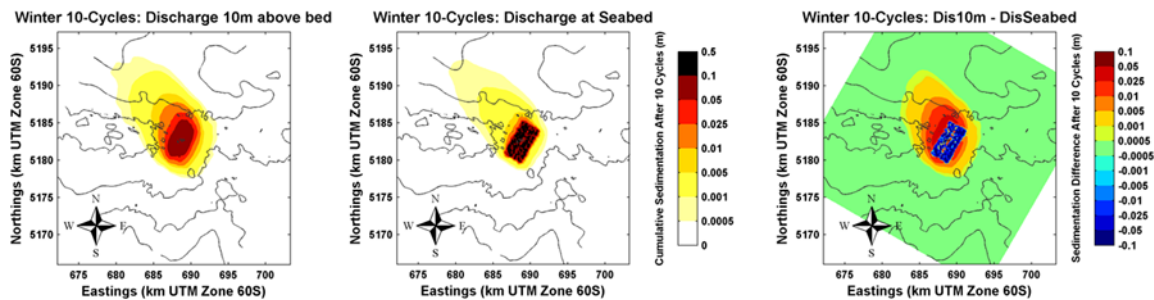


Figure 5.8 Cumulative total (fine fractions ONLY) sedimentation at 10 cycles when discharging at the bed (left) and ~10 m (right) above the seabed for the winter 2011 period.

Finally, Figure 5.9 shows time-series of the sedimentation at the RDI (iX survey) location for both discharge release scenarios. It shows the following:

- At the end of the 10-cycle simulation the total deposition at the RDI (iX survey) location is of similar magnitude for both discharge scenarios, i.e. 0.07-0.09 m.
- Sedimentation evolves however much more gradually over time in the 10 m above bed discharge scenario when compared to discharging at the bed.
- When discharging at the bed, an almost instant deposition of fines with a thickness of some 0.05 m occurs, when the vessel moves over the ADCP mooring location.

5.4 Discussion

Temporal variations in sedimentation footprints

All three considered seasonal scenarios, viz a Spring, Winter and Summer scenario of 2011 yielded sedimentation footprints having similar general characteristics: the sedimentation patterns show a strong northwest bias during winter and spring. The summer simulation additionally showed some sedimentation to the southeast. Largest footprints occur in the Winter scenario.

The comparison of the sedimentation footprints from the multiple and single cycle simulations point at limited effects of intra-seasonal hydrodynamic variations and cumulative effects, due to resuspension and delayed settling. Separation of these factors with the available set of simulations is not possible, but is not deemed important for the sedimentation patterns given the predicted limited variations.

The foregoing implies that temporal variation in sedimentation pattern is much smaller than the variation observed in the suspended plume behaviour (section 4.4). In order to explore a likely relation between the mine tailing plumes and the sedimentation footprint, the sedimentation footprint in the 10-cycle winter simulations was compared maps with the maximum near-bed plume dispersion of silt and clay. Figure 5.10 illustrates the sedimentation footprint for the 10-cycle winter scenario in the geographical context of the Rise. The top plot shows the sedimentation footprint of the 10-cycle simulation. The two lower panels show the silt and clay plumes, respectively. The pattern of silt concentrations ranging from 0.1-10 mg/l and clay concentrations ranging from 1-10 mg/l, more or less coincide with the sedimentation footprint.

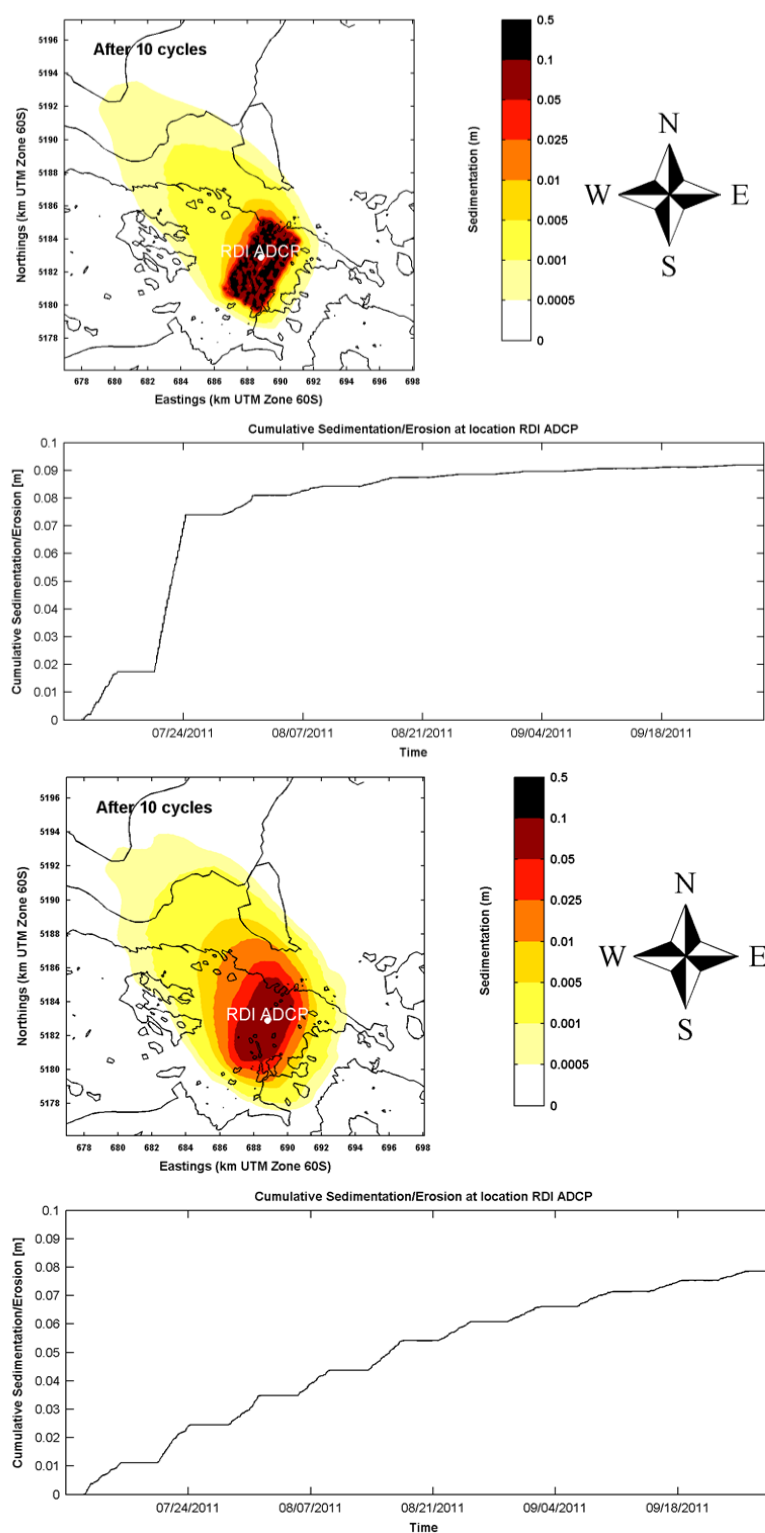


Figure 5.9 Sedimentation footprint and sedimentation rate at the RDI mooring location in the 10-cycle winter simulation. Upper two graphs refer to discharging at the bed. Lower two graphs for discharging at 10 m above the bed.

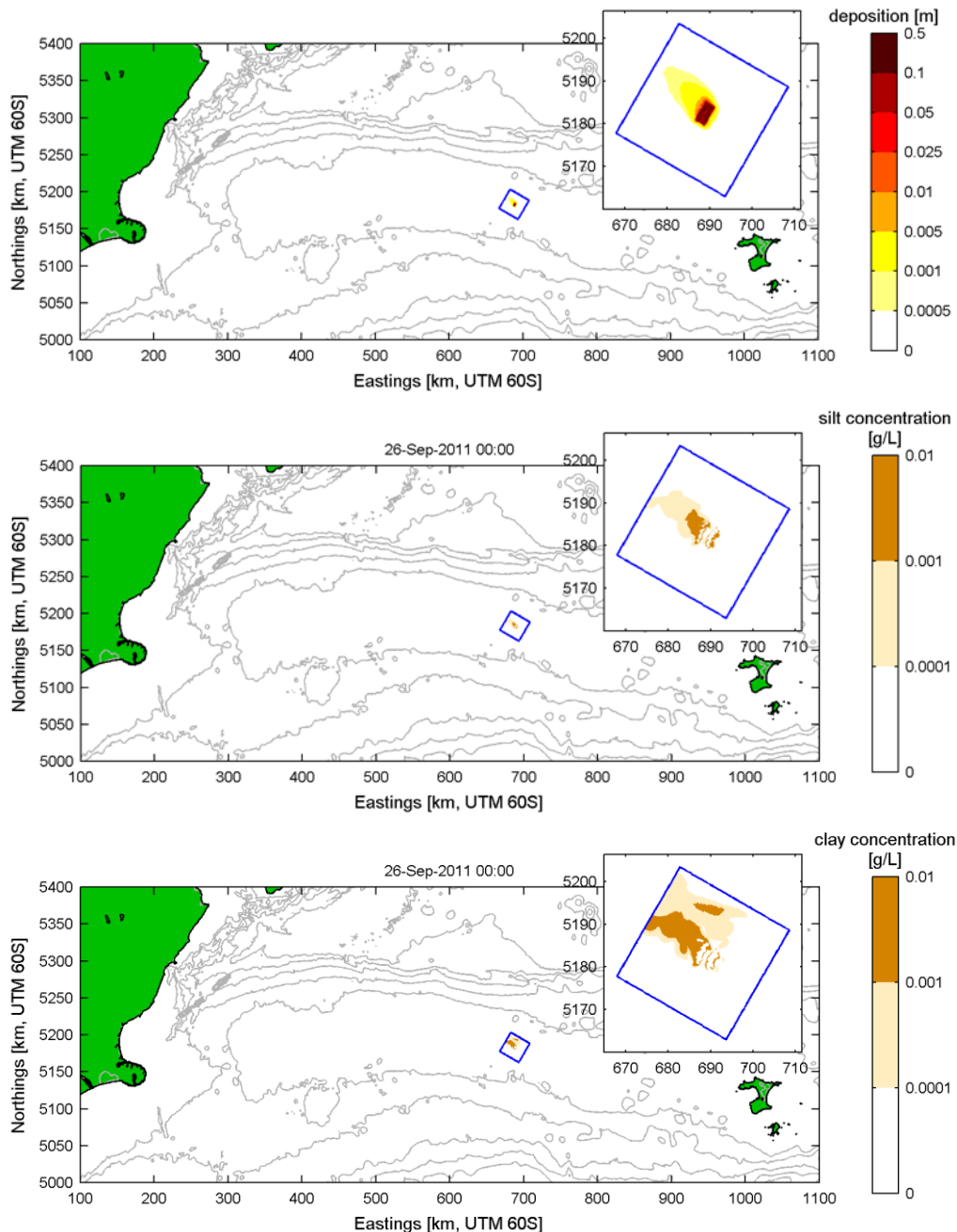


Figure 5.10. Sedimentation footprint and maximum modelled plume spreading as predicted for the 10 cycle Winter scenario for discharging near the bed. Top = sedimentation footprint, middle = silt dispersion, bottom = clay dispersion.

Effect of mine tailing release height

The sedimentation footprint changes with the discharge release height: the size of the footprint is approximately the same but spatial distribution of the sediment deposition changes. Disposal at 10 m above the bed results in a larger spreading as the sediment settles down over a larger distance and hence gets more widely dispersed. This is also reflected in the suspended sediment patterns (sections 4.2 and 4.3).

Optimized investigation – sedimentation - main findings

All three considered seasonal scenarios, Spring, Winter and Summer scenario of 2011 yielded sedimentation footprints with similar characteristics: the sedimentation patterns show a strong northwest bias during winter and spring. The Summer simulation additionally showed some sedimentation to the southeast. Largest sedimentation footprints occur in the Winter scenario.

Single cycle Simulations for a spring, summer and winter scenario (with discharge at the bed)

- The sedimentation primarily occurs along the mine tailings disposal tracks. In the mining area the mean depositional height varies between 0.08 m and 0.10 m, with small local peaks above 0.15 m. Note that this sedimentation is assumed to occur on top of the sand deposition, which is 0.05 m per single track
- In general, the sedimentation pattern shows a strong northwest bias during winter and spring, with the largest sedimentation footprint during the Winter scenario. The Summer simulation shows more sedimentation to the south-southeast of the mining area, but still with a predominant northwest bias.
- In comparison to the larger deposition within the mining discharge area, the predicted deposition outside this area is small. Approximately 2km northwest and 1 km southeast of the disposal tracks, the calculated deposition is less than 0.001 m which would not be measured in reality.

Single cycle with disposal at 10 m above the bed

- The maximum deposition height when disposing 10 m above the bed is less than 0.025 m, as compared to the predicted maximum local peaks reaching above 0.15 m when disposing at the seabed.
- The sedimentation patterns when disposing 10 m above the bed are also more diffuse closer to the mining area as compared to when discharging on the seabed.

10-Cycle Simulations

- As for the single cycle simulations, sedimentation predominantly occurs northwest of the mining area in the ten cycle simulation.
- For discharging at the bed the difference between a full cycle and ten times a single cycle are very small outside the mining area. Inside the mining area the differences are larger, but these are due to the displacement of the mining track in the full multiple cycle situation.
- When discharging at the bed, an almost instant deposition of fines with a thickness of some 0.05 m occurs
- Sedimentation evolves however much more gradually over time in the 10 m above bed discharge scenario when compared to discharging at the bed.

The comparison of the sedimentation footprints from the multiple and single cycle simulations point at limited effects of intra-seasonal hydrodynamic variations and cumulative effects, due to resuspension and delayed settling. Therefore the temporal variation in sedimentation pattern is much smaller than the variation observed in the suspended plume behaviour.

6 Model Verification

6.1 Introduction

In previous chapters, several phases with different simulations were described. An initial model performance investigation was described in Section 3.2. This comparison with measurements was done on the initial Local Model(s) with the nearest model observation point to the ADCP mooring location. The same information sources (RDI ADCP and Aquadopp) are used as described in Section 3.2.1. This chapter provides a more detailed assessment of the model performance of the optimized model in terms of hydrodynamics, focussing on:

- Tidal and non-tidal (residual) current magnitudes and direction
- Horizontal and vertical dispersion
- Mixing induced by vertical shearing of the horizontal velocity

The velocity profiles measured by the RDI ADCP and the near bed velocities measured by the Aquadopp are used. The RDI ADCP was moored at a depth of 362.74 m at location 43°29.003' S - 179°20.099' E. The centre of the first depth bin was located at 30.5 m above the bottom. An Aquadopp attached to the same frame measured velocities closer to the bed (at 8 m above the bed). All instruments are mounted on a frame about 10 meters above the seabed. All data are transformed to UTC date and time, and current directions were corrected for local magnetic declination.

A correction was applied to the time of the ADCP and Aquadopp measurements due to a post-processing error by iX Survey regarding time zones –hence the data was off by two hours. Results presented here are with measurements with a corrected time-stamp. Table 6.1 summarises the information obtained from the IX Survey mooring

Table 6.1 Overview of instruments used for data collection

	Location	Depth	Time Frame Start – end (UTC)	Parameter
ADCP	43°29.003' S 179°20.099' E	362.74 m	21/05/2011 21:00 - 13/11/2011 06:30	Current profile, pressure
Aquadopp	43°29.003' S 179°20.099' E	372.28 m	21/05/2011 21:00 - 11/12/2011 02:00	Bottom Current

The centre of the first ADCP depth bin was located at 30.5 m above the bed. The water column was divided into bins with a height of 5 m. The top 10% of the data below the surface was removed, as they may be subjected to side-lobe interference. This leads to 64 valid cells with cell centres between 30.5 and 345.5 m above the bed. Every 30 minutes an ensemble-averaged profile was recorded, consisting of 50 members spaced by 6 seconds, thus over a period of 5 minutes. This leads to a standard deviation of the velocity of 3.74 cm/s. A table was provided with the speed and direction as a function of time and depth cell from which the eastward (u) and northward component (v) of the velocity was determined.

An Aquadopp (current metre) on the same mooring below the ADCP (at 8 m), measured velocities closer to the bed. Every 15 minutes an ensemble-averaged velocity with a length of 2 minutes was recorded. The horizontal velocity precision is 1 cm/s. The Aquadopp had been measuring for a slightly longer period than the ADCP: from May 21st to December 11th, 2011. All data are transformed to UTC date and time, and current directions were corrected for local

magnetic declination. Directions in this report are given in the nautical convention, 0° to the north and 90° to the east, defined as the direction the currents are propagating towards.

The ADCP measurement bins are at a finer vertical resolution than the model layers or bins. In the local model there are 30 model layers in the vertical, with the lowest ADCP bin compared to Layer 19 of the model and the upper ADCP bin compared to Layer 9 of the model. Tests were performed to assess the variation in ADCP velocities between the bins represented by one model layer. The variation was small, however in:

- 1) *the tidal analyses* all ADCP bins were used;
- 2) *time series and tidal reconstruction* - the nearest ADCP bin to the centre of the model layer was used.

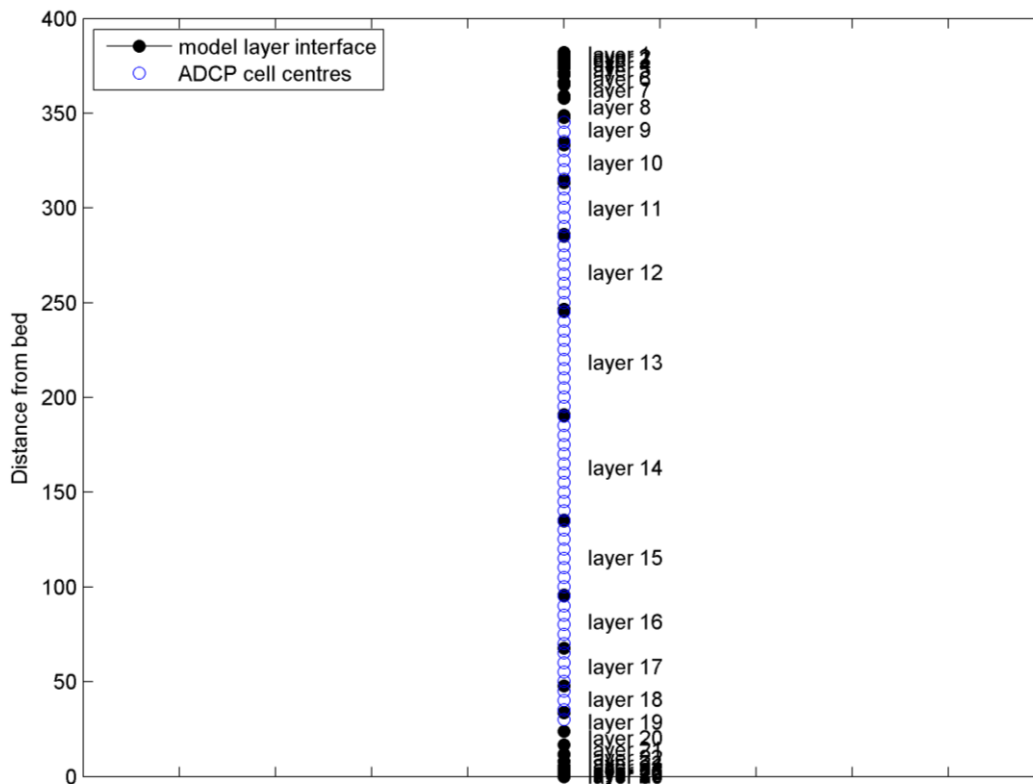


Figure 6.1 A schematic of the model layers with the higher resolution ADCP bins.

Chapter 5 previously described the various cycle simulations that were performed to assess the release of sediment during the mining operations. Simulations spanned the period from the 1st of February to the 23rd of April 2011 (summer simulations) and the 10th of July to the 30th of September (winter simulations). These simulations are used in this model verification of the hydrodynamics, though discharge of a water sediment mixture was included at certain instances in the simulations. The release of this discharge caused a temporary increase in current velocities close to the bed in the cells where the discharge was released. The effect did not propagate up into the water column and so comparisons between the model at layer 19, the layer that corresponded with the bottom ADCP bin or between the model at layer 22, the layer that corresponded with the Aquadopp, were not influenced by this discharge.

Additional simulations with the same set up as described in Chapter 5 were run to fill the entire time period recorded by the RDI ADCP, namely the 21st of May 2011 to the 13th of November 2011. In these simulations sediment disposal was not included.

6.2 Time series comparisons – Model vs. ADCP and Aquadopp

The most basic check is a time series comparison of measured versus modelled velocities and direction. The focus of this study is the dispersion and transport of the sediment plume and subsequent resuspension of sediments, so validation focusses mostly on the lower half of the water column, particularly close to the bed. However trends in the vertical are also discussed in order to understand model performance as a whole. Other parameters are shown throughout the water column later in this chapter. In addition there is a discussion on what processes or lack thereof are causing differences between the modelled and measured velocities in Section 6.5.

In the time series plots the nearest ADCP bin to the centre of the model layer was chosen (Figure 6.1). The model has 30 non-equidistant layers however the first ADCP bin corresponds to layer 19 of the model. Throughout the period considered, we see that the ADCP shows more variability compared to the modelled velocities which may be due to the high resolution of the ensemble averaged readings. In general, spring tides are overestimated by the model in the near bed layers and underestimated at the near surface layers. This may be due to wind effects in the upper layers that are taken into account in the measurements but not the model. The quality of the model performance varies over time. In some months the model captures the magnitude of measured velocities 30 m above the bed (e.g. September) and in other months velocities are overestimated by 50 % and by as much as double on certain days e.g. 22nd of June but this overestimation is not persistent in time. (Figure 6.3 - Figure 6.5).

Figure 6.2 shows the measured current velocity (ADCP) versus the modelled current velocity (in black) for the last two weeks of June. The model (layer 19) overestimates the peaks in current velocity by 0.1 – 0.2 m/s (~ 50%), though the lower velocities are captured, from the 20th-23rd of June. The model (layer 19) performance improves in September and November (Figure 6.4 and Figure 6.5) which corresponds to the period with less stratification, see section 7.4.

Figure 6.6 shows a comparison for the Aquadopp which is slightly closer to the bed than the ADCP. When the current shifts direction around the 21st of June, the model performance deteriorates. Until the 20th of June the model slightly underestimated the Aquadopp velocities (in layer 22) however from the 21st June the model overestimates the velocities again by double. Also in July the model overestimates current velocity compared to the Aquadopp (up to double). In September both velocities and direction are well captured by the model.

Given these results, it is indicated that the modelled plume travels further in late June and late July when the model overestimates the low current velocities, at times up to 100 %, compared to less stratified periods such as September and November when the model captures the majority of the modelled velocity peaks. The overestimation of currents possibly originates from the HYCOM boundary conditions that were used to run the regional model. Results of the Oceanographic Report (Deltares, 2014a) show that for the ADCP measurement period, near-bed current velocities in HYCOM are larger compared to other weakly-stratified periods and show a distinct NW-biased current direction. This trend of modelled current velocity overestimation continues up to the middle of the water column

(~200 m from the bed) above which the model begins to underestimates the current velocities.

These plots (Figure 6.1-Figure 6.9) however show the total current speed and a better indication is given in the following sections which compare both the tidal components of the flow and the residual flow components with measurements. With this information the implications for plume transport and spreading can be described in more detail.

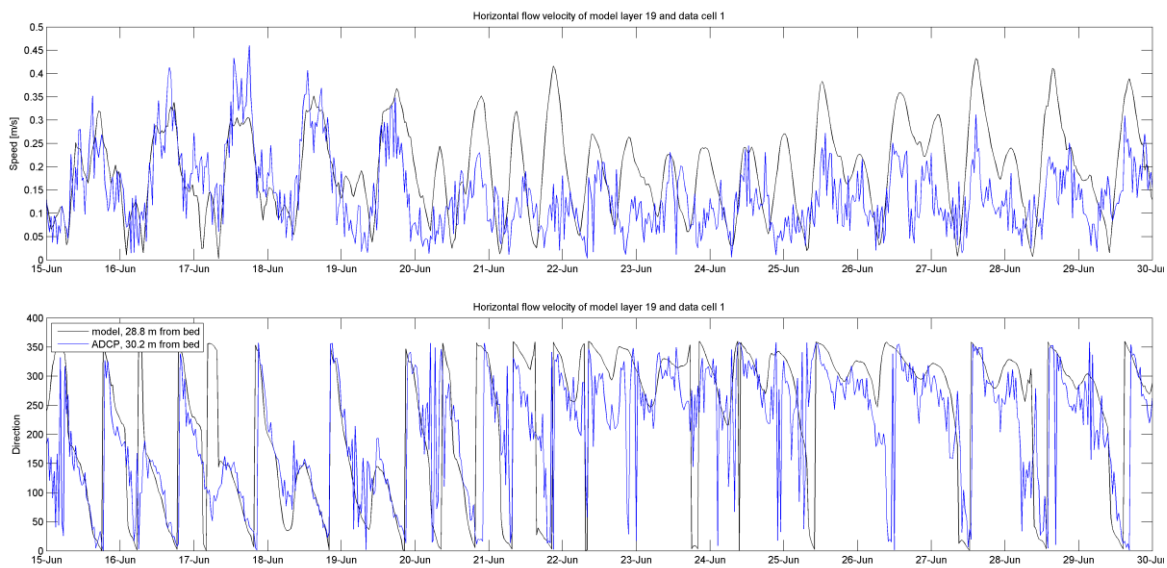


Figure 6.2 ADCP comparison of velocities and direction for 2nd half of June.

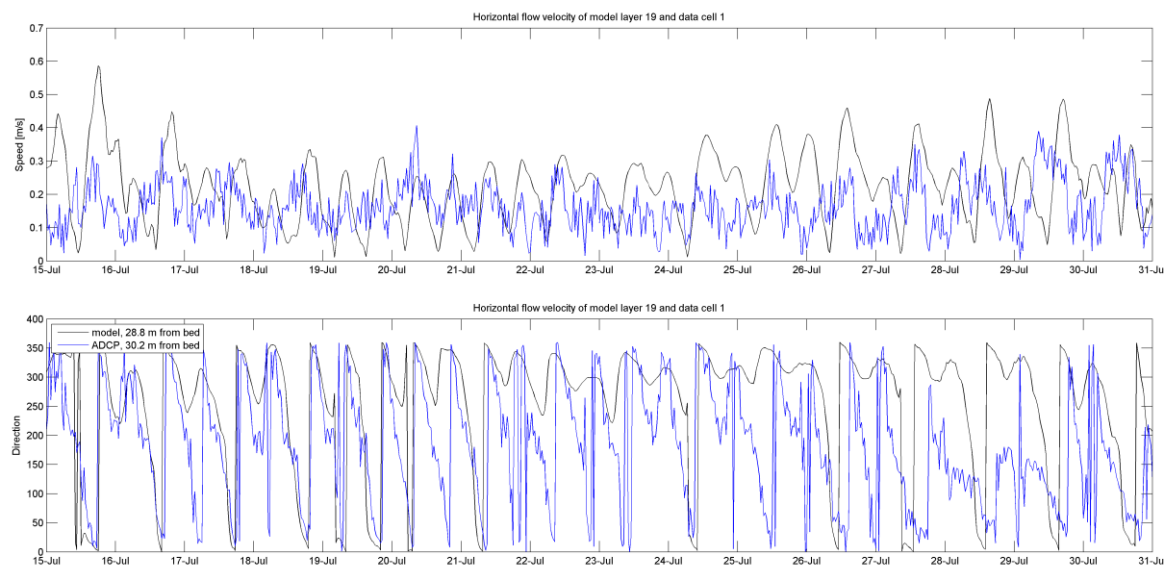


Figure 6.3 ADCP comparison of velocities and direction for 2nd half of July.

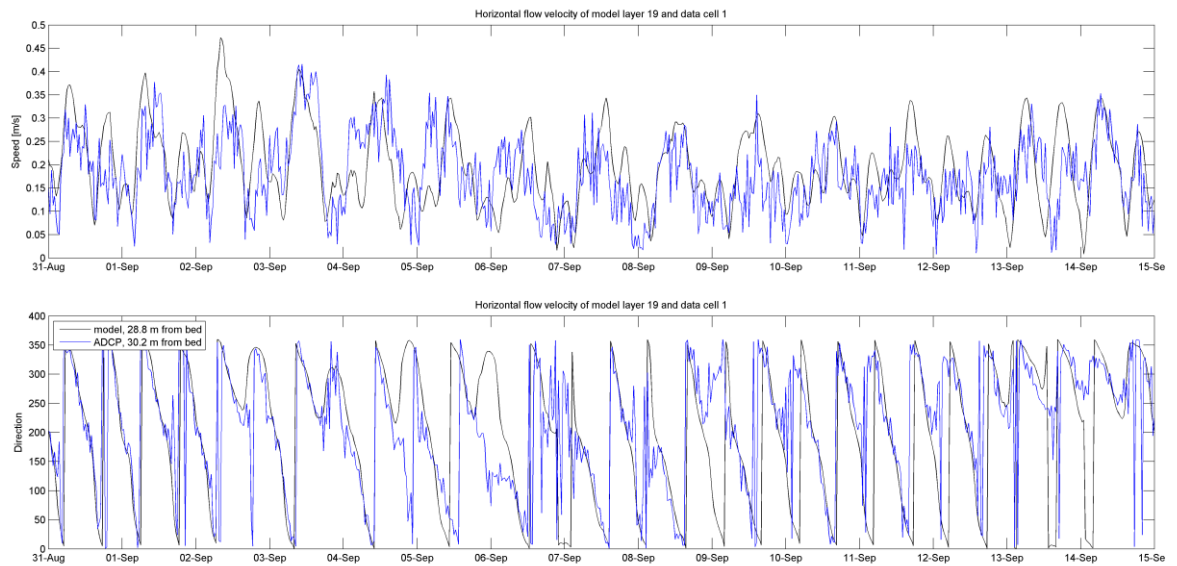


Figure 6.4 ADCP comparison of velocities and direction for 1st half of September.

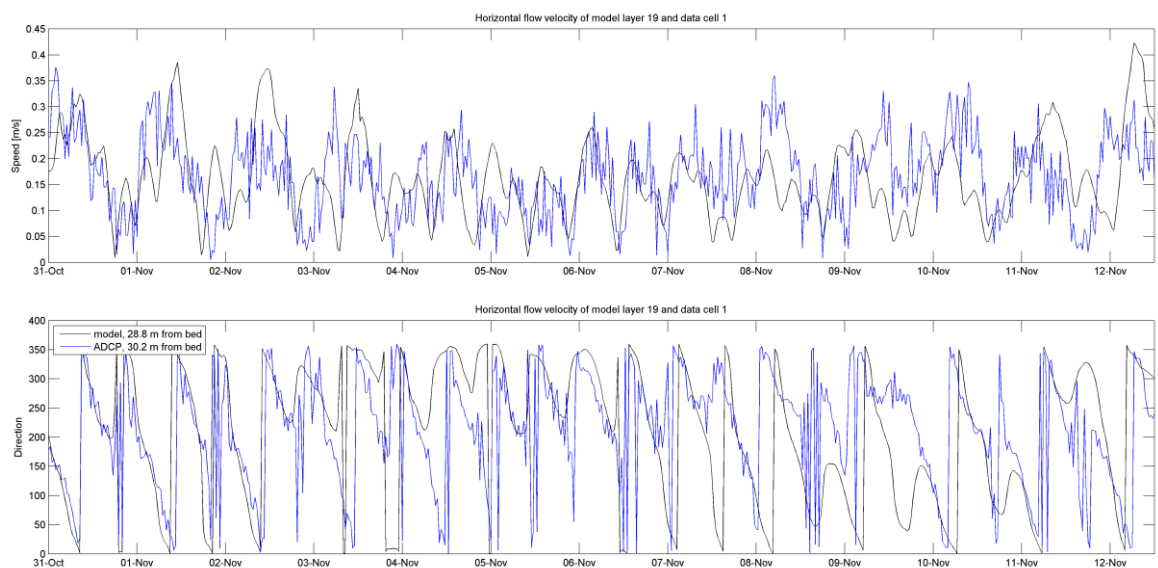


Figure 6.5 ADCP comparison of velocities and direction for 1st half of November.

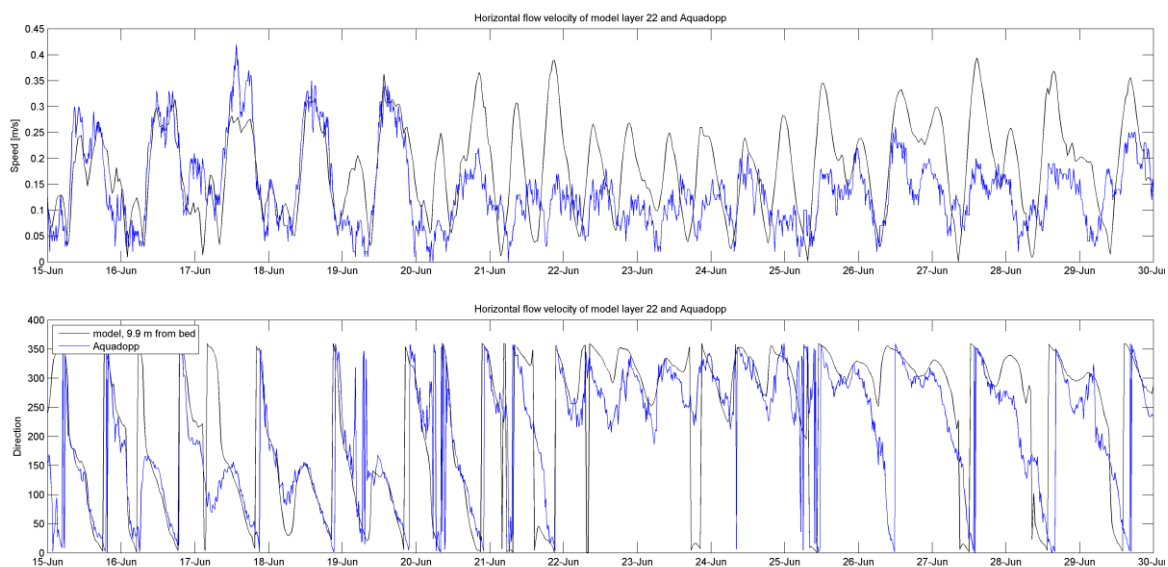


Figure 6.6 Aquadopp comparison of velocities and direction for 2nd half of June.

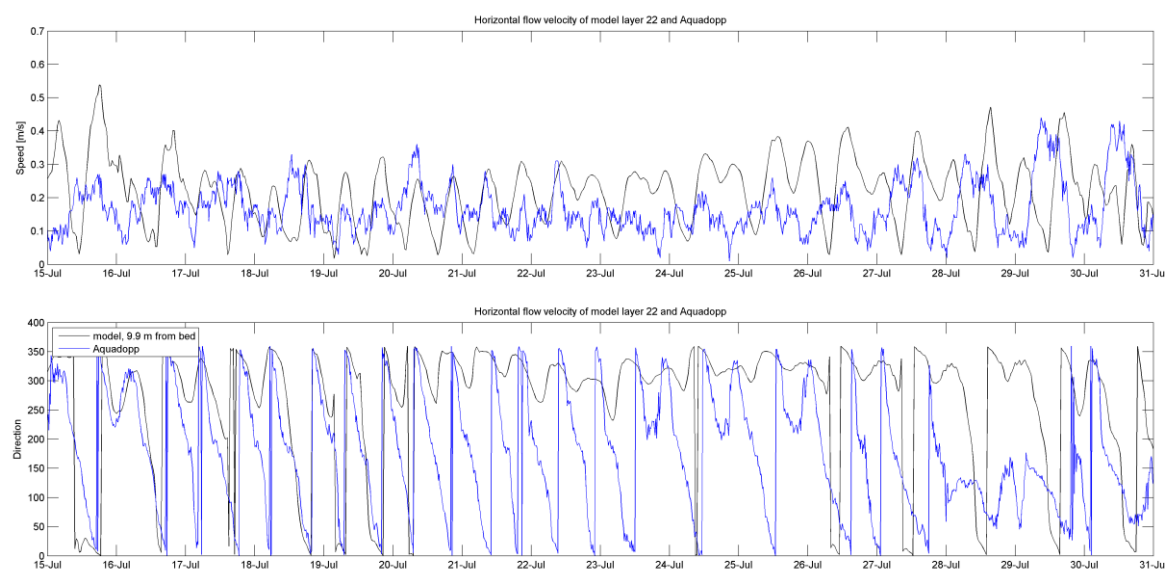


Figure 6.7 Aquadopp comparison of velocities and direction for 2nd half of July.

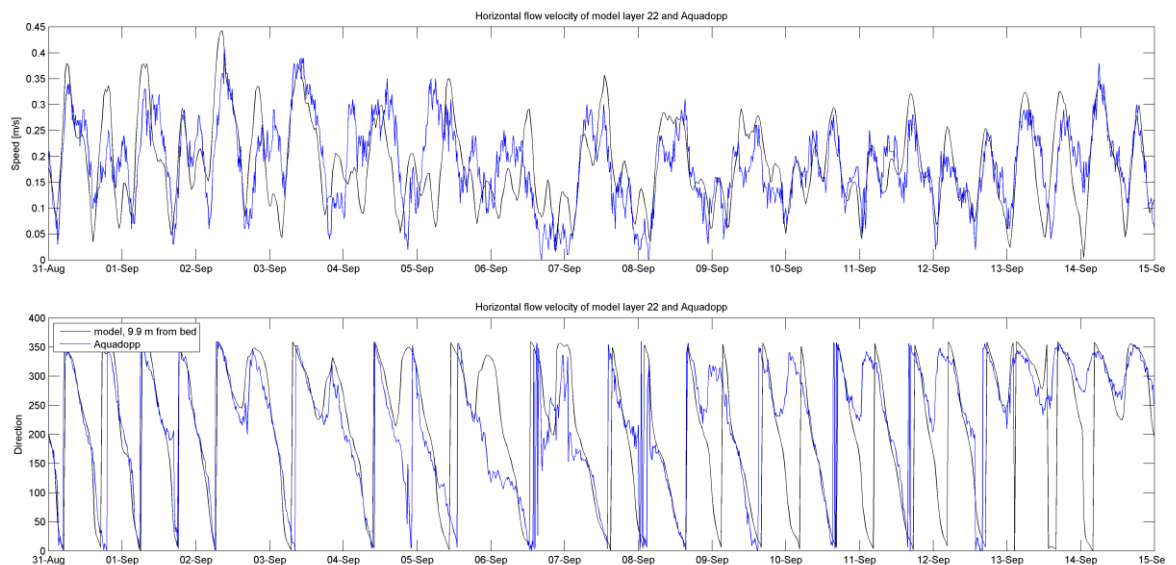


Figure 6.8 Aquadopp comparison for 1st half of September.

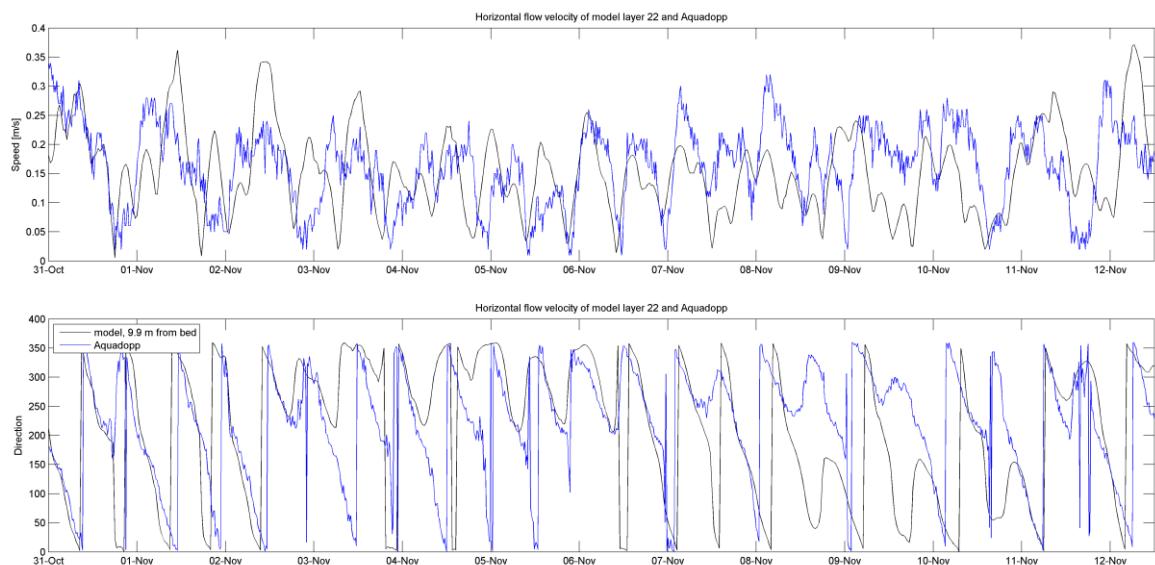


Figure 6.9 Aquadopp comparison for 1st half of November.

6.3 Tidal versus non-tidal flow

In the context of plume dispersion and sediment resuspension, the tide is mainly important for the initial transport and (re)suspension of sediments. The residual flow i.e. the part of the flow which cannot be assigned to the tidal signal, is important for the large-scale and long-term fate and transport of these resuspended sediments, and in this case, plume dispersion. Tides may also generate a residual current, but these effects are small in deep water (Deltares, 2014a).

In addition to the tides, large-scale hydrodynamics on the Chatham Rise are influenced by strong eastward flows (jets) and meso-scale eddies on the northern and southern flanks of the Rise. The combination of tides and stratified flows may result in internal tides or waves (baroclinic flows) which may also play a role over the Rise. Internal tides are internal waves with the frequency of tides. When surface tides move over a stratified water column with a varying bathymetry, internal tides will be generated. Analysis of the ADCP data in Deltares, (2014a) shows evidence of internal tides on the Chatham Rise. Although the frequency of internal tides is equal to surface tides, their phase is not the same as the phase of surface tides, because internal tides move at a much lower speed. Moreover at any given position, the phase of internal tides is not constant. Their speed depends on local stratification and bathymetry and they can be intermittent. Therefore in a tidal analysis covering longer periods, the (maximum) strength of internal tides will be underestimated by smoothing as their phase and amplitude vary in time. In addition, in areas with internal tides, the assumption of 'line' frequencies used in classical harmonic analysis is questionable (Pawlowicz *et al.*, 2002).

6.3.1 Tidal Analysis

A tidal analysis on the measured (ADCP and Aquadopp) and modelled velocity signal was performed using the t-tide toolbox (Pawlowicz *et al.* 2002). A tidal analysis has been applied to the entire half-year period covered by the ADCP measurements. Nodal corrections are applied, i.e. a correction for the 18.6 year tidal cycle. Whether a constituent can be resolved and is significant depends on the measuring interval and duration. During the six month period over which modelled and measured constituents were compared, the significance of the constituents was also taken into account. The Rayleigh criterion determines whether two tidal constituents with almost equal frequencies can be distinguished from each other. To be able to resolve the couples K1 and P1, and MSF and MF, the Rayleigh criterion is set to 0.9. This means that two waves with almost equal frequency need to differ by at least 0.9 wavelengths in the total length of the record in order to be resolved. Significance is based on the signal-to-noise power ratio, which is the square of the amplitude divided by the amplitude error. Figure 6.10 shows the significance of the ten largest constituents for the ADCP (upper panel) and the model (lower panel). In t-tide, a constituent is considered significant if the signal-to-noise ratio (SNR) is larger than 2.

For this analysis, all ADCP bins and all the model layers throughout the water column were used. It was decided not to average the ADCP bins per model layer in this case so as to resolve to full signal. The significance of constituents in the tidal analysis applied to the ADCP measurements (lines) and the Aquadopp measurements (Δ), for the period May to November 2011 (upper panel) and the modelled measurements (bottom panel) are plotted on a logarithmic scale (Figure 6.10). The signal-to-noise ratio of P1 and S2 are equal for the Aquadopp. The order of the significance is almost identical between model and measurements. This was important in deciding which tidal constituents to include in the tidal analysis. The longer period MF (lunisolar fortnightly) is less significant in the model than in the measurements. In contrast MM (lunar monthly) is more significant in the model than the measurements.

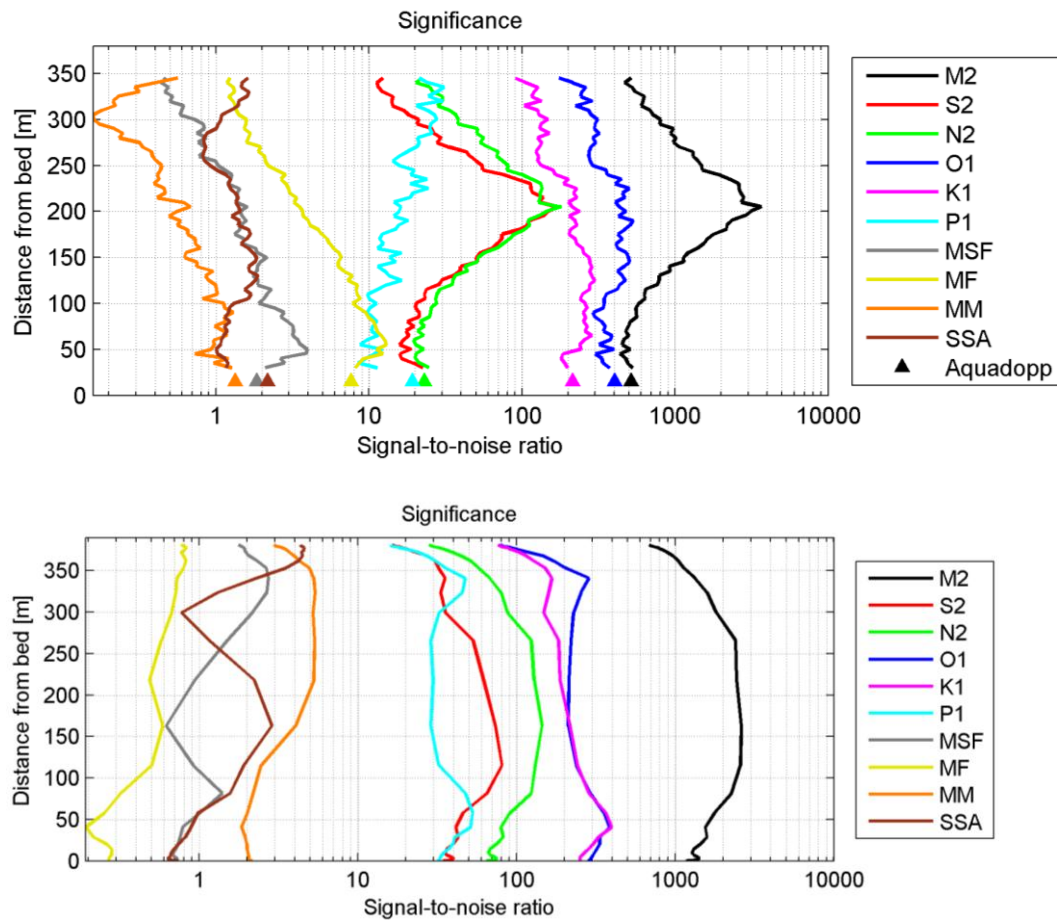


Figure 6.10 Significance of measured (top panel) and modelled constituents (lower panel).

A fast Fourier transform spectrum of the measured and modelled tidal frequencies was also performed (Figure 6.11-Figure 6.12). This determines the dominant frequencies in the ADCP velocity signal and modelled signal, the analysis was performed on the eastward (u) and northward (v) velocity component in each layer. Peaks in the spectrum show the dominant tidal constituents. The most dominant peaks in the spectrum can be related to the tidal frequencies: M2, O1, K1, MF, S2 and N2. The amplitude at the M2 tidal frequency is largest in both directions, followed by O1. The results of the ADCP and model are consistent showing that the tidal constituents are well represented in the model though the peak of the constituents is slightly lower in the model.

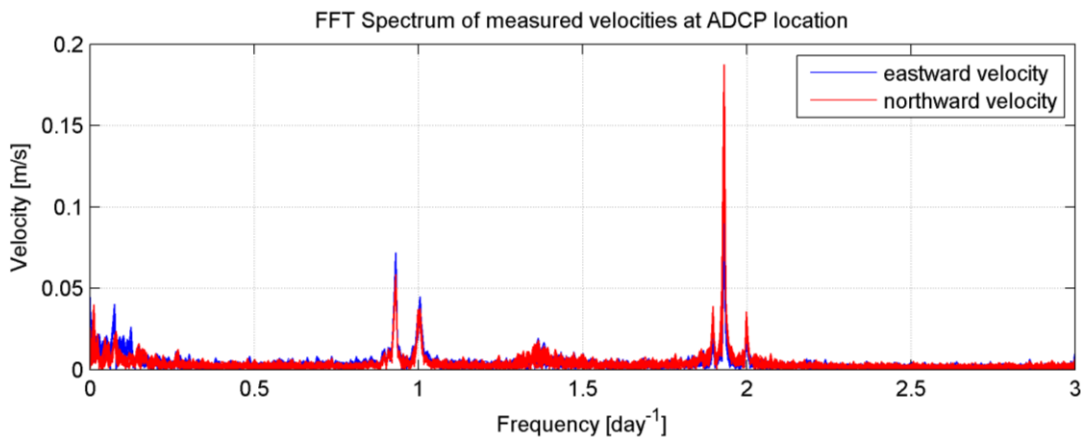


Figure 6.11 FFT spectrum of ADCP velocities.

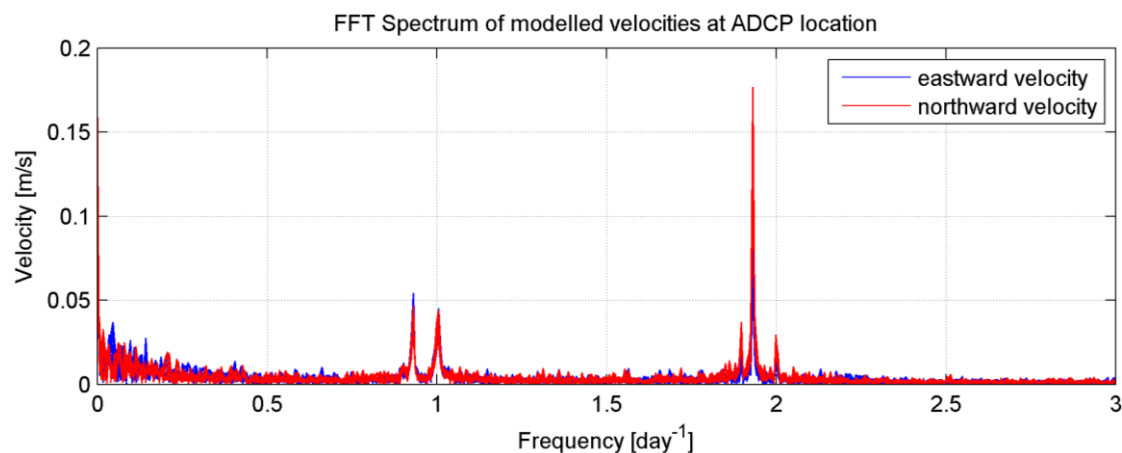


Figure 6.12 FFT spectrum of modelled velocities.

Another consideration when comparing modelled and measured velocities is that the near-bed observations of the ADCP show an artefact in the data around 50 m above the bed where current velocities reduce only to increase again towards the bed (see Figure 6.13). The Aquadopp shows slightly larger major constituents, which indicates that due to the lower velocities at ~ 50 m above the bed in the ADCP an under-prediction of the near-bed ADCP velocities might occur (Deltares 2014a). To reduce the uncertainty introduced by this artefact, the results of the Aquadopp are also used.

For the largest constituent (M2), the model is much more uniform in depth than the ADCP which shows higher velocities near the surface compared to the model and reduction in velocities moving towards the bed. The gradient of the M2 constituent over depth as is seen in the ADCP data, is an indication of internal tides. This is especially notable in June (Figure 6.13) when stratification is stronger. Later in the year (i.e. October) when the water column is well mixed a uniform profile for M2 is also observed in the measurements. This indicates that internal tides are not well reproduced by the model, which is further investigated in section 6.3.5. This concurs with earlier results of the total modelled versus measured velocities which show that the prediction of the plume is less reliable in well stratified periods (i.e. June) than in periods when stratification is less (September onwards).

The profiles of the other constituents are more similar, although O1 and K1 in the model are very close together compared to the measurements, with O1 being underestimated by the model.

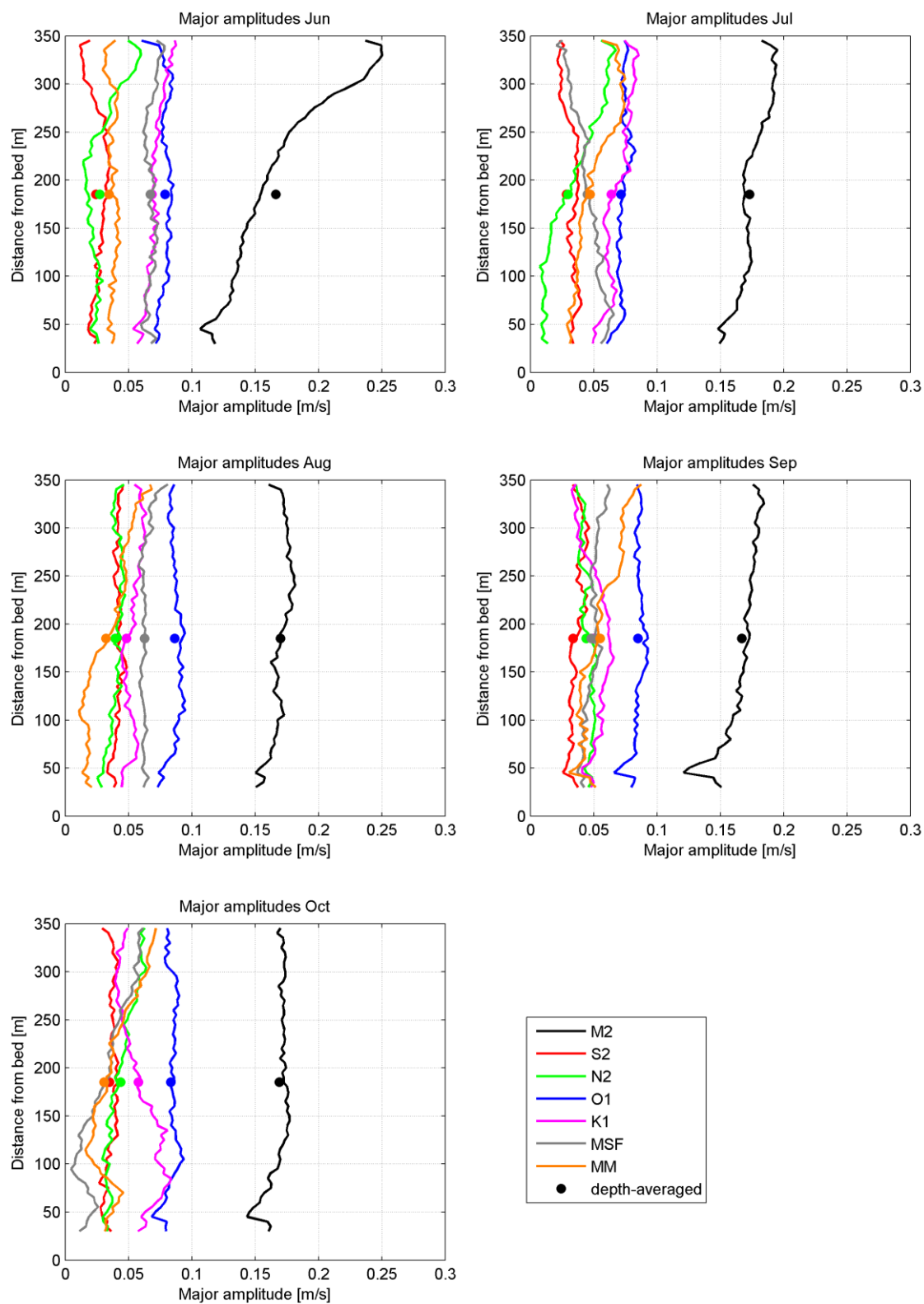


Figure 6.13 Monthly amplitudes ADCP.

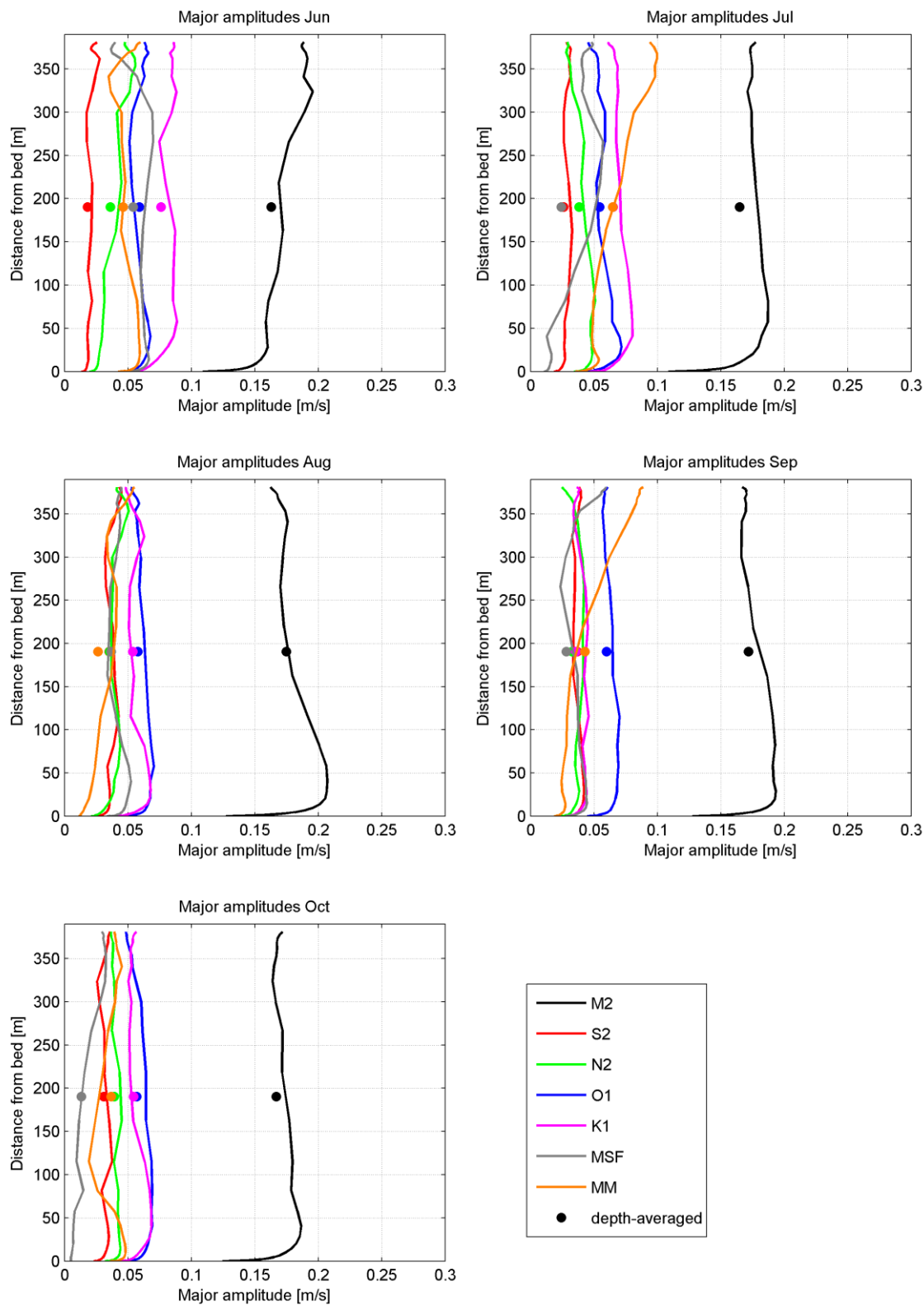


Figure 6.14 Monthly amplitudes model.

A tidal analysis with a running window of 30 days was applied to the modelled and measured velocities. This window is long enough to resolve the M2, S2, N2, O1 and K1 constituents. Internal tides may also play a role; the N2 phasing is out of sync between the model and ADCP in the 30 day running window tidal timestacks (Figure 6.15-Figure 6.16). Due to internal tides, decoupling of the phases with the barotropic tide may occur, which may result in redistribution of tidal energy over the (in this case semidiurnal) constituents such as N2 and M2 (Deltares, 2014a). The presence of an anomaly in the measurements can also be seen at 50 m above the bed in these timestack figures.

The uniformity observed in the M2 profile can also be seen in Figure 6.16 which shows the M2 constituent derived from a running window analysis on the modelled velocities. The trend in time associated with the diurnal K1 is captured by the model.

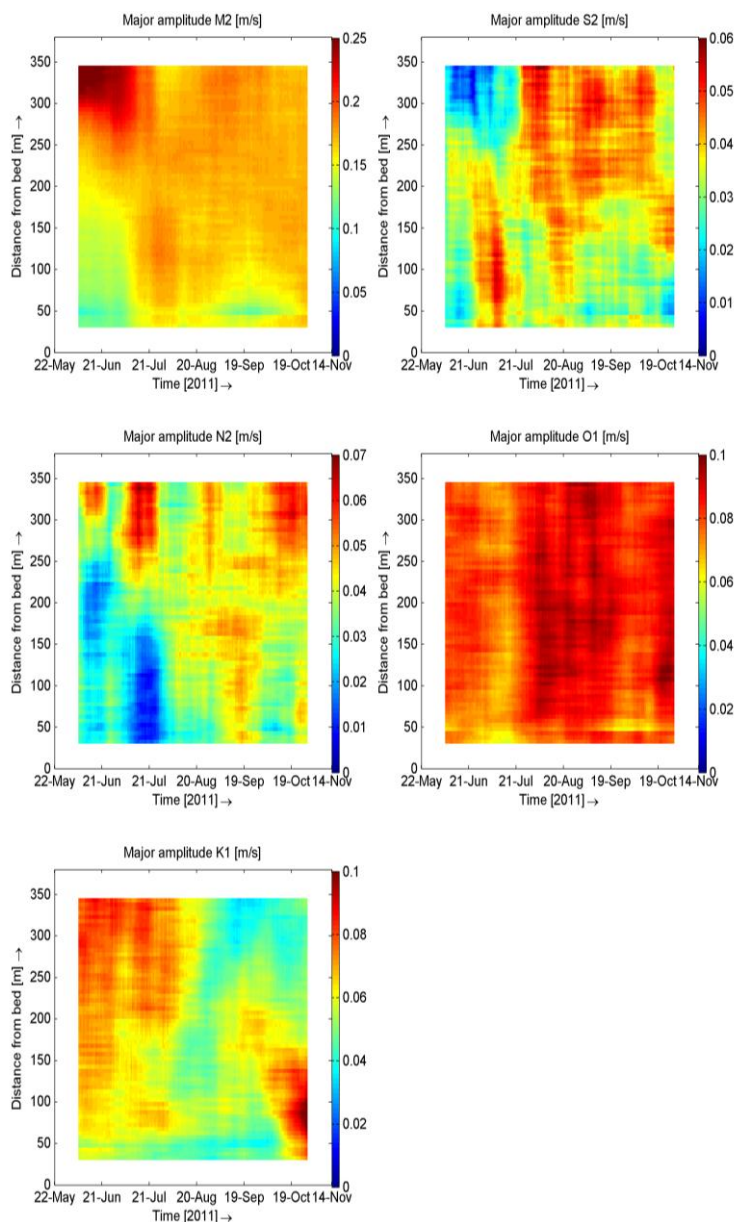


Figure 6.15 Running window timestacks of ADCP constituents.

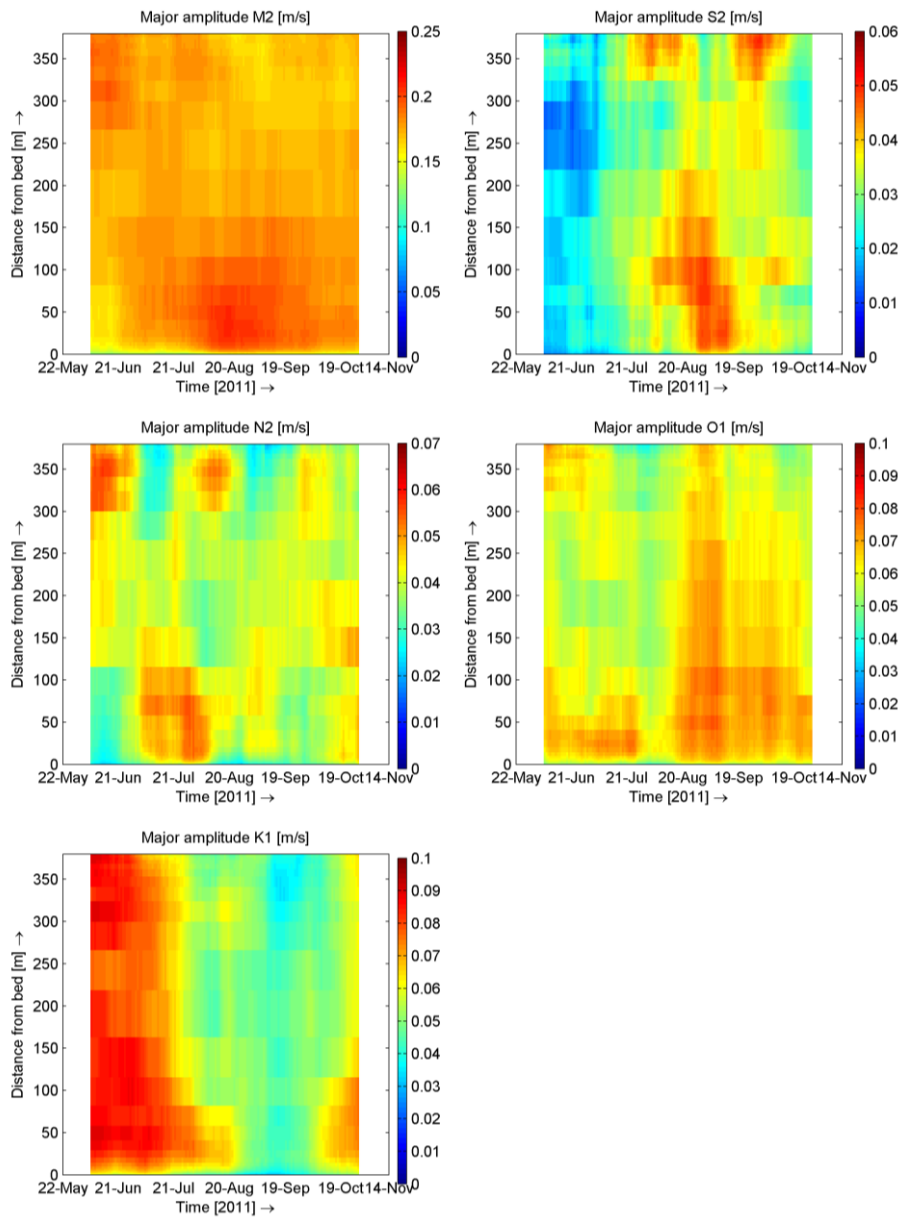


Figure 6.16 Running window timestacks of modelled constituents.

6.3.2 Tidal Ellipses

From the tidal ellipses, it can be seen that the semidiurnal constituents have a strong north-south direction while the diurnal constituents trend more towards north-west to south-east, see Figure 6.17 and Figure 6.18. The M2, N2 and P1 constituents are decreasing in size when moving from surface to bed however this reduction in amplitude is not fully captured by the model. The orientation of M2, S2 and N2 is well captured at both the surface and near the bed. K1 and P1 constituents show a varying orientation over depth. The difference in magnitude is stronger for diurnal components – O1, K1 and P1 at the surface, though the simulation of O1 improves near the bed. The difference in amplitude is larger near the bed for M2, N2, K1 and P1 where the model overestimates (the difference in scale should be noted). Eccentricity (ratio of semi-minor axis to semi-major axis) is well captured by the model for all constituents. The orientations are well simulated except for P1 in the near bed layers. The same patterns are observed comparing the model with the Aquadopp, though the difference in magnitude is smaller and the difference in rotation for P1 is less. Hence the model performs better in the area of interest: near the bed.

The differences between the modelled and measured tidal ellipses can be explained by the model forcing. Water level and flow velocity forcing is derived from the TPXO 7.2 global ocean tide model which is used to generate the tidal component of the model boundary conditions. This global tidal model uses inverse theory to find the optimal balance between the modelled hydrodynamics (water levels and flow velocities) and observations from satellite observations (water levels) and tide gauges (water levels). The forcing from TPXO 7.2 is uniform over depth. Therefore variations of the constituents over depth, which may arise from friction or internal tides, have to be generated in the Delft3D model. A tidal analysis was performed on the depth-averaged TPXO velocity data in Deltares, (2014a) and compared to the ADCP. Here it was also seen that O1 is under-predicted by TPXO and P1 over-predicted and the same phase shifts were observed. Therefore most deviations in the tidal ellipses between the model and the ADCP and Aquadopp may be traced back to the tidal forcing in the boundary conditions.

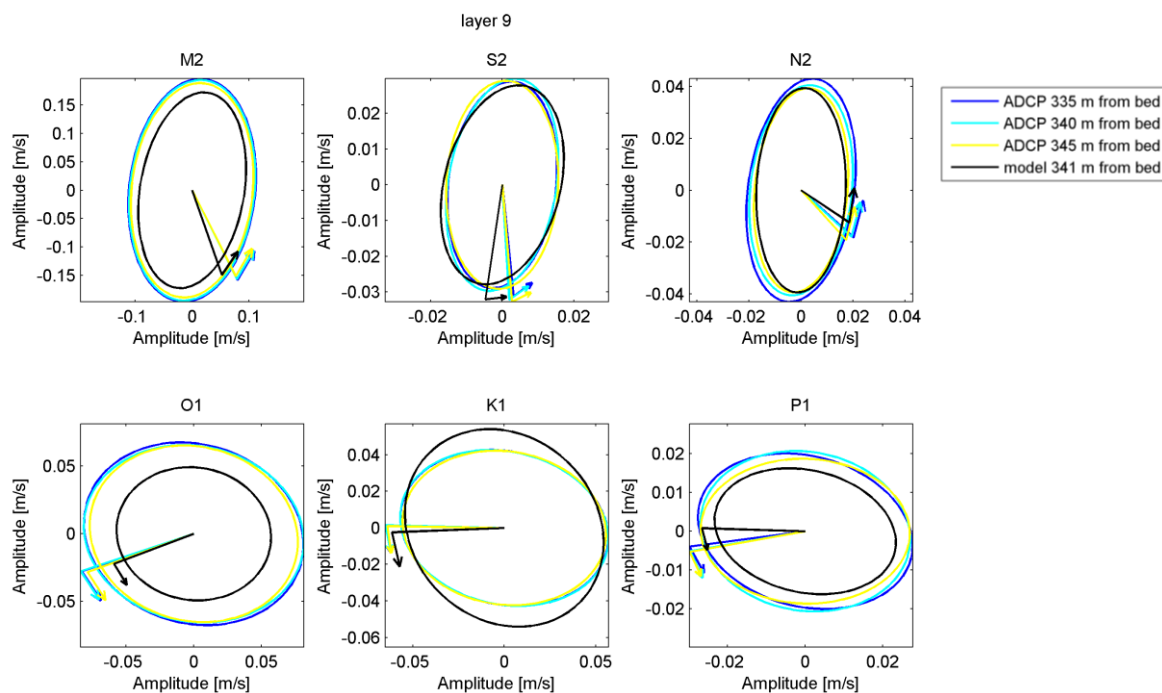


Figure 6.17 Comparison between modelled velocities from layer 9 (near surface) and ADCP.

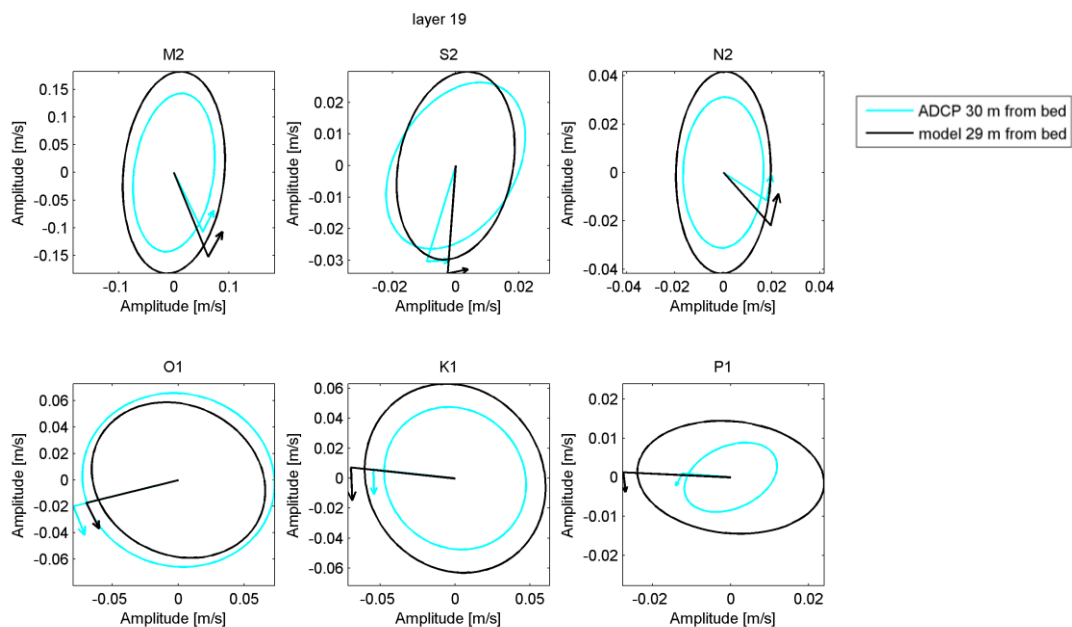


Figure 6.18 Comparison between modelled velocities from layer 19 (near bed) and ADCP.

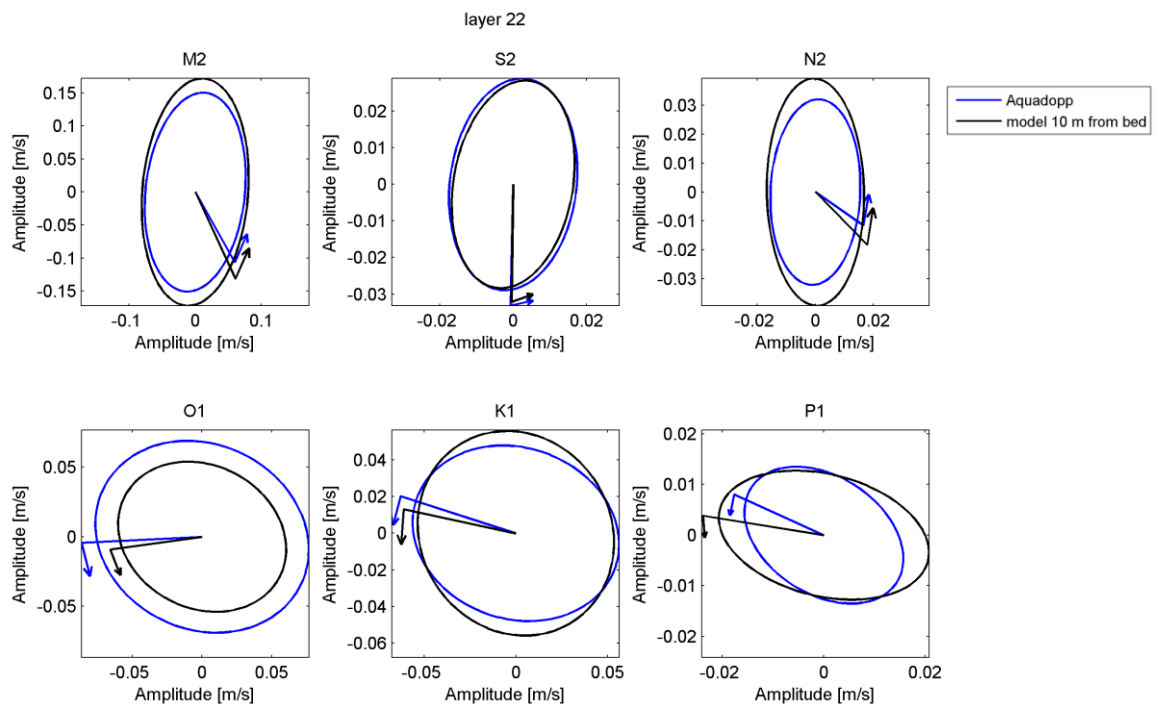


Figure 6.19 Comparison between modelled velocities from layer 22 (near bed) and Aquadopp.

6.3.3 Reconstructed tidal time series and residual flow

The modelled and measured (ADCP) tidal signal was reconstructed based on the most significant constituents from the tidal analysis. To compute the residual flow, the tidal prediction from t-tide is subtracted from the original signal. In Figure 6.20 and Figure 6.21 it is shown that the tidal signal is captured by the model, though the model overestimates the magnitude in the lower half of the water column and underestimates in the upper half of the water column (by 20-40 %). The largest differences however can be seen when comparing the residuals speeds and directions (Figure 6.22, Figure 6.23, Figure 6.24 and Figure 6.25) which at times are captured by the model but in certain periods are overestimated by up to twice the measured value. In July, the modelled residual is greater than the measured residual and the modelled direction is far more uniform. This overestimation is particularly evident in the northward component of the flow. In September the modelled residual is more in line with the measured residual, though the variability is much less. The pattern of overestimation of velocities in the lower water column and underestimation of velocities in the upper water column is also seen in the residuals (not shown here).

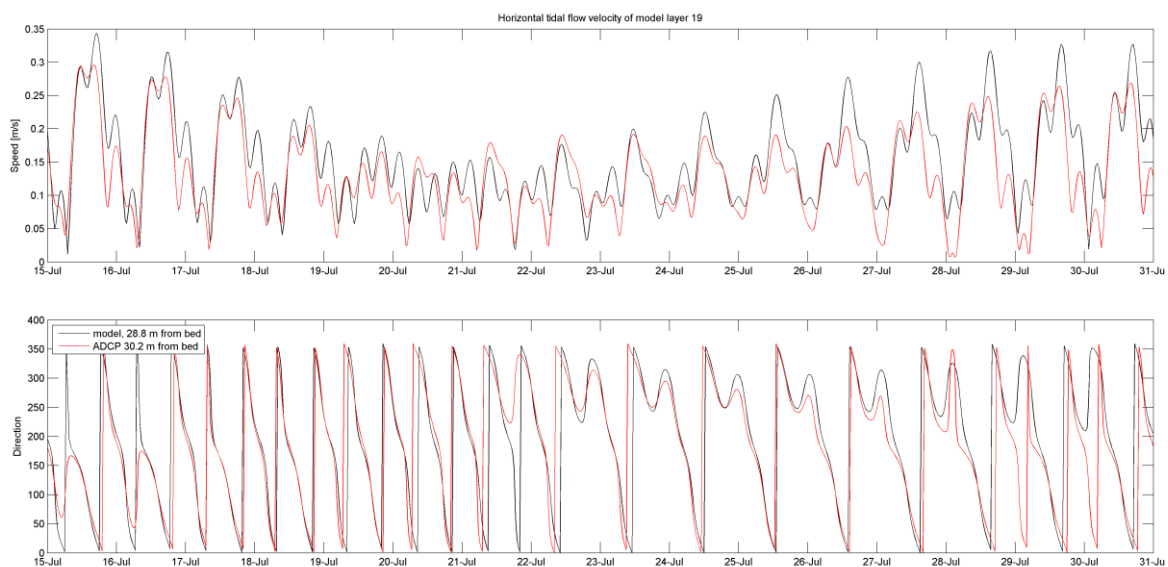


Figure 6.20 Reconstructed tidal signal for layer 19 of the model versus the measurements in the 2nd half of July.

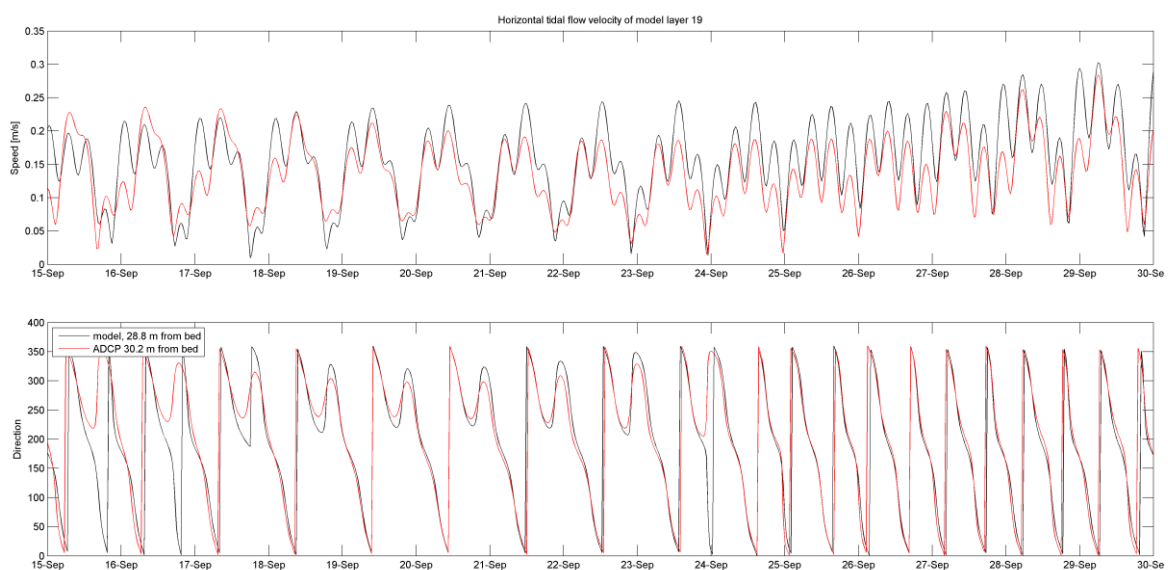


Figure 6.21 Reconstructed tidal signal for layer 19 of the model versus the measurements in the 2nd half of September.

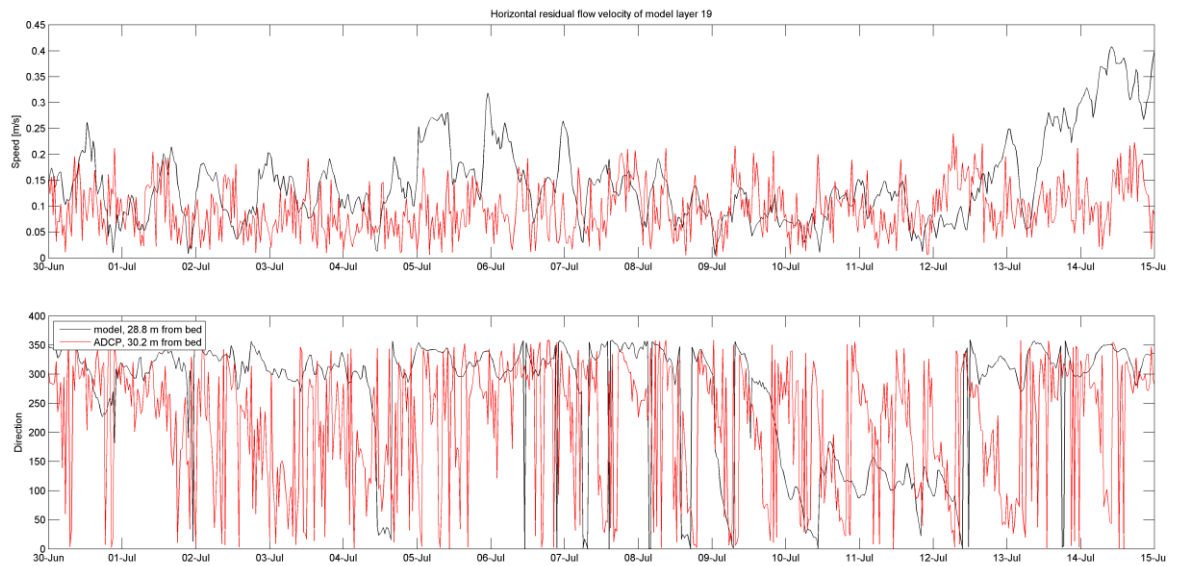


Figure 6.22 Residual signal for layer 19 of the model versus the measurements in the 1st half of July.

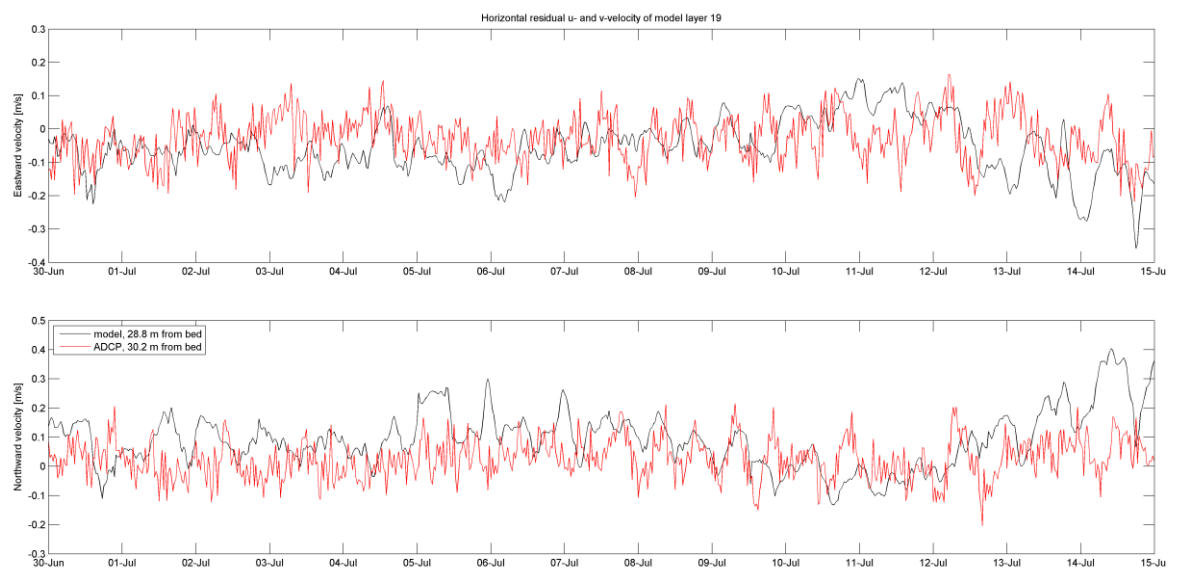


Figure 6.23 Residual u and v for layer 19 of the model versus the measurements in first half of July.

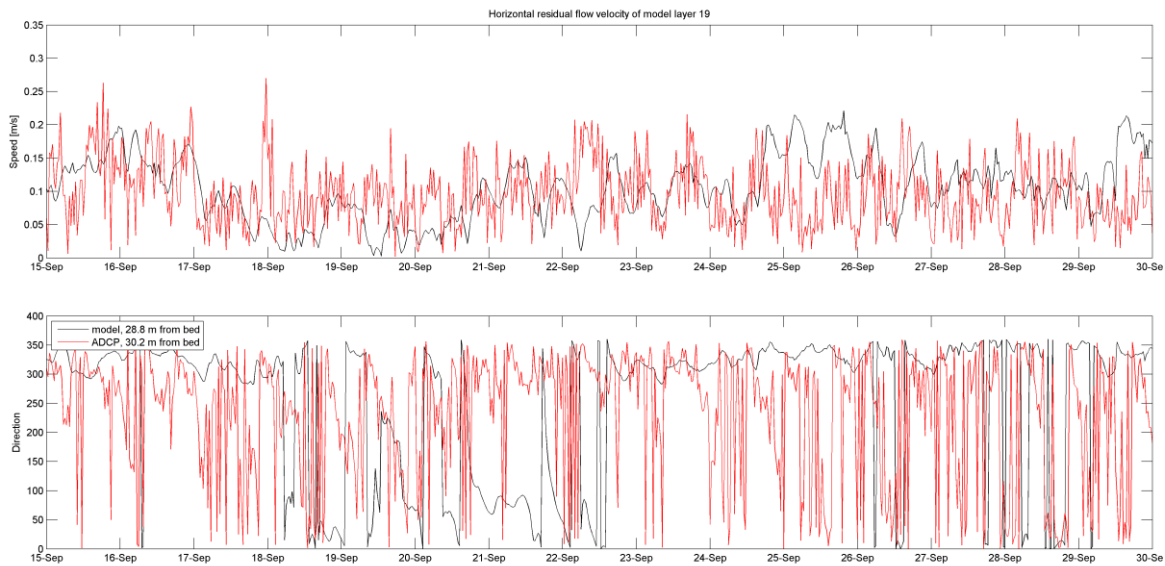


Figure 6.24 Residual signal for Layer 19 of the model versus the measurements in the 2nd half of September.

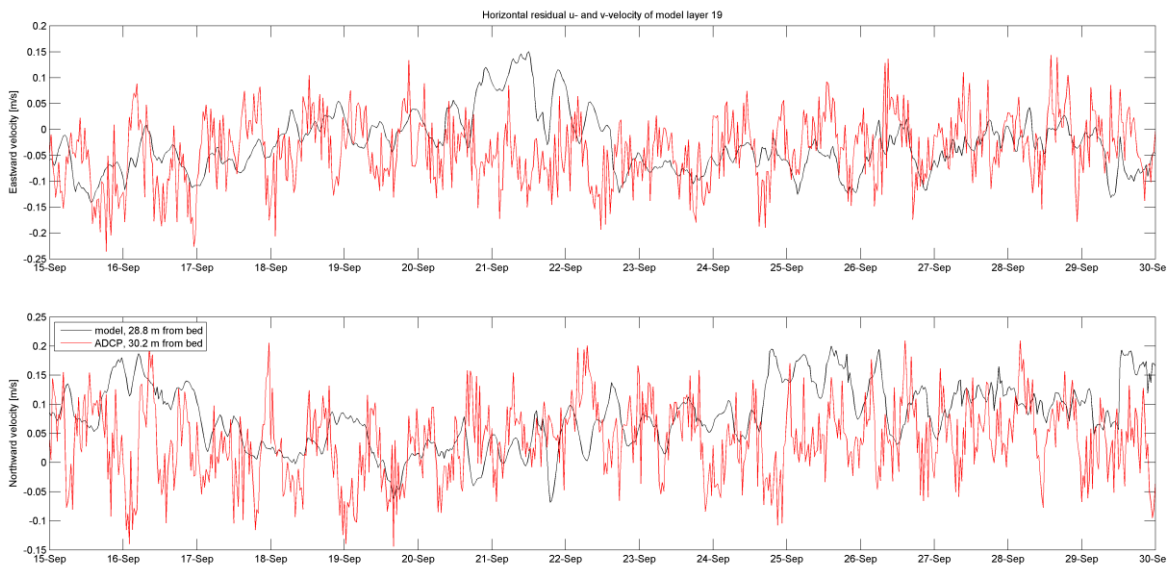


Figure 6.25 Residual u and v for layer 19 of the model versus the measurements in second half of September.

Figure 6.26 shows the eastward and northward components of the time averaged residual velocity through the water column for both the modelled and ADCP time series. Both components of velocity are overestimated by the model by a factor of 2. Figure 6.27 shows the time averaged residual speed (left panel) and direction (right panel) through the water column for the model and ADCP. There is a shift in direction about 200m above the sea bed corresponding to the level at which the model switches from underestimation to overestimation of the tidal current velocities. This is indicative of an exchange flow profile.

The advection of the modelled plume is orientated in the correct direction, though may be transported further in the model than in reality. Although the time-averaged residual speed is overestimated by the model, the modelled time-averaged residual direction in the lower half of the water column corresponds with the time-averaged residual direction of the ADCP. This

shows that, though the time-averaged residual speed may be overestimated, the direction of transport in the lower half of the water column correct.

The variability in the measured residual is also much greater than that of the modelled one, which may also influence the time-averaged residual. When looking at the time-series above there is not always a great difference in residual speed magnitudes for the u and v components of velocity.

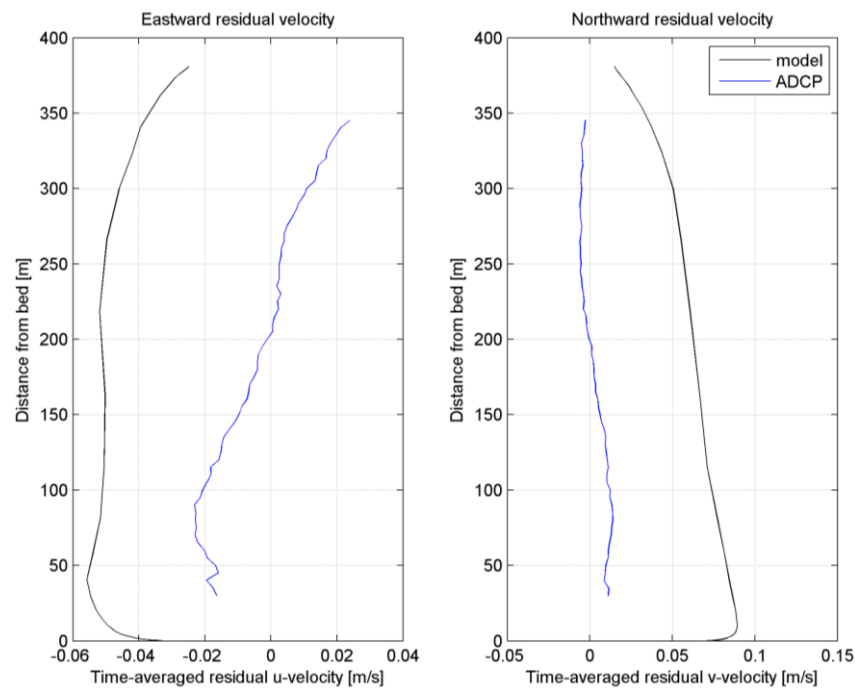


Figure 6.26 The eastward and northward residual velocities of the model versus ADCP.

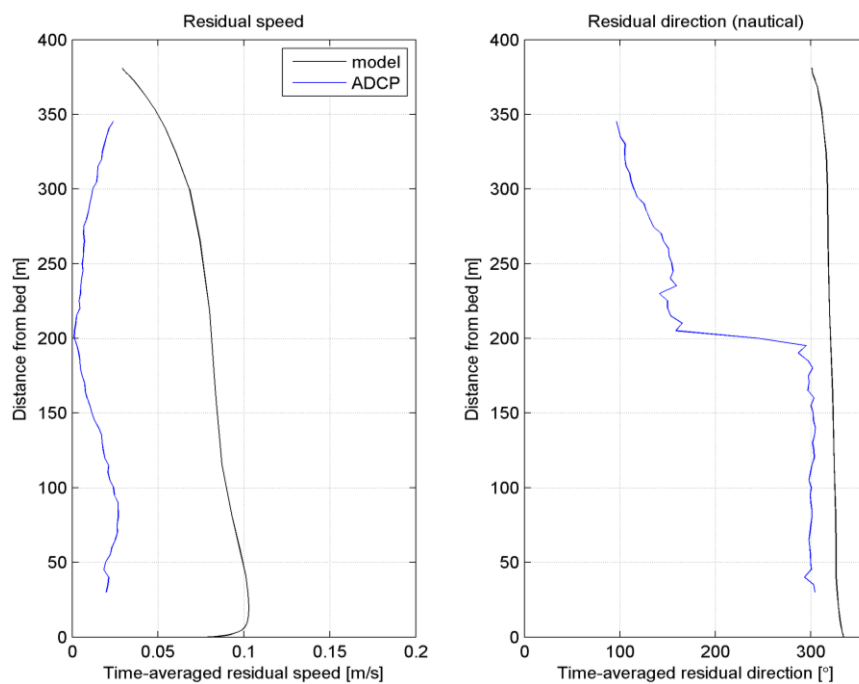


Figure 6.27 The residual speed and direction of the model.

6.3.4 Godin filtered signal

The non-tidal signal has been computed in two different ways: 1) The tidal prediction from t -tide is subtracted from the original signal (see previous section) and 2) A Godin filter was applied to the models (both regional and local) and data (ADCP) to remove high frequency components. The Godin low-pass filter effectively removes all daily tidal period energy. The HYCOM data are not filtered, because HYCOM does not contain the tidal (high-frequency) signal. The plots below show timestacks of Godin filtered speed and direction all at the ADCP mooring location for:

- The ADCP data
- The HYCOM ocean model that was used to force the regional model for currents (u and v), salinity, temperature
- The Regional Model
- The Local Model

The ADCP shows low residual current speeds throughout the water column with strong variation in direction between predominately northwest and southeast directed currents over the entire period (Figure 6.28). The HYCOM model shows higher current speeds in the near the surface layer that the ADCP does not cover, the top 10% of the water column is cut off in the ADCP data. These higher near surface speeds can be attributed to wind effects (Figure 6.29).

The Regional Model shows much less variation in direction (Figure 6.30) with flow predominately towards the northwest and slightly higher velocities throughout the water column than measurements. The easterly component of the flow seems to be under estimated in both the regional and local model – there is a strong easterly component to the flow in the measurements but almost always northerly, north westerly flow in the model, with some periods of north easterly flow. In general the direction of residual flow in the model is much more uniform than in the measurements. This may be due to the application of Riemann boundary conditions which only allow flow normal to the boundaries. Therefore the full variability in current directions, associated with the residual flow, may not be adequately represented in the model. As seen previously, the flow direction associated with the tidal signal is captured by the model.

The higher near bed velocities seen during certain periods in the regional model are further enhanced in the Local Model (upper panel of Figure 6.31) when comparing to the measured velocities (upper panel Figure 6.28). This is particularly evident around mid-June and mid-July when modelled velocities are much higher in the lower 100 m of the water column.

The uniformity in modelled direction versus measured direction can also be clearly seen in the Godin filtered rose diagrams (Figure 6.32 - Figure 6.35). The orientation and spread of the modelled directions are much closer to the measured directions near the bed than at the surface, where, although the spread in modelled direction is larger, the main orientation of flow is still north-west, whereas in the measurements it is south-east.

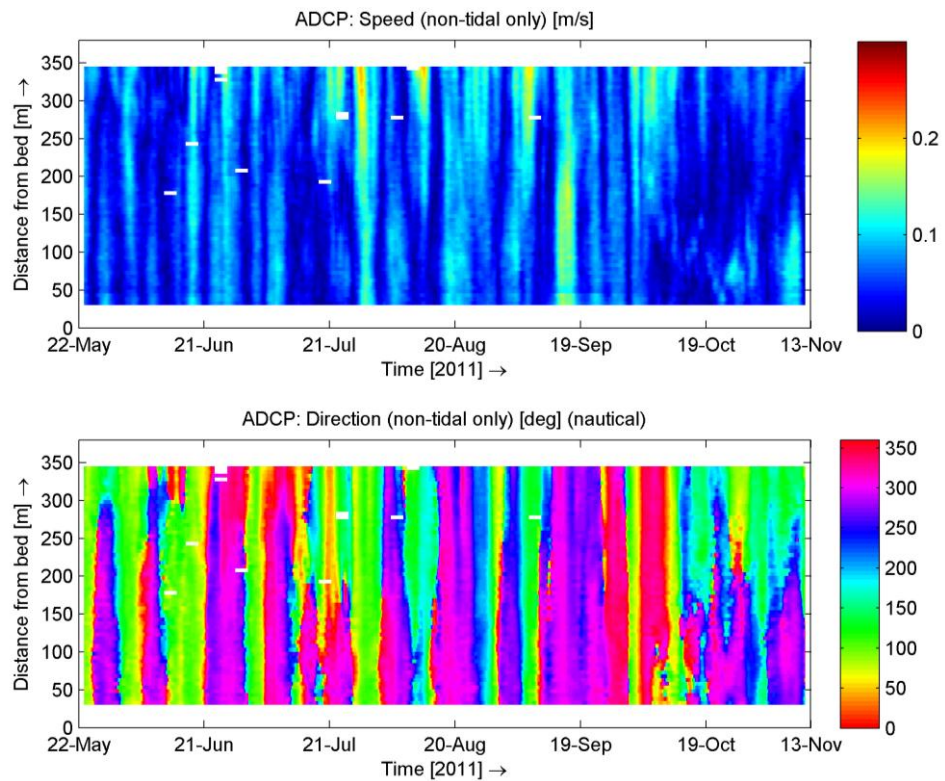


Figure 6.28 Godin filtered current speed (top) and direction (bottom) from the ADCP data.

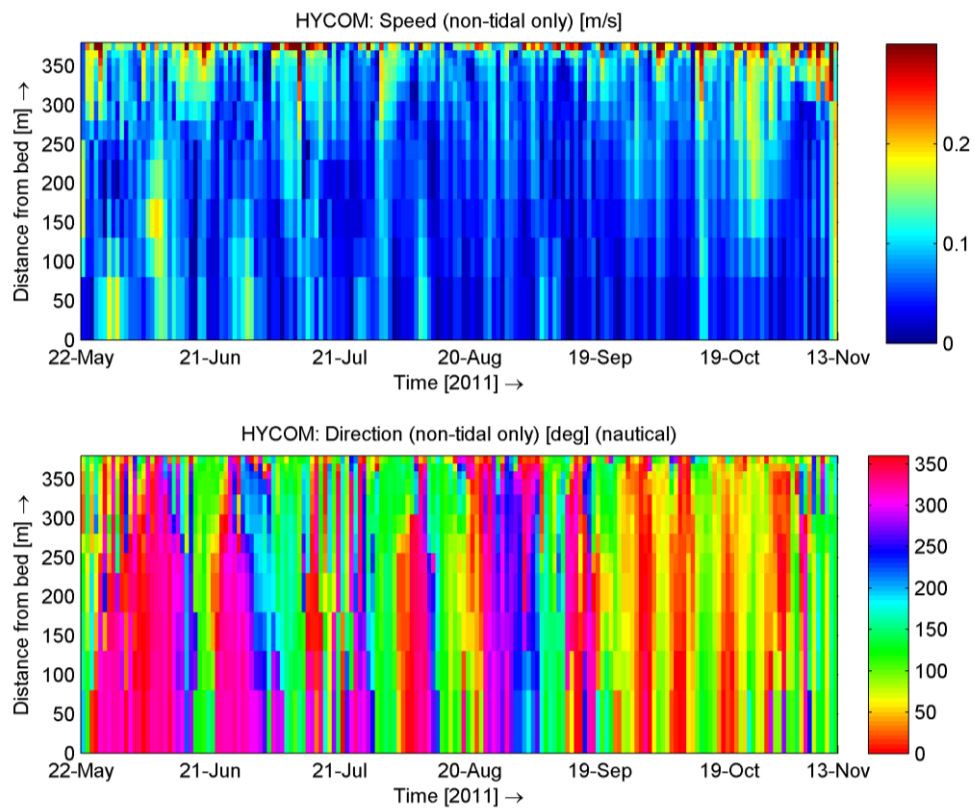


Figure 6.29 Velocities obtained from HYCOM data at the location closest to the ADCP location. No filtering applied.

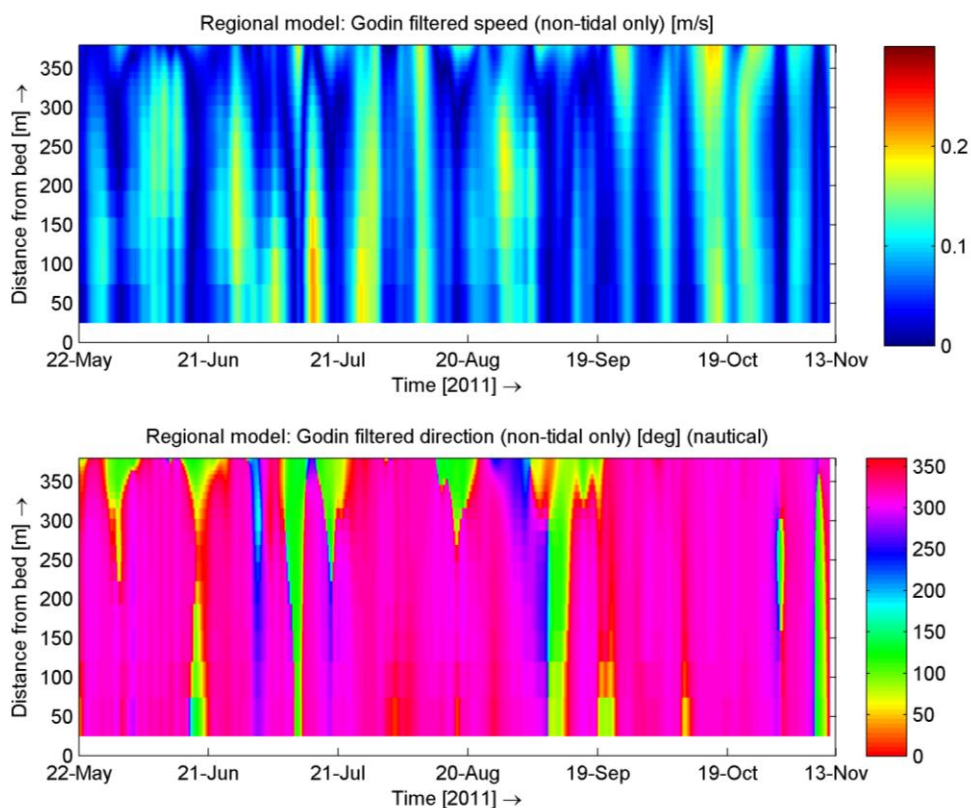


Figure 6.30 Godin filtered current speed (top) and direction (bottom) from the regional model.

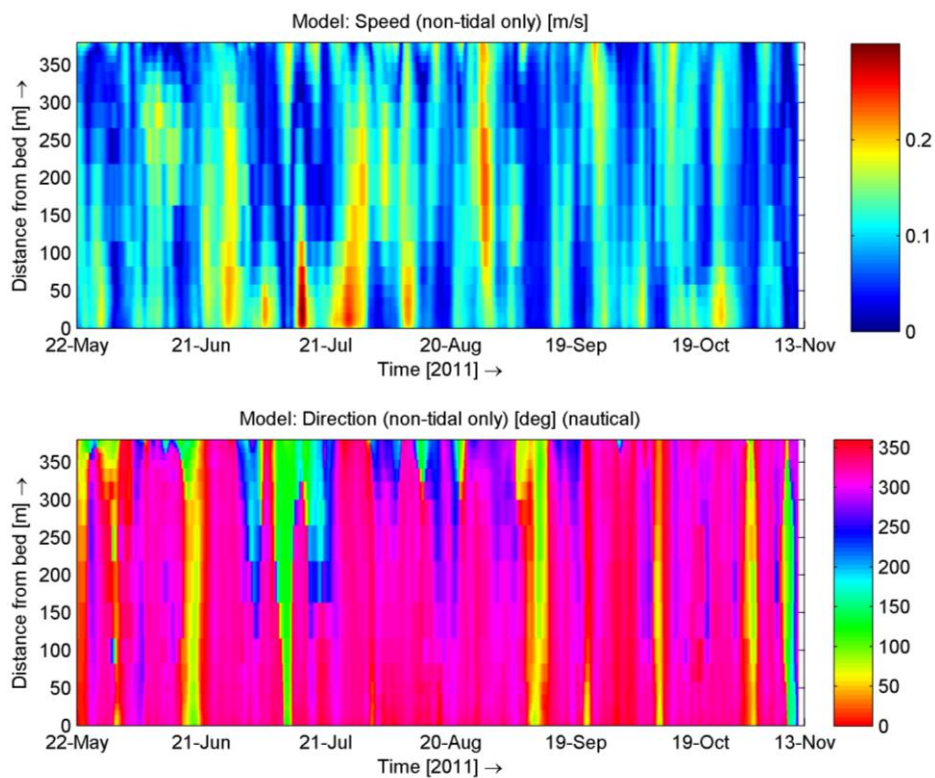


Figure 6.31 Godin filtered current speed (top) and direction (bottom) from the local model.

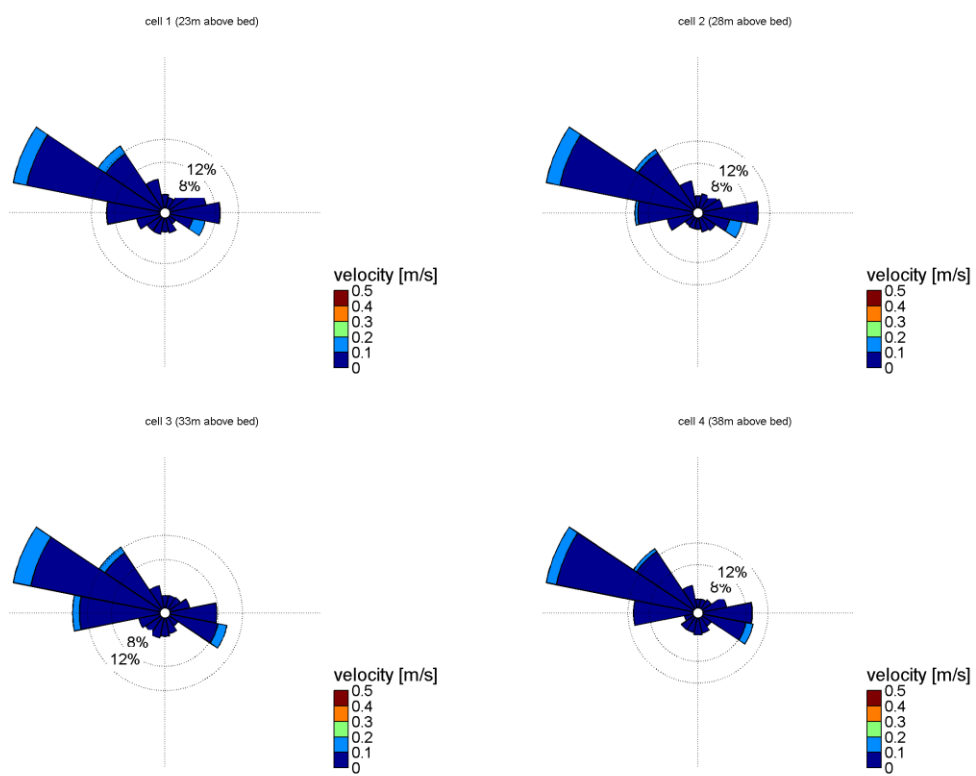


Figure 6.32 ADCP direction rose near the bed.

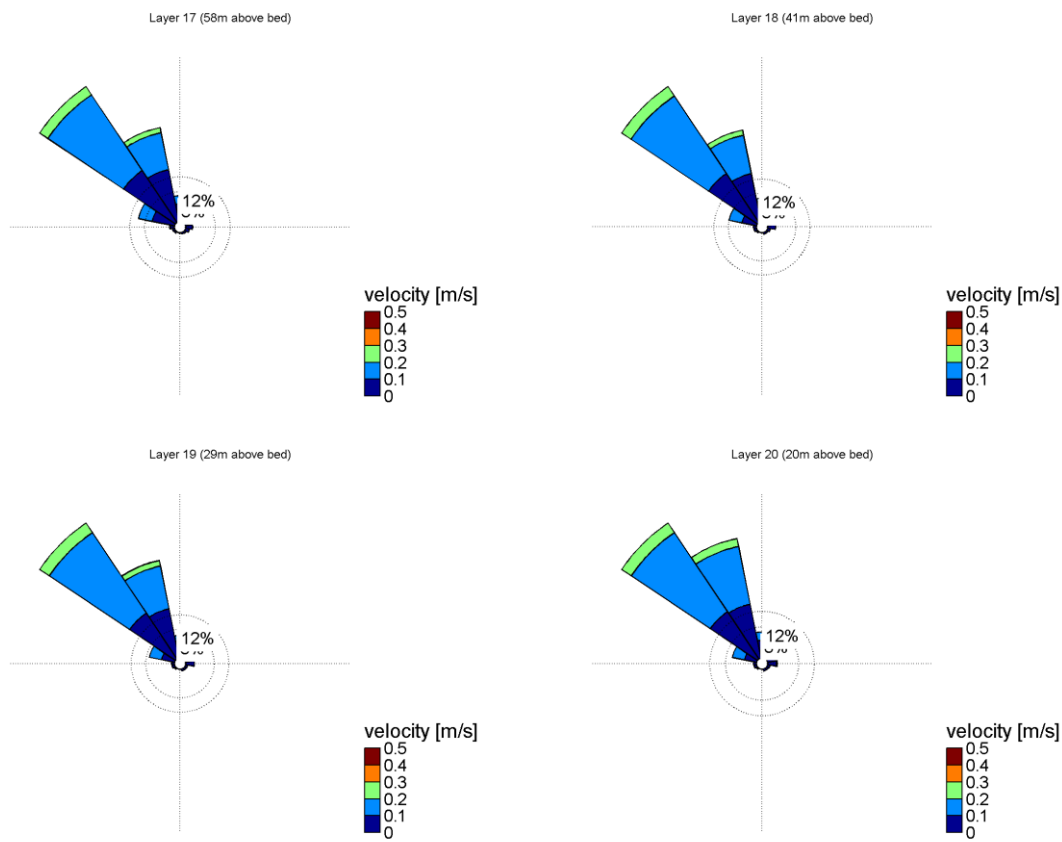


Figure 6.33 Model direction rose near the bed.

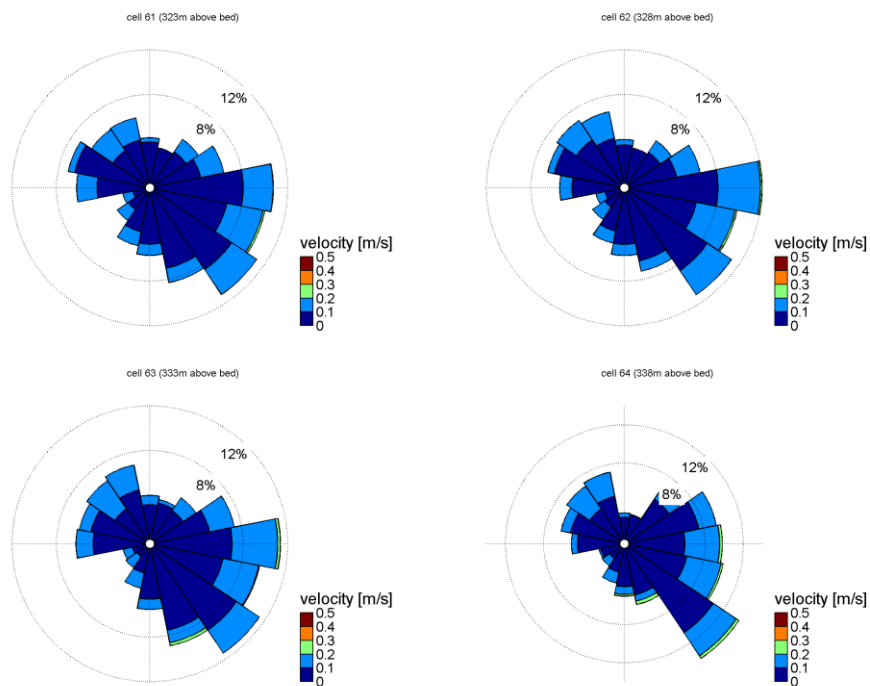


Figure 6.34 ADCP direction rose near the surface.

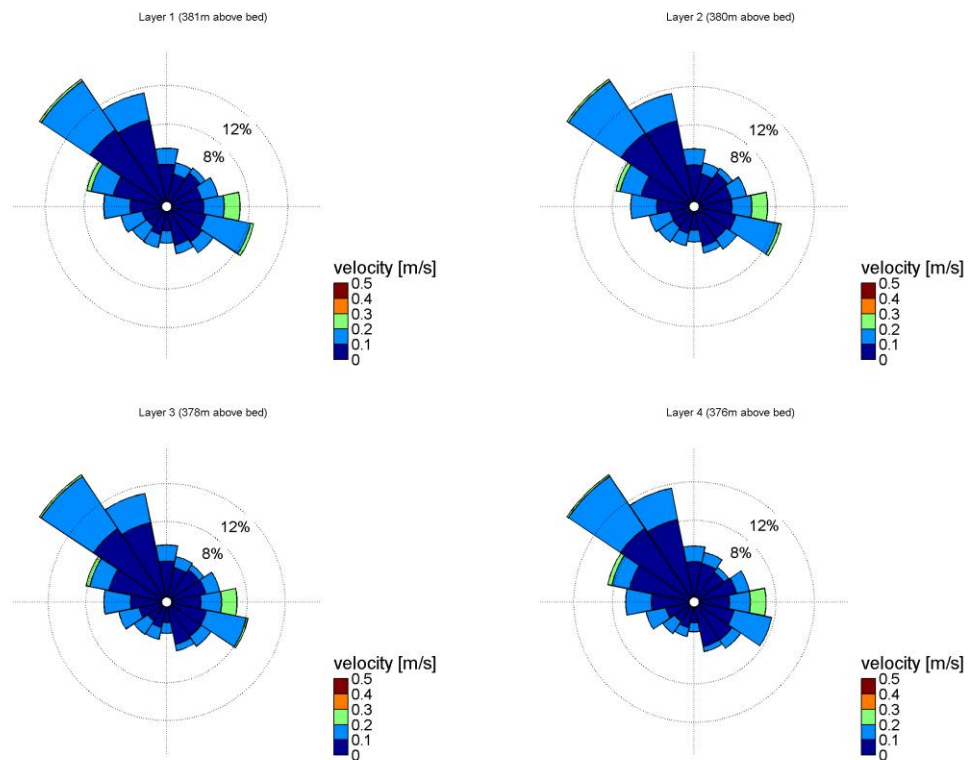


Figure 6.35 Model direction rose near the surface.

6.3.5 Internal tides

Internal tides are recognized by a strong shear in their instantaneous horizontal currents; usually the currents in the lower layer are oppositely directed to those in the upper layer. Internal tides can also have significant vertical velocities (higher than 1 cm/s) (Deltares, 2014a; van Haren, 2009). During more stratified periods, internal tides are more likely to be present and stronger, but as stratification becomes stronger their amplitude will diminish, because the density difference becomes larger. Due to the small difference in density between stratified layers compared to the large density difference between air and water, internal waves/tides have much larger elevation of internal surfaces than surface waves/tides. The degree of stratification determines the presence and magnitude of internal waves, as well as their propagation. Associated velocities extend over the full water column, including vertical velocities which are important for mixing and resuspension, thus also for plume dispersion.

To identify internal tides, the depth averaged ADCP velocity was subtracted from the eastward and northward component of the velocity. Figure 6.36 shows an example of two structures that appear frequently in the ADCP timestacks of the baroclinic eastward and northward velocities. An abrupt phase shift of 180 degrees in the vertical can be seen at about 200 m above the bed. This is indicative of internal tides. For the same period no evidence of internal tides is visible in the model (Figure 6.37). There are several reasons why internal tides are not resolved in the model.

This may be:

- 1) A result of uniform tidal constituents in the vertical from the TPXO 7.2 boundary conditions, indicating that internal tides are not forced to the model by the boundaries. Internal tides need to be generated in the model itself; however, the model size may not be large enough for these internal waves to be generated within the domain;
- 2) That density stratification in the model is not strong enough to maintain the presence of internal tides. The treatment of density in the model is described further in section 6.4. If the internal tides are not represented in the boundary conditions, the model size may not be large enough for these internal waves to be generated within the domain.

The presence or lack of internal tides in reality may also contribute to the time varying performance of the model compared to the measurements. For example, the model often performs better in September than in July. Figure 6.38 and Figure 6.39 below show that internal tides are more evident in July than September and this can also be linked to periods of density stratification. Around the 21st to the 23rd of July in particular, velocities near the surface are high (in the measurements) with strongly opposing current velocities near the bed.

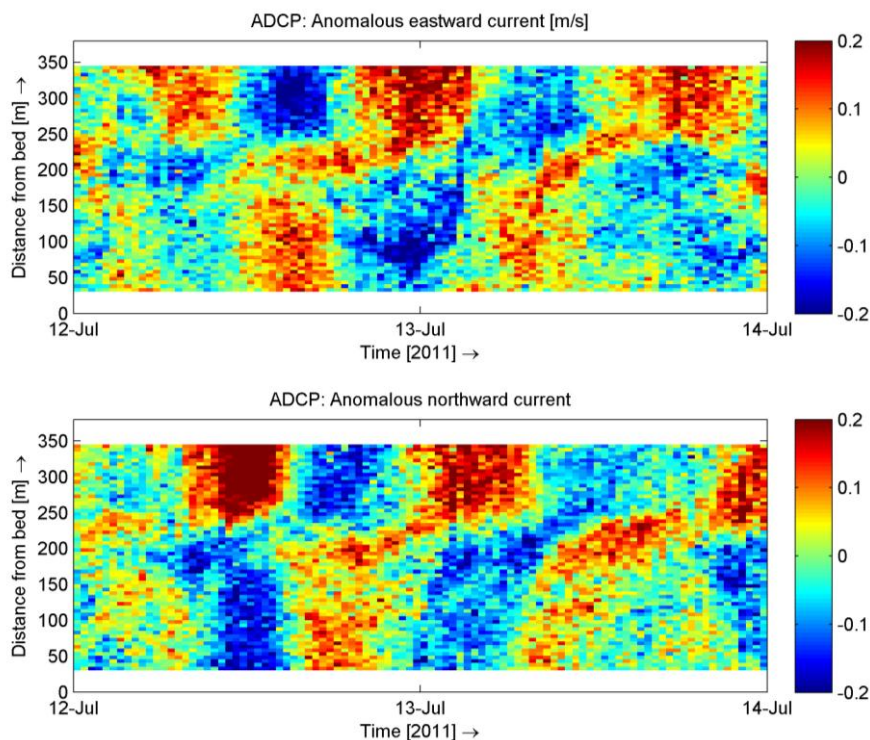


Figure 6.36 Anomalous currents from ADCP.

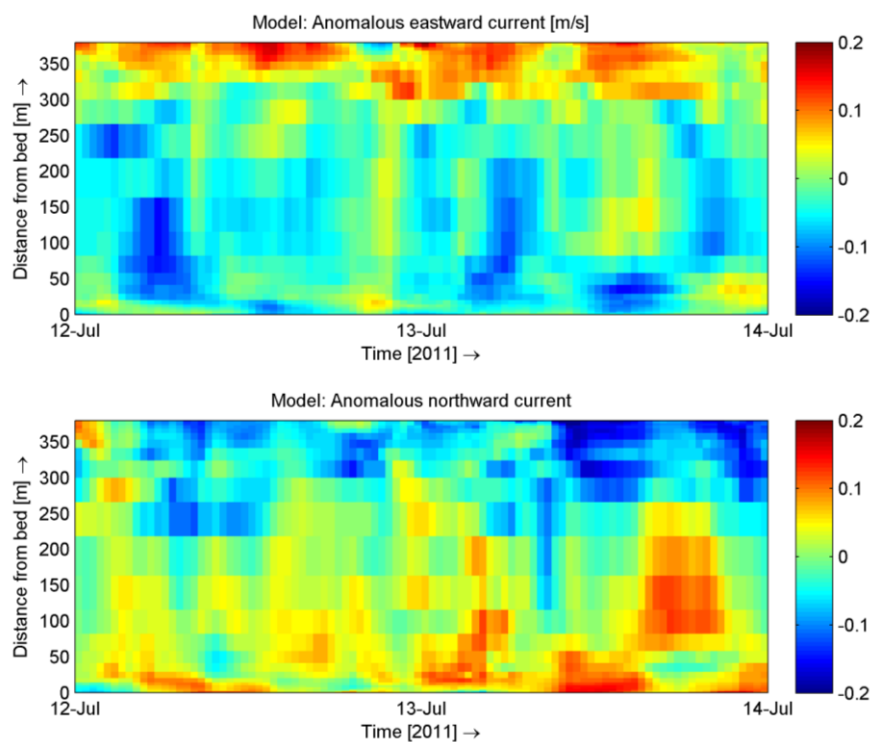


Figure 6.37 Anomalous currents from model.

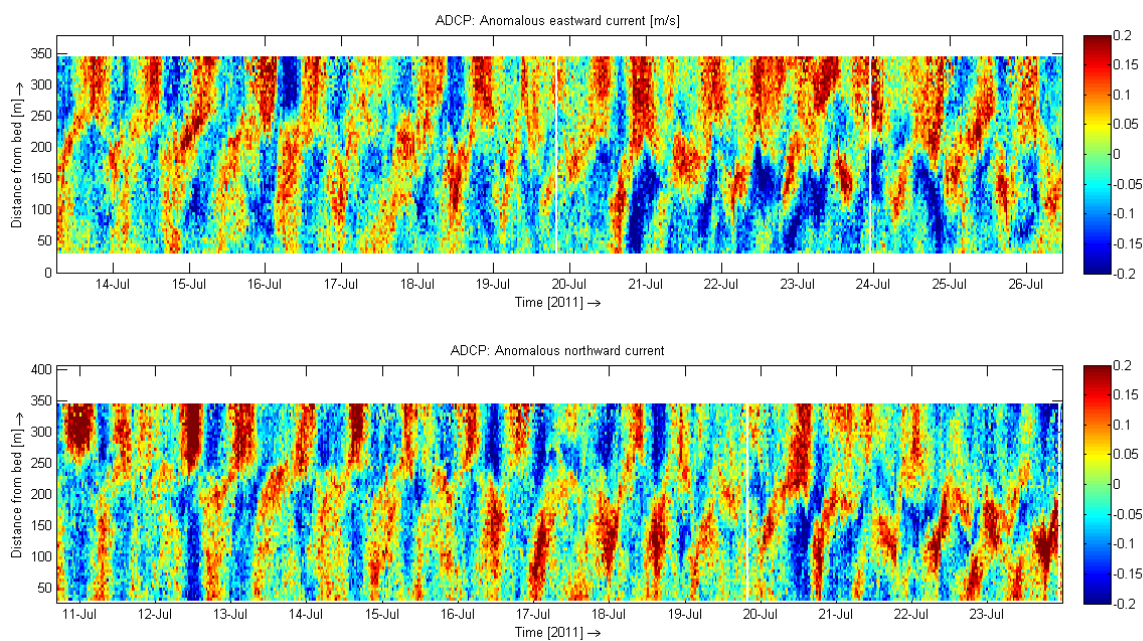


Figure 6.38 Strong internal tides in ADCP.

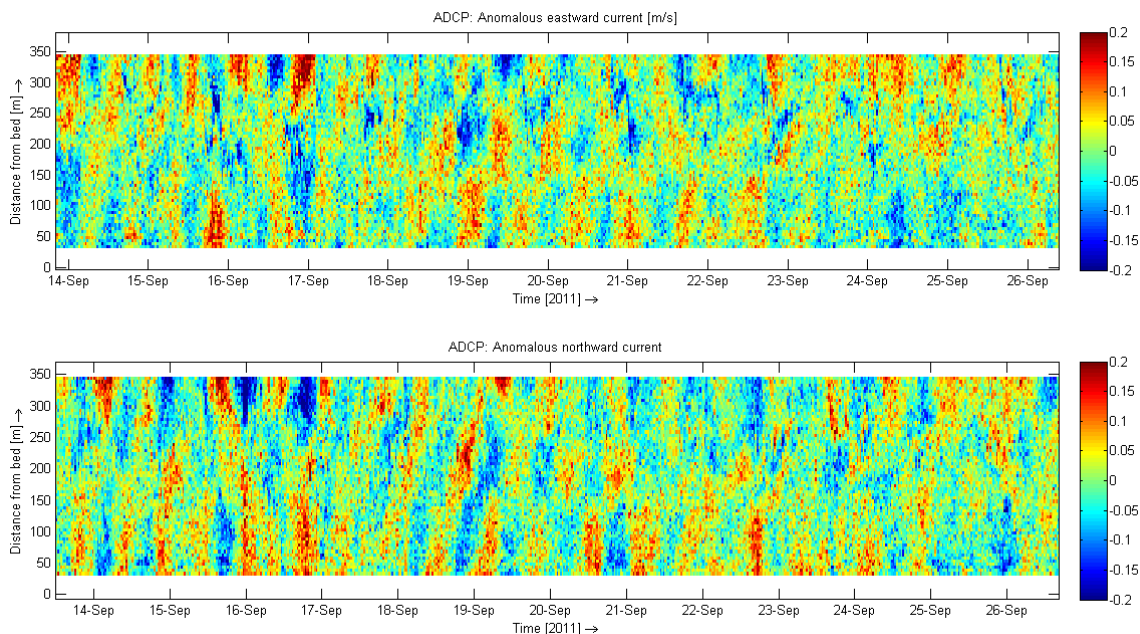


Figure 6.39 Weak(er) internal tides ADCP.

6.4 Salinity, temperature and density

A main oceanographic feature along the Chatham Rise is the Subtropical Front (STF) (Heath *et al.*, 1985). The STF separates the warm and salty subtropical water from the cold, fresher sub-Antarctic waters in the shallow ocean in the New Zealand region. Depending on the seasons and the location, waters on the crest can be subtropical, subarctic or a combination of the two. This is reflected in vertical and horizontal salinity, temperature and density gradients and associated geostrophic currents, all displaying seasonal variations.

The movement of warmer waters from the north over the rise is captured in the model. This temperature front, visible in the HYCOM forcing conditions is also present in the Delft3D model, particularly at the surface

The left panel of Figure 6.40 shows the modelled density as computed in Delft3D. Delft3D does not include the effect of pressure in the water column. This affects the vertical gradient of the density and so turbulent mixing will be underestimated. The right panel shows the density from Delft3D including the effects of pressure in the density computations at the ADCP location. Here more stratification is clearly visible and this matches with the corresponding density computed from the HYCOM forcing (Figure 6.41).

Looking at the HYCOM forcing (Figure 6.41), surface density is highest in August/September and lowest in February. Seasonal variation is visible to depths down of 200 m; this may induce turbulent mixing and affect current velocities in the upper half of the water column.

Geostrophic circulation due to density differences across the convergence zone of the STF and the sub-Antarctic waters is seen as a strong eastwards zonal flow (Heath, 1983). This component of the flow in the model may be weakened by the more gradual density gradients.

The salinity and temperature at the ADCP location in the local model show some degree of stratification (Figure 6.42 - Figure 6.43). Mixing of temperature and salinity through the water column could be suppressed by the fact that density is not as stratified in the model due to the exclusion of pressure effects.

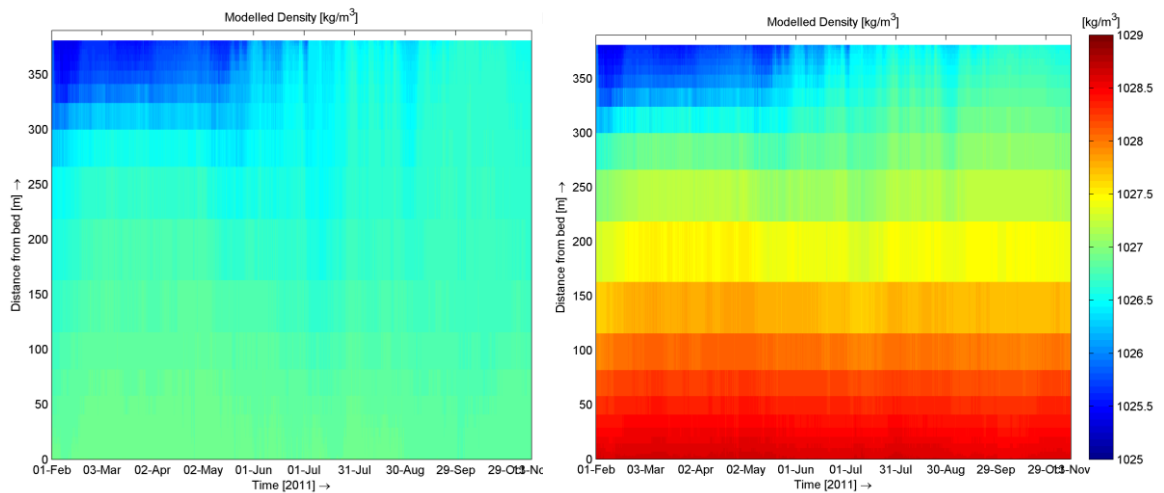


Figure 6.40 Density as computed by Delft3D at the ADCP location (left) and density from Delft3D when the pressure component is added to the UNESCO formulation (right).

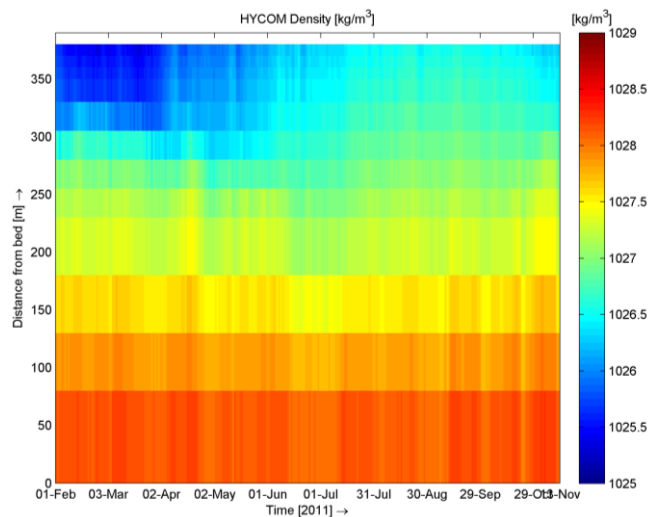


Figure 6.41 Density from HYCOM when the pressure component is added to the UNESCO formulation.

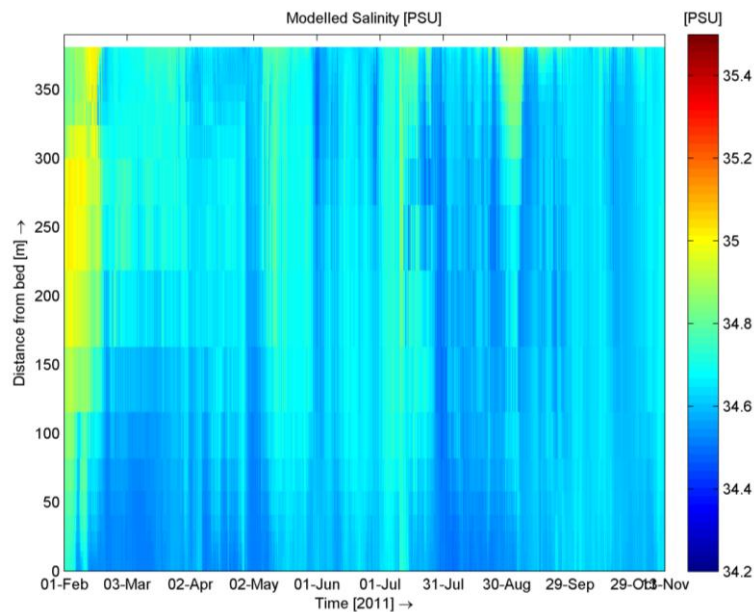


Figure 6.42 Salinity from the Local Model at ADCP location.

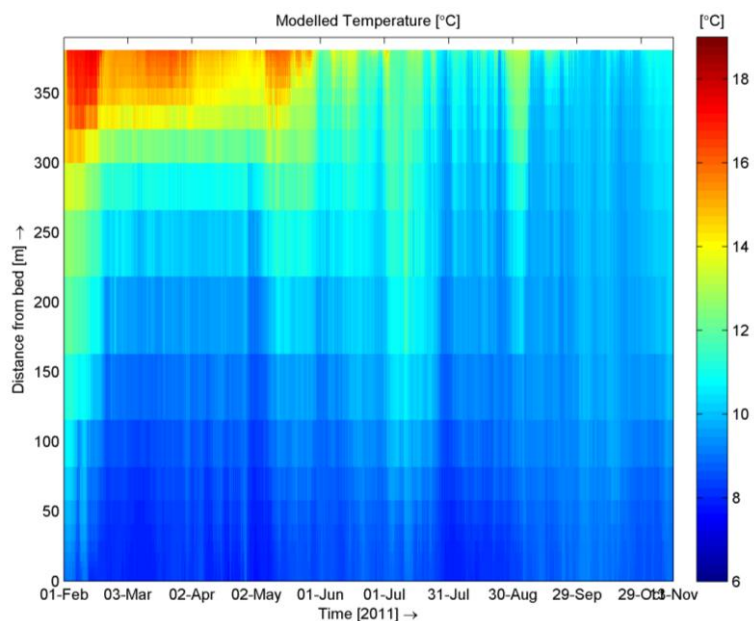


Figure 6.43 Temperature from the Local Model at ADCP location.

6.5 Implications of model verification

The objective of this study is to understand and predict the dilution and dispersion of the dredged mine tailings sediment plume discharged on the Chatham Rise. Characterisation of the plume fields by modelled suspended sediment concentrations, occurrence and durations are important to characterise the risk to biota.

The performance of the numerical model presented here is discussed in terms of the oceanographic and sediment transport mechanisms that influence the behaviour of the plume. A summary of the spreading of the plume and the concentrations modelled as well as the implications of the model verification on those results is given in Chapter 8.

Several mechanisms are of importance to accurately predict the plume dispersion:

- The near bed current velocities
- The direction and speed of the residual current
- The period and area over which the plume is spread which depends on the dilution and dispersion of the plume, which in turn depend on the hydrodynamic conditions at the time of discharge
- The bed shear stress and the critical shear stress for erosion (depending on the mine tailing characteristics) are important for the resuspension of sediment that has settled. This aspect of the study is covered in Deltares, (2014b) and not discussed further here.

Main implications of model verification

- The higher near bed currents at times predicted by the model (generally when conditions are more stratified), means that the modelled plume will be carried further from the disposal site in certain periods but not necessarily spread over a larger area. The average (residual) velocity, is overestimated by the model, ultimately determines the position of the deposition footprint relative to the position of the plume discharge. **The plume transport predicted by the model is therefore overestimated compared to reality.** This spreading of the plume is governed by vertical mixing and Taylor shear dispersion. See text box below.
- **The residual direction in the lower half of the water column where the sediment plume is discharged and is transported is on average correct.** There are times in the measurements when the residual direction of the flow is east, however the direction remains predominately to the north-west in the model.

These and other aspects of the model performance that will influence the transport and dispersion of the sediment plume are outlined in more detail in the bullet points below:

- Current velocities are at times overestimated in the lower half of the water column, with most overestimation (by a factor of two at most) occurring some days in June and July. In periods of less stratification i.e. September – November, current velocities only slightly overestimate at times. This overestimation can originate from the HYCOM boundary conditions generated for the regional model (Deltares, 2014a).
- Though Delft3D is capable of modelling internal tides (Uittenbogaard 1995), internal tides are not resolved in the model. When conditions are stratified, it is possible that vertical exchange of horizontal momentum i.e. eddy viscosity, is underestimated by the k- ϵ turbulence model due to the lack of contribution by internal tides. This may reduce the under- and overestimation of the near-surface and near-bed velocities respectively, compared to the ADCP.
- Residual flows, though small, are over estimated by the model. The time averaged residual direction however in the lower water column is simulated as north north-west in line with the measured residual direction. The depth at which the time-averaged residual direction shifts to a more easterly flow is also where the model begins to underestimate the current velocities. This shear in horizontal current direction may be as a result of internal tides.

- There are large gradients of water properties across the rise, associated with the subtropical convergence. A large temperature front across the rise, as present in HYCOM, is captured in the model. The strength and motion of this front across the rise will affect current velocities and hence the transport of the plume.
- The tidal signal and tidal ellipses are well reproduced by the model so these diurnal and semi-diurnal speeds and directions which influence the sediment plume on varying time-scales are taken into account

Further detailed discussion on the hydrodynamic processes influencing the transport and spreading of the plume is described in the text box on the next page.

Oceanographic processes influencing plume transport and dispersion – more detailed discussion

Horizontal dispersion and settling velocity determine the time scale over which sediment from an injected plume (re-) deposits. Horizontal dispersion is dependent on the degree of stratification therefore dispersion of the sediment plume will be greater during periods of stronger stratification.

Vertical mixing as well as vertical shearing of the horizontal velocity are critical processes for dilution and dispersion. The horizontal dispersion or mixing due to vertical mixing and vertical differences in horizontal transport is known as Taylor Shear dispersion (Taylor, 1953).

The stronger the vertical mixing, the less the horizontal dispersion and vice versa. Large gradients in horizontal current velocities over the vertical will induce vertical mixing. The model profiles can be qualitatively compared to the ADCP profiles (tidal currents only) to infer differences in vertical mixing between the model and ADCP, particularly in different periods. The largest difference in measured flow velocities over depth occurs in June when there is a strong gradient in the major tidal amplitude (M2) over depth and so it is expected that more vertical mixing takes place and horizontal dispersion will be less. When this occurs, the residual current will advect the sediment plume in the residual direction but if dispersion is weak then the plume may be advected further from the discharge location but necessarily dispersed over a wider area. Variation in the vertical is less in the model in June and as stratification may be under-represented in the model, more horizontal dispersion of the modelled plume will take place during this period than in reality. In addition the residual current is stronger in the model and so the plume will also be transported further in the model.

Therefore, in periods when the profiles over depth are more uniform, for both modelled and observed, the degree of horizontal dispersion simulated by the model will be closer to that in reality. The sharp gradient in velocities in the lower 50 m of the model during the entire period will also enhance the degree of dispersion in the model whereas the gradient is more gradual in the measurements.

The higher velocity of the near bed currents predicted at times by the model implies that the plume will be carried further from the disposal site but not necessarily spread over a larger area. The average (residual) velocity, also overestimated by the model, ultimately determines the position of the deposition footprint relative to the position of the plume discharge. This spreading of the plume is governed by vertical mixing and Taylor shear dispersion as described above. The residual direction in the lower half of the water column where the sediment plume is discharged and is transported is on average correct. There are times in the measurements when the residual direction of the flow is to the east, however the direction remains predominately to the north-west in the model.

It should also be noted that residual current velocities are on average very small – at ~ 0.05 m/s throughout the water column over the measurement duration (May – November 2011) and these residual currents are governed by many oceanographic features. The circulation off the east coast of the North Island, New Zealand is dominated by a number of permanent or semi-permanent mesoscale eddies embedded in the East Auckland and East Cape currents. The Wairarapa Eddy is the southernmost of these three eddies, and is found over the Hikurangi Trough, trapped between the Chatham Rise and the south-east coast of the North Island. The positioning and movement of these eddies influence current velocities and direction. HYCOM, the global ocean model used to generate boundary conditions for the Delft3D Regional Model resolves mesoscale eddies. In addition, a subtropical front, captured by the model through the boundary conditions is located over the Chatham Rise. Fronts are known to be associated with enhanced biological activity due to upwelling associated with baroclinic (internal) waves and eddies, mixing to the surface along sloping isopycnals and enhancement of near surface stratification by cross-frontal circulation (Chiswell, 2002).

7 Incident Modelling Spill plume computation

Deltares investigated the near-field plume dispersion for operational incidents assuming release of seabed material approximately 10 m to 20 m off the seabed. These incidents could arise due to blockage of the pump / riser system, requiring the pump system to be shut down, and the riser to be flushed by opening a relieve valve at the lower end of the riser. This is considered as the 'incidental release'. The riser is about 400 m long, has a diameter of 600 mm, and is filled with a mixture of sea bed material and water. The total amount of solids in the riser is estimated to be in the order of 20 m³.

The suction line, from draghead to pump, will also be back flushed. As this line section is in the order of 10 % of the riser length, about 2 m³ of solids will be released, through the draghead, at the seabed. The behaviour of this release is similar to that of the tailings release, but it is an insignificant volume, and is, therefore, not separately assessed. No other material would be released from the system if one of these incidents occurred.

Due to the excess density of the slurry in the pipeline, the spill flow rate will last for some time. The released material was assumed have a volume of 20 m³ and to have a grain size distribution representative of the fine material taken in from the seabed. Jet3D was utilized to model these operational incidents, in a similar way as the near field mid-depth tailings plume disposal, see section 3.1.1, but now only 20 m instead of 200 m above the seabed

Jet3D describes the stationary plume trajectory, velocity and density determined by initial density and flow velocity and ambient seawater conditions. The plume behaviour causes the sediment particles to settle much faster than the individual settling of fine particles.

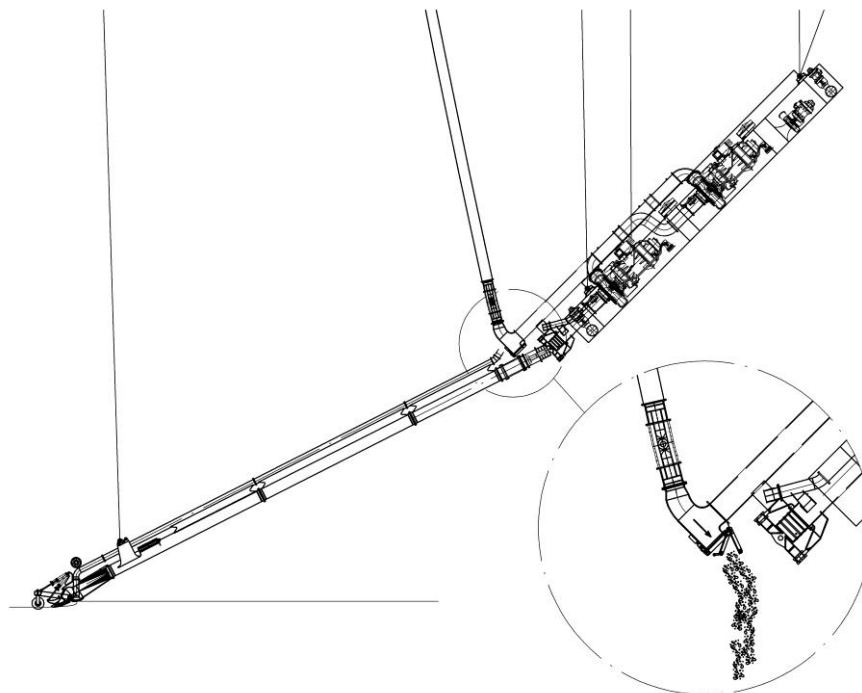


Figure 7.1 Accidental spill in riser pipeline 20 m above seabed; situation.

The grain size distribution does not influence the plume behaviour, as long as the grains are still suspended and the plume remains a coherent body with an excess density. Coarse particles (grain size diameter greater than about 1 mm) however, will settle faster than the plume subsides and will segregate whereas very fine particles remain suspended over a longer period (grain size diameter smaller than about 20 microns).

After some time and distance, the plume has diluted so much that its excess density becomes negligible (considered to be in the far-field).

With a flow rate of $2.15 \text{ m}^3/\text{s}$ and a volume of 20 m^3 of in-situ material (about 32 tonnes of sediment), the spill takes less than a minute. So the plume will exist only for a short time. The distance travelled in this time is less than 40 m.

It is assumed that the flow rate, direction, density and flow velocity during spill is comparable to the operational parameters see Table 2.3.

The **effective spill diameter** as considered in Jet3D is 1.9 m, which is the virtual initial plume diameter with an assumed horizontally backward directed flow velocity of 0.75 m/s and given flow rate, required for input in Jet3D. The plume flow establishment length ($6.2 \times 1.9 \text{ m}$ according to turbulent jet flow theory) is about 7 m. This means that at a height of 20 m, the flow is hardly established when hitting the seabed if directed downward, and the initial flow velocity and density profile is still present in the core of the flow.

During normal operation, the mining vessel with disposal pipe sails with a constant trailing speed of 0.75 m/s. The tailings sediments are deposited through the spill opening with a backward directed velocity of the same value, so the initial velocity relative to the seabed is close to 0 m/s. Relative to the spill opening, however, a horizontal flow velocity of 0.75 m/s exists and an ambient sea water flow velocity relative to the spill opening of also 0.75 m/s is present. This current velocity can increase or decrease, dependent upon the actual tidal current velocity, which varies between about 0.1 and 0.45 m/s and could add to the ambient current velocity, dependent upon sailing direction, to a maximum of 1.2 m/s.

This is all similar as in section 3.1.1.

7.1 Jet3D input

Jet3D can model the near-field plume dimensions of the spill as a result of excess density; initial momentum and ambient sea water density (see Delvigne, 1979). It can compute velocity profiles assuming (quasi-) stationary conditions, such as spill flow rate, density and currents.

Below is a summary of the Jet3D settings for this incidents study:

Jet origin

$x, y = 0$

$z = +20 \text{ m}$

Jet orientation

$\Phi = 0$ (horizontal direction)

$\Theta = 0$ (backward direction)

$D_0 = 1.9$ m initial effective spill diameter
 $\rho_0 = 1265$ kg/m³ initial density

The conditions are similar to Table 2.3 with a flow rate of 2.15 m³/s and sediment deposition rate of 827 kg/s, the same as for the tailings disposal during normal operation.

Water depth = 400 m
 Temperature = 9 °C
 Salinity = 35 ppt
 Resultant water density = 1027 kg/m³

Tidal currents considered

Min 0.10 m/s
 Max 0.45 m/s

$U_{amb} = 1.2$ m/s
 $\rho_{amb} = 1027$ kg/m³
 $u_0 = 0.75$ m/s

Particle size distribution (on fraction less than 60 µm modelled)

- 46% between 100 µm and 1000 µm
- 10% between 60 µm and 100 µm
- 20% between 20 µm and 60 µm
- 16% between 4 µm and 20 µm
- 8% smaller than 4 µm

7.2 Results and discussion

Figure 7.2 (full water depth) and Figure 7.3 (in detail 20 m above bed) show the trajectory and spatial dispersion of the plume computed with Jet3D. When the material is released at 20 m height it will hit the bed within 40 m. At this point, the density is decreased to 1037 kg/m³ (Figure 7.5) and the plume diameter is increased to 10 m.

The spill hits the seabed with 0.8 m/s (Figure 7.4), relative to the spill opening, which is assumed to sail with 0.75 m/s. So the additional velocity relative to the bed is almost completely gone and no additional resuspension of previously deposited material on the seabed or local turbidity generation is expected.

Due to a spill of 20 m³ of sediment, the computation indicates that the material is dispersed over an area of about 10 m width. In the time during the spill a distance of less than 40 m is covered, resulting in a thickness of less than 5 cm (and a footprint of 10 m x 40 m). Only the fines that are not buried in the sand may segregate and will remain suspended over a longer distance, but in the lower 20 m above the bed mainly.

Even a multiple of 20 m³ spill is unlikely to have any impact on far-field suspended sediment concentration.

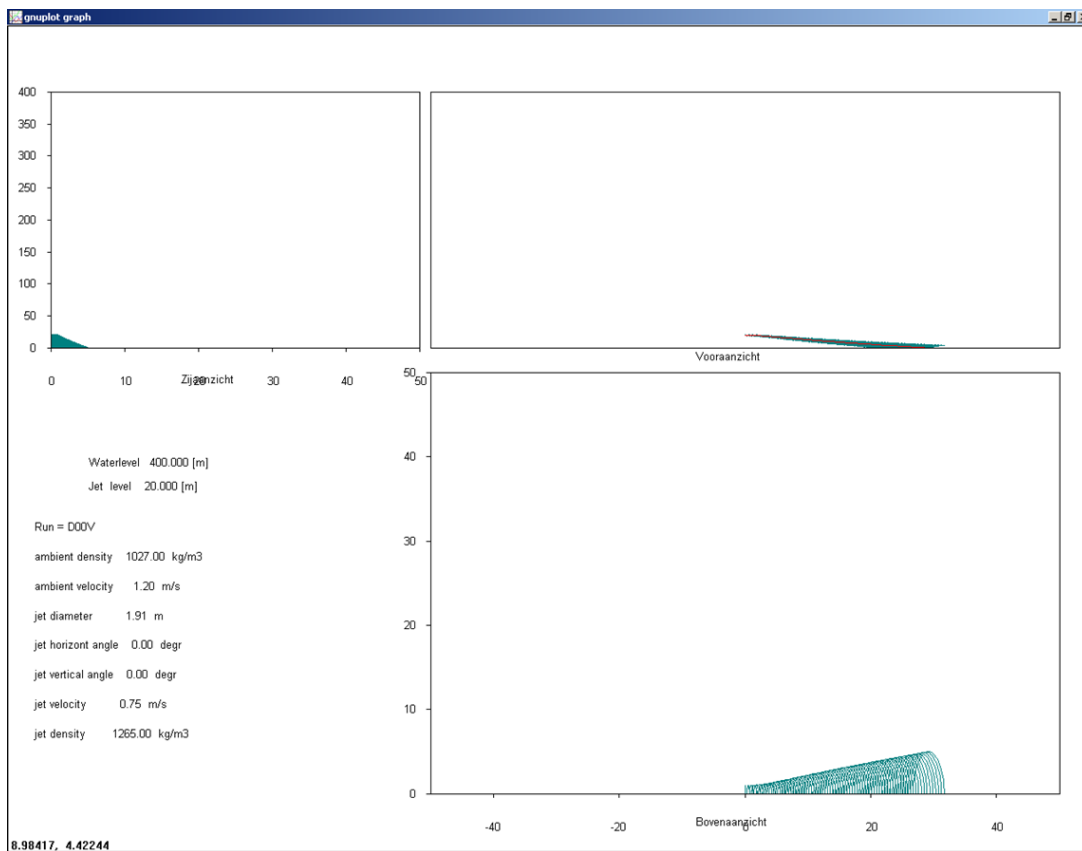


Figure 7.2 Jet3D predicted near-field plume dispersion.

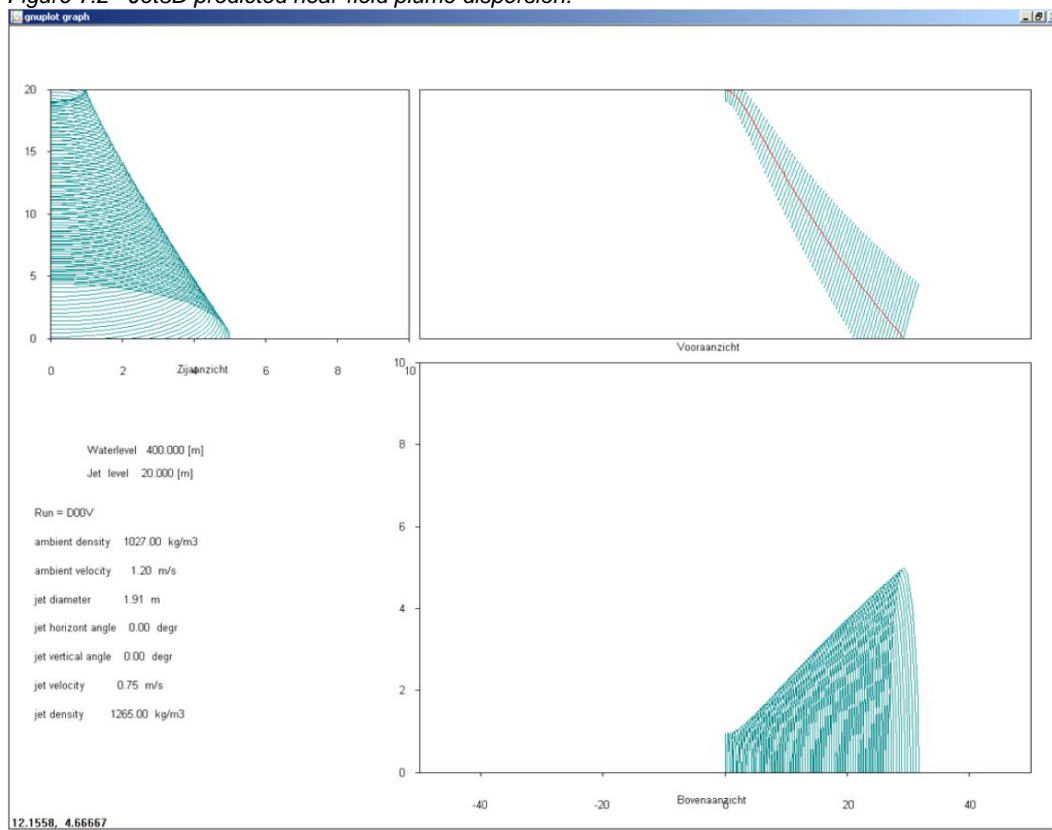


Figure 7.3 Jet3D predicted near-field plume dispersion (zoomed-in).

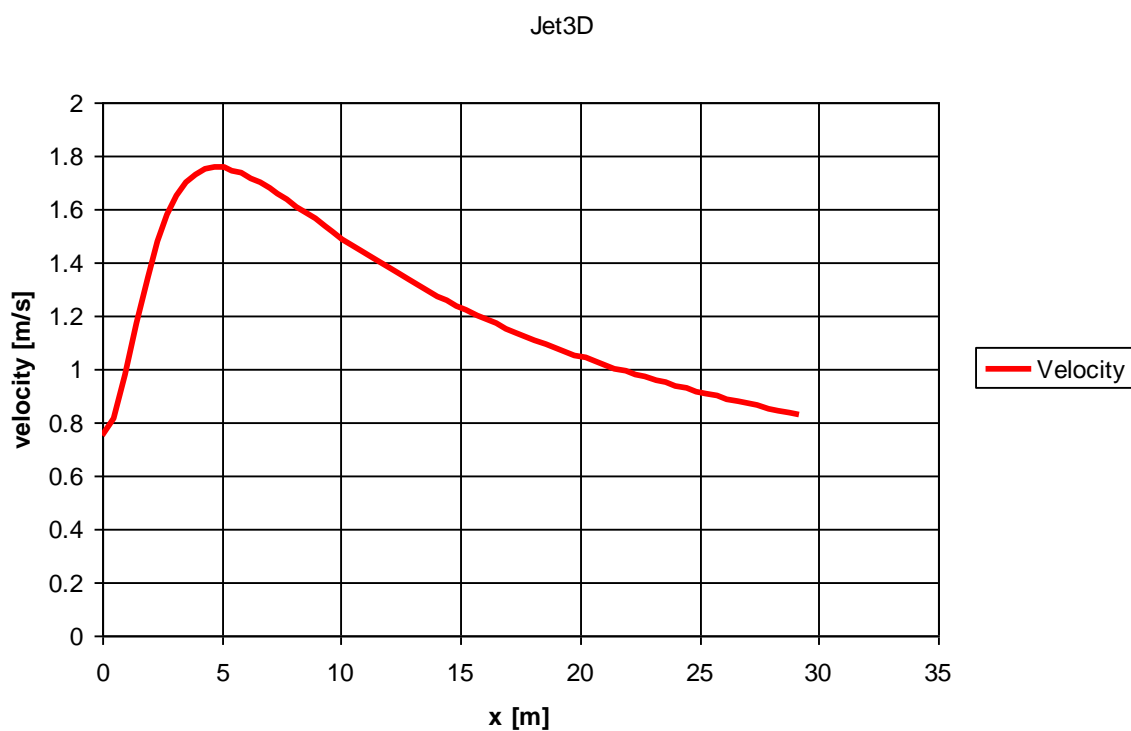


Figure 7.4 Jet3D predicted plume velocity with horizontal distance from the discharge point.

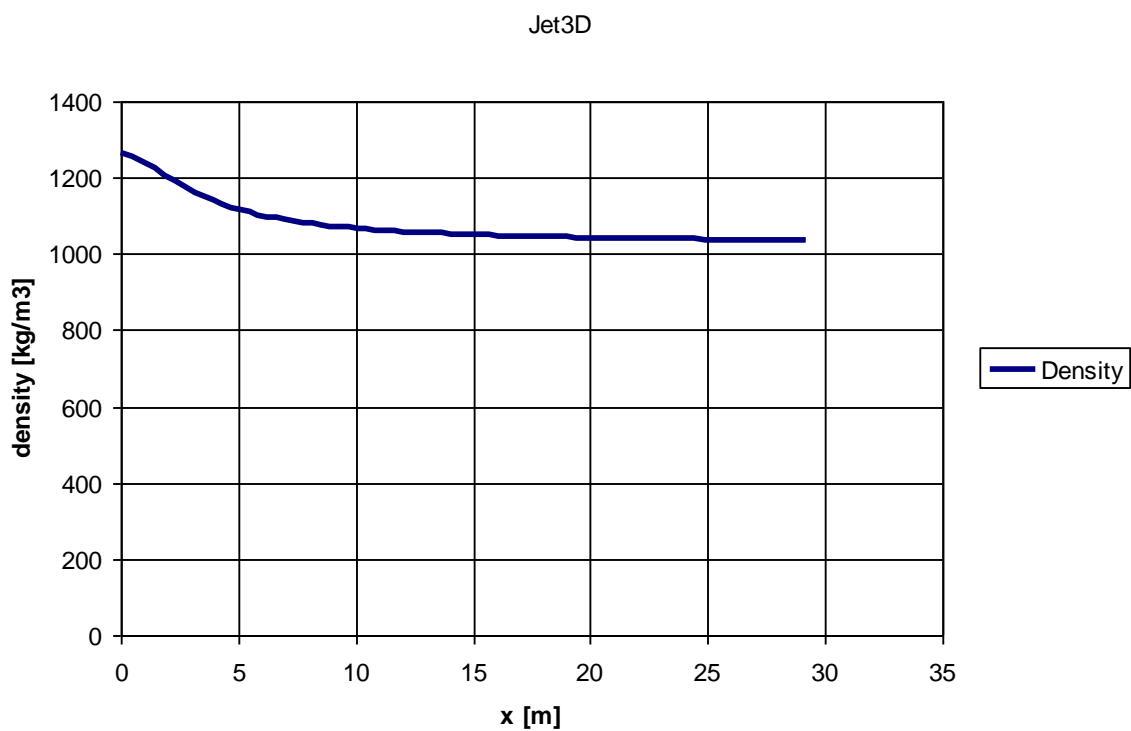


Figure 7.5 Jet3D predicted plume density with horizontal distance from the discharge point.

8 Conclusions

The plume investigations performed during several project phases using near and far-field models, testing model setup and sensitivities and analysing model performance are summarized in this chapter. The Northern and Southern Models were set-up and utilized to perform preliminary investigations on plume dispersion, including sensitivity testing during the first phase of the operations study. The model results and insights in model performance and sensitivities (Chapter 3) were used to optimize the grid schematization and resolution of the model during the 2nd phase of the operations study. In addition the model domain was moved to correspond with the iX Survey mooring.

Model simulations - initial investigation

The goal of the initial modelling study presented in Phase 1 was (1) to verify the performance of the far-field Delft3D Model using the moored RDI ADCP current data, and (2) to provide indicative (far-field) computations of fine sediment dispersal due to mining activities for a new mining operation scenario.

The results of Phase 1 illustrated that the regional hydrodynamic model reproduces the depth-averaged measured flow velocities and water levels (near the location of the measurement). Comparisons of time-series show accurately resolved water levels. Depth-averaged velocity magnitudes are reproduced for the tidally driven flows. However, in Phase 3 of the study a more detailed analysis determine how well the local optimized model performs at simulating the residual flows and tidal flows. A description and analysis of trends in the available measurement data is discussed in Deltares (2014a).

Sensitivity testing involved running the Delft3D Model using various processes and parameter settings and showed indicated that the Regional Model is robust. In addition, fall velocity was tested in the Local Model and the results showed that the effect of increased clay sedimentation thickness with increasing clay fall velocity on the computed total suspended sediment concentrations was minor. Similarly the vertical extent of the silt and clay plume for both fall velocity test cases was compared to the main setup over the shorter period of time simulated in these single cycle simulations. Effects of flocculation or aggregation of fines (clay) is implicitly taken into account with these fall velocity sensitivity tests.

In addition, as sediments were released directly onto the bed with a low discharge velocity, the far field sediment plume dynamics and the complete mining discharge process could be resolved fully with Delft3D. The Delft3D Model results predicted comparable sedimentation and concentration values between all simulations. From Phase 1 therefore the following model conclusions should be noted:

Regarding the near-field plume:

- The initial conditions at the diffuser have negligible effects.
- Due to the density effect of the plume, the major turbidity generation takes place near the seabed.
- When silt and clay particles do settle, they will also likely move around on the bed and some of this material may be resuspended due to shear stresses.
- Density flow effects increase as the release moves closer to the sea bed, however the density flow effects decrease rapidly due to mild bed slope and ambient mixing.

Far-field

- Suspended sediment concentrations outside the mining area are generally low (< 1 mg/l), however there are periods when the concentrations can locally reach over 100 mg/l in the disposal area
- Clay and silt migrate both vertically and horizontally in water column; the average vertical dispersion is limited for direct placement on the seabed; sediment concentrations decay rapidly upwards within 10 m of the sea bed
- Once mining activities are interrupted, maximum sediment concentration values reduce below negligible amounts for both the clay and silt fraction (0.02 mg/l for the clay fraction within 72 hours and below 0.01 mg/l for the silt fraction throughout the domain within 24 hours).
- Plume dispersion patterns of clay and silt display both seasonal and spatial variations.
- In all simulations with disposal at the bed, the largest deposition heights of silt and clay (0.1 – 0.15 m on average) occur along the mining discharge tracks.
- Within 1 km of the tracks, deposition reduces down to below 1 cm (0.01 m).
- Sedimentation during spring and winter shows a northwestwardly bias. During summer, sedimentation also occurs to the southeast of the mining area.

General

The results of the initial investigations indicated that the model domain needed to be increased (1.5 times) to ensure that the fine suspended sediment concentrations above 5 mg/l remain within the model domain for a single mining cycle simulation. Additionally, the horizontal grid resolution of the optimized model is now coarser than that of the previous Local Delft3D Models by 2.5 times in the mine tailings disposal area.

Model Simulations – Optimized Investigation

Based on the initial investigations, the model was optimized by: moving it to cover the iX Survey mooring location and modifying the grid extent and resolution. The simulations use a sediment outflow from the diffuser directly into the bottom grid cell because the diffuser is towed over the seabed. The results of the optimized investigation illustrate that the Delft3D model plume dispersal and sedimentation predictions are comparable between all simulations, as well as with the initial investigation runs when the mining areas in the Local Model domains were located east and southeast of the mining area in the present Optimized Local domain.

The following predictions from the seasonal scenarios, single cycle should be noted (these conclusions also hold for the 10-cycle simulations):

- Clay and silt migrate both vertically and horizontally in the water column; however, due to direct placement on the seabed, the average vertical dispersion is typically less than 50 m off the bed. This dispersion considers the hydrodynamic conditions modelled at the time.
- The relatively small clay fraction results in a low maximum suspended sediment concentration more than 10 m above the bed, with a limited duration of suspended concentrations higher than 1 mg/l outside the mining area.
- Suspended sediment concentrations decay rapidly in the lower 10 m of the water column with increasing height above the bed.
- The sedimentation footprint changes with the discharge release height: the size of the footprint is approximately the same but the spatial distribution of the sediment deposition changes. Disposal at 10 m above the bed results in a larger spreading as the sediment settles down over a larger distance and hence gets more widely dispersed. This is also reflected in the suspended sediment patterns

- Suspended sediment concentrations outside the mining area are generally low (< 1 mg/l), however there are periods when the concentrations can reach over 100 mg/l in the mining area.
- Once mining activities are interrupted, maximum sediment concentration values reduce to below 0.01 mg/l for the clay fraction (within 72 hours) and below 0.01 mg/l for the silt fraction (within 24 hours).
- Sedimentation during spring and winter shows a northwestwardly bias. During summer, sedimentation is also slightly skewed to the southeast of the mining area.
- Maximum sedimentation occurs along the mine tailings disposal tracks in all simulations.
- The maximum deposition height is on average 0.08-0.1 m along the disposal tracks
- Within 1 km of the tracks, deposition reduces down to well below 0.01 m.

10- cycle simulations:

- Plume dispersion patterns of clay and silt display both seasonal and intra-seasonal variations.
- The fine clay particles remain in suspension between mining cycles and are still present in the water column when the next mining cycle begins, therefore contributing further to a temporary cumulative effect in the water column
- Lower maximum deposition heights are predicted for the multiple-cycle scenario as compared to the multiplication of the single-cycle scenario due to the outward migration of the disposal tracks.
- The majority of the sedimentation is predicted to occur in the mine disposal area, with higher maximum sedimentation heights (order 30-35 cm) when discharging at the seabed, excluding the initial deposition of sand (ranging between 0.05 -0.15 m for a single track).
- A larger sedimentation footprint is predicted when discharging approximately 10 m above the bed, particularly for sedimentation thicknesses on the order of 0.5 – 2.5 cm.
- Summer and winter sedimentation footprints are quite similar, particularly when discharging at the seabed. However, there is slightly less dispersion and slightly higher local sedimentation heights in Summer scenarios compared to the Winter scenarios.
- The comparison of the sedimentation footprints from the multiple and single cycle simulations point at limited effects of intra-seasonal hydrodynamic variations and cumulative effects, due to resuspension and delayed settling. Separation of these factors is with the available set of simulations not possible, but is not deemed important for the sedimentation patterns given the predicted limited variations

Incidents:

Deltares investigated the near-field plume dispersion for operational incidents assuming release of seabed material approximately 10 m to 20 m off the seabed. Results show that contribution of incidents to turbidity levels and footprint on the seabed would be insignificant compared to the operational contribution.

General Modelling Conclusions

Regarding DELFT3D input:

- The schematized input of sediment release from the plume into DELFT3D is still conservative, since no burial effect of fines is taken into account, which may occur when the sediment is released with the diffuser near the bed.
- The sand fraction, which is predicted to initially settle on the bed by the original near-field investigation, is not included in the Delft3D simulations. Only the suspended fractions (composed of silt and clay) are included.

- Any sedimentation that occurs will come on top of the sand deposition, which is concentrated in an approximately 10 -15 m wide path, directly behind the diffuser: the thickness of this deposit is in the order of 0.1 to 0.2 m.
- The present (default) input settings results in little to no resuspension from the seabed after deposition, which is supported by the critical shear stress for erosion of the mine tailings calculated in the Resuspension Study (Deltares, 2014b). This is because modelled bed shear stresses are almost always below the critical shear stress for erosion of the mine tailings. If resuspension occurred under very energetic hydrodynamic conditions then, concentration levels might increase.
- A small part of the fine sediment fraction, the clay fraction in particular, leaves the model domain through the boundaries of the domain and cannot return into the domain. As a result cumulative effects due to temporal uploading of suspended sediments between subsequent mining cycles may be slightly underestimated.

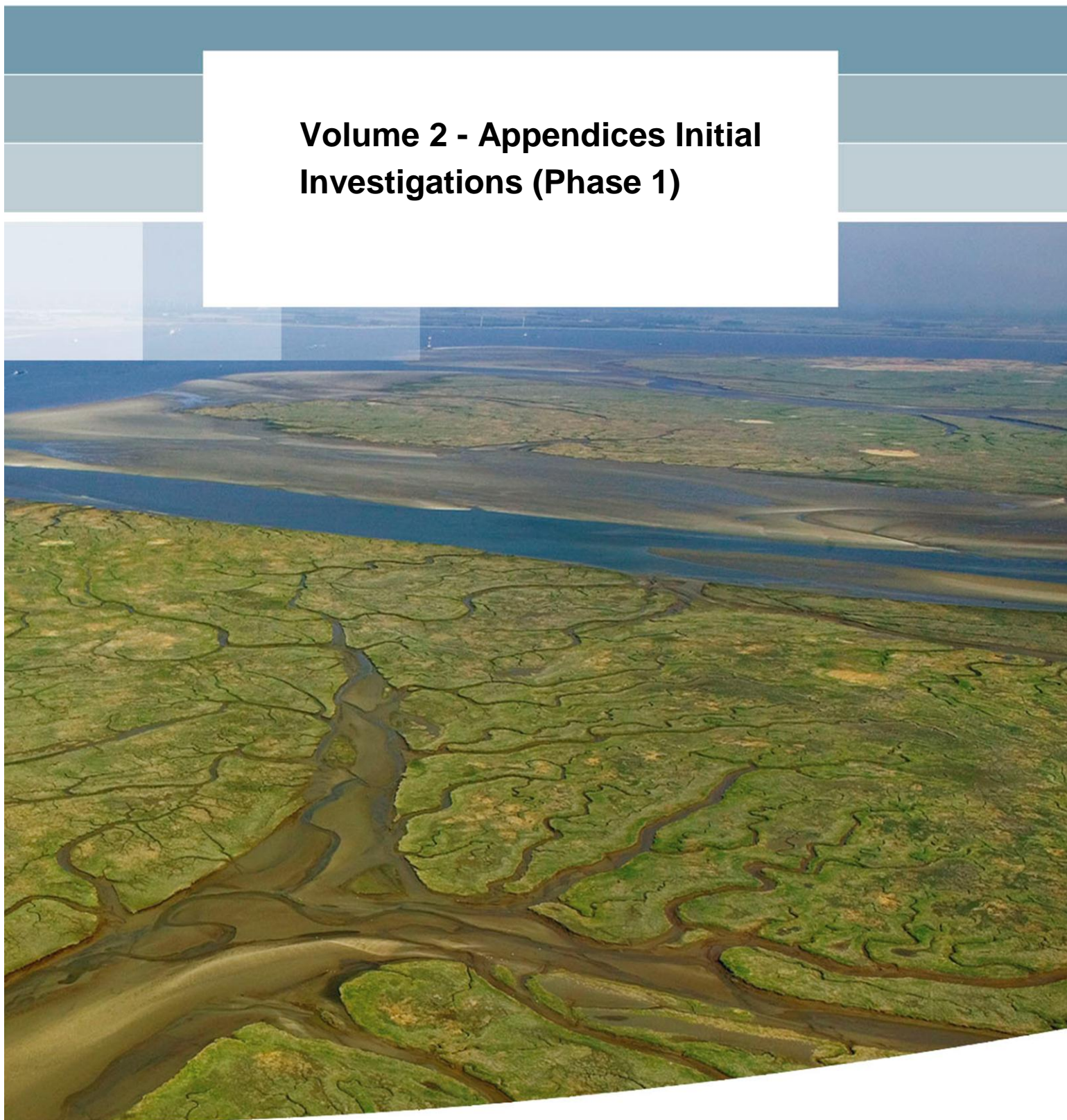
Model Verification conclusions:

- The higher near bed currents predicted by the model implies that the plume will be carried further from the disposal site but not necessarily spread over a larger area. The average (residual) velocity, also overestimated by the model, ultimately determines the position of the deposition footprint relative to the position of the plume discharge. This spreading of the plume is governed by vertical mixing and Taylor shear dispersion. Both of these factors tend to overestimate the extent of the plume effects, resulting in conservative estimates of the effects of tailings disposal.
- Comparison of model speeds and residual velocities against measurements show that the sediment plumes in the model are predicted to extend farther from the discharge point than is likely to be observed. The residual direction in the lower half of the water column where the sediment plume is discharged and is transported is on average correct. There are times in the measurements when the residual direction of the flow is east, however the direction remains predominately to the north-west in the model.

9 References

- Bowen, M. (2012). Summary of Velocity and Turbidity data from the Chatham Rise Moorings, Report for Chatham Rise Phosphate, School of Environment, University of Auckland, New Zealand.
- Chiswell, S.M. (2002). Temperature and salinity mean and variability within the subtropical front over the Chatham Rise, New Zealand, *New Zealand Journal of Marine and Freshwater Research*, 36:2, 281-298.
- Chiswell (2011). Data on the physical oceanography of the Chatham Rise. NIWA Client Report WLG2011-9
- Cronin, K.M., van Ormondt, M., Storlazzi, C., Presto, K. and Tonnon, P. (2011). Nearshore disposal of fine-grained sediment in a high-energy environment: Santa Cruz Harbor Case Study. Proceedings of the 7th Coastal Sediments conference, 2-6 May 2011, Miami, Florida, USA.
- Deltares (2014a). Chatham Rise Phase 2, Oceanographic Study. Report 1207562-000-ZKS-0012. Deltares, Delft, the Netherlands.
- Deltares (2014b). Chatham Rise Phase 2, Resuspension Study. Report 1207562-000-ZKS-0013. Deltares, Delft, the Netherlands.
- Delvigne, G., (1979). "Round buoyant jet with three dimensional trajectory in ambient flow", Paper presented at the 18th congress of the IAHR, Cagliari, Italy, September 1979
- Lesser, G. R., J. A. Roelvink, J. A. T. M. van Kester and G. S. Stelling, (2004). "Development and validation of a three-dimensional morphological model." *Coastal Engineering* 51: 883-915.
- Heath, R.A. (1983). Tidal currents in the southwestern Pacific Basin and Campbell Plateau, southeast of New Zealand, *Deep Sea Research*, Vol. 30, No. 4A, 393-409.
- Heath, R.A. (1985). A review of the physical oceanography of the seas around New Zealand - 1982, *New Zealand Journal of Marine and Freshwater Research*, 19:1, 79-124.
- Pawlowicz, R., B. Breardsley, and S. Lentz (2002). Classical tidal harmonic analysis including error estimates in MATLAB using T_TIDE, *Comput. Geosci.*, 28(8), 929-937.
- Niwa (2011). Oceanographic models of Chatham Rise for sediment dispersal estimates. NIWA Client report: WLG2010-70 March 2011, 27 pp.
- Taylor, G.I., (1953). Dispersion of soluble matter in solvent flowing slowly through a tube. *Proc. Roy. Soc. London*, A219, 186-203
- Uittenbogaard, R. E., J. A. T. M. van Kester and G. S. Stelling, (1992). Implementation of three turbulence models in 3D-TRISULA for rectangular grids. Tech. Rep. Z81, WL j Delft Hydraulics, Delft, The Netherlands.
- Uittenbogaard, R. E., (1995). The importance of internal waves for mixing in a stratified estuarine tidal flow. Ph.D. thesis, Delft University of Technology, Delft, The Netherlands. 217
- Van Haren, H. (2009). High frequency vertical current observations in stratified seas, *Continental Shelf Research* 29, 1251-1263.
- Van Kessel, T. & van Maren, D.S., (2013). Far-field and long-term dispersion of released dredged material. WodCon XX. The Art of Dredging, Brussels, Belgium, 2013, Proceedings
- Van Prooijen, B.C. & Winterwerp, J.C. (2010). A stochastic formulation for erosion of cohesive sediment. *Journal of Geophysical Research*, Vol 115, C01005, doi:10.1029/2008JC005189

**Volume 2 - Appendices Initial
Investigations (Phase 1)**



Volume 2 - Appendices Initial Investigations (Phase 1)

dr. M.C.J.L. Jeuken
J.M. Lescinski MSc
K. Cronin PhD
ir. J. Vroom
dr. E.P.L. Elias

1209110-000

Title

Volume 2 - Appendices Initial Investigations (Phase 1)

Project

1209110-000

Reference

1209110-000-ZKS-0008

Pages

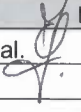
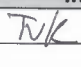

31

Keywords

Deep sea mining, Modelling, Mine tailing dispersion, Chatham Rise.

Summary

In the framework of the Chatham Rise Rock Phosphates (CRP) Mining Project, Boskalis and CRP asked Deltares to conduct an operations study investigating the dispersion behaviour of sediments released during the mining process. The main interest is in the turbidity generated in the water column and the deposition footprint on the seabed resulting from the mining discharge. The Chatham Rise is a submarine feature that is approximately 1000 km in length, extending eastward from the South Island of New Zealand. The rise has water depths that range from roughly 80 m to 500 m, with the Chatham Islands near the eastern extent of the submarine feature. Just north and south of the Rise, water depths quickly approach 3000 m. This document is an appendix of that study (Deltares, 2014) which uses a dedicated modelling approach to assess the near and far-field dispersion, and sedimentation behaviour of sediments released during the mining process.

Version	Date	Author	Initials	Review	Initials	Approval	Initials
1.0	Mar. 2014	C. Jeuken et al.		T. van Kessel		F. Hoozemans	

State

final

Contents

Appendices

A Complementary Jet3D scenario's (200 m depth discharge)	A-1
B Initial Far Field investigations – Phase 1a	B-1
B.1 Initial Local Models set-up	B-1
B.2 Input to far-field modelling with Delft3D	B-3
B.3 Reference simulation - summer North model	B-5
B.4 Fall Velocity Sensitivity	B-8
B.5 Geographical location Sensitivity	B-12
C Additional Figures Initial Far-field Investigations – Phase 1b	C-1
C.1 Spring	C-2
C.2 Summer	C-5
C.3 Winter	C-8
D References	D-1

A Complementary Jet3D scenario's (200 m depth discharge)

This section gives complementary Jet3D results for the near-field plume development in case of discharging at 200 m water depth using the sediment characteristics of phase 1b and enables a comparison with the results of phase 1a, presented in section 3.1.1.

Input JET3D computation (see Figure A-1):

1. Ambient density: assumed constant over depth.
2. Ambient velocity: = trail velocity since plume is computed relative to vessel.
3. Jet diameter, initial horizontal (0 is in horizontal plane) and vertical angle (-90° is vertically downward direction, 0 is backwards, in direction of ambient velocity).
4. "virtual" input jet diameter of 1.91 m is chosen to satisfy sediment mass flow rate with initial velocity at diffuser as given by Boskalis (0.75 m/s).
5. initial jet density 1265 kg/m³

Figure A-1 shows the plume in 3 directions. When the bed is hit, the flow width is about 100 m. When evenly spread over a width of 100 m, the sediment release results in a sediment layer thickness of 7 mm. Initial flow velocity and direction have minor impact, the plume flow at some distance from the diffuser is defined by density and dilution only. When the plume hits the bed, the height is about 50 m, the density is only 0.2 kg/m³ in excess of the ambient water density and velocity less than 0.2 m/s according the JET3D computation.

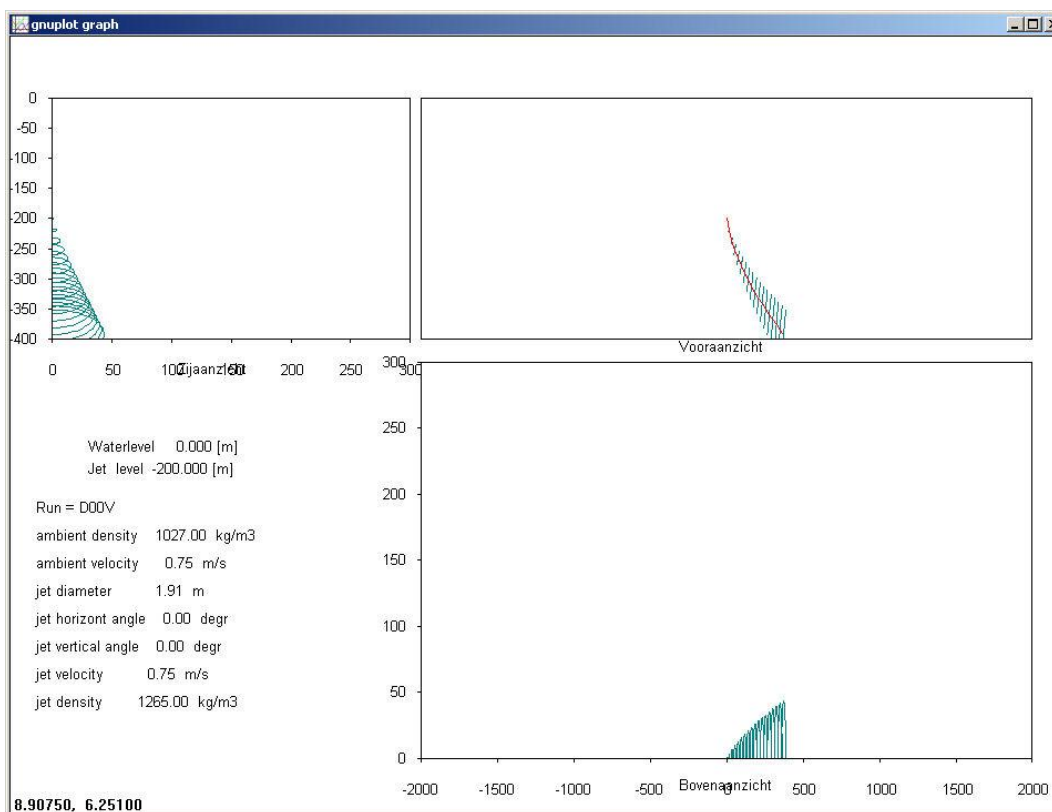


Figure A-1: Sediment plume development JET3D. Scenario 2, vessel speed 0.75 m/s, no sea water currents or density stratification. Plume hits seabed at 600 m.

B Initial Far Field investigations – Phase 1a

B.1 Initial Local Models set-up

Two initial Local Delft3D model domains were utilized in Phase 1a of the study: a northern domain, which is used as the base domain, and a southern domain, which is used in one of the sensitivity test cases (Figure B.1). For both of these domains, the vertical extent is resolved using 25 sigma layers (more commonly for coastal modelling and when modelling sediment transport), which are vertical model layers that have a constant percentage of the water depth, i.e. their absolute height change with fluctuations in the total water depth. The Local models are nested in the Regional Delft3D Model to obtain their boundary conditions.

The horizontal model resolution ranges from 100 m in the centre of the domains where the mine tailing disposal is discharged, to 200 m at the edges of the domains. A one-minute time step is employed, which was found to be satisfactory through sensitivity testing.

The water depth ranges from 420-465 m in the northern domain (Figure B.2) and from 415-520 m in the southern domain (Figure B.3). These locations were chosen to get as close to the slope as possible, while still remaining on the ‘top’ of the Rise.

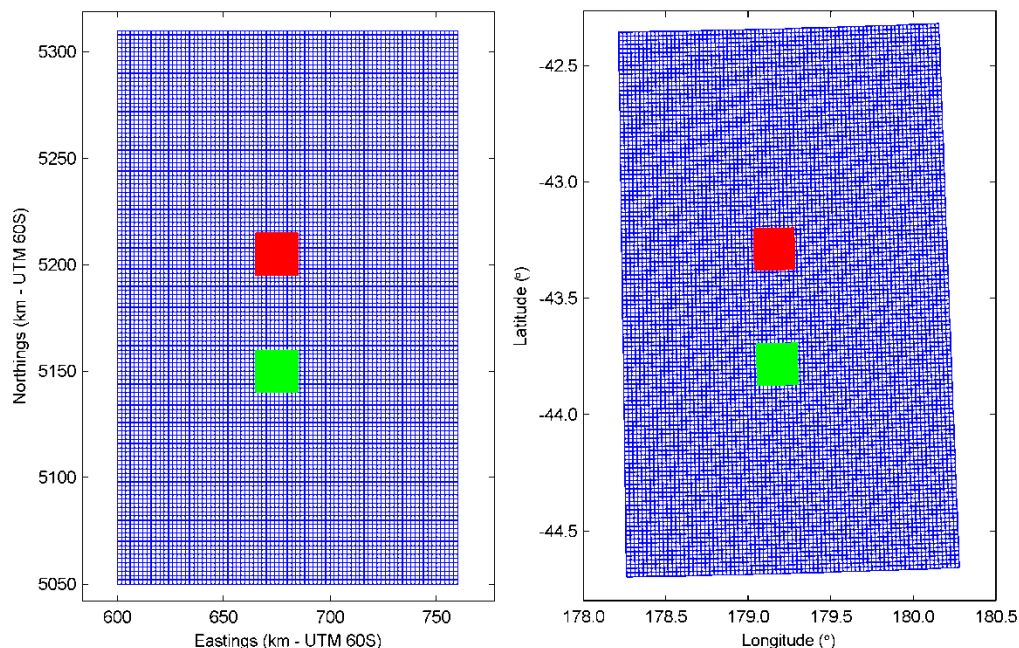


Figure B.1 Regional Delft3D grid (blue), local northern domain Delft3D grid (red), and local southern domain Delft3D grid (green).

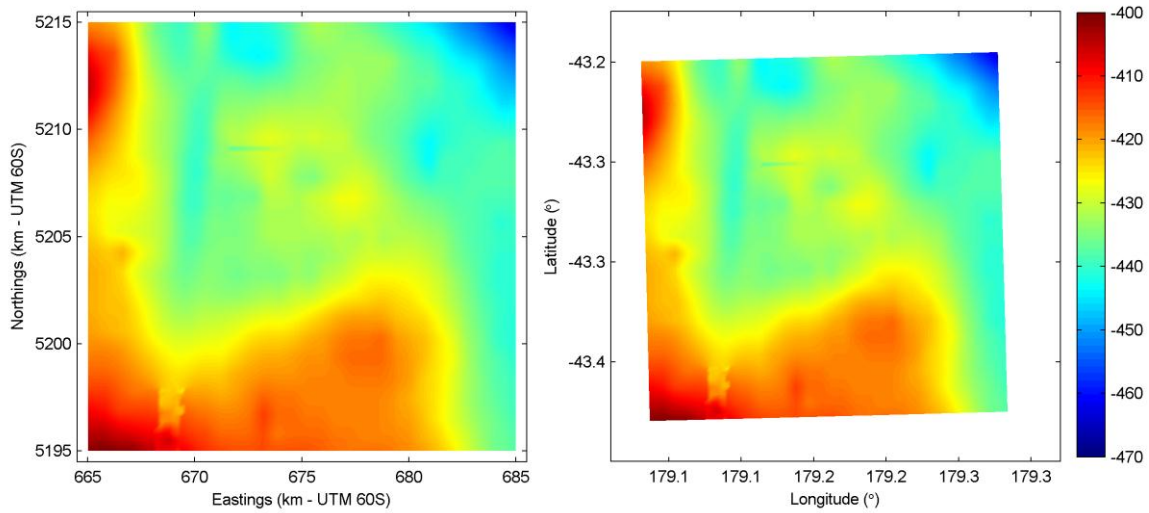


Figure B.2 Initial bed level (m) of northern local domain

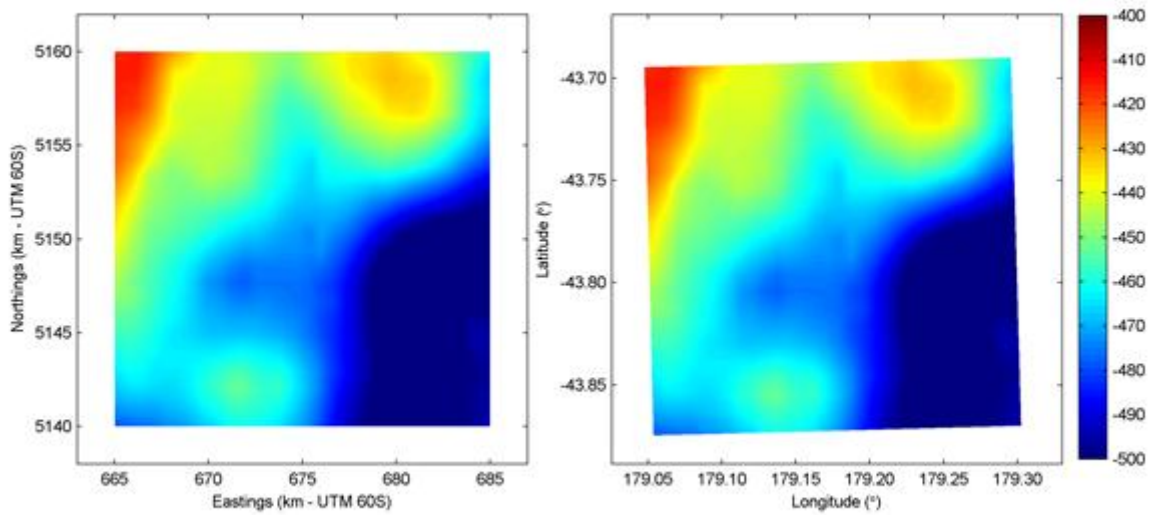


Figure B.3 Initial bed level (m) of local southern domain

B.2 Input to far-field modelling with Delft3D

As part of the preliminary study, phase 1a, the near-field mine tailing plume development was investigated using JET3D for a specific outflow parameter definition and two base scenarios, as defined by Boskalis:

- Outflow parameters
 - Sediment flow : 0.75 m³/s or 1200 kg dry solids/s (dry density 1.6 ton/m³)
 - Concentration of outflow 1.325 ton/m³ (seawater 1.025 ton/m³)
 - Mixture outflow: 2.48 m³/s (0.44 m³/s dry solids and 2.04 m³/s water)
 - The total sediment release rate is 1195 kg/s
 - For sediment characteristics see Table 2.2 Main report.
- Scenario 1:
 - Release height is 395 m below sea level = 5 m above sea bed
 - Diffuser with radial horizontal outflow, reducing outflow velocity to below 0.5 m/s (e.g. diameter 6 m, gap height 0.25 m)
 - Duration 72 hours, followed by at least 120 hours of no release
 - Linear speed of 1 m/s, up and down over stretch of 4 km
- Scenario 2:
 - Release height at 200 m below sea level = 200 m above seabed
 - Another type of diffuser was proposed with outflow velocity at least below 2 m/s, however no diffuser was used in the study because the effects of a diffuser would be negligible at this height above the seabed.
 - Duration 72 hours, followed by at least 120 hours of no release
 - Linear speed of 1 m/s, up and down over stretch of 4 km

Section 4.1 of the report (Deltares, 2014) presents the results of the near-field study. This section describes how input for far-field modelling with Delft3D (section B.3) was derived.

For both Scenario 1 and 2, a discharge file is employed within Delft3D to input the schematized output of the JET3D simulations along a mining track, which is approximately 40 km in total length, (4km stretches times 10 lengths), where mining is continuous. It is a 70-hour total mining period which is simulated, as opposed to 72 hours. The mining track for the northern domain is shown in Figure B.4 below.

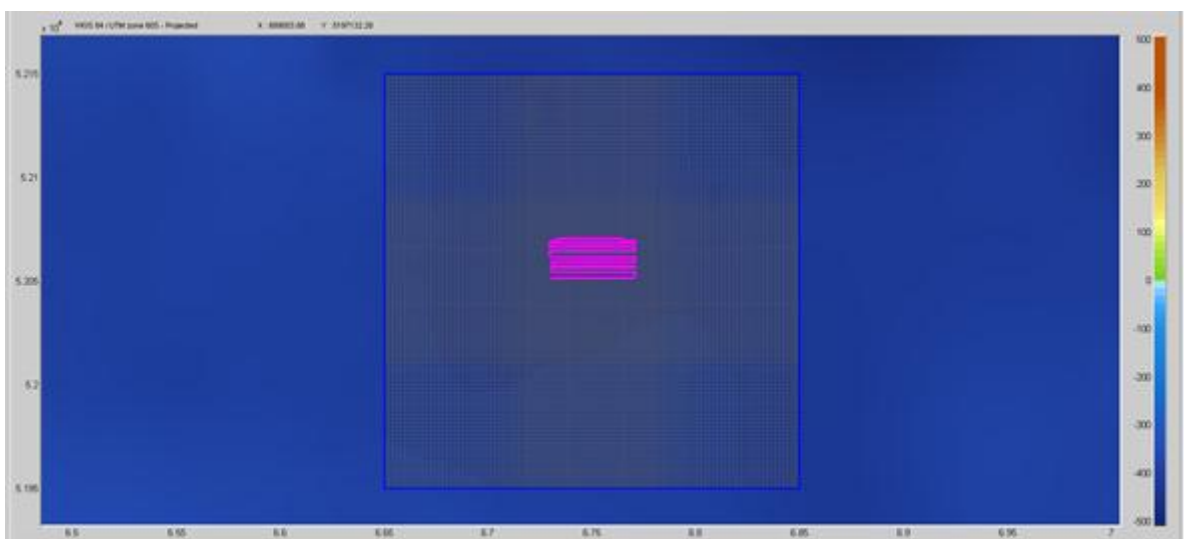


Figure B.4 Dredge track (magenta) for northern Local Delft3D domain

Scenario 2

The clay fraction, which is 10 % of the suspended sediment plume (120 kg /s, with a fall velocity of $2.7 \cdot 10^{-6}$ m /s = 0.0027 mm/s), is assumed to be fully in suspension between the seabed and roughly 50 m above the seabed at the end of the mining plume descent (end of near-field) from the mining vessel discharge point 200 m above the bed. This suspended plume results from the mining plume descending as a somewhat intact until (no stripping is assumed) hitting the seabed, at which point a fine sediment suspended plume is expected to form, which extends from the seabed to approximately 50 m off the bed.

The silt fraction, which is 20% of the sediment plume (240 kg /s, with a fall velocity of $2.5 \cdot 10^{-4}$ m /s = 0.25 mm/s), is assumed to be fully in suspension between the seabed and roughly 50 m above the seabed. This silt fraction is discharged into the Delft3D local domain spread over an approximate height of 50 m above the bed, along the dredge track.

This suspended fine sediment fraction (composed of the clay and silt fractions) is discharged into the Delft3D local domain at an approximate height of 50 m above the bed, along the mining track, to schematically input the JET3D-predicted plume when the mining discharge is released from a height 200 m above the seabed.

It is not necessary to take into account the sand sediment fraction in the Delft3D modelling, which is 54% of the total sediment plume (650 kg/s, with grain size $63 \mu\text{m} < d < 400 \mu\text{m}$), because this sediment fraction is assumed to settle nearly immediately. Thus, it is assumed to not contribute to the suspended sediment plume after the plume makes contact with the bed. It is important to note that due to the predicted shear stresses in the Delft3D modelling, it is assumed that the sand fraction will not go into suspension, but will be transported as bed load along the seabed. However, the current modelling study did not investigate this possibility, but it could affect future dredge operations if the sand footprint migrates.

The stripping of the plume (entrainment of fines into the ambient water during the plume flow to the bed) from release point to seabed is neglected. It is included in the suspended sediment layer near the bed. This could be about 10% of the fines but this effect takes place only during the plume subsidence in the first couple of hundred meters of the total plume track so is minor anyway.

Scenario 1

The same silt and clay discharge rates from Scenario 2 are utilized as the input discharge rates into Delft3D for Scenario 1; however, these fractions are discharged into the vertical grid cell just above the seabed, following the mining track. This is a conservative estimate for Scenario 1 because it is assuming that all the fine material will make it into suspension from the plume, therefore, no flocculation effects are included and no burial effects are included. Additionally, the grid cell thickness is more than 5 m.

Three sensitivity tests cases are also performed for Scenario 2 looking into the effect of the modelled clay fall velocity and the location of the mining activities. There are two fall velocity sensitivity tests, with a clay fall velocity of 0.025 mm/s (Fall Velocity 1, 10X computed value) and 0.25 mm/s (Fall Velocity 2, 100X computed value), respectively. The third test case uses the southern Local domain as opposed to the northern Local domain.

B.3 Reference simulation - summer North model

The preliminary summer simulations used the input as described in section 4.1. During the summer simulations, the currents in the lower half of the water column have velocities on the order of 0.3 m/s, with peak velocities reaching 0.5 m/s.

Scenario 1-mine tailing release at 5m above the bed

For Scenario 1 (Figure B.4), the mine tailing plume is predicted to move along with the oscillatory tidal motions in a circular pattern around the mining track. The mining plume signal is clearly visible near the seabed, within the same vertical grid layer as the discharge, with peak concentrations on the order of 100mg/L being predicted near the discharge location, and quickly dispersing. Approximately 80 m above the seabed, a plume signal is predicted which is on the order of 3 mg/L 24 hours after the mining activities, have concluded. After the mining activities conclude, the plume concentrations near the seabed drop below 20 mg/L within 24 hours.

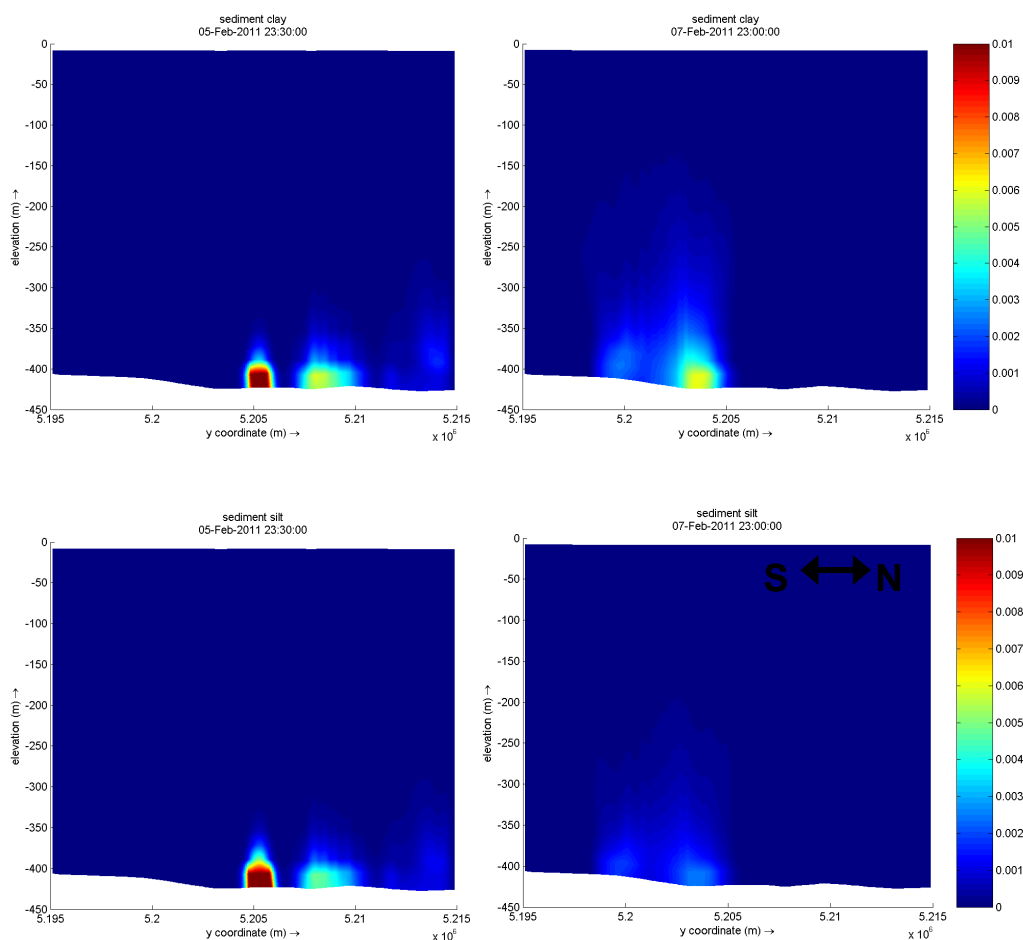


Figure B.4 Scenario 1: Clay (upper) and Silt (lower) suspended concentrations (g/L) at $x=675$ km 47.5 hours after discharging began (left) and 47 hours after discharging concluded (right).

The maximum vertical extent of the suspended clay plume is within 150 m of the water surface nearly 48 hours after the mining concludes, and with a clay concentration on the order of 6 mg/L near the seabed. The SSC panels 47.5 hours after the mining has commenced contains two plume signals (Figure B.4).

At the end of the 10-day simulation period, the cumulative maximum sedimentation of the clay and silt sediments at the seabed is on the order of 1.5 mm near the dredge track (Figure B.5). The sedimentation footprint is centred on the discharge track.

Note: to determine the total sedimentation the computed sedimentation layer thickness (in Fig. B.5) has to be added to the value that was computed for the near field because this settled layer (mainly composed of the sand fraction) is not included in the Delft3D simulations.

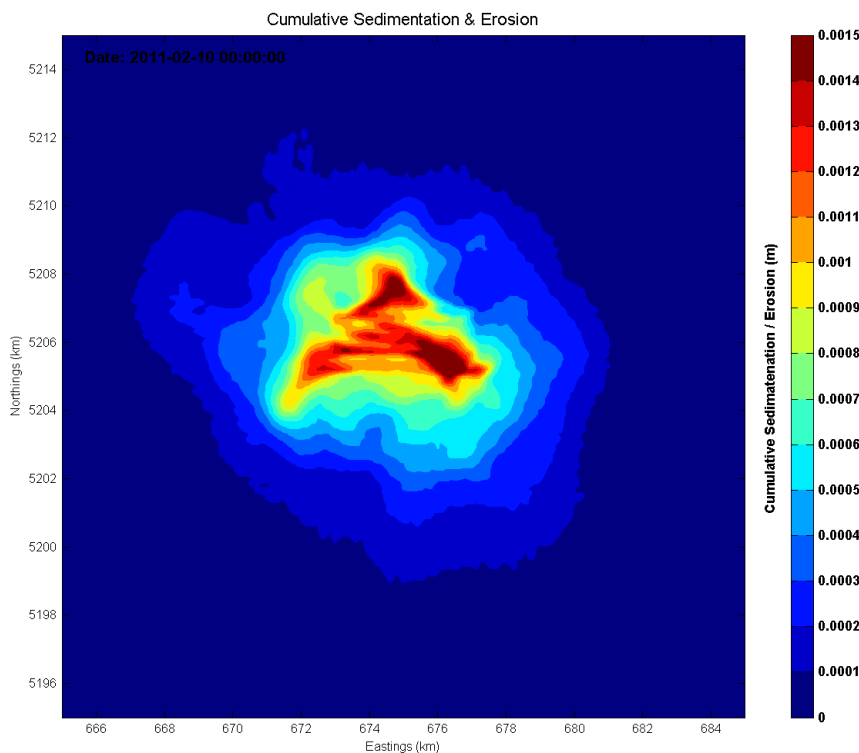


Figure B.5 Scenario 1 cumulative sedimentation (m) of silt and clay dredge discharge material at end of simulation period.

Scenario 2 - mine tailing release at 200 m above the bed

In Scenario 2, the plume signal approximately 80 m above the seabed is much larger than in the Scenario 1 simulation. The plume signal persists for a similar length of time at 80 m above the bed, as at the Delft3D discharge depth. Maximum clay concentrations after the mining activities conclude are on the order of 20 mg/L after 24 hours at approximately 50 m above the bed and 5 mg/L approximately 80 m above the bed.

The maximum vertical extent of the suspended clay plume is within 100 m of the water surface, and within 125 m of the water surface for the suspended silt plume (Figure B.6). Now the SSC panels 47.5 hours after the mining has commenced contains three plume signals. The vertical velocities during the summer lead to continued suspension, as well as vertical spreading, of the plume, particularly when discharging 200 m above the seabed, when compared to discharged just above the seabed (Figure B.6).

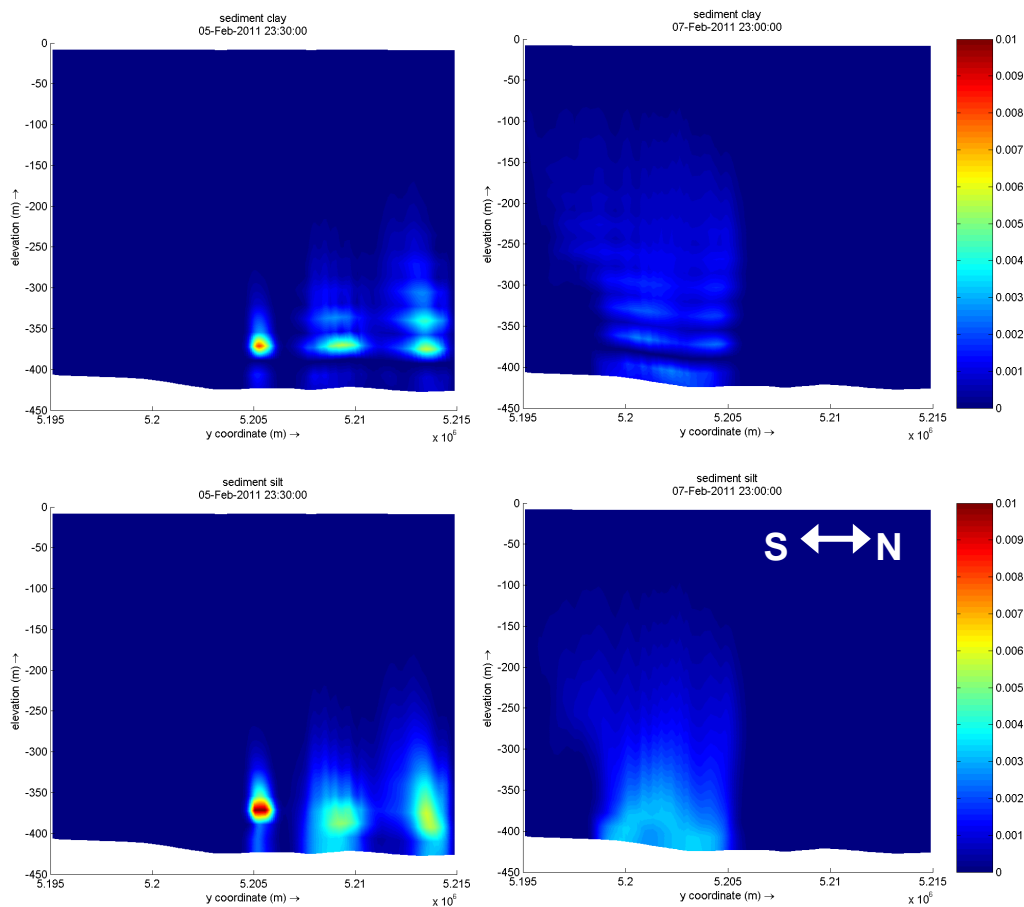


Figure B.6 Scenario 2: Clay (upper) and Silt (lower) suspended concentrations (g/L) at $x=675$ km 47.5 hours after discharging began (left) and 47 hours after discharging concluded (right).

At the end of the 10-day simulation period, the maximum cumulative sedimentation of the clay and silt sediments at the seabed is less than 0.5 mm (Figure B.7). The sedimentation footprint is centred on discharge track.

Note: the computed sedimentation layer thickness has to be added to the value that was computed for the near field because this settled layer (mainly composed of the sand fraction) is not included in the Delft3D simulations.

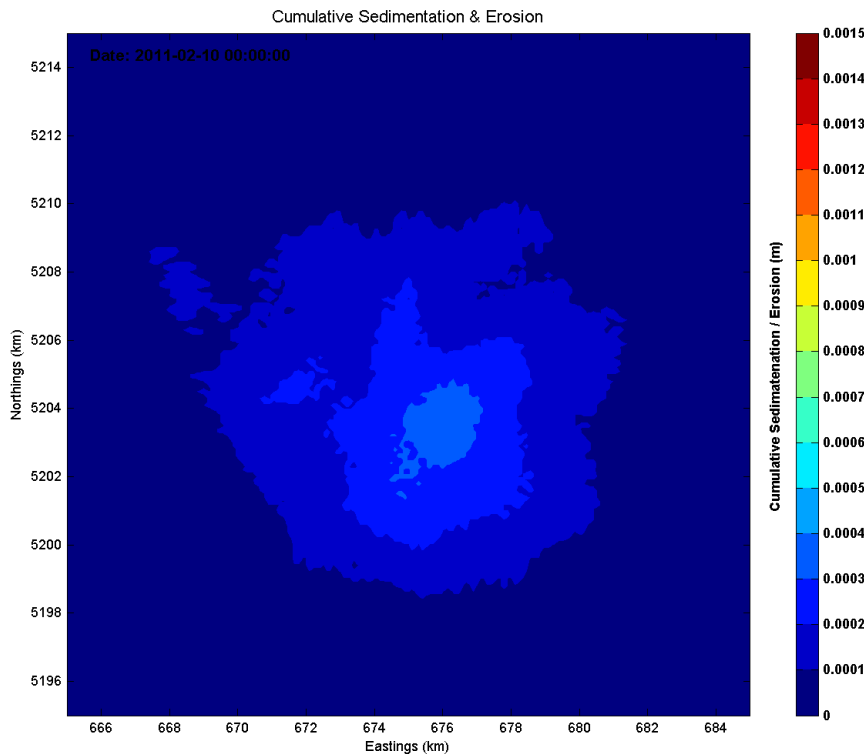


Figure B.7 Scenario 2 cumulative sedimentation (m) of silt and clay dredge discharge material at end of simulation period.

B.4 Fall Velocity Sensitivity

In the fall velocity sensitivity test cases, two larger fall velocities (compared to $w_s = 0.0027 \text{ mm/s}$ in base case) were employed for the clay fraction:

- Fall Velocity 1, the clay fraction has a fall velocity of 0.025 mm/s , which is roughly one order of magnitude larger than for the base case, and
- Fall Velocity 2, the clay fraction has a fall velocity of 0.25 mm/s , two orders larger, which is the same fall velocity as the silt fraction in this modelling study.

These two fall velocity test cases are run for Scenario 2 only, i.e. a mine tailing release at 200 m above the bed.

In the Fall Velocity 1 test case, the plume signal approximately 80 m and 50 m above the seabed is similar to that of the summer Scenario 2 simulation; however, with clay concentrations which decrease slightly more rapidly after the dredge activities conclude. The maximum clay concentration is on the order of 20 mg/L 24 hours after the dredge discharging concludes approximately 50 m above the bed and 4.5 mg/L approximately 80 m above the bed.

Similar to the summer Scenario 2 simulation, the maximum vertical extent of the suspended clay plume is within 100 m of the water surface, and within 125 m of the water surface for the suspended silt plume (Figure B.8).

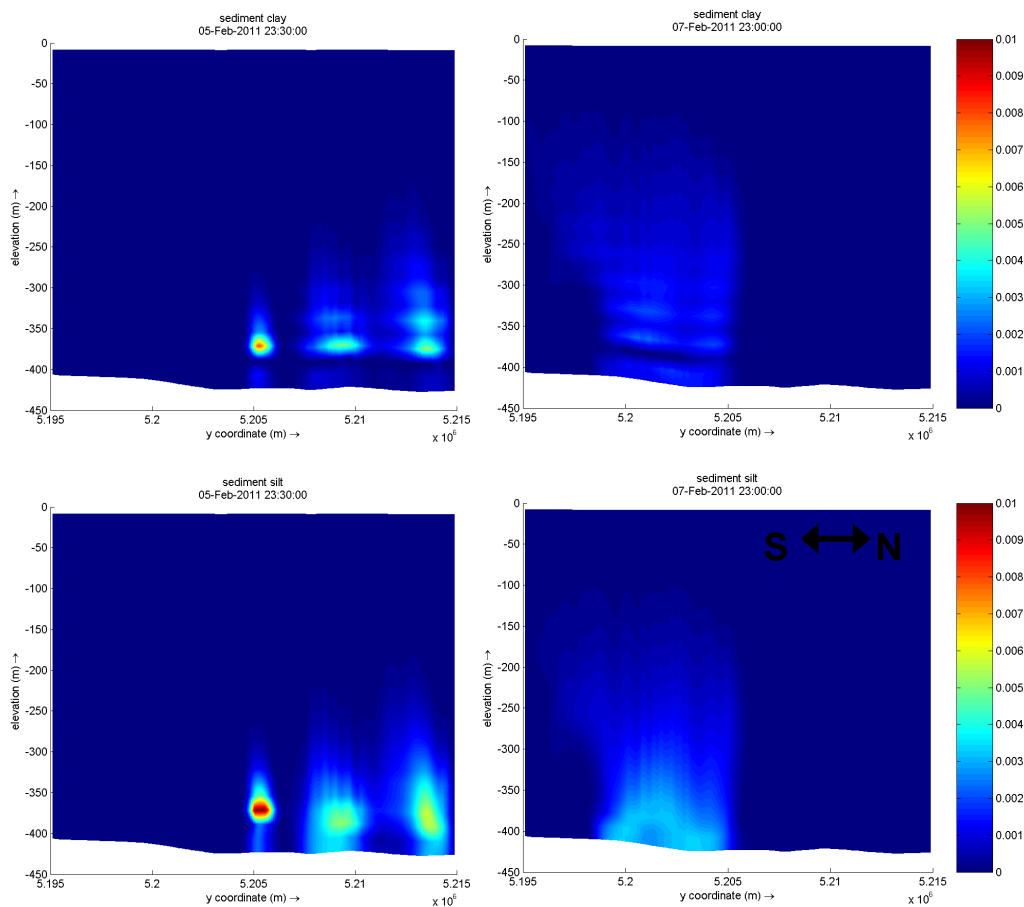


Figure B.8 Scenario 2, Fall velocity 1: Clay (upper) and Silt (lower) suspended concentrations (g/L) at $x=675$ km 47.5 hours after discharging began (left) and 47 hours after discharging concluded (right). w_s , clay = 0.025 mm/s

At the end of the 10-day simulation period, the maximum cumulative sedimentation of the clay and silt sediments at the seabed is less than 0.5 mm (Figure B.9). The sedimentation footprint is centred on the discharge track, with a slightly more pronounced south-western lobe of the footprint as compared to the summer Scenario 2 simulation.

Note: the computed sedimentation layer thickness has to be added to the value that was computed for the near field because this settled layer (mainly composed of the sand fraction) is not included in the Delft3D simulations.

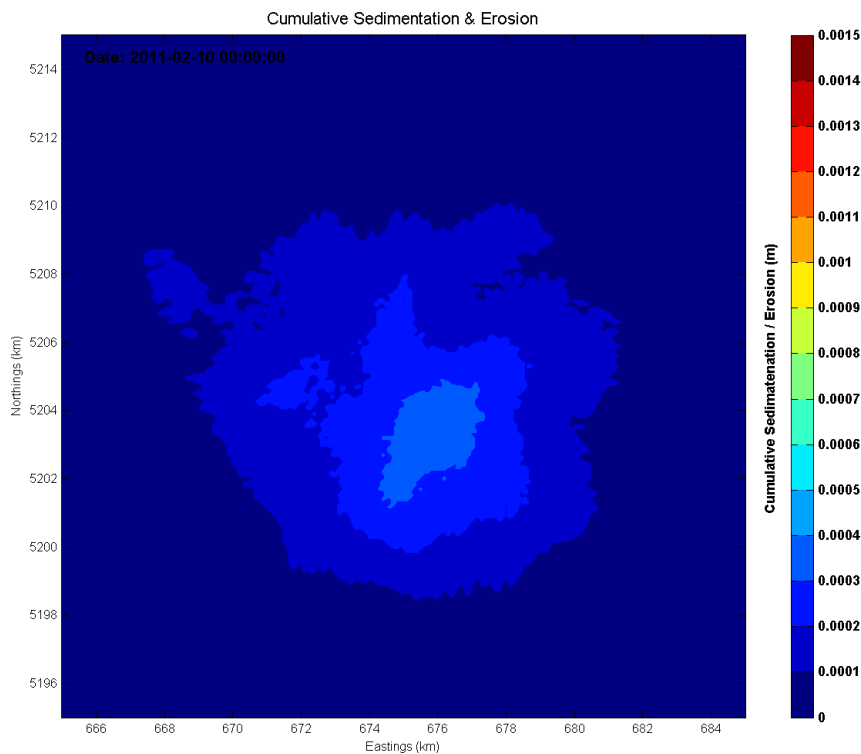


Figure B.9 Scenario 2 Fall Velocity 1 cumulative sedimentation (m) of silt and clay dredge discharge material at end of simulation period.

In the Fall Velocity 2 test case, the plume signal approximately 80 m and 50 m above the seabed is similar to that of the summer Scenario 2 simulation (c.f. Fig. B.10, B8); however, with clay concentrations which decrease slightly more rapidly after the dredge activities conclude. The maximum silt concentration is on the order of 10 mg/L 24 hours after the dredge discharging concludes approximately 50 m above the bed and 4 mg/L approximately 80 m above the bed. In this test case, the silt fraction has a larger concentration than the clay fraction 24 hours after the dredge works have concluded because the silt fraction is double that of the clay fraction and the fall velocities are set equal for the silt and clay fractions.

Again, similar to the summer Scenario 2 simulation, the maximum vertical extent of the suspended clay plume is within 100 m of the water surface, and within 125 m of the water surface for the suspended silt plume (Figure B.10).

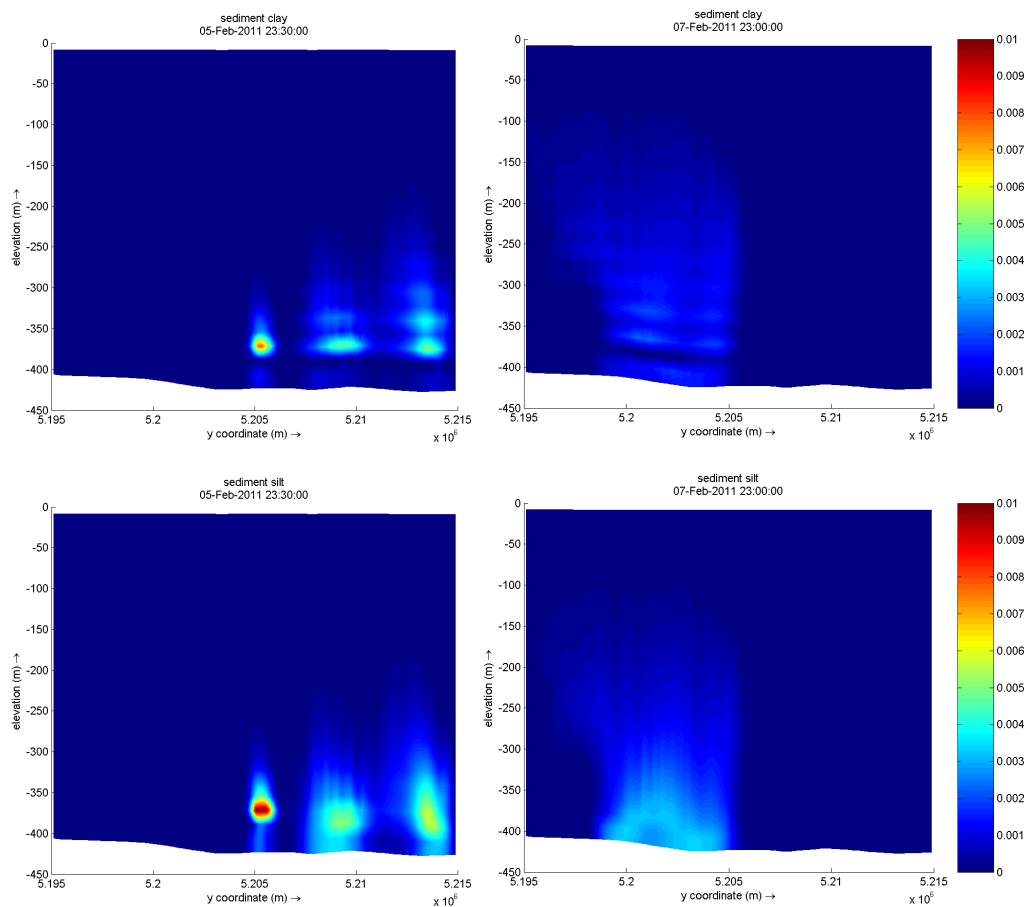


Figure B.10 Scenario 2, Fall velocity 2: Clay (upper) and Silt (lower) suspended concentrations (g/L) at $x=675$ km 47.5 hours after discharging began (left) and 47 hours after discharging concluded (right). w_s , clay = 0.25 mm/s

At the end of the 10-day simulation period, the maximum cumulative sedimentation of the clay and silt sediments at the seabed is less than 0.6 mm (Figure B.11). The sedimentation footprint is centred on the discharge track, with a slightly more pronounced south-western lobe of the footprint as compared to the summer Scenario 2 simulation and a slightly larger footprint overall compared to the Fall Velocity 1 test case.

Note: the computed sedimentation layer thickness has to be added to the value that was computed for the near field because this settled layer (mainly composed of the sand fraction) is not included in the Delft3D simulations.

There is little difference in the results for a clay fall velocity ranging between $w_s = 0.0027$ mm/s, 0.025 mm/s and 0.25 mm/s. This suggests that at the temporal and spatial scale considered, settling of the clay fraction is very small. At larger scales, there should be a significant difference, but the question is whether this is relevant: due to dilution, the concentration levels have become quite small. Note, however, that on the long timescale, the deposition flux of fines should match the 'production' rate of fines (150 kg/s) to avoid further loading of the water column. For $w_s = 0.25$ mm/s and a uniform concentration of 0.1 mg/L, you will need about 100×100 km to get equilibrium between production and deposition. Comparatively, for a uniform concentration of 10 mg/L, you will need roughly a 10×10 km area to get equilibrium between production and deposition. So long-term uploading of the

water column could become an issue for scenario 2, depending upon the environmental regulations and habitat sensitivity of the surrounding waters. In order to have a better understanding of this potential long-term impact, comparisons should be made between the natural flux towards the seabed and the range in ambient concentrations in the dredge plume dispersion region (see also 10-cycle simulations in Chapters 5 and 6).

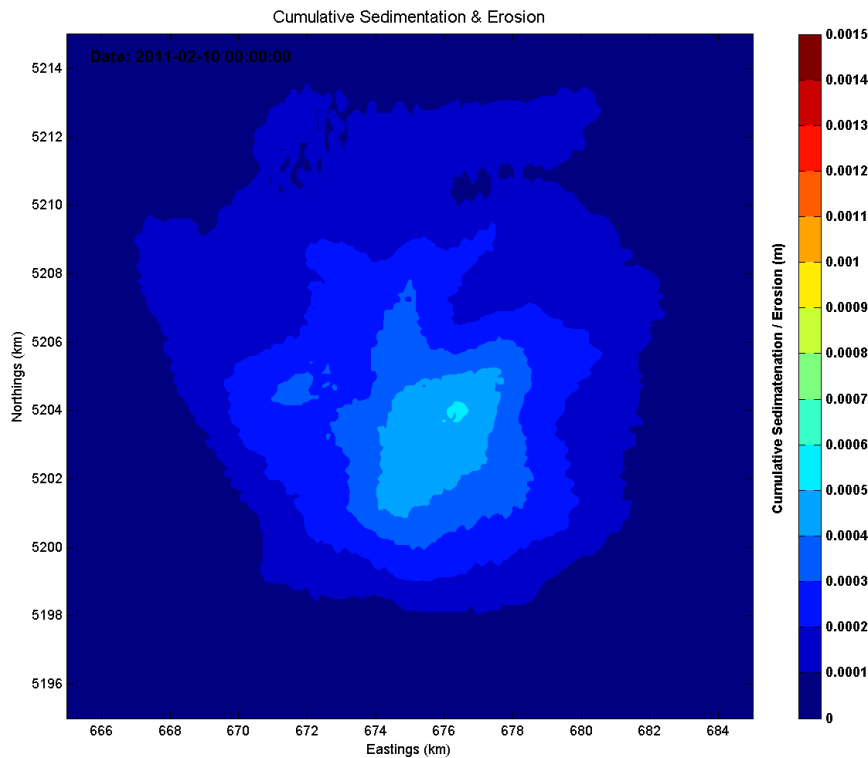


Figure B.11 Scenario 2 Fall Velocity 2 cumulative sedimentation (m) of silt and clay dredge discharge material at end of simulation period.

In general, the change in the footprint between the two Fall Velocity test cases and the base summer Scenario 2 test case is only attributable to the increase in the settled clay fraction due to the increased clay fall velocity.

B.5 Geographical location Sensitivity

In the Southern Chatham Rise test case, the southern Local model domain is used. This test case is only run for *Scenario 2*, with a mine tailing release halfway the water column. The purpose of this test case is to investigate if there is any significant difference in the plume dispersion and settlement patterns between the southern side of the Chatham Rise and the northern side.

During the Southern Chatham Rise test case simulation, the currents in the lower half of the water column have velocities on the order of 0.25 m/s, with peak velocities reaching 0.5 m/s. The average and maximum velocities are similar to those for the northern summer Scenario 2 simulation; however the residual direction of the flow is oriented towards the east, as opposed to a circular pattern around the dredge track.

In the Southern Chatham Rise test case, the plume signal approximately 80 m and 50 m above the seabed tend to oscillate around the dredge track, with a residual flow towards the east. The maximum clay and silt concentrations are on the order of 10 mg/L 12 hours after the dredge discharging concludes approximately 50 m above the bed and 2 mg/L approximately 80 m above the bed. The mine tailing plume is predicted to settle out and disperse more quickly in this southern domain simulation compared to the northern domain simulation (Fig. B.12).

The maximum vertical extent of the suspended clay and silt plumes is within 100 m of the seabed, and which is quite different from the summer Scenario 2 simulation for the North domain.

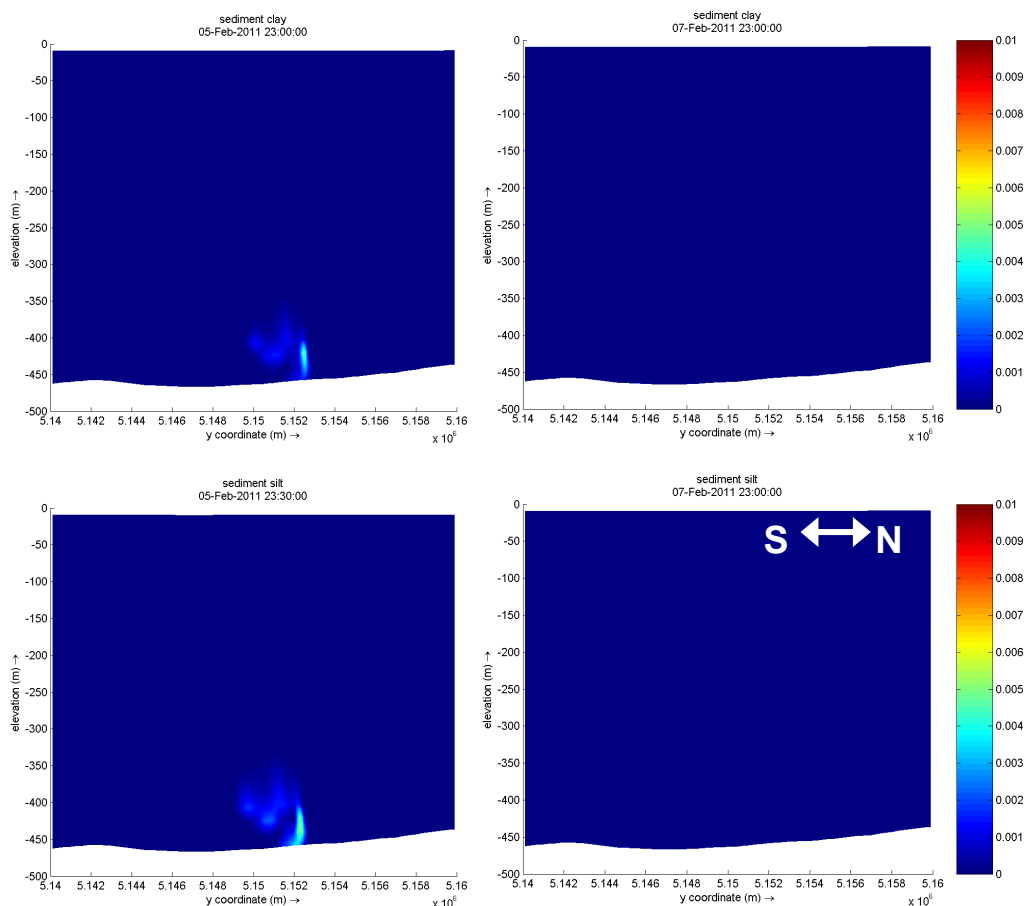


Figure B.12 Scenario 2, Southern domain: Clay (upper) and Silt (lower) suspended concentrations (g/L) at $x=675$ km 47.5 hours after discharging began (left) and 47 hours after discharging concluded (right).

Figure B.13 and Figure B.14 are timestacks of silt and clay SSC, respectively, for scenarios 1, 2, 2 with fall velocity 1, 2 with fall velocity 2 and 2 for the southern domain. These images illustrate the transport of the plume across this central point, which is located along the mining track, approximately half way along track. Again, the maximum SSC of both the silt and clay fractions are on the order of 5 mg/L around the far-field model discharge depth (i.e. bottom grid cell for scenario 1 and approximately 50 m off the bed for scenario 2). Once the discharge concludes (i.e. three days after it begins), the plume is present at this central point for the northern domain scenarios, though with a diluted concentration and more spread over the water column. For the southern domain test case, the plume is predicted to be quickly

transported away from this central point and diluted after the mining concludes, similarly to the winter and spring northern domain scenarios.

As to be expected, the silt predictions for scenarios 2, 2 with fall velocity 1 and 2 with fall velocity 2 are identical because the hydrodynamics and the silt input are the same for all three scenarios. However, there is variability between the clay timestacks. The scenario 2 and scenario 2 with fall velocity 1 have strikingly similar patterns; however the timestack for scenario 2 with fall velocity 2 has a reduced SSC comparatively, particularly once the mining works conclude. This implies that there is virtually no difference (assuming no flocculation) in transport and dilution patterns between clay with a fall velocity of 0.025 mm/s and 0.0027 mm/s. Comparatively, there is somewhat increased settling predicted for clay particles with a fall velocity of 0.25 mm/s, which is the same settling velocity as the silt fraction in this study.

At the end of the 10-day simulation period, the maximum cumulative sedimentation of the clay and silt sediments at the seabed is less than 1.1 mm (Figure B.15), which is slightly more than double the predicted maximum clay and silt sedimentation for the northern summer Scenario 2 simulation. The sedimentation footprint is skewed to the east of the discharge track, which is different from the footprint patterns predicted in all the other simulations. This eastern skew is expected because there is a known eastward residual flow along the Chatham Rise.

Note: the computed sedimentation layer thickness has to be added to the value that was computed for the near field because this settled layer (mainly composed of the sand fraction) is not included in the Delft3D simulations.

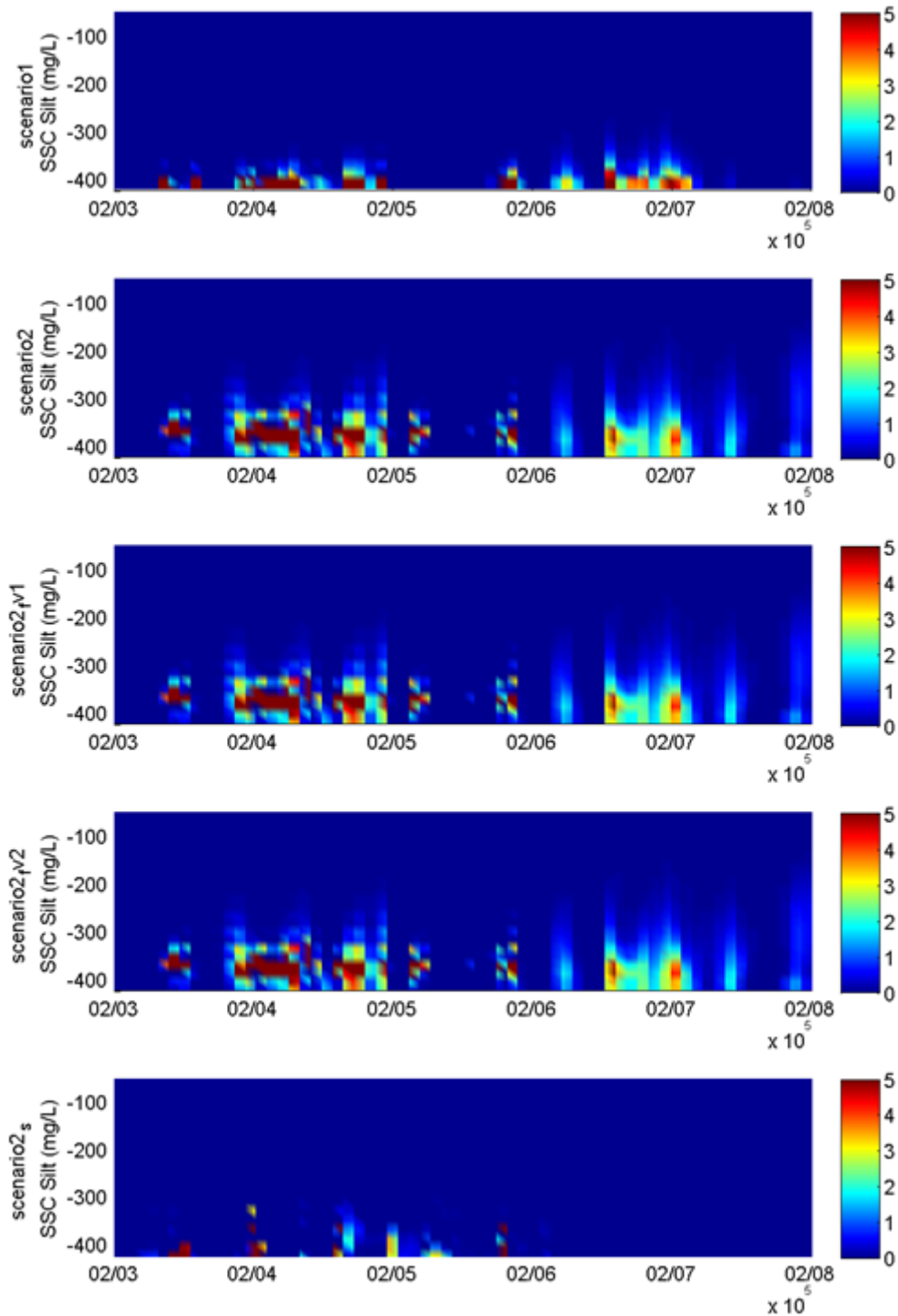


Figure B.13 Scenario 1 (upper), scenario 2 (2nd panel), scenario 2 for fall velocity 1 (3rd panel), scenario 2 for fall velocity 2 (4th panel), and scenario 2 for the southern domain (bottom) timestacks of Silt SSC (mg/L) for a central point along the mining track.

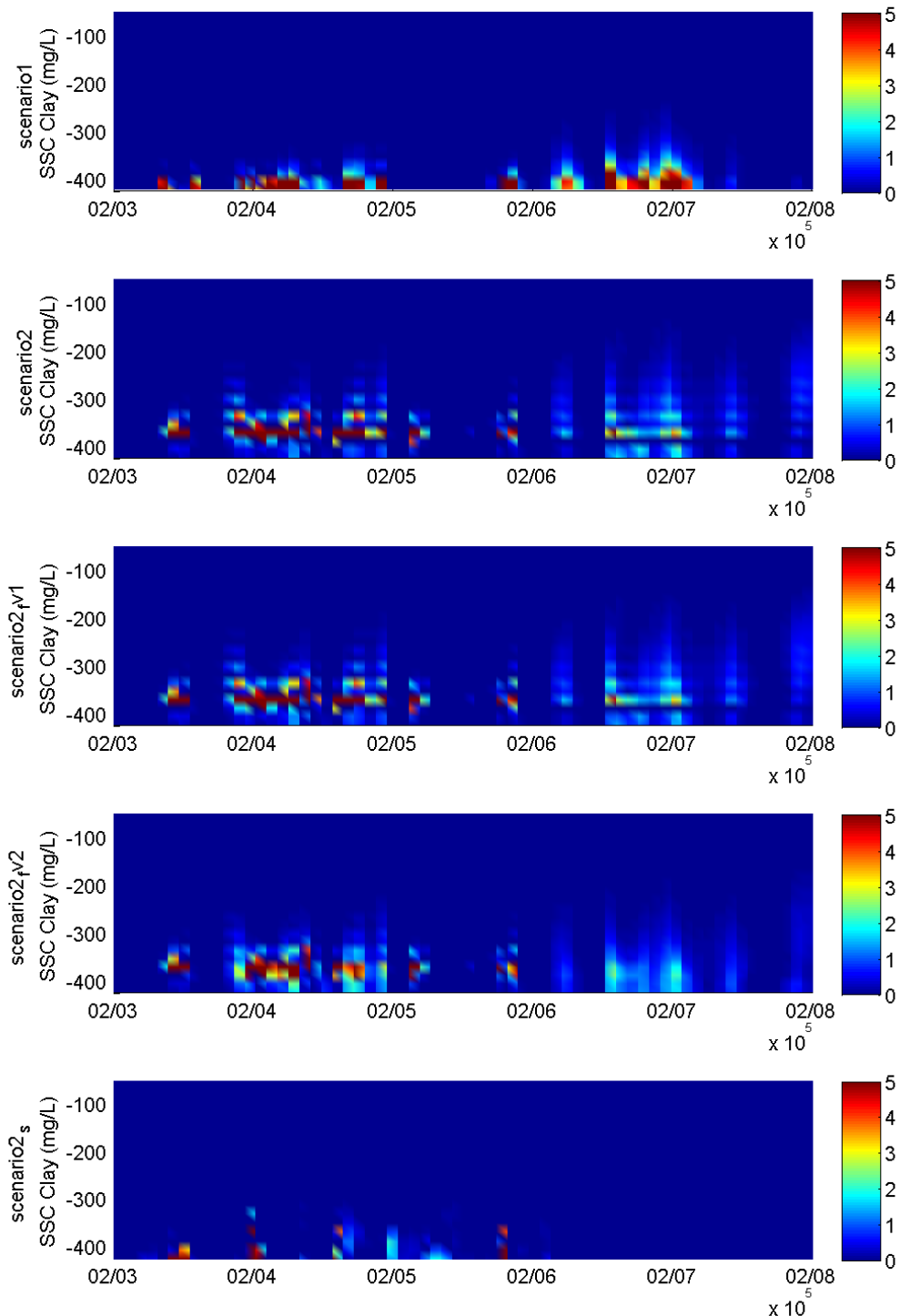


Figure B.14 Scenario 1 (upper), scenario 2 (2nd panel), scenario 2 for fall velocity 1 (3rd panel), scenario 2 for fall velocity 2 (4th panel), and scenario 2 for the southern domain (bottom) timestacks of Clay SSC (mg/L) for a central point along the mining track.

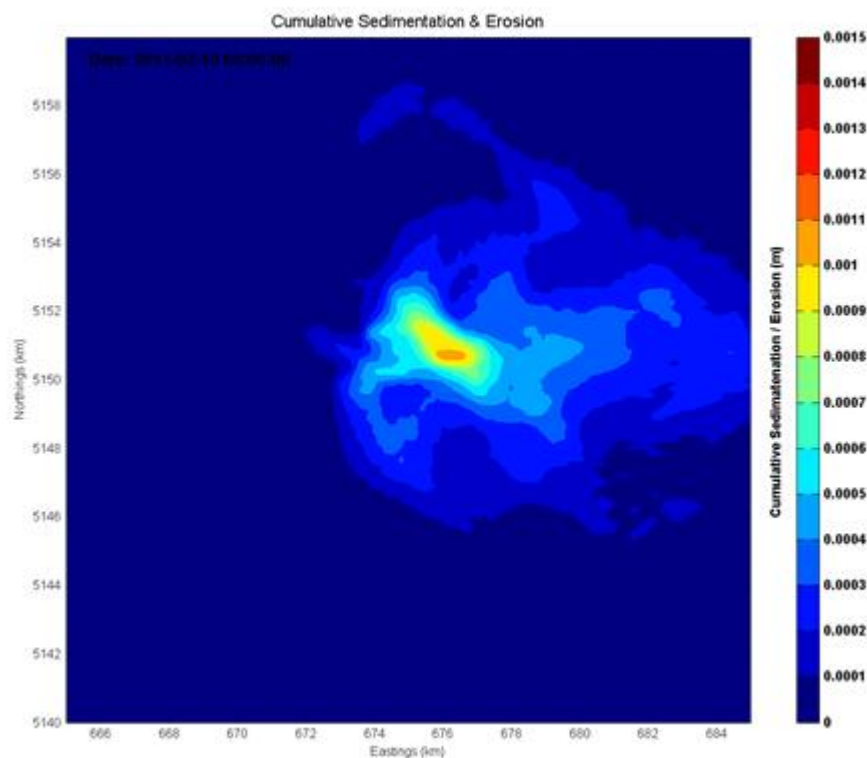


Figure B.15 Scenario 2 cumulative sedimentation (m) of silt and clay dredge discharge material at end of simulation period.

C Additional Figures Initial Far-field Investigations – Phase 1b

This appendix contains more snapshots over a cycle and other threshold levels, such as 10, 30 and 50 mg/l. These plots are also shown for 10 and 50 m above the bed for spring, summer and winter.

C.1 Spring

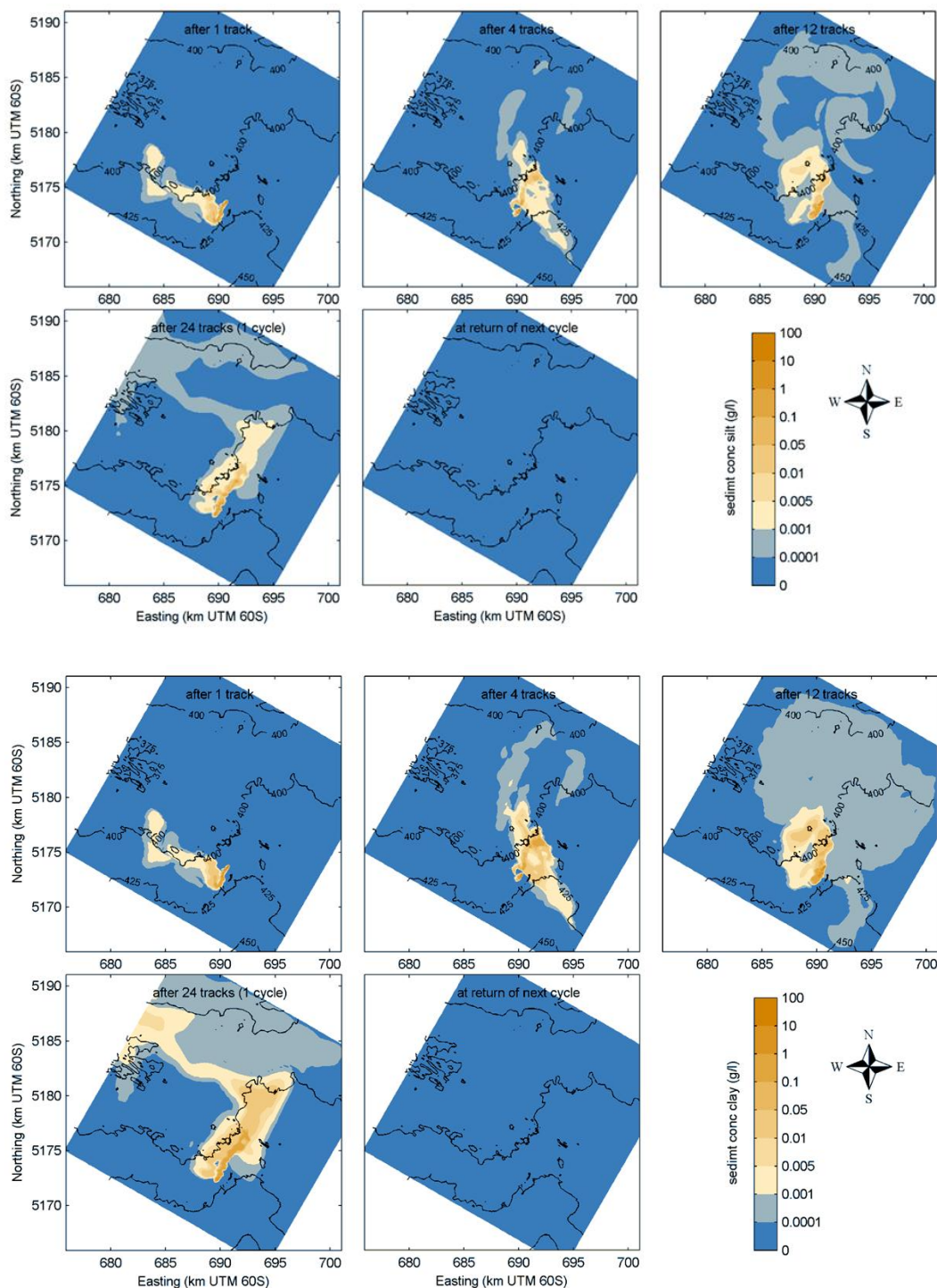


Figure C.1 Overview of the near-bed (bottom grid cell) suspended sediment concentration of the **silt (top) and clay (bottom)** fraction (g/l) over 1 completed track line, 4 track lines, 12 track lines, a complete cycle, and at the start of a new cycle. **South Domain Spring.**

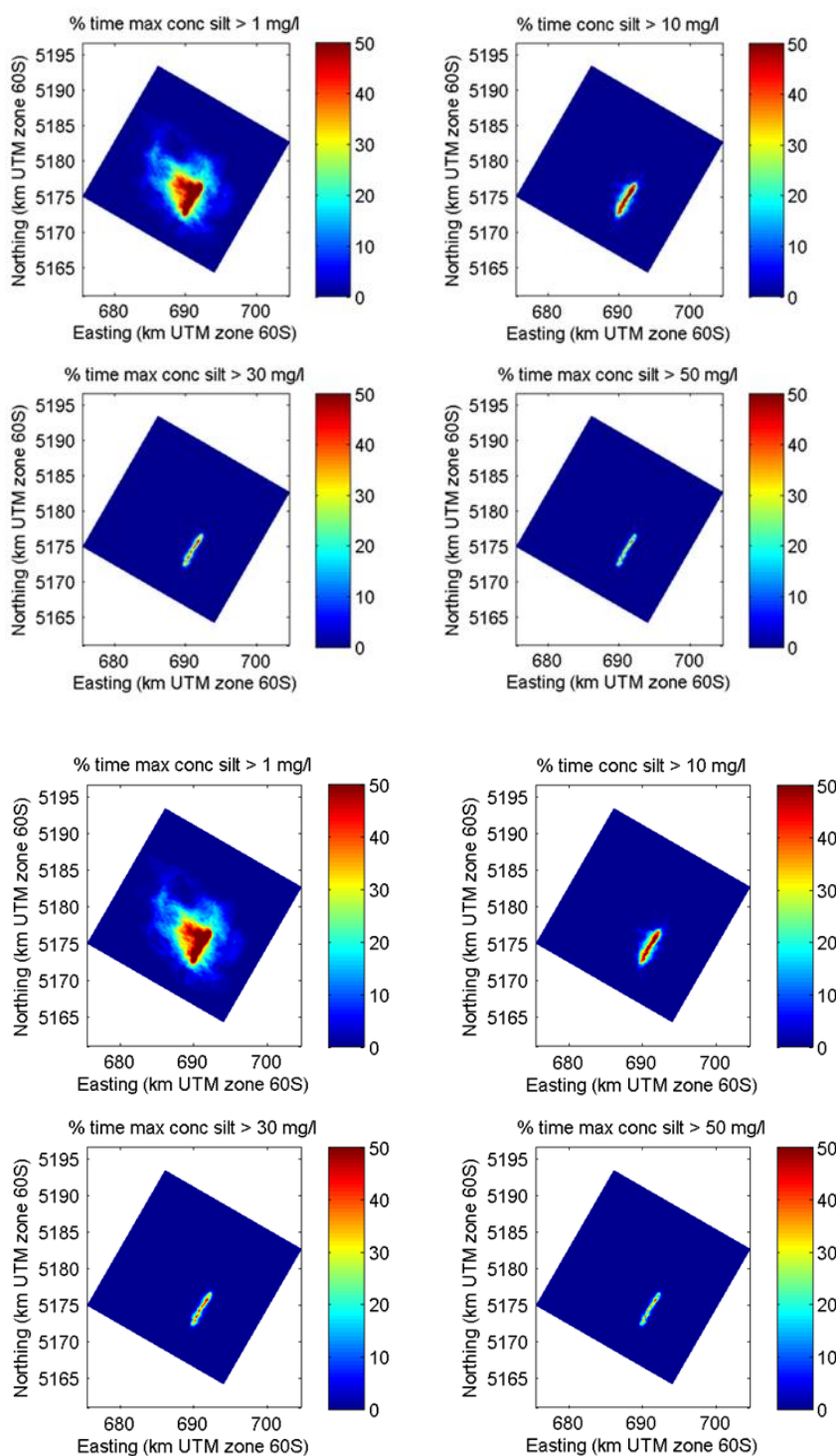


Figure C.2 Overview of the % time that the observed maximum suspended sediment concentration **over the height of the water column** of the silt fraction exceeds 1 mg/l (upper left), 10 mg/l (upper right), 30 mg/l (lower left) and 50 mg/l (lower right). **South Domain Spring.**

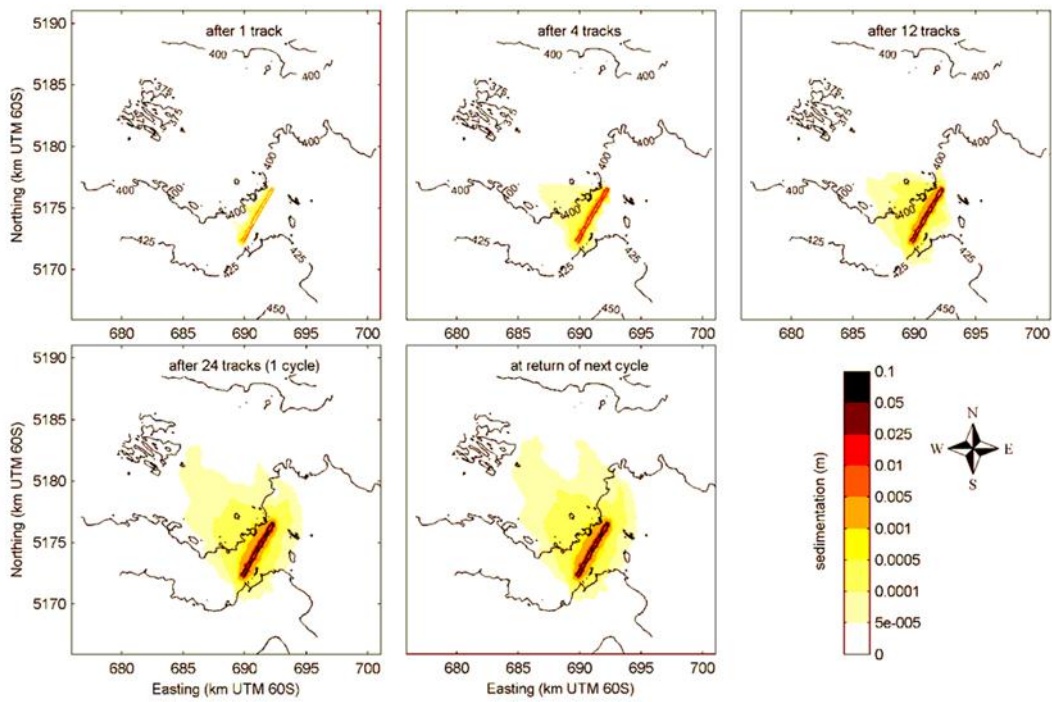


Figure C.3 Overview silt + clay sedimentation (m) over 1 completed track line, 4 track lines, 12 track lines, a complete cycle, and at the start of a new cycle. South Domain Spring

C.2 Summer

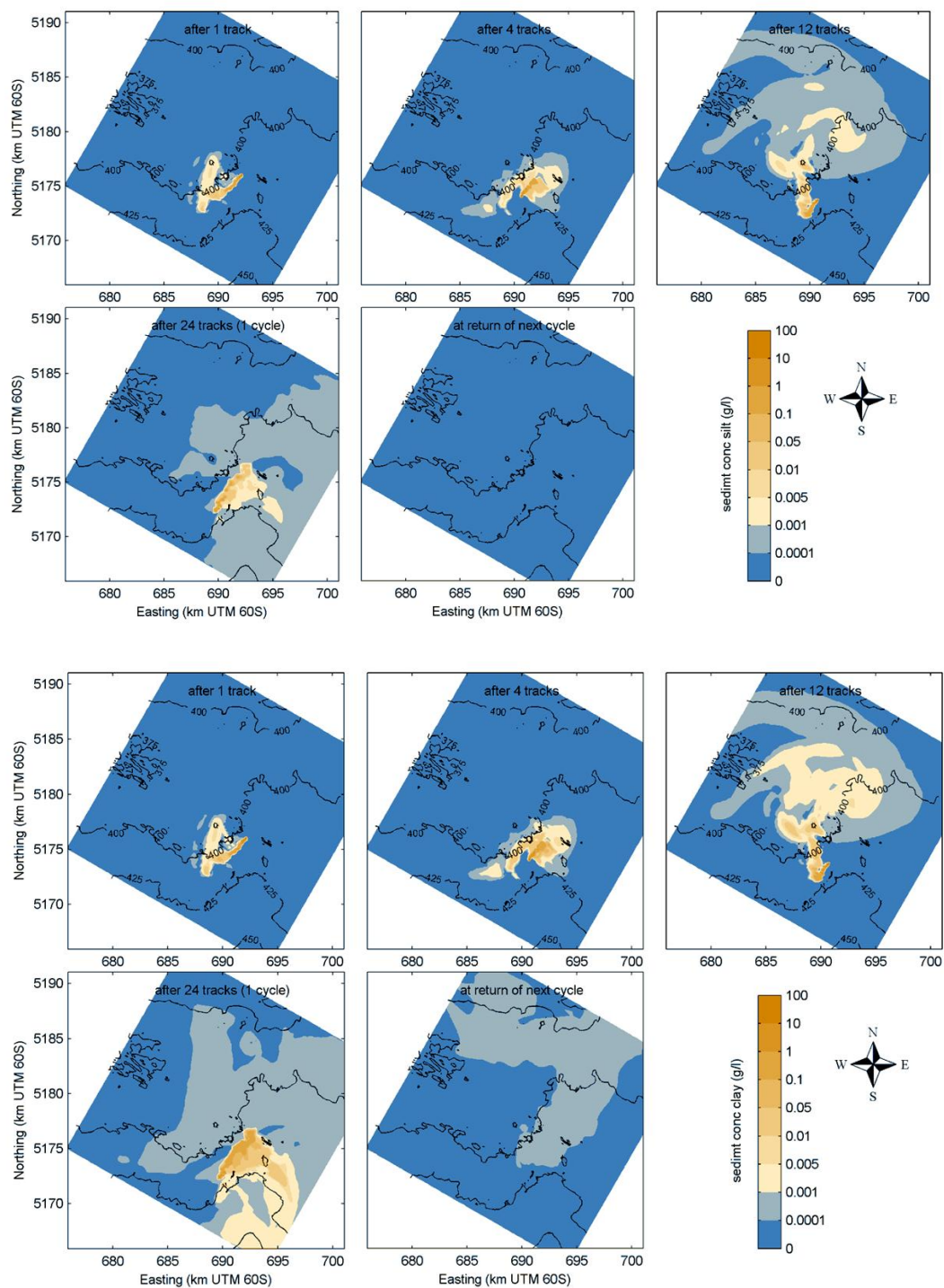


Figure C.4 Overview of the near-bed (bottom grid cell) suspended sediment concentration of the silt (top) and clay (bottom) fraction (g/l) over 1 completed track line, 4 track lines, 12 track lines, a complete cycle, and at the start of a new cycle. **South Domain Summer.**

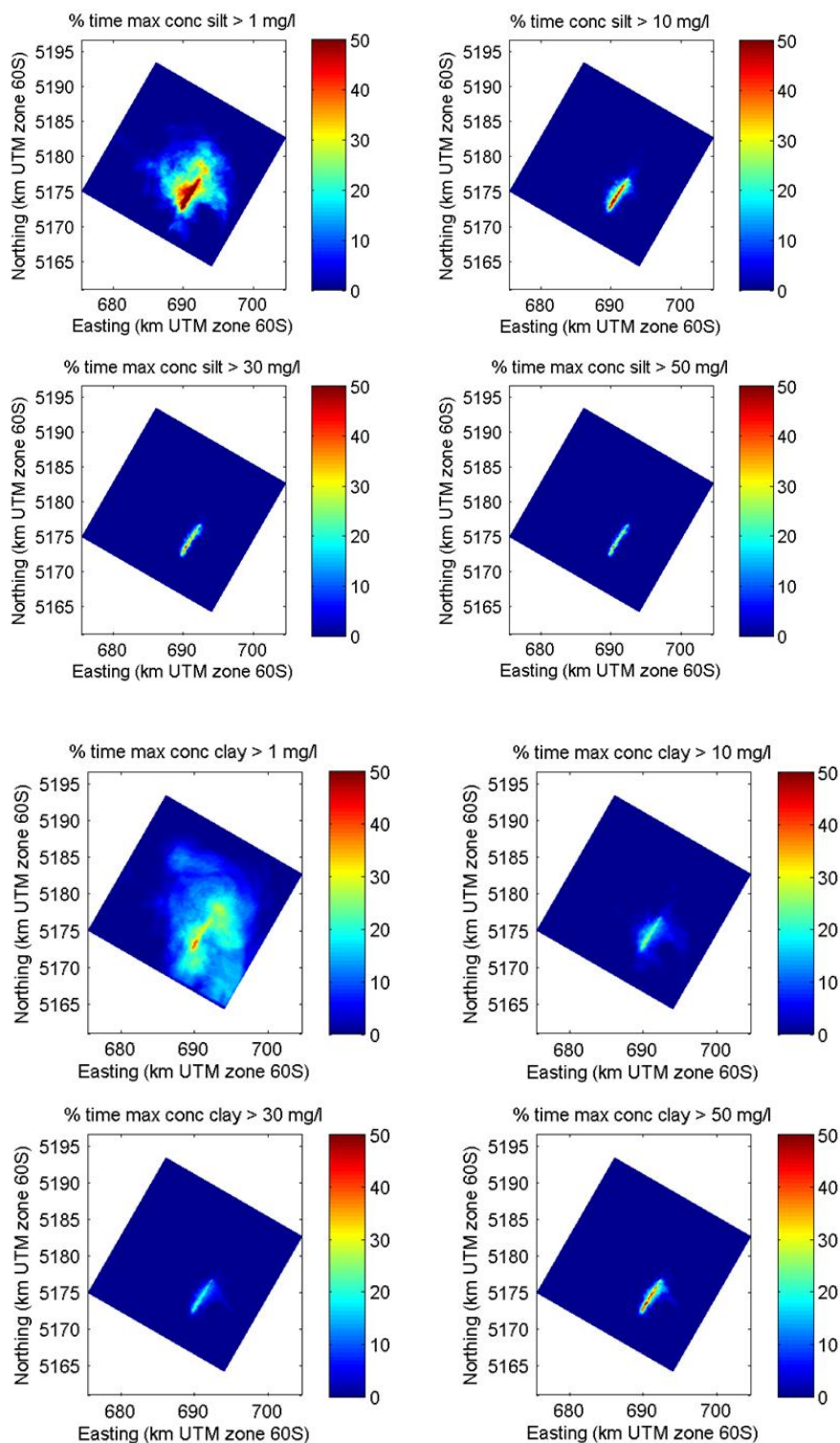


Figure C.5 Overview of the % time that the observed maximum suspended sediment concentration over the height of the water column of the **silt fraction** and clay (bottom) exceeds 1 mg/l (upper left), 10 mg/l (upper right), 30 mg/l (lower left) and 50 mg/l (lower right). South Domain Summer.

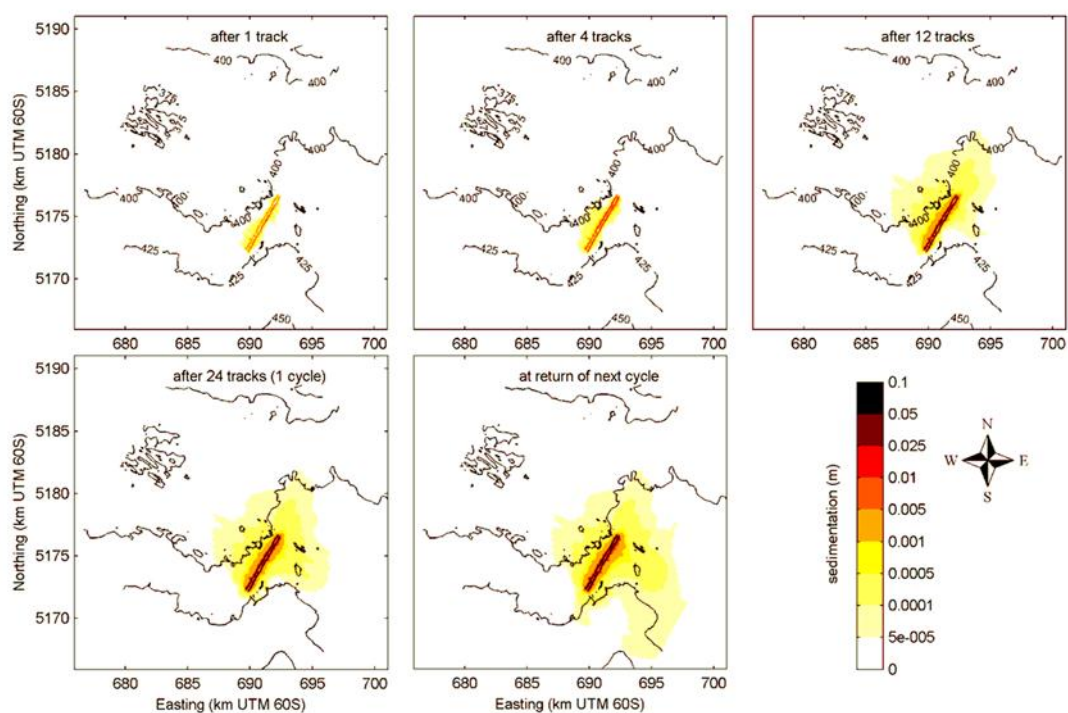


Figure C.6 Overview silt + clay sedimentation (m) over 1 completed track line, 4 track lines, 12 track lines, a complete cycle, and at the start of a new cycle. **South Domain Summer**

C.3 Winter

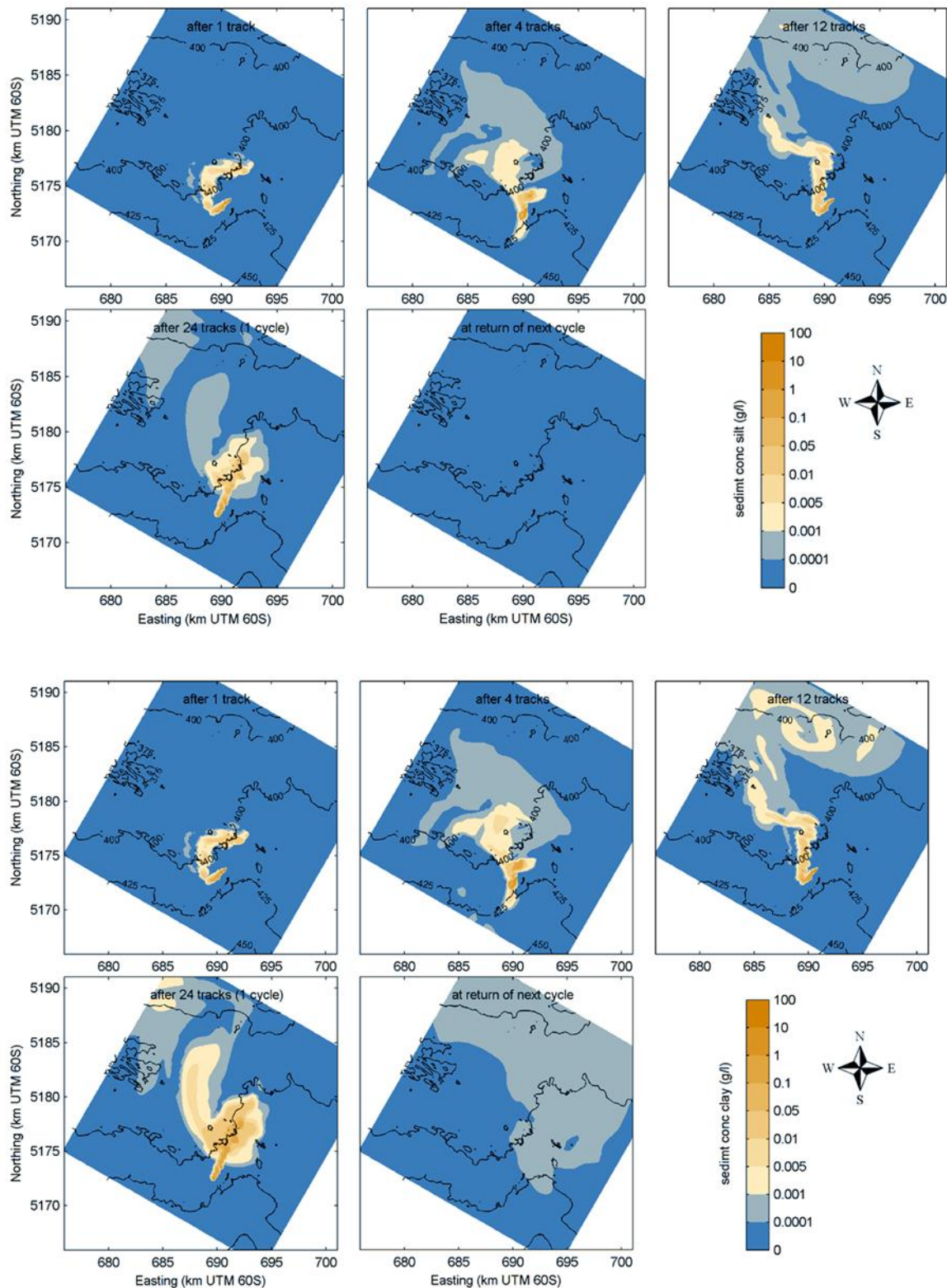


Figure C.7 Overview of the near-bed (bottom grid cell) suspended sediment concentration of the silt fraction (g/l) over 1 completed track line, 4 track lines, 12 track lines, a complete cycle, and at the start of a new cycle. South Domain Winter

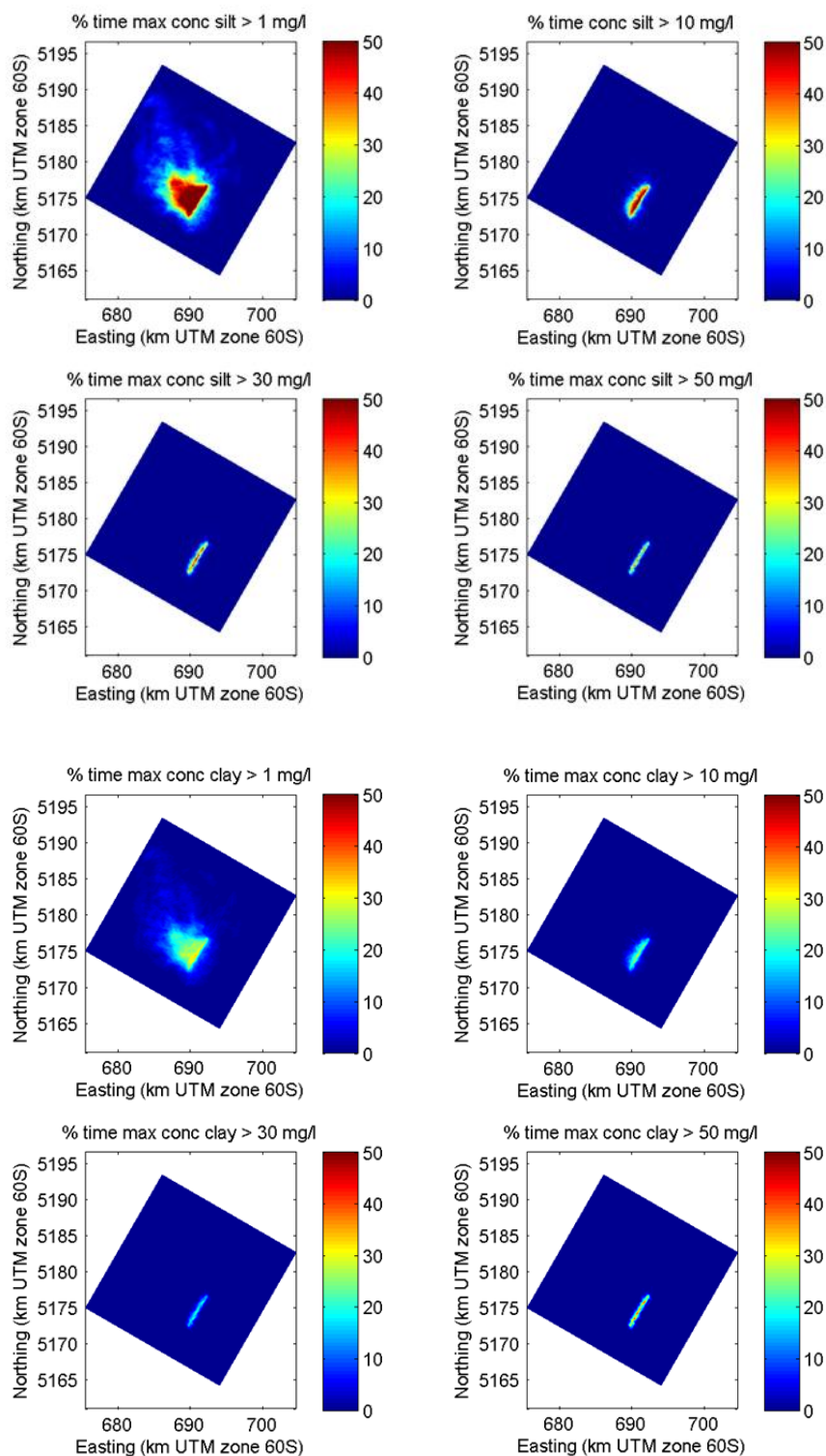


Figure C.8 Overview of the % time that the observed maximum suspended sediment concentration over the height of the water column of the clay fraction exceeds 1 mg/l (upper left), 10 mg/l (upper right), 30 mg/l (lower left) and 50 mg/l (lower right). **South Domain Winter.**

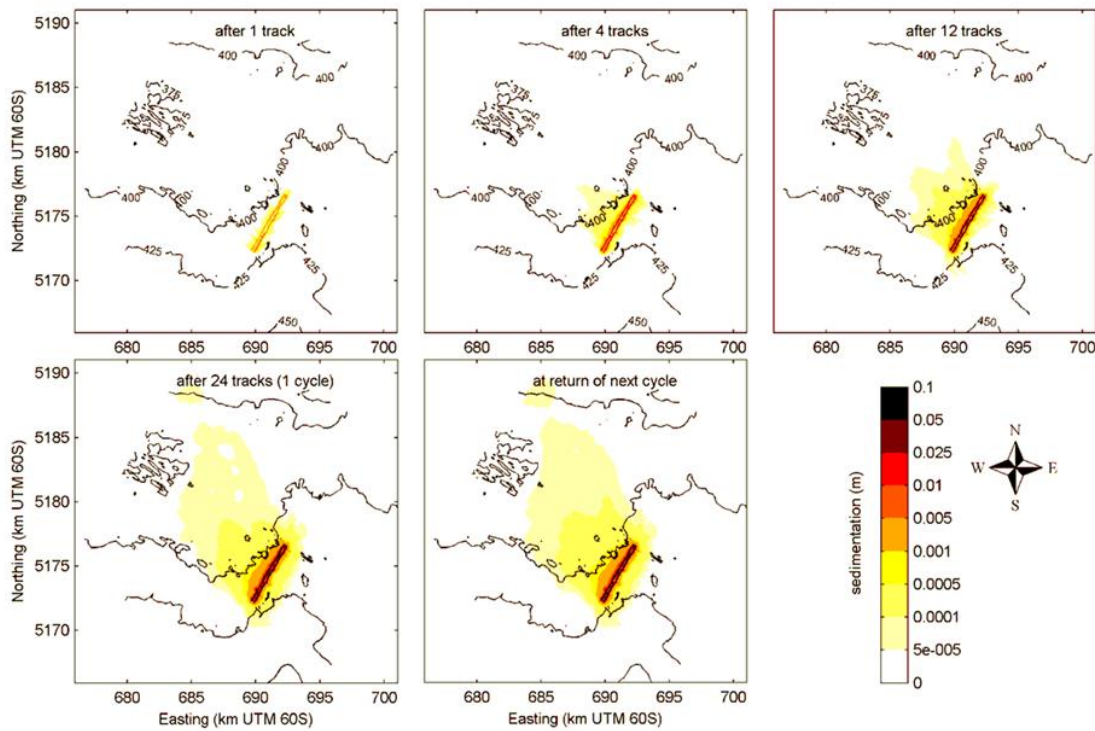


Figure C.9 Overview silt + clay sedimentation (m) over 1 completed track line, 4 track lines, 12 track lines, a complete cycle, and at the start of a new cycle. **South Domain Winter.**

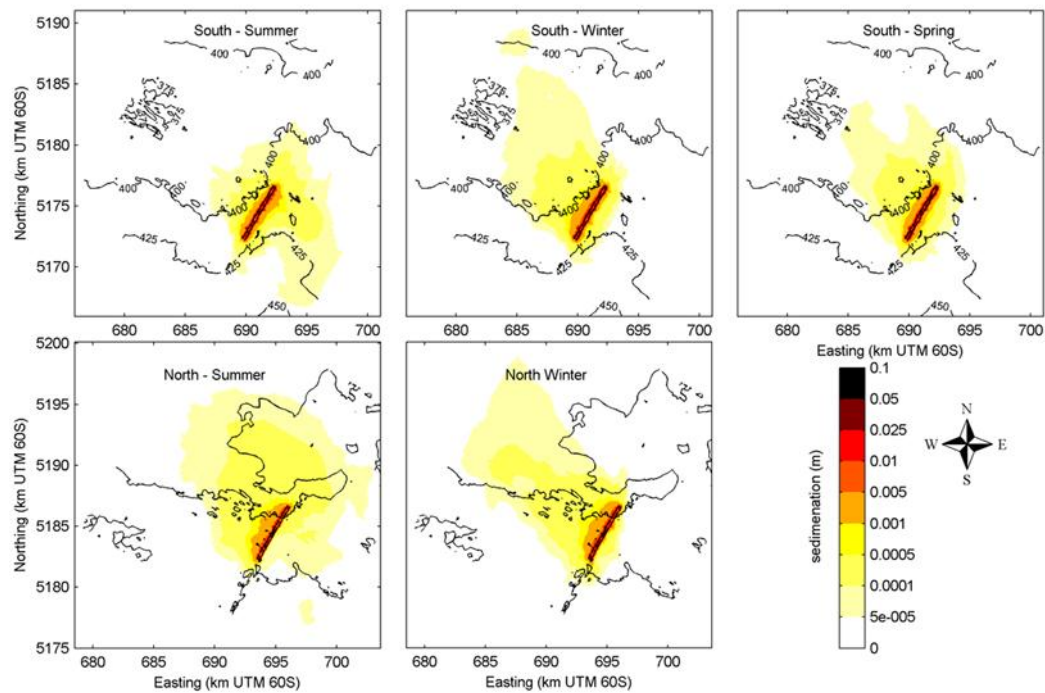
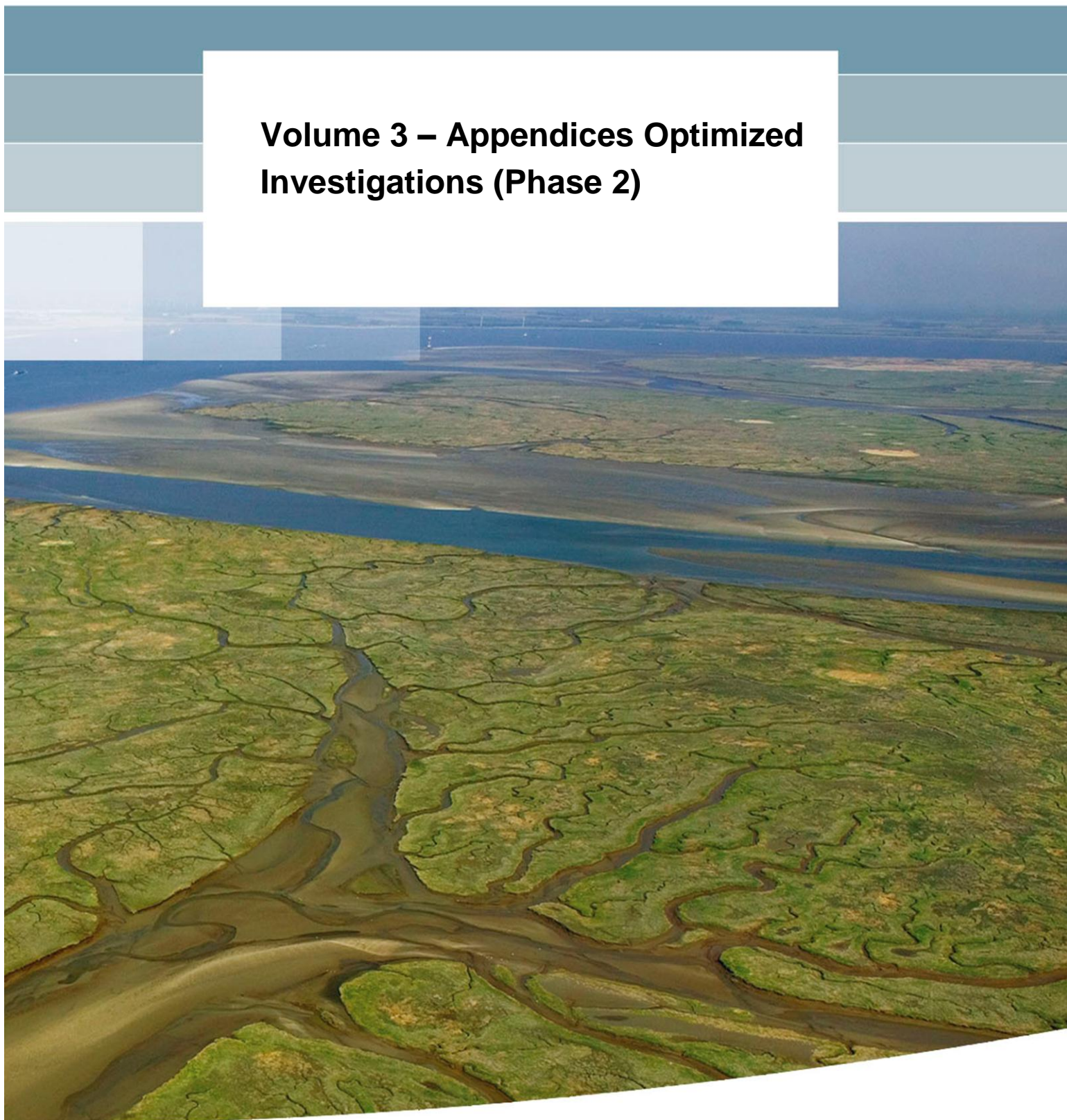


Figure C.10 Overview of cumulative sedimentation (m) of silt and clay fractions of discharged material at the end of a completed dredge cycle (24 tracks + 114 hour return time) for South domain (winter, summer, spring) and North domain (Summer and Winter).

D References

Deltares, 2014. *Modelling investigations on mine tailing plume dispersion on the Chatham Rise*. Deltares Final Report 1209110-000-ZKS-0007, 57 pp

**Volume 3 – Appendices Optimized
Investigations (Phase 2)**



Volume 3 – Appendices Optimized Investigations (Phase 2)

dr. M.C.J.L. Jeuken
J.M. Lescinski MSc
K. Cronin PhD
ir. J. Vroom
dr. E.P.L. Elias

1209110-000

Title

Volume 3 – Appendices Optimized Investigations (Phase 2)

Project	Reference	Pages
1209110-000	1209110-000-ZKS-0009	14

Keywords

Deep sea mining, Modelling, Mine tailing dispersion, Chatham Rise.

Summary

In the framework of the Chatham Rise Rock Phosphates (CRP) Mining Project, Boskalis and CRP asked Deltares to conduct an operations study investigating the dispersion behaviour of sediments released during the mining process. The main interest is in the turbidity generated in the water column and the deposition footprint on the seabed resulting from the mining discharge. The Chatham Rise is a submarine feature that is approximately 1000 km in length, extending eastward from the South Island of New Zealand. The rise has water depths that range from roughly 80 m to 500 m, with the Chatham Islands near the eastern extent of the submarine feature. Just north and south of the Rise, water depths quickly approach 3000 m. This document is an appendix of that study (Deltares, 2014a) which uses a dedicated modelling approach to assess the near and far-field dispersion, and sedimentation behaviour of sediments released during the mining process.

Version	Date	Author	Initials	Review	Initials	Approval	Initials
	Mar. 2014	Claire Jeuken					

State

final

Contents

Appendices

A Single cycle simulations- threshold maps	A-1
A.1 Spring	A-1
A.2 Summer	A-3
A.3 Winter	A-5
B Disposal release 10 m above bed	B-7
B.1 Single Cycle simulations	B-8
B.2 10-Cycle Simulations	B-13
C Sedimentation	C-1
D References	D-1

A Single cycle simulations- threshold maps

This section contains additional time exceedence plots corresponding to Section 4.1 and Section 4.2 of the main report (Deltares, 2014a). Here additional threshold sediment concentrations are shown.

A.1 Spring

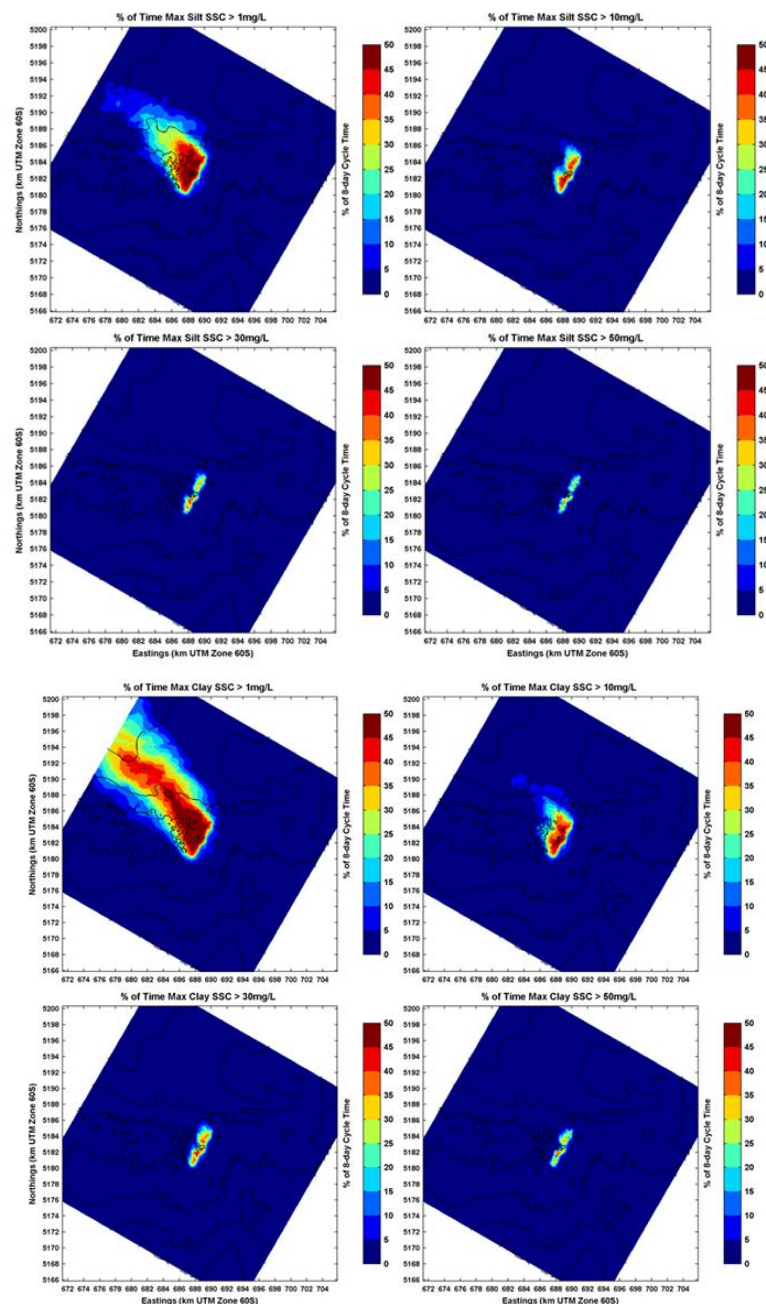


Figure A.1 Overview of the % time (of the mining cycle) that the observed **maximum** SSC suspended sediment concentration **over the height of the water column** of the **silt** (top) and **clay** (bottom) fraction

exceeds 1 mg/l (upper left), 10 mg/l (upper right), 30 mg/l (lower left) and 50 mg/l (lower right). **Local domain – Spring** Colour scale 0-50%, with 5% increment.

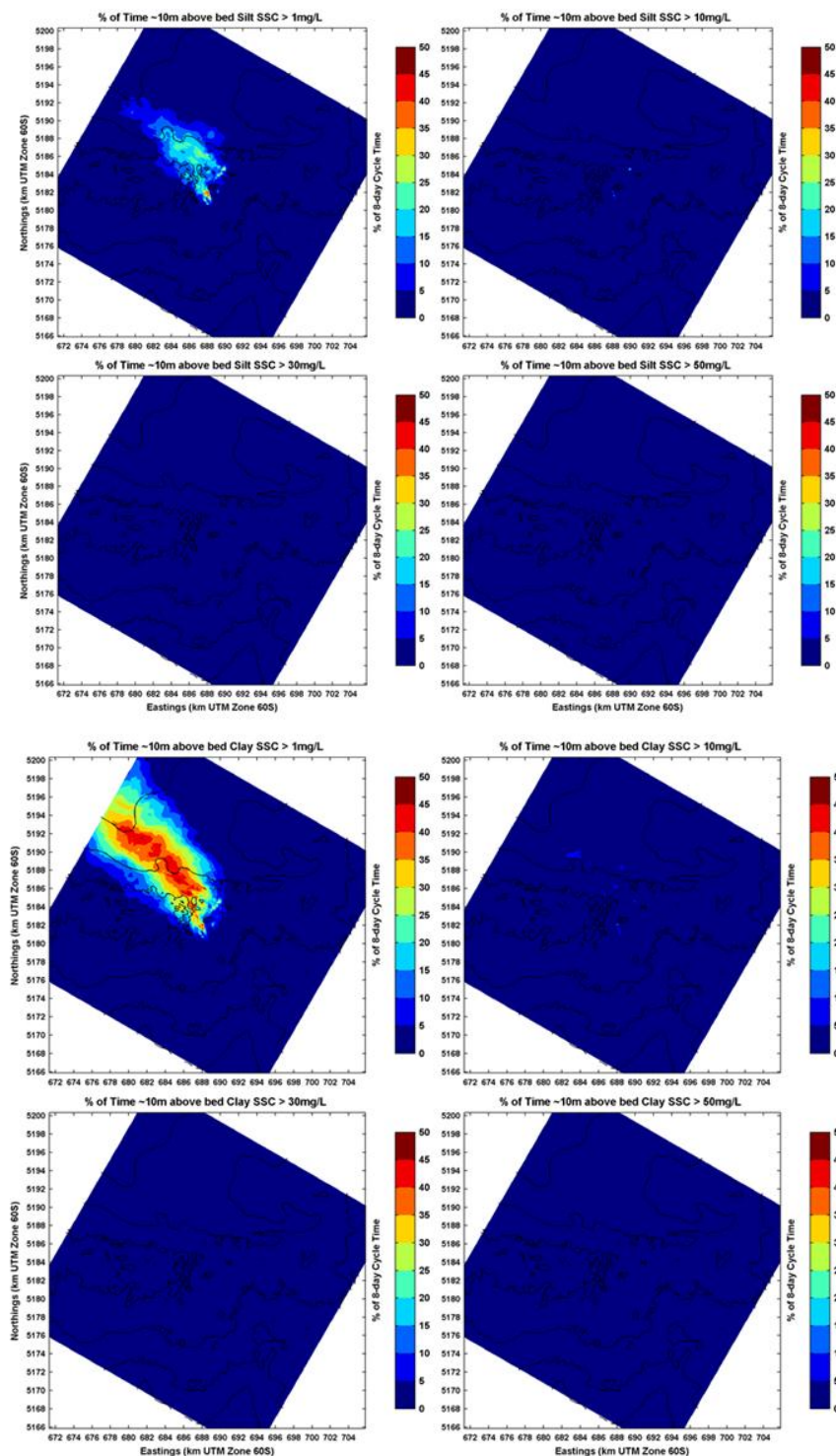


Figure A.2 Overview of the % time that the observed suspended sediment concentration approximately **10 m above the bed** of the **silt** (top) and **clay** (bottom) fraction exceeds 1 mg/l (upper left), 10 mg/l (upper right), 30 mg/l (lower left) and 50 mg/l (lower right). **Local Domain Spring**

A.2 Summer

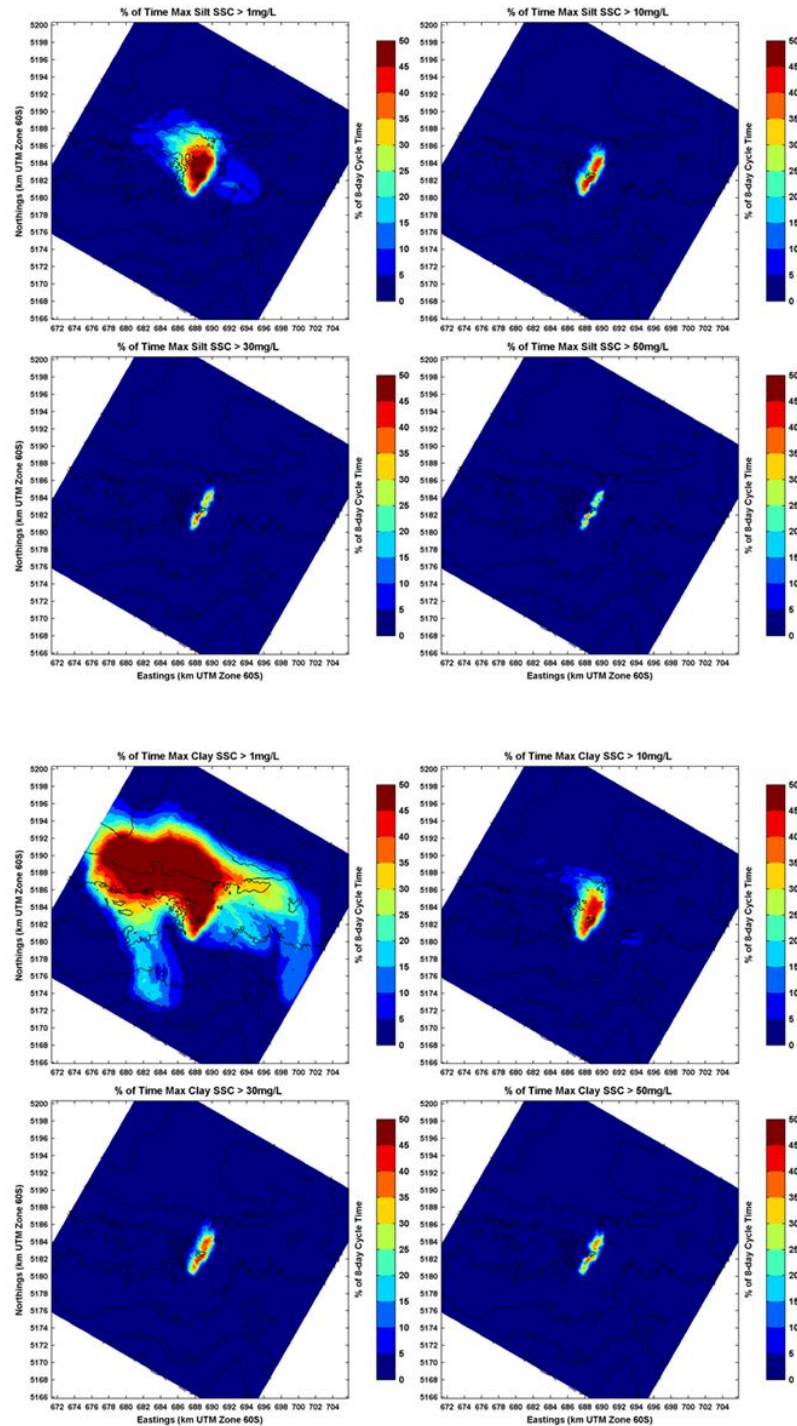


Figure A.3 Overview of the % time (of the mining cycle) that the observed **maximum SSC** suspended sediment concentration **over the height of the water column** of the **silt** (top) and **clay** (bottom panels) fraction exceeds 1 mg/l (upper left), 10 mg/l (upper right), 30 mg/l (lower left) and 50 mg/l (lower right). **Local domain – Spring** Colour scale 0-50%, with 5% increment.

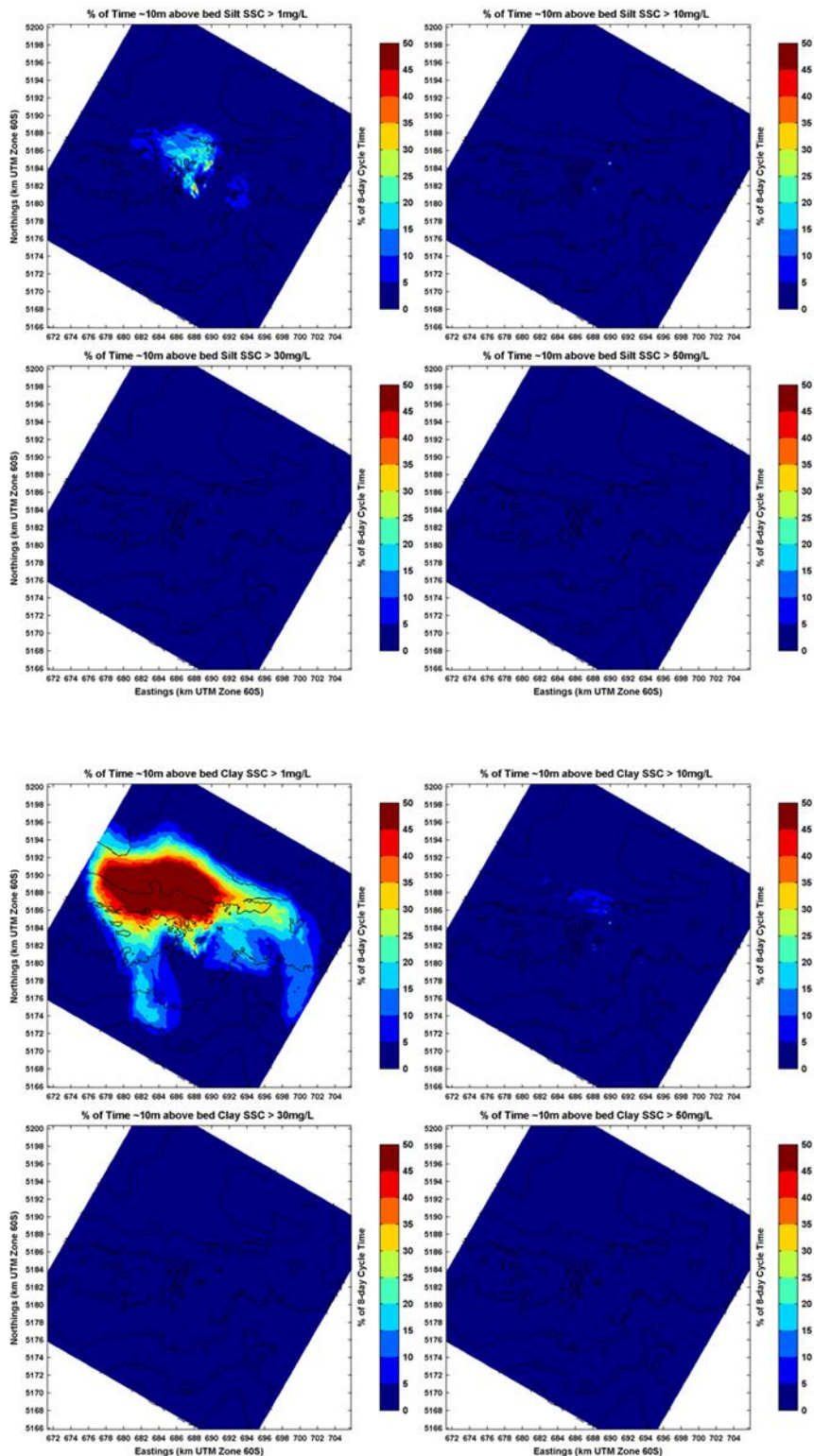


Figure A.4 Overview of the % time that the observed suspended sediment concentration approximately **10 m above the bed** of the **silt** (top) and **clay** (bottom) fraction exceeds 1 mg/l (upper left), 10 mg/l (upper right), 30 mg/l (lower left) and 50 mg/l (lower right). **Local Domain Spring**

A.3 Winter

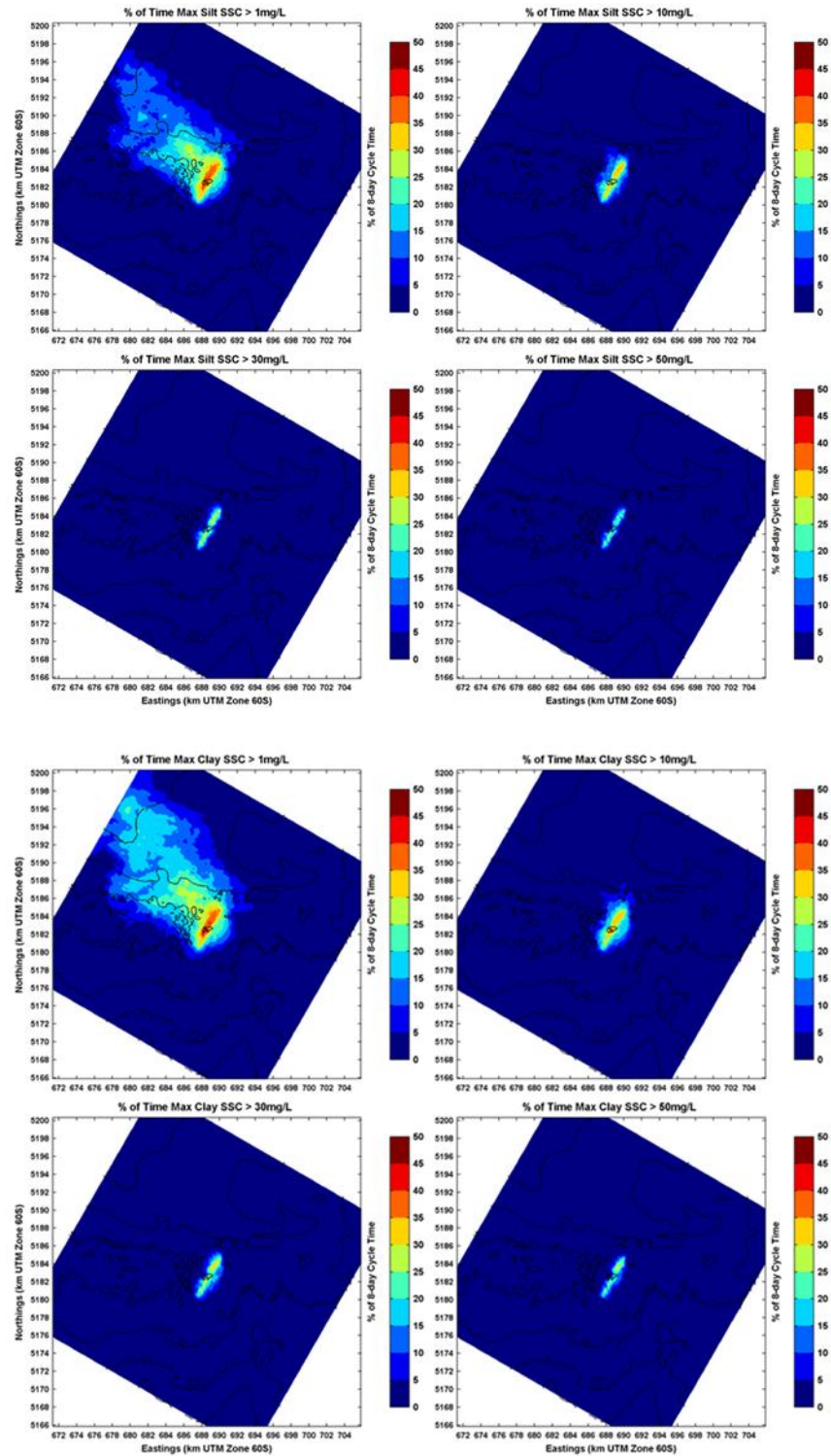


Figure A.5 Overview of the % time (of the mining cycle) that the observed **maximum SSC** suspended sediment concentration **over the height of the water column** of the **silt** (top) and **clay** (bottom panels) fraction exceeds 1 mg/l (upper left), 10 mg/l (upper right), 30 mg/l (lower left) and 50 mg/l (lower right). **Local domain – Winter.**

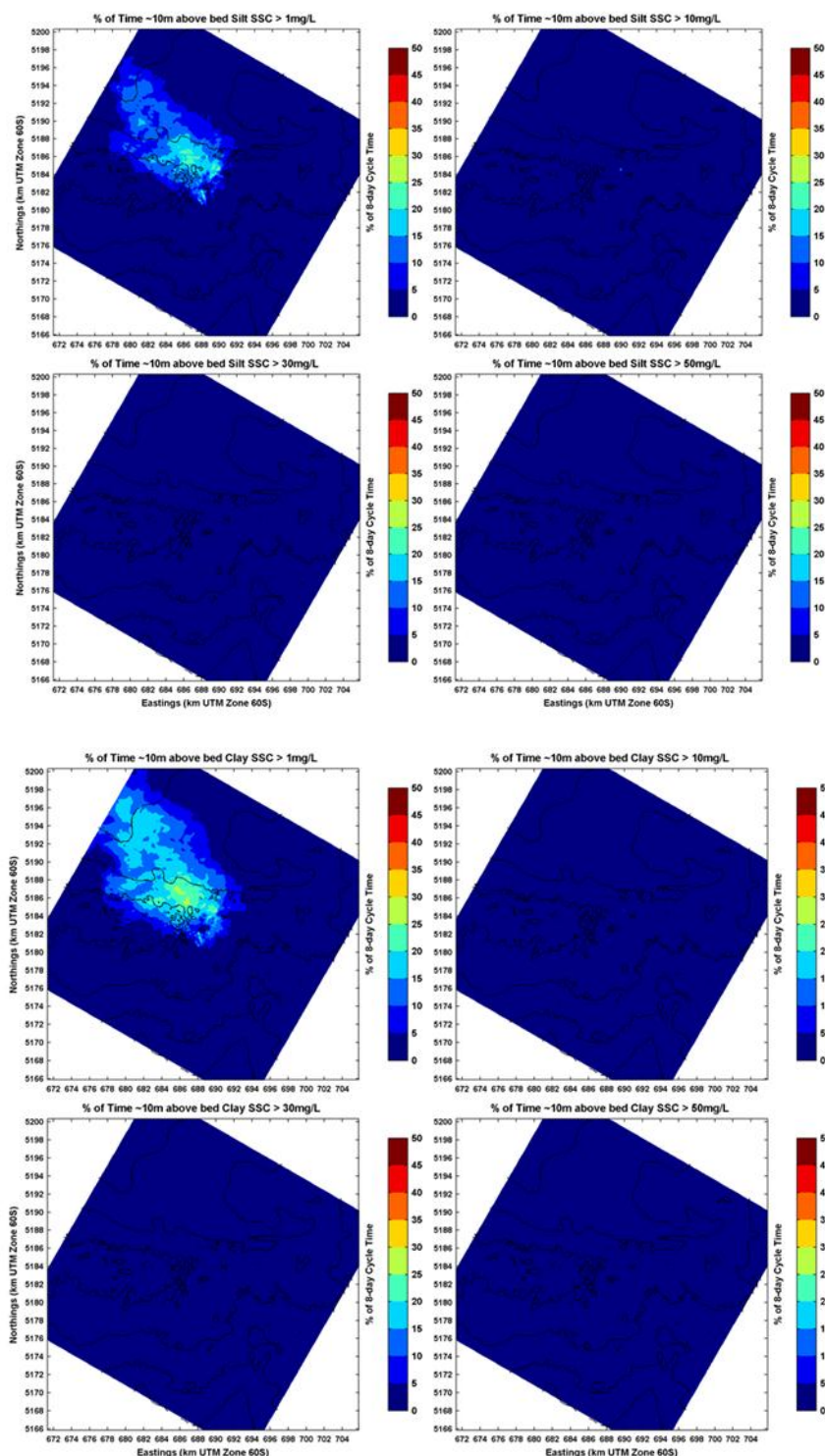


Figure A.6 Overview of the % time that the observed suspended sediment concentration approximately 10 m above the bed of the **silt** (top) and **clay** (bottom) fraction exceeds 1 mg/l (upper left), 10 mg/l (upper right), 30 mg/l (lower left) and 50 mg/l (lower right). **Local Domain Winter**

B Disposal release 10 m above bed

This section contains additional plots corresponding to Section 4.1, Section 4.2 and Section 4.3 of the main report (Deltares, 2014a). Plots include:

- An overview of the suspended sediment concentration of silt and clay near the bed and 10 m above the bed over 1 completed track line, 4 track lines, 12 track lines, a complete cycle, and at the start of a new cycle when disposing 10 m above bed for summer and winter (Figures B1 and B2).
- Near-bed suspended clay concentrations after Cycle 2 and Cycle 8 during the 5-days break in mining, prior to commencement of a new mining cycle in the Summer scenario after disposing 10 m above the bed (Figure B3).
- Overview of the % time that the observed maximum suspended sediment concentration over the height of the water column of the silt fraction exceeds 1 mg/l, 10 mg/l, 30 mg/l and 50 mg/l when disposing 10 m above bed in the Summer scenario (Figure B4).
- Overview of the % time that the observed suspended sediment concentration approximately 10 m above the bed of the silt fraction exceeds 1 mg/l, 10 mg/l, 30 mg/l and 50 mg/l for disposing 10 m above bed in the Summer scenario (Figure B5).
- Intra-seasonal variations in near-bed suspended clay concentrations at the end of cycles 1-10 during the 10-cycles simulation for discharging 10 m above the bed in the Summer scenario (Figure B6).
- Intra-seasonal variations in near-bed suspended clay concentrations at the end of cycles 1-10 during the 10-cycles simulation for discharging 10 m above the bed in the Winter scenario (Figure B7).
- Intra-seasonal variations in near-bed suspended silt concentrations at the end of cycles 1-10 during the 10-cycles simulation for discharging 10 m above the bed in the Summer scenario (Figure B8).
- Intra-seasonal variations in near-bed suspended silt concentrations at the end of cycles 1-10 during the 10-cycles simulation for discharging 10 m above the bed in the Winter Scenario (Figure B9).

B.1 Single Cycle simulations

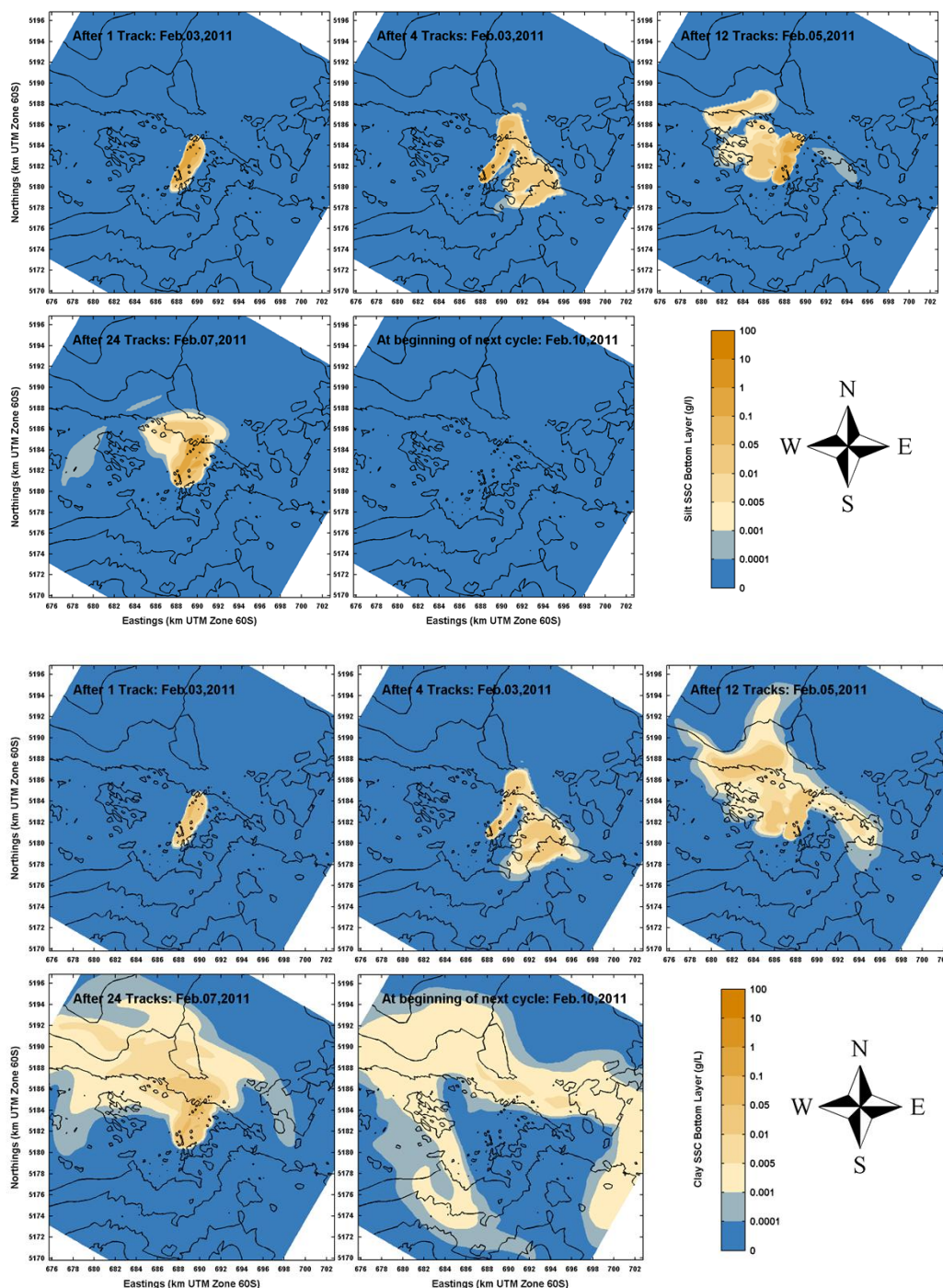


Figure B.1 Overview of the **near-bed** (bottom grid cell) suspended sediment concentration of the **silt** (upper) and **clay** (bottom) fraction (g/l) over 1 completed track line, 4 track lines, 12 track lines, a complete cycle, and at the start of a new cycle. **Disposing 10 m above bed. Local Domain Summer**

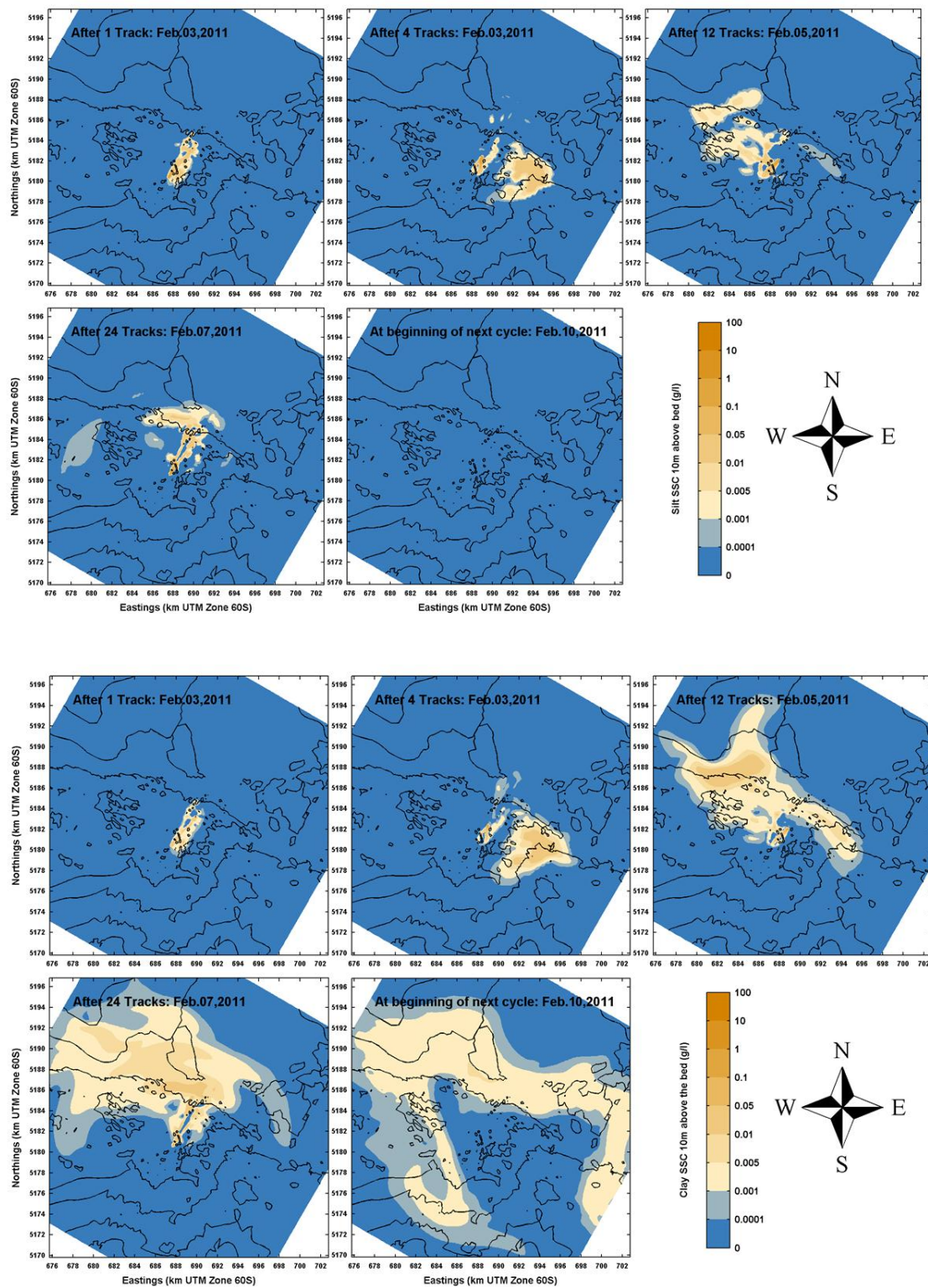


Figure B.2 Overview of approximately 10 m above the bed suspended sediment concentration (g/l) of the **silt** fraction (upper) and **clay** fraction (bottom) over 1 completed track line, 4 track lines, 12 track lines, a complete cycle, and at the start of a new cycle. **Disposing 10 m above bed. Local Domain Summer**

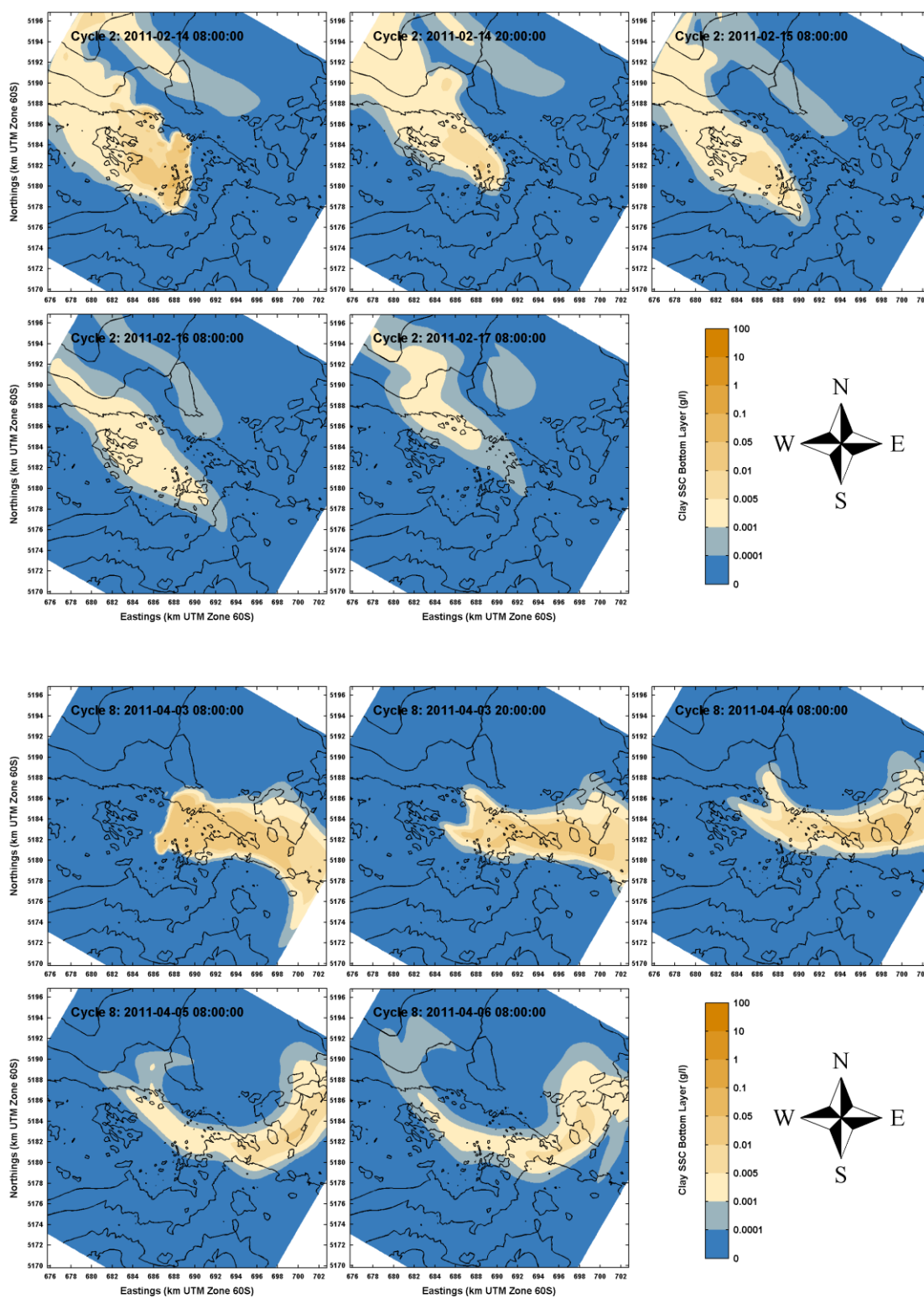


Figure B.3 Cycle 2 (upper) and Cycle 8 (bottom) near-bed suspended clay concentrations during the 5-days break in mining, prior to commencement of a new mining cycle. **Summer, disposal 10 m above the bed**

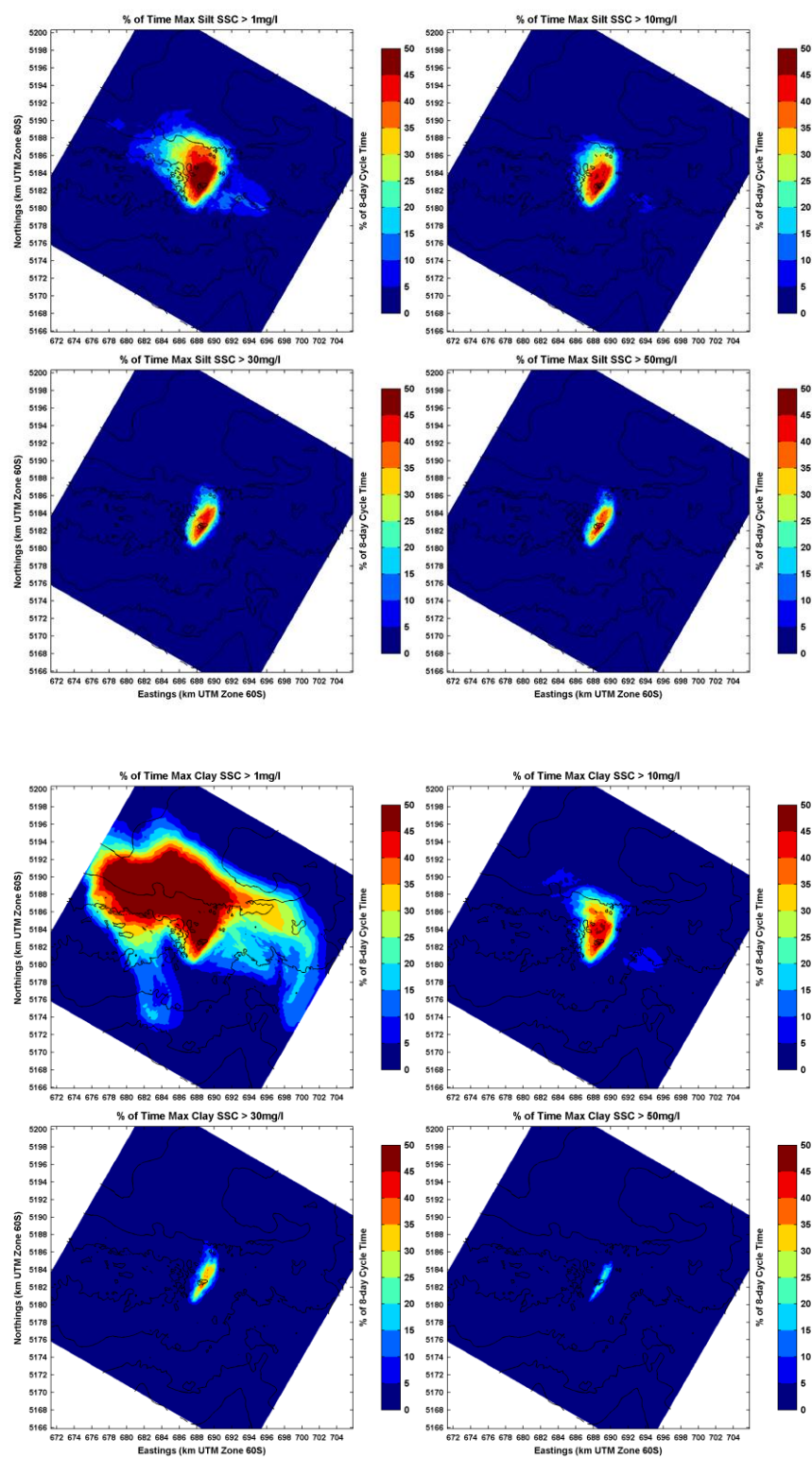


Figure B.4 Overview of the % time that the observed maximum suspended sediment concentration **over the height of the water column** of the **silt** fraction exceeds 1 mg/l (upper left), 10 mg/l (upper right), 30 mg/l (lower left) and 50 mg/l (lower right). **Disposing 10 m above bed. Local Domain Summer**

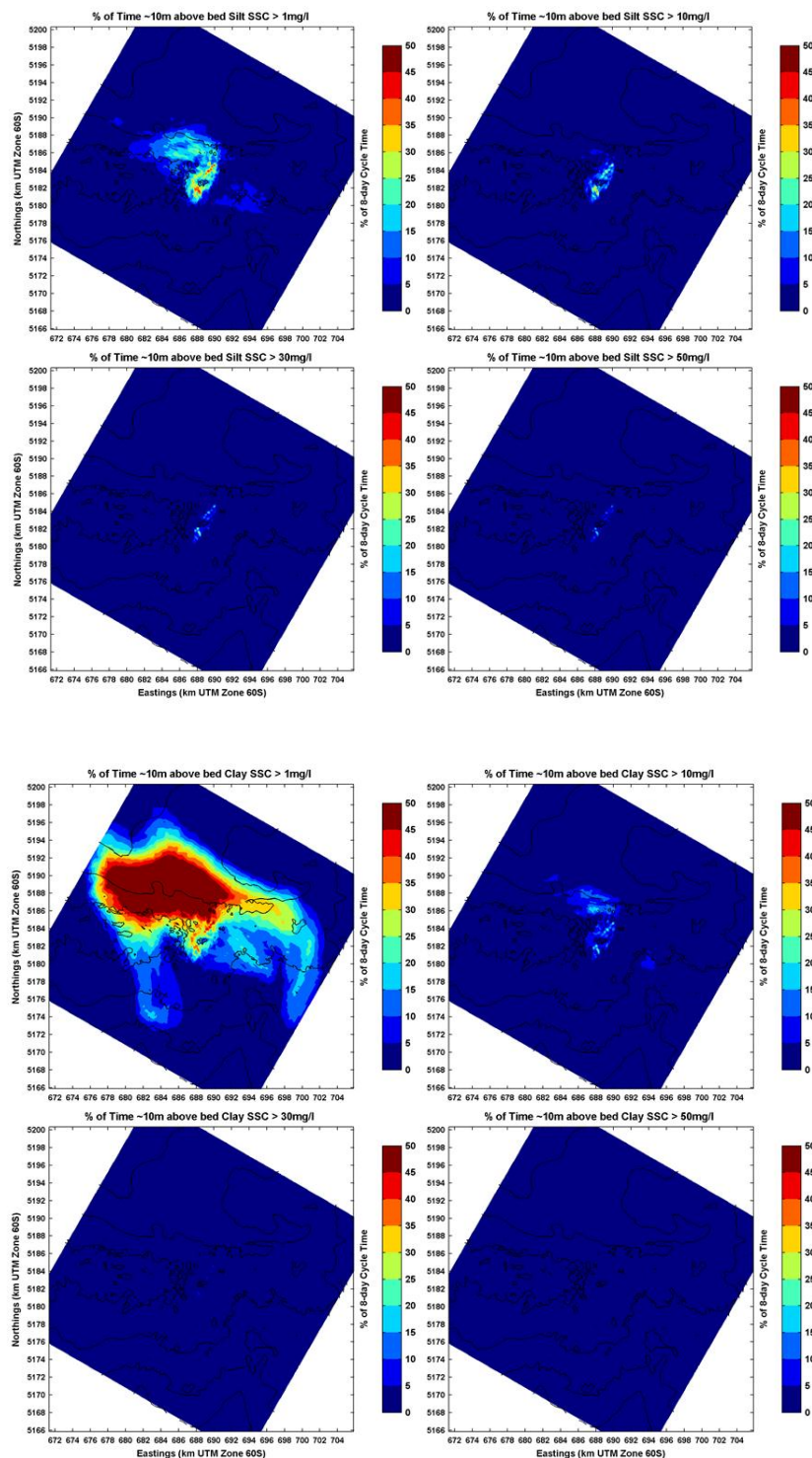


Figure B.5 Overview of the % time that the observed suspended sediment concentration approximately 10 m above the bed of the silt fraction exceeds 1 mg/l (upper left), 10 mg/l (upper right), 30 mg/l (lower left) and 50 mg/l (lower right). **Disposing 10 m above bed. Local Domain Summer**

B.2 10-Cycle Simulations

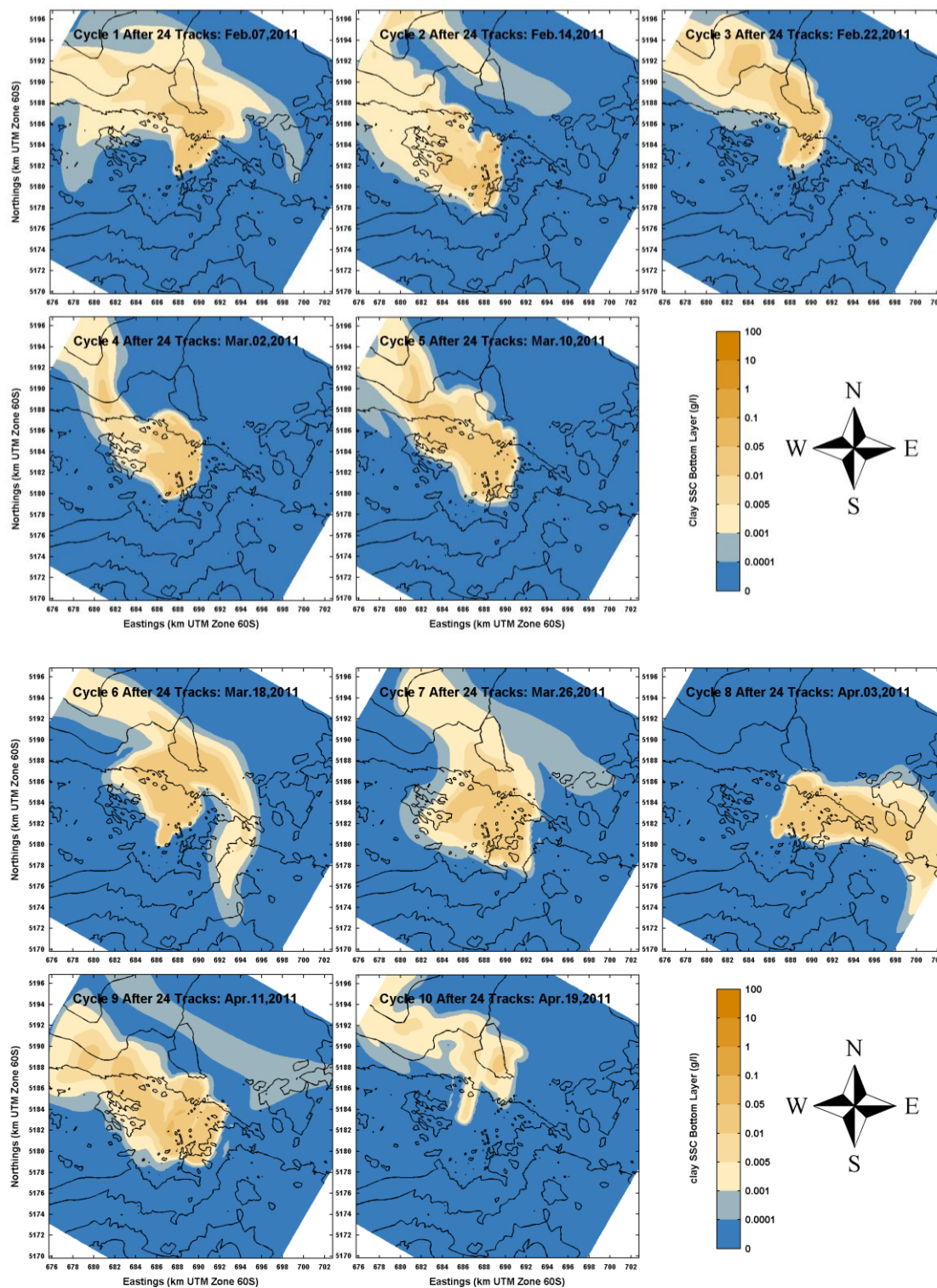


Figure B.6 Intra-seasonal variations in near-bed suspended **clay** concentrations at the end of cycles 1-10 during the 10-cycles simulation for **discharging 10 m above the bed. Summer**. Optimized Local Model domain.

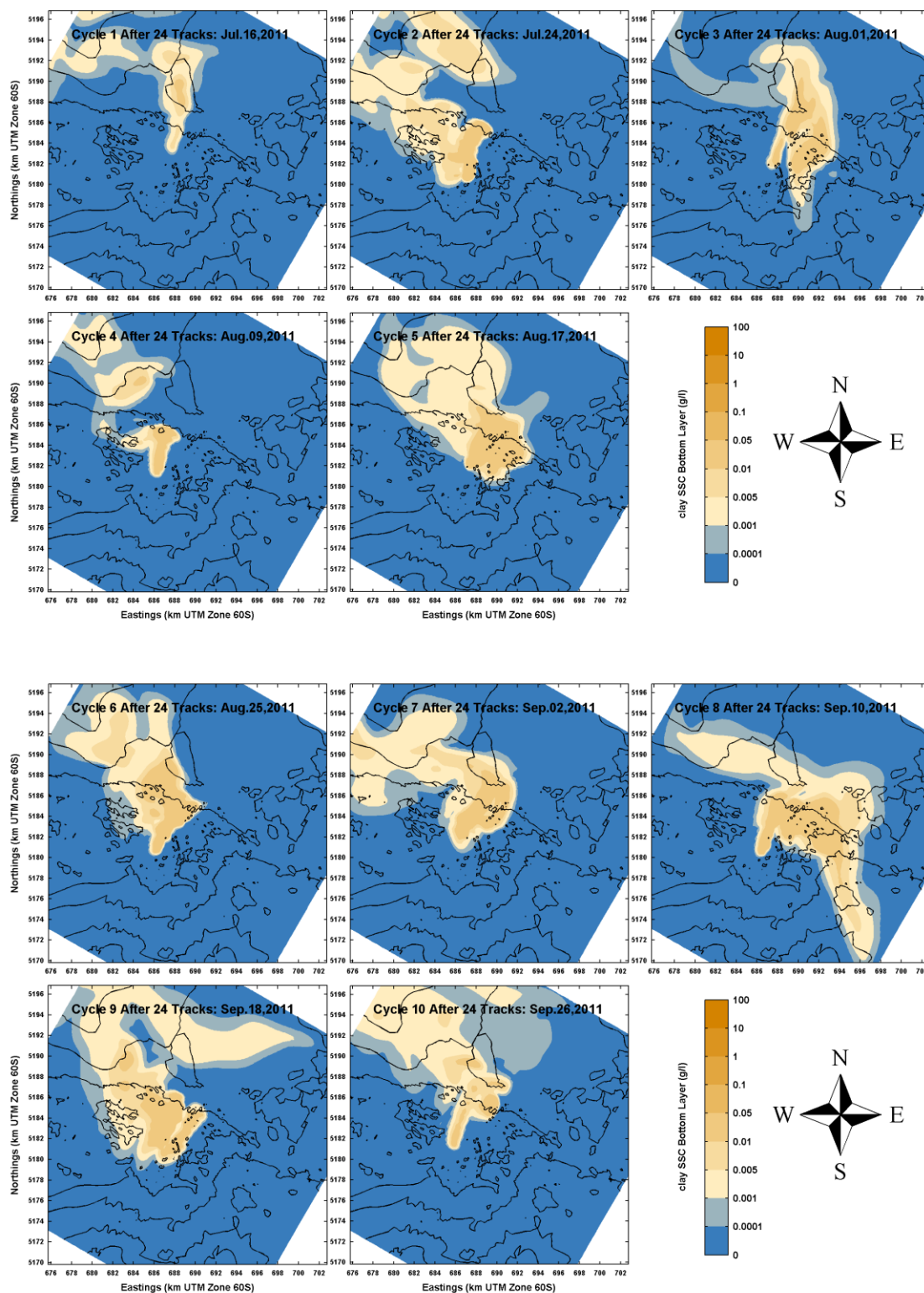


Figure B.7 Intra-seasonal variations in near-bed suspended **clay** concentrations (g/l) at the end of cycles 1-10 during the 10-cycles simulation for **discharging 10 m above the bed. Winter. Optimized Local Model domain.**

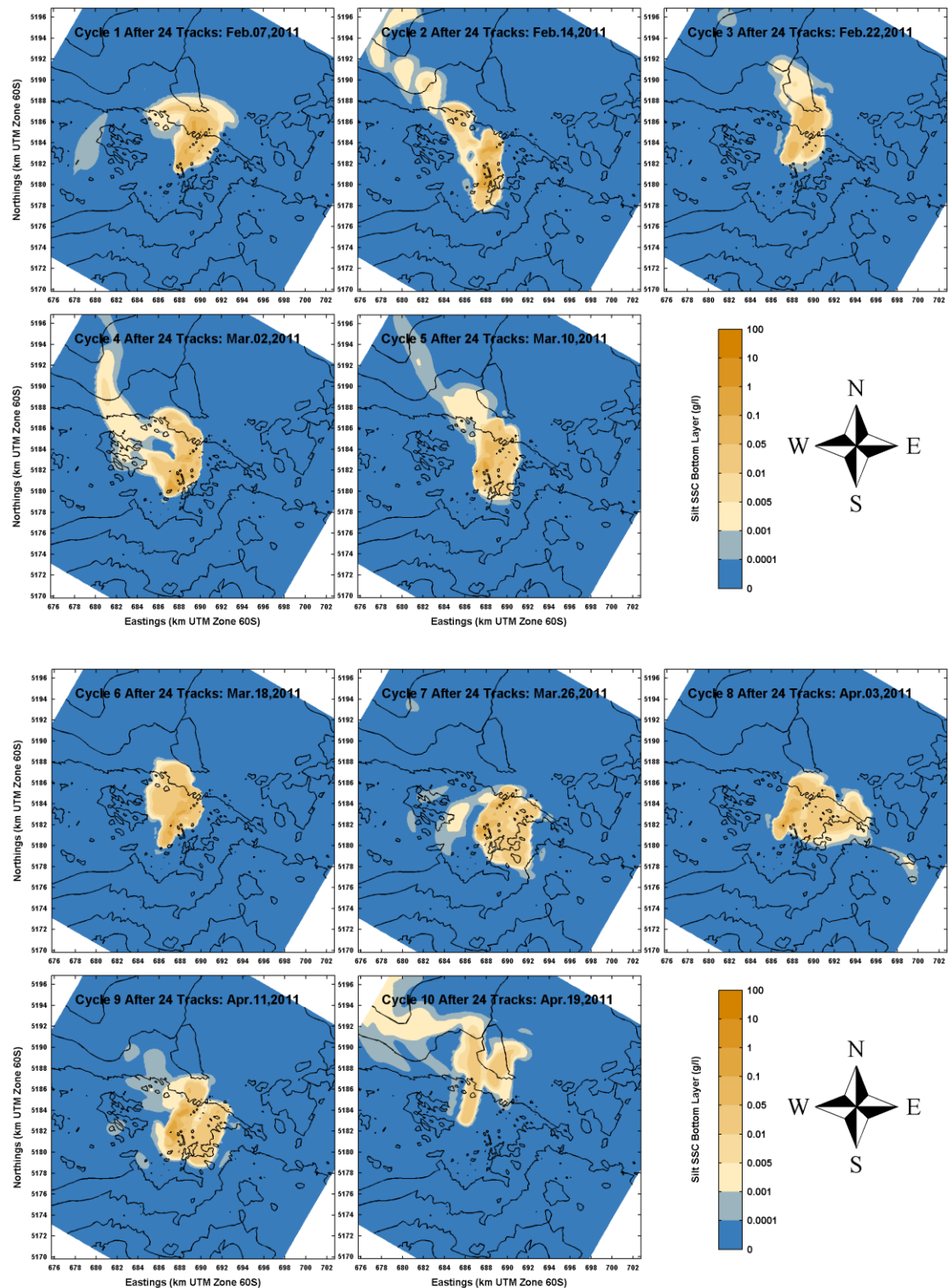


Figure B.8 Intra-seasonal variations in near-bed suspended *silt* concentrations (g/l) at the end of cycles 1-10 during the 10-cycles simulation for **discharging 10 m above the bed. Summer**. Optimized Local Model domain.

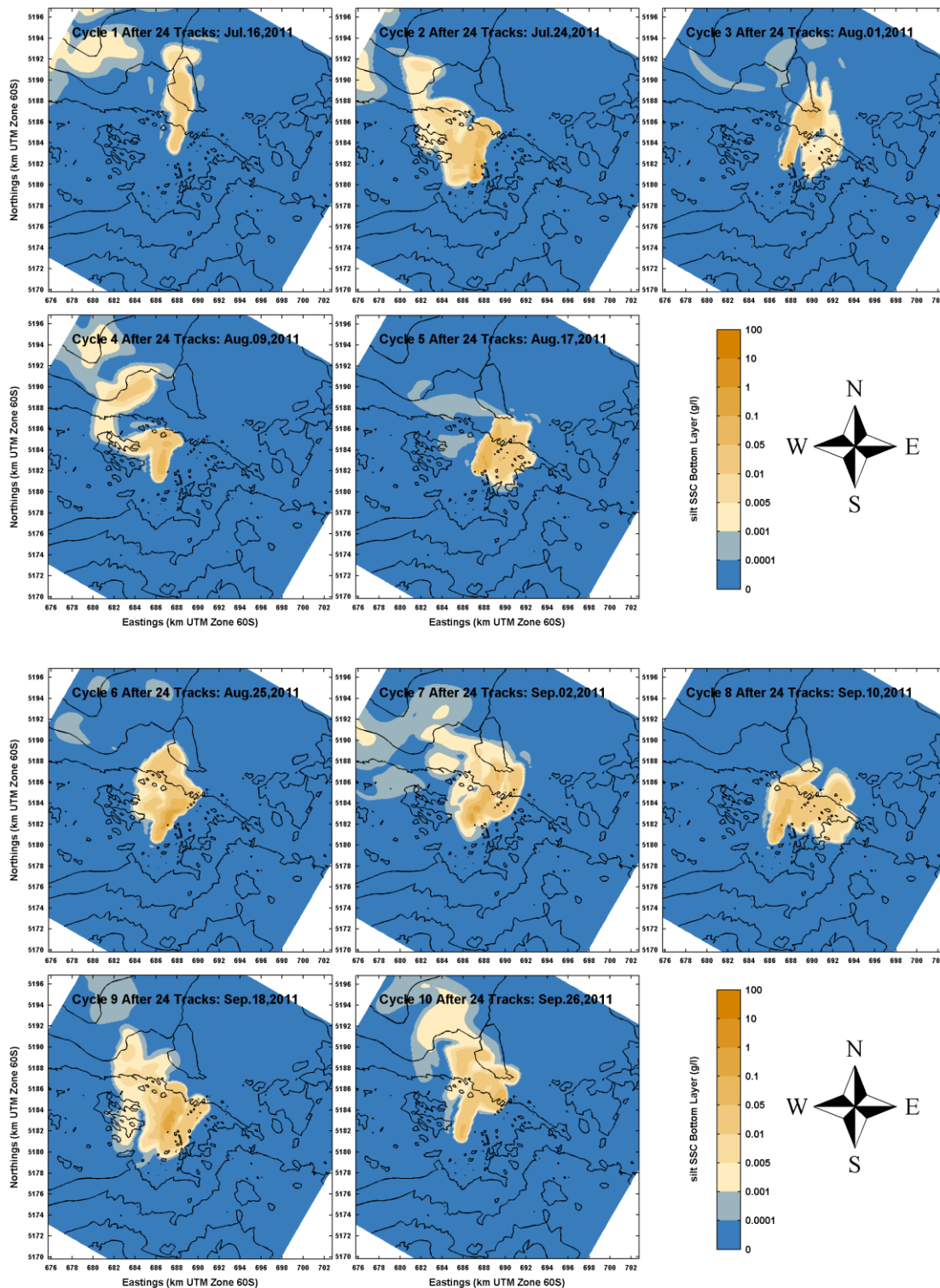


Figure B.9 Intra-seasonal variations in near-bed suspended **silt** concentrations (g/l) at the end of cycles 1-10 during the 10-cycles simulation for **discharging 10 m above the bed. Winter. Optimized Local Model domain.**

C Sedimentation

Figures C2 and C3 provide snapshots of the development of the sedimentation footprint over a single mining cycle for Winter and Spring scenarios for discharging at the bed. The Summer scenario for discharging at the bed is given in the main body of text in Section 5.1 and for discharge 10 m above the bed below in Figure C4. The sedimentation is expressed in [m] deposited sediment layer thickness or height. The darkest colour represents 0.1 m of sedimentation, brighter red 0.01 m and the predominately yellow colour 0.001 m (less than 1 mm) of sedimentation.

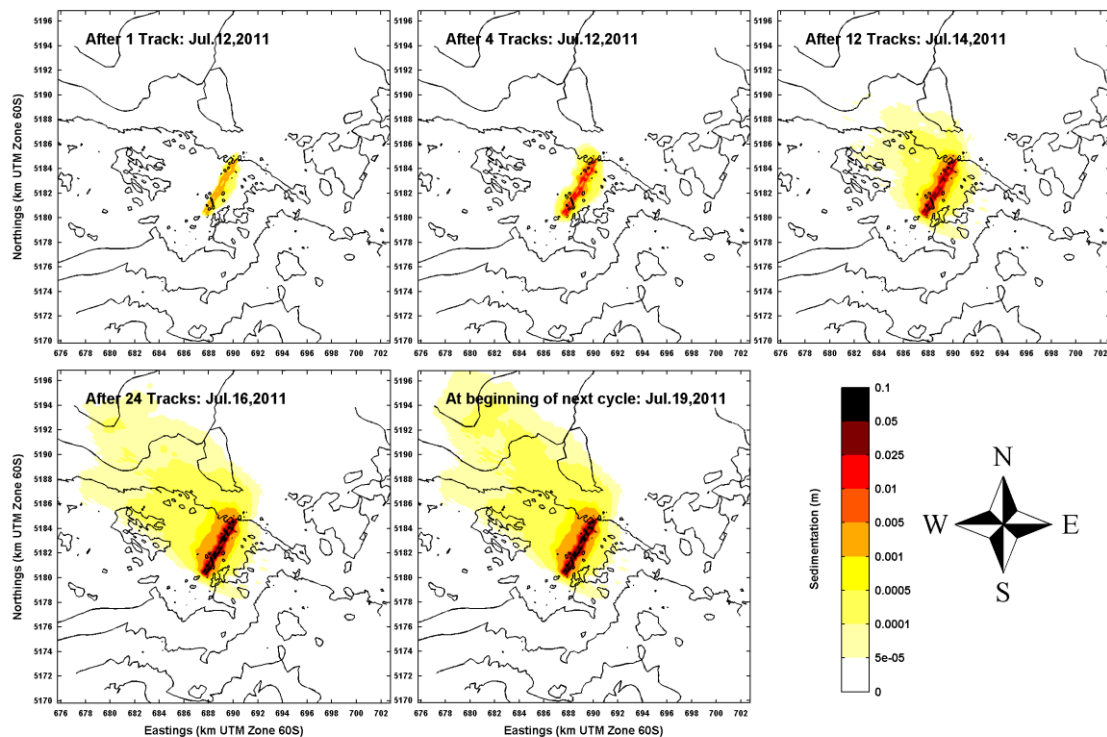


Figure C.1 Snapshots of single cycle footprint development in the Winter scenario. Example overview silt and clay sedimentation (m) over 1 completed track line, 4 track lines, 12 track lines, a complete cycle, and at the start of a new cycle for discharging at the bed.

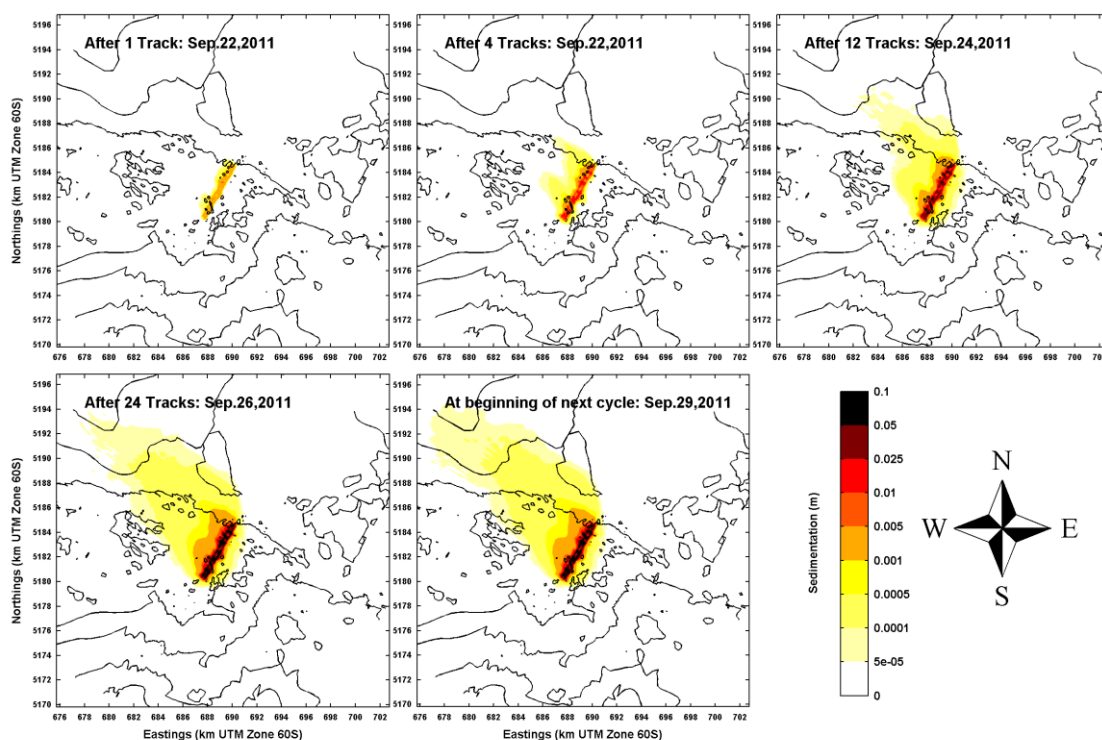


Figure C.2 Snapshots of single cycle footprint development in the Spring scenario. Example overview silt and clay sedimentation (m) over 1 completed track line, 4 track lines, 12 track lines, a complete cycle, and at the start of a new cycle for discharging at the bed.

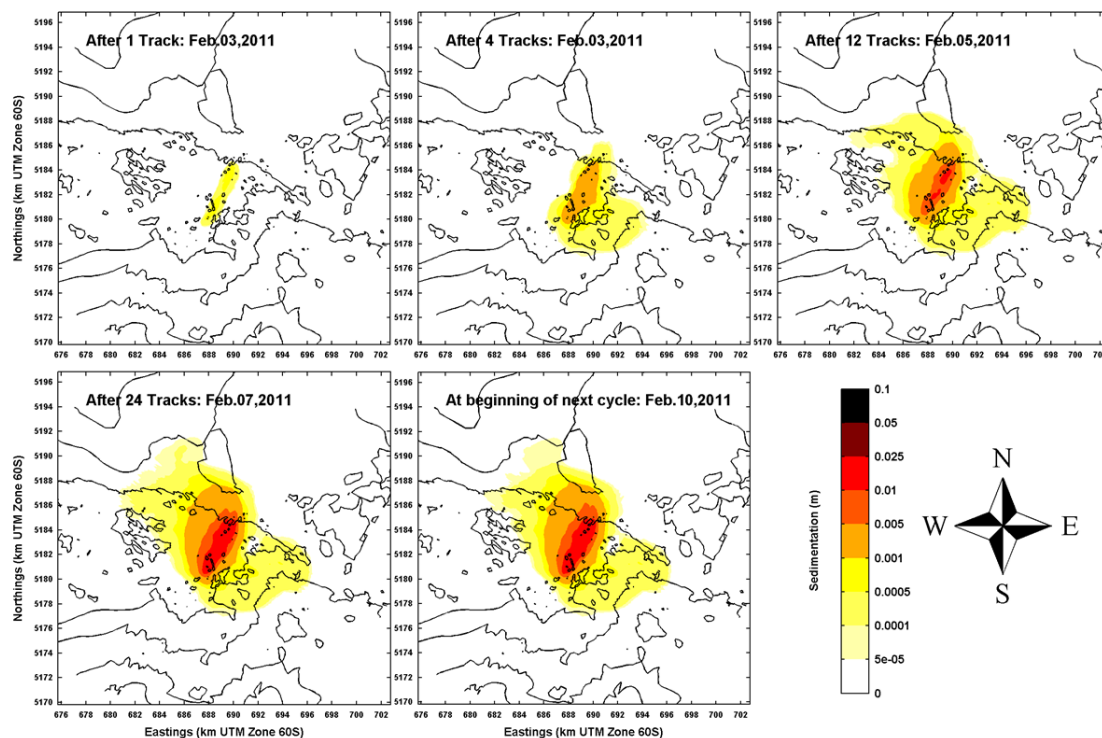


Figure C.3 Overview silt + clay sedimentation (m) over 1 completed track line, 4 track lines, 12 track lines, a complete cycle, and at the start of a new cycle. Disposing 10 m above bed. **Local Domain Summer**

D References

Deltares, 2014a *Modelling investigations on mine tailing plume dispersion on the Chatham Rise*. Deltares Final Report 1209110-000-ZKS-0007, 57 pp

Deltares, 2014b *Chatham Rise Phase 2, Resuspension Study*. Report 1207562-000-ZKS-0013. Deltares, Delft, the Netherlands.